Earth Syst. Sci. Data, 17, 965–1039, 2025
https://doi.org/10.5194/essd-17-965-2025

Open Access Earth System Science Data

Global Carbon Budget 2024

Pierre Friedlingstein[1,2], Michael O'Sullivan[1], Matthew W. Jones[3], Robbie M. Andrew[4], Judith Hauck[5,6], Peter Landschützer[7], Corinne Le Quéré[3], Hongmei Li[8,9], Ingrid T. Luijkx[10], Are Olsen[11,12], Glen P. Peters[4], Wouter Peters[10,13], Julia Pongratz[14,9], Clemens Schwingshackl[14], Stephen Sitch[1], Josep G. Canadell[15], Philippe Ciais[16], Robert B. Jackson[17,18], Simone R. Alin[19], Almut Arneth[20], Vivek Arora[21], Nicholas R. Bates[22], Meike Becker[11,12], Nicolas Bellouin[23], Carla F. Berghoff[24], Henry C. Bittig[25], Laurent Bopp[2], Patricia Cadule[2], Katie Campbell[26], Matthew A. Chamberlain[27], Naveen Chandra[28], Frédéric Chevallier[16], Louise P. Chini[29], Thomas Colligan[30], Jeanne Decayeux[31], Laique M. Djeutchouang[32,33], Xinyu Dou[34], Carolina Duran Rojas[1], Kazutaka Enyo[35], Wiley Evans[26], Amanda R. Fay[36], Richard A. Feely[19], Daniel J. Ford[1], Adrianna Foster[37], Thomas Gasser[38], Marion Gehlen[16], Thanos Gkritzalis[7], Giacomo Grassi[39], Luke Gregor[40], Nicolas Gruber[40], Özgür Gürses[5], Ian Harris[41], Matthew Hefner[42,43], Jens Heinke[44], George C. Hurtt[29], Yosuke Iida[35], Tatiana Ilyina[45,8,9], Andrew R. Jacobson[46,47], Atul K. Jain[48], Tereza Jarníková[49], Annika Jersild[30], Fei Jiang[50], Zhe Jin[51,52], Etsushi Kato[53], Ralph F. Keeling[54], Kees Klein Goldewijk[55], Jürgen Knauer[56,15], Jan Ivar Korsbakken[4], Xin Lan[46,47], Siv K. Lauvset[57,12], Nathalie Lefèvre[58], Zhu Liu[34], Junjie Liu[59,60], Lei Ma[29], Shamil Maksyutov[61], Gregg Marland[42,43], Nicolas Mayot[62], Patrick C. McGuire[63], Nicolas Metzl[58], Natalie M. Monacci[64], Eric J. Morgan[54], Shin-Ichiro Nakaoka[61], Craig Neill[27], Yosuke Niwa[61], Tobias Nützel[14], Lea Olivier[5,14], Tsuneo Ono[65], Paul I. Palmer[66,67], Denis Pierrot[68], Zhangcai Qin[69], Laure Resplandy[70,71], Alizée Roobaert[7], Thais M. Rosan[1], Christian Rödenbeck[72], Jörg Schwinger[57,12], T. Luke Smallman[66,67], Stephen M. Smith[73], Reinel Sospedra-Alfonso[21], Tobias Steinhoff[74,57], Qing Sun[75], Adrienne J. Sutton[19], Roland Séférian[31], Shintaro Takao[61], Hiroaki Tatebe[76,77], Hanqin Tian[78], Bronte Tilbrook[27,79], Olivier Torres[2], Etienne Tourigny[80], Hiroyuki Tsujino[81], Francesco Tubiello[82], Guido van der Werf[10], Rik Wanninkhof[68], Xuhui Wang[52], Dongxu Yang[83], Xiaojuan Yang[84], Zhen Yu[85], Wenping Yuan[86], Xu Yue[87], Sönke Zaehle[71], Ning Zeng[88,30], and Jiye Zeng[61]

[1]Faculty of Environment, Science and Economy, University of Exeter, Exeter, EX4 4QF, UK
[2]Laboratoire de Météorologie Dynamique, Institut Pierre-Simon Laplace, CNRS, École Normale Supérieure, Université PSL, Sorbonne Université, École Polytechnique, Paris, France
[3]Tyndall Centre for Climate Change Research, School of Environmental Sciences, University of East Anglia, Norwich Research Park, Norwich, NR4 7TJ, UK
[4]CICERO Center for International Climate Research, Oslo 0349, Norway
[5]Alfred-Wegener-Institut, Helmholtz-Zentrum für Polar- und Meeresforschung, Am Handelshafen 12, 27570 Bremerhaven, Germany
[6]Faculty of Biology/Chemistry, Universität Bremen, Bremen, Germany
[7]Flanders Marine Institute (VLIZ), Jacobsenstraat 1, 8400, Ostend, Belgium
[8]Helmholtz-Zentrum Hereon, Max-Planck-Straße 1, 21502 Geesthacht, Germany
[9]Max Planck Institute for Meteorology, Bundesstraße 53, 20146 Hamburg, Germany
[10]Environmental Sciences Group, Wageningen University, P.O. Box 47, 6700 AA, Wageningen, the Netherlands
[11]Geophysical Institute, University of Bergen, Allégaten 70, 5007 Bergen, Norway
[12]Bjerknes Centre for Climate Research, Bergen, Norway
[13]Centre for Isotope Research, University of Groningen, Groningen, the Netherlands
[14]Department of Geography, Ludwig-Maximilians-Universität München, Luisenstr. 37, 80333 Munich, Germany
[15]CSIRO Environment, Canberra, ACT 2101, Australia

Published by Copernicus Publications.

[16]Laboratoire des Sciences du Climat et de l'Environnement, LSCE–IPSL, CEA–CNRS–UVSQ, Université Paris-Saclay, 91198 Gif-sur-Yvette, France
[17]Department of Earth System Science, Stanford University, Stanford, CA 94305-2210, USA
[18]Woods Institute for the Environment and Precourt Institute for Energy, Stanford University, Stanford, CA 94305-2210, USA
[19]National Oceanic and Atmospheric Administration, Pacific Marine Environmental Laboratory (NOAA/PMEL), 7600 Sand Point Way NE, Seattle, WA 98115, USA
[20]Institute of Meteorology and Climate Research Atmospheric Environmental Research, Karlsruhe Institute of Technology, 82467 Garmisch-Partenkirchen, Germany
[21]Canadian Centre for Climate Modelling and Analysis, Environment and Climate Change Canada, Victoria, BC, Canada
[22]Bermuda Institute of Ocean Sciences (ASU BIOS), 31 Biological Lane, Ferry Reach, St. George's, GE01, Bermuda
[23]Department of Meteorology, University of Reading, Reading, RG6 6BB, UK
[24]Instituto Nacional de Investigación y Desarrollo Pesquero, Paseo Victoria Ocampo No 1, Escollera Norte, B7602HSA, Mar del Plata, Argentina
[25]Leibniz Institute for Baltic Sea Research Warnemünde (IOW), Seestrasse 15, 18119 Rostock, Germany
[26]Hakai Institute, Heriot Bay, BC, V0P 1H0, Canada
[27]CSIRO Environment, Castray Esplanade, Hobart, TAS 7004, Australia
[28]Research Institute for Global Change, Japan Agency for Marine-Earth Science and Technology (JAMSTEC), 3173-25 Showa-machi, Kanazawa, Yokohama, 236-0001, Japan
[29]Department of Geographical Sciences, University of Maryland, College Park, MD 20742, USA
[30]Earth System Science Interdisciplinary Center, University of Maryland, College Park, MD 20740, USA
[31]Centre National de Recherches Météorologiques, Université de Toulouse, Météo-France, CNRS, UMR 3589, Toulouse, France
[32]School for Climate Studies, Stellenbosch University, Private Bag X1, Matieland, Stellenbosch, 7602, South Africa
[33]Southern Ocean Carbon and Climate Observatory, CSIR, Rosebank, Cape Town, 7700, South Africa
[34]Department of Earth System Science, Tsinghua University, Beijing, China
[35]Japan Meteorological Agency, 3-6-9 Toranomon, Minato City, Tokyo, 105-8431, Japan
[36]Lamont-Doherty Earth Observatory, Columbia University, New York, NY, USA
[37]Climate and Global Dynamics Laboratory, National Center for Atmospheric Research, Boulder, CO 80305, USA
[38]International Institute for Applied Systems Analysis (IIASA), Schlossplatz 1, 2361 Laxenburg, Austria
[39]Joint Research Centre (JRC), European Commission, Ispra, Italy
[40]Environmental Physics Group, Institute of Biogeochemistry and Pollutant Dynamics and Center for Climate Systems Modeling (C2SM), ETH Zürich, Zurich, Switzerland
[41]NCAS-Climate, Climatic Research Unit, School of Environmental Sciences, University of East Anglia, Norwich Research Park, Norwich, NR4 7TJ, UK
[42]Research Institute for Environment, Energy, and Economics, Appalachian State University, Boone, NC, USA
[43]Department of Geological and Environmental Sciences, Appalachian State University, Boone, NC, USA
[44]Potsdam Institute for Climate Impact Research (PIK), Leibniz Association, P.O. Box 60 12 03, 14412 Potsdam, Germany
[45]Department of Earth System Sciences, Universität Hamburg, Bundesstraße 55, 20146 Hamburg, Germany
[46]Cooperative Institute for Research in Environmental Sciences (CIRES), University of Colorado Boulder, Boulder, CO 80309, USA
[47]National Oceanic and Atmospheric Administration Global Monitoring Laboratory (NOAA/GML), 325 Broadway R/GML, Boulder, CO 80305, USA
[48]Department of Climate, Meteorology and Atmospheric Sciences, University of Illinois, Urbana, IL 61821, USA
[49]School of Environmental Sciences, University of East Anglia, Norwich, UK

[50]Jiangsu Provincial Key Laboratory of Geographic Information Science and Technology, International Institute for Earth System Science, Nanjing University, Nanjing 210023, China
[51]State Key Laboratory of Tibetan Plateau Earth System and Resource Environment, Institute of Tibetan Plateau Research, Chinese Academy of Sciences, Beijing 100101, China
[52]Institute of Carbon Neutrality, Sino-French Institute for Earth System Science, College of Urban and Environmental Sciences, Peking University, Beijing 100871, China
[53]Institute of Applied Energy (IAE), Minato City, Tokyo, 105-0003, Japan
[54]Scripps Institution of Oceanography, University of California, San Diego, La Jolla, CA 92093-0244, USA
[55]Faculty of Geosciences, Department IMEW, Copernicus Institute of Sustainable Development, Utrecht University, Heidelberglaan 2, P.O. Box 80115, 3508 TC, Utrecht, the Netherlands
[56]Hawkesbury Institute for the Environment, Western Sydney University, Penrith, NSW, Australia
[57]NORCE Norwegian Research Centre, Jahnebakken 5, 5007 Bergen, Norway
[58]LOCEAN/IPSL, Sorbonne Université, CNRS–IRD–MNHN, 75252 Paris, France
[59]Jet Propulsion Laboratory, California Institute of Technology, Pasadena, CA, USA
[60]Division of Geological and Planetary Sciences, California Institute of Technology, Pasadena, CA, USA
[61]Earth System Division, National Institute for Environmental Studies, 16-2 Onogawa, Tsukuba, Ibaraki, 305-8506, Japan
[62]Laboratoire d'Océanographie de Villefranche, Sorbonne Université, Villefranche-sur-Mer, France
[63]Department of Meteorology and National Centre for Atmospheric Science (NCAS), University of Reading, Reading, UK
[64]College of Fisheries and Ocean Sciences, University of Alaska Fairbanks, Fairbanks, AK 99709, USA
[65]Fisheries Research and Education Agency, 2-12-4 Fukuura, Kanazawa, Yokohama, 236-8648, Japan
[66]National Centre for Earth Observation, University of Edinburgh, Edinburgh, EH9 3FF, UK
[67]School of GeoSciences, University of Edinburgh, Edinburgh, EH9 3FF, UK
[68]NOAA Atlantic Oceanographic and Meteorological Laboratory (NOAA/AOML), 4301 Rickenbacker Causeway, Miami, FL 33149, USA
[69]School of Atmospheric Sciences, Sun Yat-sen University, Zhuhai 519000, China
[70]Department of Geosciences, Princeton University, Princeton, NJ, USA
[71]High Meadows Environmental Institute, Princeton University, Princeton, NJ, USA
[72]Max Planck Institute for Biogeochemistry, P.O. Box 600164, Hans-Knöll-Str. 10, 07745 Jena, Germany
[73]Smith School of Enterprise and the Environment, University of Oxford, Oxford, UK
[74]GEOMAR Helmholtz Centre for Ocean Research Kiel, Wischhofstr. 1–3, 24148 Kiel, Germany
[75]Climate and Environmental Physics, Physics Institute, University of Bern, Bern, Switzerland
[76]Research Center for Environmental Modeling and Application, Japan Agency for Marine-Earth Science and Technology (JAMSTEC), Yokohama, Japan
[77]Advanced Institute for Marine Ecosystem Change, Japan Agency for Marine-Earth Science and Technology (JAMSTEC), Yokohama, Japan
[78]Schiller Institute of Integrated Science and Society, Department of Earth and Environmental Sciences, Boston College, Chestnut Hill, MA 02467, USA
[79]Australian Antarctic Partnership Program, University of Tasmania, Hobart, TAS, Australia
[80]Barcelona Supercomputing Center, Barcelona, Spain
[81]JMA Meteorological Research Institute, Tsukuba, Ibaraki, Japan
[82]Statistics Division, Food and Agriculture Organization of the United Nations, Via Terme di Caracalla, Rome 00153, Italy
[83]Institute of Atmospheric Physics, Chinese Academy of Sciences, Beijing, China
[84]Climate Change Science Institute and Environmental Sciences Division, Oak Ridge National Laboratory, Oak Ridge, TN 37831, USA
[85]School of Ecology and Applied Meteorology, Nanjing University of Information Science and Technology (NUIST), Nanjing 210044, China
[86]Institute of Carbon Neutrality, College of Urban and Environmental Sciences, Peking University, Beijing 100091, China

[87]School of Environmental Science and Engineering, Nanjing University of Information Science and Technology (NUIST), Nanjing 210044, China
[88]Department of Atmospheric and Oceanic Science, University of Maryland, College Park, MD, USA

Correspondence: Pierre Friedlingstein (p.friedlingstein@exeter.ac.uk)

Received: 6 November 2024 – Discussion started: 13 November 2024
Revised: 24 January 2025 – Accepted: 30 January 2025 – Published: 14 March 2025

Abstract. Accurate assessment of anthropogenic carbon dioxide (CO_2) emissions and their redistribution among the atmosphere, ocean, and terrestrial biosphere in a changing climate is critical to better understand the global carbon cycle, support the development of climate policies, and project future climate change. Here we describe and synthesize datasets and methodologies to quantify the five major components of the global carbon budget and their uncertainties. Fossil CO_2 emissions (E_{FOS}) are based on energy statistics and cement production data, while emissions from land-use change (E_{LUC}) are based on land-use and land-use change data and bookkeeping models. Atmospheric CO_2 concentration is measured directly, and its growth rate (G_{ATM}) is computed from the annual changes in concentration. The global net uptake of CO_2 by the ocean (S_{OCEAN}, called the ocean sink) is estimated with global ocean biogeochemistry models and observation-based fCO_2 products (fCO_2 is the fugacity of CO_2). The global net uptake of CO_2 by the land (S_{LAND}, called the land sink) is estimated with dynamic global vegetation models. Additional lines of evidence on land and ocean sinks are provided by atmospheric inversions, atmospheric oxygen measurements, and Earth system models. The sum of all sources and sinks results in the carbon budget imbalance (B_{IM}), a measure of imperfect data and incomplete understanding of the contemporary carbon cycle. All uncertainties are reported as $\pm 1\sigma$.

For the year 2023, E_{FOS} increased by 1.3 % relative to 2022, with fossil emissions at $10.1 \pm 0.5\,GtC\,yr^{-1}$ ($10.3 \pm 0.5\,GtC\,yr^{-1}$ when the cement carbonation sink is not included), and E_{LUC} was $1.0 \pm 0.7\,GtC\,yr^{-1}$, for a total anthropogenic CO_2 emission (including the cement carbonation sink) of $11.1 \pm 0.9\,GtC\,yr^{-1}$ ($40.6 \pm 3.2\,GtCO_2\,yr^{-1}$). Also, for 2023, G_{ATM} was $5.9 \pm 0.2\,GtC\,yr^{-1}$ ($2.79 \pm 0.1\,ppm\,yr^{-1}$; ppm denotes parts per million), S_{OCEAN} was $2.9 \pm 0.4\,GtC\,yr^{-1}$, and S_{LAND} was $2.3 \pm 1.0\,GtC\,yr^{-1}$, with a near-zero B_{IM} ($-0.02\,GtC\,yr^{-1}$). The global atmospheric CO_2 concentration averaged over 2023 reached 419.31 ± 0.1 ppm. Preliminary data for 2024 suggest an increase in E_{FOS} relative to 2023 of +0.8 % (−0.2 % to 1.7 %) globally and an atmospheric CO_2 concentration increase by 2.87 ppm, reaching 422.45 ppm, 52 % above the pre-industrial level (around 278 ppm in 1750). Overall, the mean of and trend in the components of the global carbon budget are consistently estimated over the period 1959–2023, with a near-zero overall budget imbalance, although discrepancies of up to around $1\,GtC\,yr^{-1}$ persist for the representation of annual to semi-decadal variability in CO_2 fluxes. Comparison of estimates from multiple approaches and observations shows the following: (1) a persistent large uncertainty in the estimate of land-use change emissions, (2) low agreement between the different methods on the magnitude of the land CO_2 flux in the northern extra-tropics, and (3) a discrepancy between the different methods on the mean ocean sink.

This living-data update documents changes in methods and datasets applied to this most recent global carbon budget as well as evolving community understanding of the global carbon cycle. The data presented in this work are available at https://doi.org/10.18160/GCP-2024 (Friedlingstein et al., 2024).

Executive summary. Global fossil CO_2 emissions (including cement carbonation) are expected to further increase in 2024 by 0.8 %. The 2023 emissions increase was $0.14\,GtC\,yr^{-1}$ ($0.5\,GtCO_2\,yr^{-1}$) relative to 2022, bringing 2023 fossil CO_2 emissions to $10.1 \pm 0.5\,GtC\,yr^{-1}$ ($36.8 \pm 1.8\,GtCO_2\,yr^{-1}$). Preliminary estimates based on data available suggest fossil CO_2 emissions have increased further in 2024, by 0.8 % relative to 2023 (−0.2 % to 1.7 %), bringing emissions to $10.2\,GtC\,yr^{-1}$ ($37.4\,GtCO_2\,yr^{-1}$).[1]

Emissions from coal, oil, and gas in 2024 are expected to be slightly above their 2023 levels (by 0.1 %, 0.9 %, and 2.5 %, respectively). Regionally, fossil emissions in 2024 are expected to have decreased by 2.8 % in the European Union, reaching 0.7 GtC (2.4 $GtCO_2$), and by 0.9 % in the United States (1.3 GtC, 4.9 $GtCO_2$). Emissions in China are expected to have increased in 2024 by 0.1 % (3.3 GtC, 11.9 $GtCO_2$). Fossil emissions are also expected to have increased by 3.7 % in India (0.9 GtC, 3.2 $GtCO_2$) and by 1.2 % for the rest of the world (4.0 GtC, 14.5 $GtCO_2$) in 2024. Emissions from international aviation and shipping (IAS) are also expected to have increased by 7.8 % (0.3 GtC, 1.2 $GtCO_2$) in 2024.

[1] All 2024 growth rates use a leap year adjustment that corrects for the extra day in 2024.

Fossil CO_2 emissions decreased significantly in 23 countries with significantly growing economies during the decade 2014–2023. Altogether, these 23 countries have contributed about 2.2 GtC yr^{-1} (8.2 $GtCO_2$) to fossil fuel CO_2 emissions over the last decade, representing about 23 % of world CO_2 fossil emissions.

Global CO_2 emissions from land-use, land-use change, and forestry (LULUCF) averaged 1.1 ± 0.7 GtC yr^{-1} (4.1 ± 2.6 $GtCO_2$ yr^{-1}) for the 2014–2023 period with a similar preliminary projection for 2024 of 1.2 ± 0.7 GtC yr^{-1} (4.2 ± 2.6 $GtCO_2$ yr^{-1}). Since the late 1990s, emissions from LULUCF have shown a statistically significant decrease at a rate of around 0.2 GtC per decade. Emissions from deforestation, the main driver of global gross sources, remain high at around 1.7 GtC yr^{-1} over the 2014–2023 period, highlighting the strong potential of halting deforestation for emissions reductions. Sequestration of 1.2 GtC yr^{-1} through re-/afforestation and forest regrowth in shifting cultivation cycles offsets two-thirds of the deforestation emissions. Further, smaller emissions are due to other land-use transitions and peat drainage and peat fire. The highest emitters during 2014–2023 in descending order were Brazil, Indonesia, and the Democratic Republic of the Congo, with these three countries contributing more than half of global land-use CO_2 emissions.

Total anthropogenic emissions (fossil and LULUCF, including the cement carbonation sink) were 11.1 GtC yr^{-1} (40.6 $GtCO_2$ yr^{-1}) in 2023, with a slightly higher preliminary estimate of 11.4 GtC yr^{-1} (41.6 $GtCO_2$ yr^{-1}) for 2024. Total anthropogenic emissions have been stable over the last decade (zero growth rate over the 2014–2023 period) and much slower than over the previous decade (2004–2013), with an average growth rate of 2.0 % yr^{-1}.

The remaining carbon budget for a 50 % likelihood to limit global warming to 1.5, 1.7, and 2 °C above the 1850–1900 level has been reduced to 65 GtC (235 $GtCO_2$), 160 GtC (585 $GtCO_2$), and 305 GtC (1110 $GtCO_2$), respectively, from the beginning of 2025, equivalent to around 6, 14, and 27 years, assuming 2024 emissions levels.

The concentration of CO_2 in the atmosphere is set to reach 422.45 parts per million (ppm) in 2024, 52 % above pre-industrial levels. The atmospheric CO_2 growth was 5.2 ± 0.02 GtC yr^{-1} (2.5 ppm) during the decade 2014–2023 (48 % of total CO_2 emissions), with a preliminary 2024 growth rate estimate of around 6.1 GtC (2.87 ppm).

The ocean sink, the global net uptake of CO_2 by the ocean, has been stagnant since 2016 after rapid growth during 2002–2016, largely in response to large interannual climate variability. The ocean CO_2 sink was 2.9 ± 0.4 GtC yr^{-1} during the decade 2014–2023 (26 % of total CO_2 emissions). A slightly higher value of 3.0 GtC yr^{-1} is preliminarily estimated for 2024, which marks an increase in the sink since 2023 due to the prevailing El Niño and neutral conditions in 2024.

The land sink, the global net uptake of CO_2 by the land, continued to increase during the 2014–2023 period primarily in response to increased atmospheric CO_2, albeit with large interannual variability. The land CO_2 sink was 3.2 ± 0.9 GtC yr^{-1} during the 2014–2023 decade (30 % of total CO_2 emissions). The land sink in 2023 was 2.3 ± 1 GtC yr^{-1}, which is 1.6 GtC lower than in 2022 and the lowest estimate since 2015. This reduced sink is primarily driven by a response of tropical land ecosystems to the onset of the 2023–2024 El Niño event, combined with large wildfires in Canada in 2023. The preliminary 2024 estimate is around 3.2 GtC yr^{-1}, similar to the decadal average, consistent with a land sink emerging from the El Niño state.

So far in 2024 (at the time of writing), global fire CO_2 emissions have been 11 %–32 % higher than the 2014–2023 average due to high fire activity in both North America and South America, reaching 1.6–2.2 GtC during January–September. In Canada, emissions through September were 0.2–0.3 GtC yr^{-1}, down from 0.5–0.8 GtC yr^{-1} in 2023 but still more than twice the 2014–2023 average. In Brazil, fires through September emitted 0.2–0.3 GtC yr^{-1}, 91 %–118 % above the 2014–2023 average due to intense drought. These fire emissions estimates should not be directly compared with the land-use emissions or the land sink because they represent a gross carbon flux to the atmosphere and do not account for post-fire recovery or distinguish between natural, climate-driven, and land-use-related fires.

1 Introduction

The concentration of carbon dioxide (CO_2) in the atmosphere has increased from approximately 278 parts per million (ppm) in 1750 (Gulev et al., 2021), the beginning of the industrial era, to 419.3 ± 0.1 ppm in 2023 (Lan et al., 2024; Fig. 1). The atmospheric CO_2 increase above pre-industrial levels was, initially, primarily caused by the release of carbon to the atmosphere from deforestation and other land-use change activities (Canadell et al., 2021). While emissions from fossil fuels started before the industrial era, they became the dominant source of anthropogenic emissions to the atmosphere from around 1950, and their relative share has continued to increase until the present. Anthropogenic emissions occur on top of an active natural carbon cycle that circulates carbon between the reservoirs of the atmosphere, ocean, and terrestrial biosphere on timescales from sub-daily to millennial, while exchanges with geologic reservoirs occur on longer timescales (Archer et al., 2009).

The global carbon budget (GCB) presented here refers to the mean of, variations in, and trends in the perturbation of CO_2 in the environment, referenced to the beginning of the industrial era (defined here as 1750). This paper describes the components of the global carbon cycle over the historical period, with a stronger focus on the recent period (since 1958, onset of robust atmospheric CO_2 measurements), the last decade (2014–2023), the last year (2023), and the current year (2024) at the time of writing. Finally, it provides cumulative emissions from fossil fuels and land-use change since the year 1750 and since the year 1850 (the reference year for historical simulations in the Intergovernmental Panel on Climate Change Sixth Assessment Report, IPCC AR6) (Eyring et al., 2016).

We quantify the input of CO_2 to the atmosphere by emissions from human activities; the growth rate of atmospheric CO_2 concentration; and the resulting changes in the storage of carbon in the land and ocean reservoirs in response to increasing atmospheric CO_2 levels, climate change, and variability and other anthropogenic and natural changes (Fig. 2). An understanding of this perturbation budget over time and

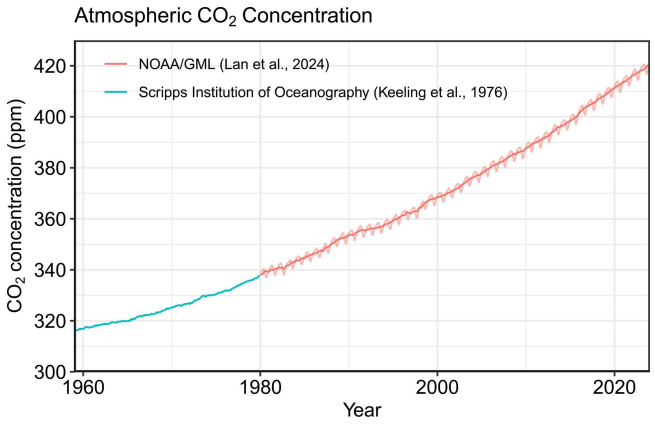

Figure 1. Surface average atmospheric CO_2 concentration (ppm). From 1980, monthly data are from NOAA/GML (Lan et al., 2024) and are based on an average of direct atmospheric CO_2 measurements from multiple stations in the marine boundary layer (Masarie and Tans, 1995). The 1958–1979 monthly data are from Scripps Institution of Oceanography, based on an average of direct atmospheric CO_2 measurements from the Mauna Loa and South Pole stations (Keeling et al., 1976). To account for the difference in mean CO_2 and seasonality between the NOAA/GML and the Scripps station networks used here, the Scripps surface average (from two stations) was de-seasonalized and adjusted to match the NOAA/GML surface average (from multiple stations) by adding the mean difference of 0.667 ppm, calculated here from overlapping data during 1980–2012.

the underlying variability in and trends of the natural carbon cycle is necessary to understand the response of natural sinks to changes in climate, CO_2, and land-use change drivers and to quantify emissions compatible with a given climate stabilization target.

The components of the CO_2 budget that are reported annually in this paper include separate and independent estimates for the CO_2 emissions from (1) fossil fuel combustion and oxidation from all energy and industrial processes, also including cement production and carbonation (E_{FOS}; GtC yr^{-1}), and (2) deliberate human activities on land, including those leading to land-use change (E_{LUC}; GtC yr^{-1}), and their partitioning among (3) the growth rate of atmospheric CO_2 concentration (G_{ATM}; GtC yr^{-1}) and the uptake of CO_2 (the "CO_2 sinks") in (4) the ocean (S_{OCEAN}; GtC yr^{-1}) and (5) on land (S_{LAND}; GtC yr^{-1}). The CO_2 sinks as defined here conceptually include the response of the land (including inland waters and estuaries) and ocean (including coastal and marginal seas) to elevated CO_2 and changes in climate and other environmental conditions, although in practice not all processes are fully accounted for (see Sect. 2.10). Note that the term sink means that the net transfer of carbon is from the atmosphere to land or the ocean, but it does not imply any permanence of that sink in the future.

Global emissions and their partitioning among the atmosphere, ocean, and land are in balance in the real world. Due to the combination of imperfect spatial and/or temporal data coverage, errors in each estimate, and smaller terms not included in our budget estimate (discussed in Sect. 2.10), the independent estimates (1) to (5) above do not necessarily add up to zero. We hence estimate a budget imbalance (B_{IM}), which is a measure of the mismatch between the estimated emissions and the estimated changes in the atmosphere, land, and ocean, as follows:

$$B_{IM} = E_{FOS} + E_{LUC} - (G_{ATM} + S_{OCEAN} + S_{LAND}). \quad (1)$$

G_{ATM} is usually reported in ppm yr^{-1}, which we convert to units of carbon mass per year, GtC yr^{-1}, using 1 ppm = 2.124 GtC (Ballantyne et al., 2012; Table 1). Units of gigatonnes of CO_2 (or billion tonnes of CO_2) used in policy are equal to 3.664 multiplied by the value in units of gigatonnes of carbon (GtC).

We also assess a set of additional lines of evidence derived from global atmospheric inversion system results (Sect. 2.7), observed changes in oxygen concentration (Sect. 2.8), and Earth system model (ESM) simulations (Sect. 2.9), with all of these methods closing the global carbon balance (zero B_{IM}).

We further quantify E_{FOS} and E_{LUC} by country, including both territorial and consumption-based accounting for E_{FOS} (see Sect. 2), and discuss missing terms from sources other than the combustion of fossil fuels (see Sects. 2.10 and S1 and S2 in the Supplement). We also assess carbon dioxide removal (CDR) (see Sect. 2.2 and 2.3). Land-based CDR is significant but already accounted for in E_{LUC} in Eq. (1) (Sect. 3.2.2). Other CDR methods, not based on vegetation, are currently several orders of magnitude smaller than the other components of the budget (Sect. 3.3); hence these are not included in Eq. (1) or in the global carbon budget tables or figures (with the exception of Fig. 2, where CDR is shown primarily for illustrative purposes).

The global CO_2 budget has been assessed by the Intergovernmental Panel on Climate Change (IPCC) in all assessment reports (Prentice et al., 2001; Schimel et al., 1995; Watson et al., 1990; Denman et al., 2007; Ciais et al., 2013; Canadell et al., 2021) and by others (e.g. Ballantyne et al., 2012). The Global Carbon Project (GCP; https://www.globalcarbonproject.org/, last access: 21 January 2025) has coordinated this cooperative community effort for the annual publication of global carbon budgets for the year 2005 (Raupach et al., 2007; including fossil emissions only), year 2006 (Canadell et al., 2007), year 2007 (GCP, 2007), year 2008 (Le Quéré et al., 2009), year 2009 (Friedlingstein et al., 2010), year 2010 (Peters et al., 2012), year 2012 (Le Quéré et al., 2013; Peters et al., 2013), year 2013 (Le Quéré et al., 2014), year 2014 (Le Quéré et al., 2015a; Friedlingstein et al., 2014), year 2015 (Jackson et al., 2016; Le Quéré et al., 2015b), year 2016 (Le Quéré et al., 2016), year 2017 (Le Quéré et al., 2018a; Peters et al., 2017a), year 2018

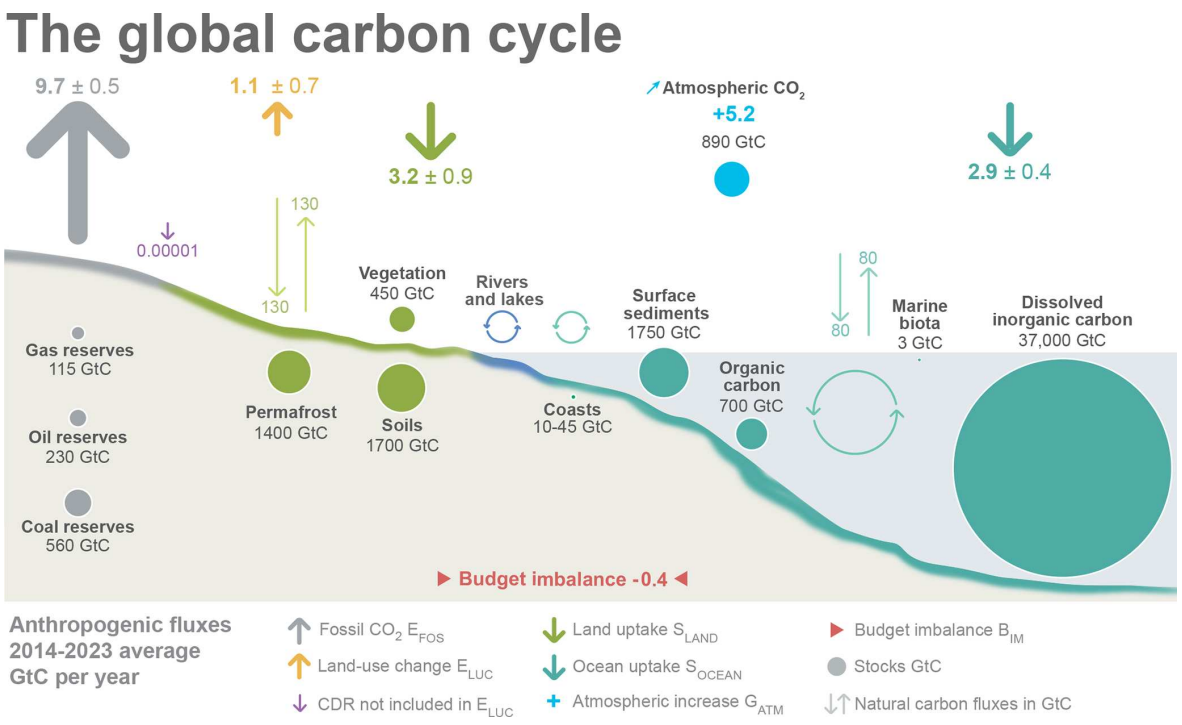

Figure 2. Schematic representation of the overall perturbation of the global carbon cycle caused by anthropogenic activities, averaged globally for the decade 2014–2023. See legend for the corresponding arrows. Flux estimates and their 1 standard deviation uncertainty are as reported in Table 7. The CDR estimate is for the year 2023 only. The uncertainty in the atmospheric CO_2 growth rate is very small ($\pm 0.02\,GtC\,yr^{-1}$) and is neglected for the figure. The anthropogenic perturbation occurs on top of an active carbon cycle, with fluxes and stocks represented in the background and taken from Canadell et al. (2021) for all numbers, except for the carbon stocks in coasts, which is from a literature review of coastal marine sediments (Price and Warren, 2016). Fluxes are in gigatonnes of carbon per year ($GtC\,yr^{-1}$) and reservoirs in gigatonnes of carbon (GtC). This figure was produced by Nigel Hawtin.

Table 1. Factors used to convert carbon in various units (by convention, unit 1 = unit 2 × conversion).

Unit 1	Unit 2	Conversion	Source
GtC (gigatonnes of carbon)	ppm (parts per million)[a]	2.124[b]	Ballantyne et al. (2012)
GtC (gigatonnes of carbon)	PgC (petagrams of carbon)	1	SI unit conversion
$GtCO_2$ (gigatonnes of carbon dioxide)	GtC (gigatonnes of carbon)	3.664	44.01/12.011 in mass equivalent

[a] Measurements of atmospheric CO_2 concentration have units of dry-air mole fraction; "ppm" is an abbreviation for micromoles per mole, dry air. [b] The use of a factor of 2.124 assumes that all the atmosphere is well mixed within 1 year. In reality, only the troposphere is well mixed and the growth rate of CO_2 concentration in the less well mixed stratosphere is not measured by sites from the NOAA network. Using a factor of 2.124 gives an approximation that the growth rate of CO_2 concentration in the stratosphere equals that of the troposphere on a yearly basis.

(Le Quéré et al., 2018b; Jackson et al., 2018), year 2019 (Friedlingstein et al., 2019; Jackson et al., 2019; Peters et al., 2020), year 2020 (Friedlingstein et al., 2020; Le Quéré et al., 2021), year 2021 (Friedlingstein et al., 2022a; Jackson et al., 2022), year 2022 (Friedlingstein et al., 2022b), and most recently year 2023 (Friedlingstein et al., 2023). Each of these papers updated previous estimates with the latest available information for the entire time series.

We adopt a range of ± 1 standard deviation (σ) to report the uncertainties in our global estimates, representing a likelihood of 68 % that the true value will be within the provided range if the errors have a Gaussian distribution, and no bias is assumed. This choice reflects the difficulty of characterizing the uncertainty in the CO_2 fluxes between the atmosphere and the ocean and land reservoirs individually, particularly on an annual basis, as well as the difficulty of updating the CO_2 emissions from land-use change. A likelihood of 68 % provides an indication of our current capability to quantify each term and its uncertainty given the available information. The uncertainties reported here combine statistical analysis of the underlying data, assessments of uncertainties in the generation of the datasets, and expert judgement of the likelihood of results lying outside this range. The limitations of current information are discussed in the paper and have

been examined in detail elsewhere (Ballantyne et al., 2015; Zscheischler et al., 2017). We also use a qualitative assessment of the confidence level to characterize the annual estimates from each term based on the type, quantity, quality, and consistency of the different lines of evidence as defined by the IPCC (Stocker et al., 2013).

This paper provides a detailed description of the datasets and methodology used to compute the global carbon budget estimates for the industrial period, from 1750 to 2024, and goes into more detail for the period since 1959. This paper is updated every year using the format of "living data" to keep a record of budget versions and the changes in new data, revision of data, and changes in methodology that lead to changes in estimates of the carbon budget. Additional materials associated with the release of each new version will be posted at the Global Carbon Project (GCP) website (https://www.globalcarbonproject.org/carbonbudget, last access: 21 January 2025), with fossil fuel emissions also available through the Global Carbon Atlas (https://www.globalcarbonatlas.org, last access: 21 January 2025). All underlying data used to produce the budget can also be found at https://globalcarbonbudget.org/ (last access: 21 January 2025). With this approach, we aim to provide the highest transparency and traceability in the reporting of CO_2, the key driver of climate change.

2 Methods

Multiple organizations and research groups around the world have generated the original measurements and data used to complete the global carbon budget. The effort presented here is thus mainly one of synthesis, where results from individual groups are collated, analysed, and evaluated for consistency. We facilitate access to original data with the understanding that primary datasets will be referenced in future work (see Table 2 for how to cite the datasets and the "Data availability" section). Descriptions of the measurements, models, and methodologies follow below, with more detailed descriptions of each component provided in the Supplement (Sects. S1 to S5).

This is the 19th version of the global carbon budget and the 13th revised version in the format of a living-data update in *Earth System Science Data*. It builds on the latest published global carbon budget of Friedlingstein et al. (2023). The main changes this year are the inclusion of (1) data to the year 2023 and a projection for the global carbon budget for the year 2024 and (2) an estimate of the 2024 projection of fossil emissions from Carbon Monitor. Other methodological differences between recent annual carbon budgets (2020 to 2024) are summarized in Table 3, and previous changes since 2006 are provided in Table S9.

2.1 Fossil CO_2 emissions (E_{FOS})

2.1.1 Historical period 1850–2023

The estimates of global and national fossil CO_2 emissions (E_{FOS}) include the oxidation of fossil fuels through both combustion (e.g. transport, heating) and chemical oxidation (e.g. carbon anode decomposition in aluminium refining) activities and the decomposition of carbonates in industrial processes (e.g. the production of cement). We also include CO_2 uptake from the cement carbonation process. Several emissions sources are not estimated or not fully covered: coverage of emissions from lime production are not global, and decomposition of carbonates in glass and ceramic production is included only for the "Annex I" countries of the United Nations Framework Convention on Climate Change (UNFCCC) for lack of activity data. These omissions are considered to be minor. Short-cycle carbon emissions – for example from combustion of biomass – are not included here but are accounted for in the CO_2 emissions from land use (see Sect. 2.2).

Our estimates of fossil CO_2 emissions rely on data collection by many other parties. Our goal is to produce the best estimate of this flux, and we therefore use a prioritization framework to combine data from different sources that have used different methods while being careful to avoid double counting and undercounting of emissions sources. The CDIAC-FF emissions dataset, derived largely from UN energy data, forms the foundation, and we extend emissions to 2023 using energy growth rates reported by the Energy Institute (a dataset formerly produced by BP). We then proceed to replace estimates using data from what we consider to be superior sources, for example Annex I countries' official submissions to the UNFCCC. All data points, not just those of the latest year, are potentially subject to revision. For full details see Andrew and Peters (2024).

Other estimates of global fossil CO_2 emissions exist, and these are compared by Andrew (2020a). The most common reason for differences in estimates of global fossil CO_2 emissions is a difference in which emissions sources are included in the datasets. Datasets such as those published by the Energy Institute, the US Energy Information Administration, and the International Energy Agency's "CO_2 emissions from fuel combustion" are all generally limited to emissions from combustion of fossil fuels. In contrast, datasets such as PRIMAP-hist, CEDS, EDGAR, and that of GCP aim to include all sources of fossil CO_2 emissions. See Andrew (2020a) for detailed comparisons and discussion.

Cement absorbs CO_2 from the atmosphere over its lifetime, a process known as "cement carbonation". We estimate this CO_2 sink, from 1931 onwards, as the average of two studies in the literature (Cao et al., 2020; Guo et al., 2021). Both studies use the same model, developed by Xi et al. (2016), with different parameterizations and input data, with the estimate of Guo and colleagues being a revision of

Table 2. How to cite the individual components of the global carbon budget presented here.

Component	Primary reference
Global fossil CO_2 emissions (E_{FOS}), total and by fuel type	Andrew and Peters (2024)
National territorial fossil CO_2 emissions (E_{FOS})	Hefner and Marland (2023), UNFCCC (2022)
National consumption-based fossil CO_2 emissions (E_{FOS}) by country (consumption)	Peters et al. (2011) updated as described in this paper
Net land-use change flux (E_{LUC})	This paper (see Table 4 for individual model references)
Growth rate in atmospheric CO_2 concentration (G_{ATM})	Lan et al. (2024)
Ocean and land CO_2 sinks (S_{OCEAN} and S_{LAND})	This paper (see Table 4 for individual model and data product references)

that of Xi et al. (2016). The trends of the two studies are very similar. Since carbonation is a function of both current and previous cement production, we extend these estimates to 2023 using the growth rate derived from the smoothed cement emissions (10-year smoothing) fitted to the carbonation data. In the present budget, we always include the cement carbonation carbon sink in the fossil CO_2 emission component (E_{FOS}).

We use the Kaya identity for a simple decomposition of CO_2 emissions into the key drivers (Raupach et al., 2007). While there are variations (Peters et al., 2017a), we focus here on a decomposition of CO_2 emissions into population, GDP per person, energy use per GDP, and CO_2 emissions per energy unit. Multiplying these individual components together returns the CO_2 emissions. Using the decomposition, it is possible to attribute the change in CO_2 emissions to the change in each of the drivers. This method gives a first-order understanding of what causes CO_2 emissions to change each year.

2.1.2 Year 2024 projection

We provide a projection of global fossil CO_2 emissions in 2024 by combining separate projections for China, the USA, the European Union (EU), India, and all other countries combined. The methods are different for each of these. For China we combine monthly fossil fuel production data from the National Bureau of Statistics and trade data from the customs administration, giving us partial data for the growth rates to date of natural gas, petroleum, and cement and of the apparent consumption itself for raw coal. We then use a regression model to project full-year emissions based on historical observations. For the USA our projection is taken directly from the Energy Information Administration (EIA) Short-Term Energy Outlook (EIA, 2024), combined with the year-to-date growth rate of cement clinker production. For the EU we use monthly energy data from Eurostat to derive estimates of monthly CO_2 emissions, with coal emissions extended using a statistical relationship with reported electricity generation from coal and other factors. For natural gas, preliminary observations are available through December. EU emissions from oil are derived using the EIA's projection of oil consumption for Europe. EU cement emissions are based on available year-to-date data from three of the largest producers, Germany, Poland, and Spain. India's projected emissions are derived from monthly estimates using the methods of Andrew (2020b) and are extrapolated through December assuming seasonal patterns from before 2019. Emissions from international transportation (bunkers) are estimated separately for aviation and shipping. Changes in aviation emissions are derived primarily from Organisation for Economic Co-operation and Development (OECD) monthly estimates, extrapolated using the growth rates of global flight miles from Airportia, and then the final months are projected assuming normal patterns from previous years. Changes in shipping emissions are derived from OECD monthly estimates for global shipping. Emissions for the rest of the world are derived for coal and cement using projected growth in economic production from the IMF (2024) combined with extrapolated changes in emissions intensity of economic production, for oil using a global constraint from the EIA, and for natural gas using a global constraint from the International Energy Agency (IEA). More details on the E_{FOS} methodology and its 2024 projection can be found in the Supplement, Sect. S1.

For the first time this year, we cross-check our 2024 projection with a 2024 projection from Carbon Monitor. Carbon Monitor is an open-access dataset (https://carbonmonitor.org/, last access: 21 January 2025) of daily emissions constructed using hourly to daily proxy data (e.g. electricity consumption, travel patterns) instead of energy use data. Available Carbon Monitor estimated emissions from January to November are combined into a new projection for December to give a full-year 2024 estimate. The December projections are estimated by leveraging seasonal patterns from 2019–2023 daily CO_2 emissions data from Carbon Monitor. A regression model is applied separately for individual countries to obtain their respective forecast. First, the season-

Table 3. The main methodological changes in the global carbon budget since 2020. Methodological changes introduced in one year are kept for the following years unless noted. Empty cells mean there were no methodological changes introduced that year. LUC denotes land-use change; DGVM denotes dynamic global vegetation model; GHG denotes greenhouse gas; NH and SH denote the Northern Hemisphere and Southern Hemisphere, respectively; GOBM denotes global ocean biogeochemistry model. Table S9 lists methodological changes from the first global carbon budget publication up to 2019.

Year (and publication)	Fossil fuel emissions		LUC emissions	Reservoirs			Other changes
	Global	Country (territorial)		Atmosphere	Ocean	Land	
2020 Friedlingstein et al. (2020) GCB2020	Cement carbonation now included in the E_{FOS} estimate, reducing E_{FOS} by about 0.2 GtC yr^{-1} for the last decade	India's emissions from Andrew (2020b); corrections to Netherlands Antilles and Aruba and Soviet emissions before 1950 as per Andrew (2020a); China's coal emissions in 2019 derived from official statistics, emissions now shown for EU27 instead of EU28; projection for 2020 based on assessment of four approaches	Average of three bookkeeping models; use of 17 DGVMs; estimate of gross land-use sources and sinks provided	Use of six atmospheric inversions	Based on nine models; river flux revised and partitioned into NH, the tropics, and SH	Based on 17 models	
2021 Friedlingstein et al. (2022a) GCB2021	Projections no longer an assessment of four approaches	Official data included for a number of additional countries; new estimates for South Korea; added emissions from lime production in China	E_{LUC} estimate compared to the estimates adopted in national GHG inventories		Average of means of eight models and means of seven data products; current-year prediction of S_{OCEAN} using a feed-forward neural network method	Current-year prediction of S_{LAND} using a feed-forward neural network method	
2022 Friedlingstein et al. (2022b) GCB2022			E_{LUC} provided at country level; revised component decomposition of E_{LUC} fluxes; revision of LUC maps for Brazil; new datasets for peat drainage	Use of nine atmospheric inversions	Average of means of 10 models and means of 7 data products	Based on 16 models; revision of LUC maps for Brazil	

Table 3. Continued.

Year (and publication)	Fossil fuel emissions		LUC emissions	Reservoirs			Other changes
	Global	Country (territorial)		Atmosphere	Ocean	Land	
2023			Refined component decomposition of E_{LUC}; revision of LUC maps for Indonesia; use of updated peat drainage estimates	Use of 14 atmospheric inversions; additional use of four Earth system models to estimate current-year CO_2	Additional use of four Earth system models and an atmospheric oxygen method to assess S_{OCEAN}; regional distribution of river flux adjustment revised	Based on 20 models; additional use of four Earth system models and an atmospheric oxygen method to assess the net atmosphere–land flux	Inclusion of an estimate of carbon dioxide removal
Friedlingstein et al. (2023) GCB2023							
2024	Inclusion of 2024 projections from Carbon Monitor	Inclusion of 2024 projections from Carbon Monitor for China, the USA, EU27, India, and the rest of the world	Fourth bookkeeping estimate (LUCE); update of land-use data (HYDE 3.4) including revision of LUC maps for China; updated definition of forest (re)growth fluxes (consistent with second State of CDR report)	Use of 14 atmospheric inversion models	Use of 10 GOBMs and 8 fCO_2 products; added evaluation for fCO_2 products	Use of 20 DGVMs	
This study							

ality component for each month is assessed based on daily average emissions from 2019 to 2023, excluding 2020 due to the COVID-19 pandemic. Then a linear regression model is constructed using the calculated seasonal components and the daily average emissions for the months from January to November 2024. The resulting model is used to project carbon emissions for December 2024. The uncertainty range is calculated using historical monthly variance of seasonal components.

2.2 CO_2 emissions from land-use, land-use change, and forestry (E_{LUC})

2.2.1 Historical period 1850–2023

The net CO_2 flux from land-use, land-use change, and forestry (E_{LUC}, called land-use change emissions in the rest of the text) includes CO_2 fluxes from deforestation, afforestation, logging and forest degradation (including harvest activity), shifting cultivation (cycle of cutting forest for agriculture and then abandoning), regrowth of forests (following wood harvest or agriculture abandonment), peat burning, and peat drainage.

Four bookkeeping approaches were used to quantify gross emissions and gross removals and the resulting net E_{LUC}: the updated estimates for each of BLUE (Hansis et al., 2015), OSCAR (Gasser et al., 2020), and H&C2023 (Houghton and Castanho, 2023) and the new estimates of LUCE (Qin et al., 2024). Emissions from peat burning and peat drainage are added from external datasets (see the Supplement, Sect. S2.1): peat fire emissions from the Global Fire Emissions Database (GFED4.1s; van der Werf et al., 2017) and peat drainage emissions averaged from estimates of the Food and Agriculture Organization (Conchedda and Tubiello, 2020; FAO, 2023a, b) and from simulations with the dynamic global vegetation model (DGVM) ORCHIDEE-PEAT (Qiu et al., 2021) and the DGVM LPX-Bern (Lienert and Joos, 2018; Müller and Joos, 2021). Uncertainty estimates were derived from the DGVM ensemble for the time period prior to 1960, and for the recent decades an uncertainty range of $\pm 0.7\,GtC\,yr^{-1}$ was used, which is a semi-quantitative measure for annual and decadal emissions and reflects our best value judgement that there is at least a 68 % chance ($\pm 1\sigma$) that the true land-use change emission lies within the given range for the range of processes considered here.

The GCB E_{LUC} estimates follow the CO_2 flux definition of global carbon cycle models and differ from IPCC definitions adopted in national greenhouse gas inventories (NGHGIs) for reporting under the UNFCCC. The latter typically include terrestrial fluxes occurring on all land that countries define as managed, following the IPCC managed-land proxy approach (Grassi et al., 2018). This partly includes fluxes due to environmental change (e.g. atmospheric CO_2 increase), which are part of S_{LAND} in our definition. As a result, global emissions estimates are smaller for NGHGIs than for the global carbon budget definition (Grassi et al., 2023). The same is the case for the FAO estimates of carbon fluxes on forest land, which include both anthropogenic and natural fluxes on managed land (Tubiello et al., 2021). We map the GCB and NGHGI definitions onto each other to provide a comparison of the anthropogenic carbon budget as reported in the GCB to the official country reporting to the UNFCCC convention. We further compare these estimates with the net atmosphere-to-land flux from atmospheric inversion systems (see Sect. 2.7), averaged over managed land only.

E_{LUC} contains a range of fluxes that are related to carbon dioxide removal (CDR). CDR is defined as the set of anthropogenic activities that remove CO_2 from the atmosphere, in addition to the Earth's natural processes (such as carbon uptake in response to atmospheric CO_2 increase), and store it in durable form, such as in forest biomass, soils, long-lived products, the ocean, or geological reservoirs. Here, we quantify vegetation-based CDR that is implicitly or explicitly captured by land-use fluxes (CDR not based on vegetation is discussed in Sect. 2.3). We quantify re-/afforestation from the four bookkeeping estimates by separating forest regrowth into shifting cultivation cycles from permanent increases in forest cover (see the Supplement, Sect. S2.1). The latter count as CDR, but it should be noted that the permanence of the storage under climate risks such as fire is increasingly questioned. Other CDR activities related to land use but not fully accounted for in our E_{LUC} estimate include the transfer of carbon to harvested wood products (HWPs), bioenergy with carbon capture and storage (BECCS), and biochar production (Babiker et al., 2022; Smith et al., 2024). The different bookkeeping models all represent HWPs but with varying details concerning product usage and their lifetimes. BECCS and biochar are currently only represented in bookkeeping and TRENDY models with regard to the CO_2 removal through photosynthesis, without accounting for the durable storage. HWPs, BECCS, and biochar are typically counted as CDR once the transfer to the durable storage site occurs and not when the CO_2 is removed from the atmosphere, which complicates a direct comparison to the GCB approach to quantify annual fluxes to and from the atmosphere. We provide estimates for CDR through HWPs, BECCS, and biochar based on independent studies in Sect. 3.2.2, but we do not add them to our E_{LUC} estimate to avoid potential double counting that arises from the partial consideration of HWPs, BECCS, and biochar in the bookkeeping and TRENDY models and to avoid inconsistencies from the temporal discrepancy between transfer to storage and removal from the atmosphere.

2.2.2 Year 2024 projection

We project the 2024 land-use emissions for BLUE, H&C2023, OSCAR, and LUCE based on their E_{LUC} estimates for 2023 and on adding the change in carbon emissions from peat fires and tropical deforestation and degradation fires (2024 emissions relative to 2023 emissions) estimated using active fire data (MCD14ML; Giglio et al., 2016). Peat drainage is assumed to be unaltered as it has low interannual variability. More details on the E_{LUC} methodology can be found in the Supplement, Sect. S2.

2.3 Carbon dioxide removal (CDR) not based on vegetation

While some CDR involves CO_2 fluxes via land use and is included in our estimate of E_{LUC} (re-/afforestation) or provided from other data sources (biochar, HWPs, and BECCS), other CDR occurs through fluxes of CO_2 directly from the air to the geosphere. The majority of this derives from enhanced weathering through the application of crushed rock to soils, with a smaller contribution from direct air carbon capture and storage (DACCS). We use data from the State of CDR report (Smith et al., 2024), which compiles and harmonizes reported removal rates from a combination of existing databases, surveys, and novel research. Currently there are no internationally agreed methods for reporting these CDR types, meaning estimates are based on self-disclosure by projects following their own protocols. As such, the fractional uncertainty in these numbers should be viewed as substantial, and they are liable to change in future years as protocols are harmonized and improved.

2.4 Growth rate in atmospheric CO_2 concentration (G_{ATM})

2.4.1 Historical period 1850–2023

The rate of growth of the atmospheric CO_2 concentration is provided for the years 1959–2023 by the US National Oceanic and Atmospheric Administration Global Monitoring Laboratory (NOAA/GML; Lan et al., 2024), which includes recent revisions to the calibration scale of atmospheric CO_2 measurements (WMO CO_2 X2019; Hall et al., 2021). For the 1959–1979 period, the global growth rate is based on measurements of atmospheric CO_2 concentration averaged from the Mauna Loa and South Pole stations, as observed by the CO_2 Program at Scripps Institution of Oceanography (Keeling et al., 1976). For the 1980–2021 time period, the global growth rate is based on the average of multiple stations selected from the marine boundary layer sites with well-mixed background air (Lan et al., 2023) after fitting a smooth curve

through the data for each station as a function of time and averaging by latitude band (Masarie and Tans, 1995). The annual growth rate is estimated by Lan et al. (2024) from atmospheric CO_2 concentration by taking the average of the most recent December–January months corrected for the average seasonal cycle and subtracting this same average 1 year earlier. The growth rate in units of ppm yr^{-1} is converted to units of GtC yr^{-1} by multiplying by a factor of 2.124 GtC ppm^{-1}, assuming instantaneous mixing of CO_2 throughout the atmosphere (Ballantyne et al., 2012; Table 1).

The uncertainty around the atmospheric growth rate is due to three main factors. The first uncertainty is related to the network composition of the marine boundary layer sites with some sites coming or going, gaps in the time series at each site, etc. This uncertainty was estimated with a bootstrap method by constructing 100 "alternative" networks (Steele et al., 1992; Masarie and Tans, 1995; Lan et al., 2024). The second uncertainty is the analytical uncertainty that describes the short- and long-term uncertainties associated with the CO_2 analysers. A Monte Carlo method was used to estimate the total analytical uncertainty by randomly selecting errors to add to each observation from a normal distribution of combined short- and long-term uncertainties. Prior to the 1980s when analysers were less precise and the CO_2 measurement scale was slightly less well defined, larger analytical errors were assigned to account for these factors. However, the network uncertainty remains the larger term of uncertainty. The first and second uncertainties are reported as 1σ standard deviations (i.e. 68 % confidence interval) and are summed in quadrature to determine the global surface growth rate uncertainty, which averaged to 0.085 ppm. The third uncertainty is the uncertainty associated with using the average CO_2 concentration from a surface network to approximate the true atmospheric average CO_2 concentration (mass-weighted, in three dimensions) as needed to assess the total atmospheric CO_2 burden. In reality, CO_2 variations measured at the stations will not exactly track the changes in total atmospheric burden, with offsets in magnitude and phasing due to vertical and horizontal mixing. This effect must be very small on decadal and longer timescales, when the atmosphere can be considered well mixed. The long-term CO_2 increase in the stratosphere lags the increase (meaning lower concentrations) that we observe in the marine boundary layer, while the continental boundary layer (where most of the emissions take place) leads the marine boundary layer with higher concentrations. These effects nearly cancel each other out. In addition, the growth rate is nearly the same everywhere (Ballantyne et al., 2012). We therefore maintain an uncertainty around the annual growth rate based on the multiple-station dataset ranges between 0.11 and 0.72 GtC yr^{-1}, with a mean of 0.61 GtC yr^{-1} for 1959–1979 and 0.17 GtC yr^{-1} for 1980–2023, when more measurement sites were available (Lan et al., 2024). We estimate the uncertainty in the decadally averaged growth rate after 1980 at 0.02 GtC yr^{-1} based on the annual growth rate uncertainty but stretched over a 10-year interval. For years prior to 1980, we estimate the decadally averaged uncertainty to be 0.07 GtC yr^{-1} based on a factor proportional to the annual uncertainty prior to and after 1980 ($0.02 \times (0.61/0.17)$ GtC yr^{-1}).

We assign a high confidence to the annual estimates of G_{ATM} because they are based on direct measurements from stations distributed around the world (Lan et al., 2023) with all CO_2 measurements consistently measured against the same CO_2 standard scale (WMO CO_2 X2019) defined by a suite of gas standards (Hall et al., 2021).

To estimate the total carbon accumulated in the atmosphere since 1750 and 1850, we use an atmospheric CO_2 concentration of 278.3 ± 3 ppm and 285.1 ± 3 ppm, respectively (Gulev et al., 2021). For the construction of the cumulative budget shown in Fig. 3, we use the fitted estimates of CO_2 concentration from Joos and Spahni (2008) and the conversion factors shown in Table 1 to estimate the annual atmospheric growth rate. The uncertainty of ± 3 ppm (converted into $\pm 1\sigma$) is taken directly from the IPCC's AR5 (Ciais et al., 2013). Typical uncertainties in the growth rate in atmospheric CO_2 concentration from ice core data are equivalent to ± 0.1–0.15 GtC yr^{-1}, as evaluated from the Law Dome data (Etheridge et al., 1996) for individual 20-year intervals over the period from 1850 to 1960 (Bruno and Joos, 1997).

2.4.2 Year 2024 projection

We provide an assessment of G_{ATM} for 2024 as the average of two methods. The GCB regression method models monthly global-average atmospheric CO_2 concentrations and derives the increment and annual average from these. The model uses lagged observations of concentration (Lan et al., 2024): both a 12-month lag and the lowest lag that will allow the model prediction to produce an estimate for the following January, recalling that the G_{ATM} increment is derived from December–January pairs. The largest driver of interannual changes is the El Niño–Southern Oscillation (ENSO) signal (Betts et al., 2016), so the monthly Niño 3.4 index (Huang et al., 2017) is included in the model. Given the natural lag between sea-surface temperatures and effects on the biosphere and in turn effects on globally mixed atmospheric CO_2 concentration, a lagged ENSO index is used, and we use both a 5-month and a 6-month lag. The combination of the two lagged ENSO values helps reduce possible effects of noise in a single month. To help characterize the seasonal variation, we add "month" as a categorical variable. Finally, we flag the period affected by the Pinatubo eruption (August 1991–November 1993) as a categorical variable. Note that while emissions of CO_2 are the largest driver of the trend in atmospheric CO_2 concentration, our goal here is to predict divergence from that trend. Because changes in emissions from year to year are relatively minor in comparison to total emissions, this has little effect on the variation in concentration from the trend line. Even the relatively large drop in emis-

sions in 2020 due to the COVID-19 pandemic does not cause any problems for the model.

We also use the multi-model mean and uncertainty in the 2024 G_{ATM} estimated by the ESM prediction system (see Sect. 2.9). We then take the average of the GCB regression and ESM G_{ATM} estimates, with their respective uncertainty combined quadratically.

Similarly, the projection of the 2024 global-average CO_2 concentration (in ppm) is calculated as the average of the estimates from the two methods. For the GCB regression method, it is the annual average of global concentration over the 12 months of 2024; for the ESMs, it is the observed global-average CO_2 concentration for 2023 and the annual increase in 2024 of the global-average CO_2 concentration predicted by the ESM multi-model mean.

2.5 Ocean CO_2 sink

2.5.1 Historical period 1850–2023

The reported estimate of the global ocean anthropogenic CO_2 sink S_{OCEAN} is derived as the average of two estimates. The first estimate is derived as the mean over an ensemble of 10 global ocean biogeochemistry models (GOBMs; Tables 4 and S2). The second estimate is obtained as the mean over an ensemble of eight surface ocean fCO_2 observation-based data products (fCO_2 is the fugacity of CO_2; Tables 4 and S3). A ninth fCO_2 product (UExP-FFN-U) is shown but is not included in the ensemble average as it differs from the other products by adjusting the flux to a cool, salty ocean surface skin. In previous editions of the GCB, this product was obtained following the Watson et al. (2020) method, but it has been updated following the method of Dong et al. (2022; see the Supplement, Sect. S3.1, for a discussion). The GOBMs simulate both the natural and the anthropogenic CO_2 cycles in the ocean. They constrain the anthropogenic air–sea CO_2 flux (the dominant component of S_{OCEAN}) by the transport of carbon into the ocean interior, which is also the controlling factor of present-day ocean carbon uptake in the real world. They cover the full globe and all seasons and were evaluated against surface ocean carbon observations, suggesting they are suitable for estimating the annual ocean carbon sink (Hauck et al., 2020). The fCO_2 products are tightly linked to observations of fCO_2 (fugacity of CO_2, which equals pCO_2 corrected for the non-ideal behaviour of the gas; Pfeil et al., 2013), which carry imprints of temporal and spatial variability but are also sensitive to uncertainties in gas-exchange parameterizations and data sparsity (Fay et al., 2021; Gloege et al., 2021; Hauck et al., 2023a). Their advantage is the assessment of the mean spatial pattern of variability and its seasonality (Hauck et al., 2020; Gloege et al., 2021; Hauck et al., 2023a). To benchmark trends derived from the fCO_2 products, we additionally performed a model subsampling exercise following Hauck et al. (2023a; see Sect. S3). In addition, two diagnostic ocean models are used to estimate S_{OCEAN} over the industrial era (1781–1958).

The global fCO_2-based flux estimates were adjusted to remove the pre-industrial ocean source of CO_2 to the atmosphere of $0.65 \pm 0.3\,GtC\,yr^{-1}$ from river input to the ocean (Regnier et al., 2022) in order to satisfy our definition of S_{OCEAN} (Hauck et al., 2020). The river flux adjustment was distributed over the latitudinal bands using the regional distribution of Lacroix et al. (2020; north: $0.14\,GtC\,yr^{-1}$; tropics: $0.42\,GtC\,yr^{-1}$; south: $0.09\,GtC\,yr^{-1}$). Acknowledging that this distribution is based on only one model, the advantage is that a gridded field is available, and the river flux adjustment can be calculated for the three latitudinal bands and the RECCAP (REgional Carbon Cycle Assessment and Processes) regions (RECCAP-2; Ciais et al., 2022; Poulter et al., 2022; DeVries et al., 2023). This dataset suggests that more of the riverine outgassing is located in the tropics than in the Southern Ocean and is thus opposed to the previously used dataset of Aumont et al. (2001). Accordingly, the regional distribution is associated with a major uncertainty in addition to the large uncertainty around the global estimate (Crisp et al., 2022; Gruber et al., 2023). Anthropogenic perturbations of river carbon and nutrient transport to the ocean are not considered (see Sects. 2.10 and S6.3).

We derive S_{OCEAN} from GOBMs using a simulation (sim A) with historical forcing of climate and atmospheric CO_2 from the GCB (Sect. 2.4), accounting for model biases and drift from a control simulation (sim B) with constant atmospheric CO_2 and normal-year climate forcing. A third simulation (sim C) with historical atmospheric CO_2 increase and normal-year climate forcing is used to attribute the ocean sink to CO_2 (sim C minus sim B) and climate (sim A minus sim C) effects. A fourth simulation (sim D; historical climate forcing and constant atmospheric CO_2) is used to compare the change in the anthropogenic carbon inventory in the interior ocean (sim A minus sim D) to the observational estimate of Gruber et al. (2019) with the same flux components (steady-state and non-steady-state anthropogenic carbon flux). The fCO_2 products are adjusted with respect to their original publications to represent the full ice-free ocean area, including coastal zones and marginal seas, when the area coverage is below 99 %. This is done by either area filling following Fay et al. (2021) or a simple scaling approach. GOBMs and fCO_2 products fall within the observational constraints over the 1990s ($2.2 \pm 0.7\,GtC\,yr^{-1}$; Ciais et al., 2013) before and after applying adjustments.

S_{OCEAN} is calculated as the average of the GOBM ensemble mean and the fCO_2-product ensemble mean from 1990 onwards. Prior to 1990, it is calculated as the GOBM ensemble mean and half of the offset between GOBM and fCO_2-product ensemble means over 1990–2001.

We assign an uncertainty of $\pm 0.4\,GtC\,yr^{-1}$ to the ocean sink based on a combination of random (ensemble standard deviation) and systematic uncertainties (GOBM bias in anthropogenic carbon accumulation, previously reported uncer-

Table 4. References for the process models, bookkeeping models, ocean data products, and atmospheric inversions. All models and products are updated with new data to the end of the year 2023.

Model/data name	Reference	Change from Global Carbon Budget 2023 (Friedlingstein et al., 2023)
Bookkeeping models for land-use change emissions		
BLUE	Hansis et al. (2015)	No change to model but simulations performed with LUH2-GCB2024 forcing; update in added peat drainage emissions
H&C2023	Houghton and Castanho (2023)	No change to model; data for years after last modelled year (2020) extrapolated based on anomalies in deforestation fires from GFED; update in added peat drainage emissions
OSCAR	Gasser et al. (2020)	No change to model but land-use forcing changed to LUH2-GCB2024 and FRA2020 extrapolated to 2023; constraining based on GCB2023 data for S_{LAND} over 1960–2022; update in added peat drainage emissions
LUCE	Qin et al. (2024)	New model in GCB2024
Dynamic global vegetation models		
CABLE-POP	Haverd et al. (2018)	Bug fix applied to land-use change calculations enabling variable crop and pasture fractions; corrections to the pre-industrial primary forest fraction in Europe; minor parameter changes
CLASSIC	Melton et al. (2020), Asaadi et al. (2018)	Permeable soil depth reduced to 4 m; 15 soil layers in the top 4 m of permeable soil and 5 bed rock layers from 4 to 62 m; saturated hydraulic conductivity decrease with depth in the permeable soil layers; transpiration from partially wet canopy leaves; better runoff seasonality and more realistic partitioning of precipitation into runoff and evapotranspiration
CLM6.0	Lawrence et al. (2019)	Updates to surface datasets; improvement of roughness length calculation; updates to snow optical properties and snow thermal conductivity; improved excess ice; improved simulation of burial of vegetation by snow; urban updates, including transient urban, urban properties, and air conditioning; improvements to biomass heat storage; tillage and residue removal; crop phenology and planting dates; improvement to irrigation methods; plant functional type (PFT) parameter update
DLEM	Tian et al. (2015), You et al. (2022)	Incorporation of mechanistic representations of dynamic crop growth and development processes, such as crop-specific phenological development, carbon allocation, yield formation, and biological N fixation; agricultural management practices such as N fertilizer use, irrigation, tillage, manure application, dynamic crop rotation, cover cropping, and genetic improvements also included (You et al., 2022)
EDv3	Moorcroft et al. (2001), Ma et al. (2022)	Minor bug fixes; updated fire submodule
ELM	Yang et al. (2023), Burrows et al. (2020)	No change
IBIS	Xia et al. (2024)	Improved algorithm of leaf area index
iMAPLE	Yue et al. (2024)	The updated version of the YIBs model with dynamic coupling between carbon and water cycles
ISAM	Jain et al. (2013), Meiyappan et al. (2015), Shu et al. (2020)	Vertically resolved soil biogeochemistry (carbon and nitrogen) module, following Shu et al. (2020)
ISBA-CTRIP	Delire et al. (2020)	No change
JSBACH	Mauritsen et al. (2019), Reick et al. (2021)	Minor bug fixes in post-processing
JULES-ES	Wiltshire et al. (2021), Sellar et al. (2019), Burton et al. (2019)	Minor bug fixes. (Using JULES v7.4)
LPJ-GUESS	Smith et al. (2014)	No change
LPJmL	Schaphoff et al. (2018), von Bloh et al. (2018), Lutz et al. (2019) (tillage), Heinke et al. (2023) (livestock grazing)	No change
LPJ-wsl	Poulter et al. (2011)	Minor bug fixes; weighting of fire carbon by GFED to simulate annual cycle
LPX-Bern	Lienert and Joos (2018)	No change
OCN	Zaehle and Friend (2010), Zaehle et al. (2011)	No change

Table 4. Continued.

Model/data name	Reference	Change from Global Carbon Budget 2023 (Friedlingstein et al., 2023)
ORCHIDEEv3	Krinner et al. (2005), Zaehle and Friend (2010), Vuichard et al. (2019)	No change
SDGVM	Woodward and Lomas (2004), Walker et al. (2017)	Parameter adjustment for the calculation of evapotranspiration; bug fix in model outputs; further development on gross land-use transitions and tracking of carbon fluxes from transitions
VISIT	Ito and Inatomi (2012), Kato et al. (2013)	No change
Intermediate-complexity land carbon cycle model		
CARDAMOM	Bloom et al. (2016), Smallman et al. (2021)	No change
Global ocean biogeochemistry models		
NEMO-PlankTOM12	Wright et al. (2021)	Minor bug fixes; change to salinity restoring and restart file; new atmospheric CO_2 input for simulations A and C
NEMO4.2-PISCES (IPSL)	Aumont et al. (2015)	Switch to the new model version NEMO4.2-PISCES; update following the new protocol (with 1750 pre-industrial CO_2 for spin-up); new atmospheric CO_2 input for simulations A and C
MICOM-HAMOCC (NorESM1-OCv1.2)	Schwinger et al. (2016)	No change in model set-up; new atmospheric CO_2 file for simulations A and C; corrected diagnostic output for pco2atm; diagnostic output for sfco2 and spco2 provided at the air–sea interface (not with respect to dry air at 1 atm)
MPIOM-HAMOCC6	Lacroix et al. (2021)	No change; only updated atmosphere CO_2 input for A and C experiments and run 1948–2023
NEMO3.6-PISCESv2-gas (CNRM)	Berthet et al. (2019), Séférian et al. (2019)	Updated simulations using 1750 pre-industrial conditions instead of 1850; no change to model configuration; new atmospheric CO_2 input for simulations A and C
FESOM2.1-REcoM3	Gürses et al. (2023)	Updated atmospheric CO_2 for simulations A and C
MOM6-COBALT (Princeton)	Liao et al. (2020)	No change
CESM-ETHZ	Doney et al. (2009)	Compared to the 2023 submission, the spin-up extended to 1422 years before 1750; also, starting at 1751, the new atmospheric CO_2 concentrations provided by the GCB used for simulations A and C
MRI-ESM2-3	Tsujino et al. (2024), Sakamoto et al. (2023)	Iron circulation and its limitation on primary production introduced; updated atmospheric CO_2 for simulations A and C
ACCESS (CSIRO)	Law et al. (2017)	No change in model set-up (since GCB2023); updated atmospheric CO_2 for simulations A and C
fCO_2 products		
VLIZ-SOMFFN (previously MPI-SOM-FFN)	Landschützer et al. (2016)	Time period 1982–2023; the estimate now for the full open-ocean and coastal domain as well as the Arctic Ocean extension by merging two mixed-layer depth (MLD) proxies for year-round full coverage; additionally, in the self-organizing map (SOM) step, the SeaFlux climatology now used
Jena-MLS	Rödenbeck et al. (2014) updated to Rödenbeck et al. (2022)	Time period extended to 2023
CMEMS-LSCE-FFNNv2	Chau et al. (2022)	Time period now 1985–2023
UExP-FNN-U (previously Watson et al., 2020)	Watson et al. (2020), Ford et al. (2024)	Updated CCI sea-surface temperature (SST) to v3 (Embury et al., 2024), with cool bias with respect to global drifter observations corrected following recommendations in Dong et al. (2022); updated SOM-FFN implementation to Python
NIES-ML3	Zeng et al. (2022)	Updated time period 1982–2023
JMA-MLR	Iida et al. (2021)	Time period extended to 2023
OceanSODA-ETHZv2	Gregor et al. (2024)	Updated method following Gregor et al. (2024) and time period extended to 2023

Table 4. Continued.

Model/data name	Reference	Change from Global Carbon Budget 2023 (Friedlingstein et al., 2023)
LDEO-HPD	Gloege et al. (2022), Bennington et al. (2022)	Time period extended to 2023
CSIR-ML6	Gregor et al. (2019)	Time period 1982–2023
Atmospheric inversions		
Jena CarboScope	Rödenbeck et al. (2018), Stephens et al. (2007)	Extension to end of year 2023; slight change in station set; In the NBE-T inversion, removal of the relaxation term and, instead, filtering out decadal variations from air temperature; adding an additive correction to the result of the NBE-T inversion to account for CO_2 flux interannual variation (IAV) not related to air temperature based on eight long atmospheric records available near continuously since at least 1976; TM3 driven by ERA5 rather than NCEP
CAMS	Chevallier et al. (2005), Remaud et al. (2018)	Extension to year 2023; increase in the 3D resolution with hexagonal prisms rather than rectangular parallelepipeds (3 times more 3D cells than the previous submission); update of the prior fluxes
CarbonTracker Europe (CTE)	van der Laan-Luijkx et al. (2017)	Extension to 2023; update of prior fluxes
NISMON-CO_2	Niwa et al. (2022, 2020)	Extension to 2023; update of prior fluxes
CT-NOAA	Jacobson et al. (2023a, b), Byrne et al. (2024b), Krol et al. (2005), Peiro et al. (2022)	Extended to 2023 using the CarbonTracker Near-Real Time release CT-NRT.v2024-1 (Jacobson et al., 2023b)
CMS-Flux	Liu et al. (2021)	Extension to 2023; update of prior fluxes
CAMS-FT24r1	Chevallier et al. (2005), Remaud et al. (2018)	Extension to year 2023; increase in the 3D resolution with hexagonal prisms rather than rectangular parallelepipeds (3 times more 3D cells than the previous submission); update of the prior fluxes
GONGGA	Jin et al. (2023), Nassar et al. (2010)	Extension to 2023; update of prior fluxes
COLA	Liu et al. (2022)	Extension to 2023; update of prior fluxes
GCASv2	Jiang et al. (2021), Emmons et al. (2010)	Extension to 2023; update of prior fluxes
UoE in situ	Feng et al. (2016), Palmer et al. (2019)	Extension to 2023; update of prior fluxes
IAPCAS	Yang et al. (2021), Feng et al. (2016)	Extension to 2023; update of prior fluxes
MIROC4-ACTM	Chandra et al. (2022), Patra et al. (2018)	Extension to 2023; update of prior fluxes using only CASA and not VISIT; fewer observation sites used in the assimilation (46 instead of 50)
NTFVAR	Nayagam et al. (2024), Maksyutov et al. (2021)	New this year
Earth system models		
CanESM5	Swart et al. (2019), Sospedra-Alfonso et al. (2021)	Reconstructions extended to 1960–2023; predictions extended to 2024
EC-Earth3-CC	Döscher et al. (2022), Bilbao et al. (2021), Bernardello et al. (2024)	New this year
IPSL-CM6A-CO_2-LR	Boucher et al. (2020)	Reconstructions extended to 1960–2023; predictions extended to 2024; no change to model; the CMIP6 CovidMIP CO_2 emissions after 2015 used
MIROC-ES2L	Watanabe et al. (2020)	Reconstructions extended to 1960–2023; predictions extended to 2024; no change to model; the simulations rerun including a long spin-up
MPI-ESM1-2-LR	Mauritsen et al. (2019), Li et al. (2023)	Reconstructions extended to 1960–2023; predictions extended to 2024

tainties in fCO_2 products; see the Supplement, Sect. S3.4). While this approach is consistent within the GCB, an independent uncertainty assessment of the fCO_2 products alone suggests a somewhat larger uncertainty of up to 0.7 GtC yr^{-1} (Ford et al., 2024). We assign a medium confidence level to the annual ocean CO_2 sink and its uncertainty because it is based on multiple lines of evidence, it is consistent with ocean interior carbon estimates (Gruber et al., 2019; see Sect. 3.6.5), and the interannual variability in the GOBMs and data-based estimates is largely consistent and can be explained by climate variability. We refrain from assigning a high confidence level because of the deviation between the GOBM and fCO_2-product trends between around 2002 and 2020. More details on the S_{OCEAN} methodology can be found in the Supplement, Sect. S3.

2.5.2 Year 2024 projection

The ocean CO_2 sink forecast for the year 2024 is based on (a) the historical (Lan et al., 2024) and our 2024 estimate of atmospheric CO_2 concentration, (b) the historical and our 2024 estimate of global fossil fuel emissions, and (c) the boreal spring (March, April, May) Oceanic Niño Index (ONI) (NCEP, 2024). Using a non-linear regression approach, i.e. a feed-forward neural network, atmospheric CO_2, ONI, and the fossil fuel emissions are used as training data to best match the annual ocean CO_2 sink (i.e. combined S_{OCEAN} estimate from GOBMs and data products) from 1959 through 2023 from this year's carbon budget. Using this relationship, the 2024 S_{OCEAN} can then be estimated from the projected 2024 input data using the non-linear relationship established during the network training. To avoid overfitting, the neural network training was done using a Monte Carlo approach, with a variable number of artificial neurons (varying between two and five), and 20 % of the randomly selected training data were withheld for independent internal testing.

Based on the best output performance (tested using the 20 % withheld input data), the best-performing number of neurons was selected. In a second step, we trained the network 10 times using the best number of neurons identified in step 1 and different sets of randomly selected training data. The mean of the 10 training runs is considered our best forecast, whereas the standard deviation of the 10 ensembles provides a first-order estimate of the forecast uncertainty. This uncertainty is then combined with the S_{OCEAN} uncertainty (0.4 GtC yr^{-1}) to estimate the overall uncertainty in the 2024 projection. As an additional line of evidence, we also assess the 2024 atmosphere–ocean carbon flux from the ESM prediction system (see Sect. 2.9).

2.6 Land CO_2 sink

2.6.1 Historical period 1850–2023

The terrestrial land sink (S_{LAND}) is thought to be due to the combined effects of rising atmospheric CO_2, increasing N inputs, and climate change on plant growth and terrestrial carbon storage. S_{LAND} does not include land sinks directly resulting from land-use and land-use change (e.g. regrowth of vegetation) as these are part of the land-use flux (E_{LUC}), although system boundaries make it difficult to exactly attribute CO_2 fluxes on land to S_{LAND} and E_{LUC} (Erb et al., 2013).

S_{LAND} is estimated from the multi-model mean of 20 DGVMs (Tables 4 and S1). DGVM simulations include all climate variability and CO_2 effects over land. In addition to the carbon cycle represented in all DGVMs, 14 models also account for the nitrogen cycle and hence can include the effect of N inputs on S_{LAND}. The DGVM estimate of S_{LAND} does not include the export of carbon to aquatic systems or its historical perturbation, which is discussed in the Supplement, Sect. S6.3. DGVMs need to meet several criteria to be included in this assessment. In addition, we use the International Land Model Benchmarking (ILAMB) system (Collier et al., 2018) for the DGVM evaluation (see the Supplement, Sect. S4.2), with an additional comparison of DGVMs with a data-informed Bayesian model–data fusion framework (CARDAMOM) (Bloom and Williams, 2015; Bloom et al., 2016). The uncertainty in S_{LAND} is taken from the DGVM standard deviation. More details on the S_{LAND} methodology can be found in the Supplement, Sect. S4.

2.6.2 Year 2024 projection

Like for the ocean forecast, the land CO_2 sink forecast for the year 2024 is based on (a) the historical (Lan et al., 2024) and our 2024 estimate of atmospheric CO_2 concentration, (b) the historical and our 2024 estimate of global fossil fuel emissions, and (c) the boreal summer (June, July, August) Oceanic Niño Index (ONI) (NCEP, 2024). All training data are again used to best match S_{LAND} from 1959 through 2023 from this year's carbon budget using a feed-forward neural network. To avoid overfitting, the neural network was trained with a variable number of artificial neurons (varying between 2–15), larger than for S_{OCEAN} prediction due to the stronger land carbon interannual variability. As done for S_{OCEAN}, Monte Carlo-type pre-training selects the optimal number of artificial neurons based on 20 % withheld input data, and in a second step, an ensemble of 10 forecasts is produced to provide the mean forecast and uncertainty. This uncertainty is then combined with the S_{LAND} uncertainty for 2023 (1.0 GtC yr^{-1}) to estimate the overall uncertainty in the 2024 projection.

2.7 Atmospheric inversion estimate

The worldwide network of in situ atmospheric measurements and satellite-derived atmospheric CO_2 column (XCO_2) observations put a strong constraint on changes in the atmospheric abundance of CO_2. This is true not only globally (hence our large confidence in G_{ATM}), but also in regions

with sufficient observational density, found mostly in the extra-tropics. This allows atmospheric inversion methods to constrain the magnitude and location of the combined total surface CO_2 fluxes from all sources, including fossil and land-use change emissions and land and ocean CO_2 fluxes. The inversions assume E_{FOS} to be well known, and they solve for the spatial and temporal distribution of land and ocean fluxes from the residual gradients of CO_2 between stations that are not explained by fossil fuel emissions. By design, such systems thus close the carbon balance ($B_{IM} = 0$) and provide an additional perspective on the independent estimates of the ocean and land fluxes.

This year's release includes 14 inversion systems that are described in Table S4. Each system is rooted in Bayesian inversion principles but uses different methodologies. These differences concern the selection of atmospheric CO_2 data or XCO_2 and the choice of a priori fluxes to refine. They also differ in spatial and temporal resolution, assumed correlation structures, and the mathematical approach of their models (see references in Table S4 for details). Importantly, the systems use a variety of transport models, which was demonstrated to be a driving factor behind differences in atmospheric-inversion-based flux estimates and specifically their distribution across latitudinal bands (Gaubert et al., 2019; Schuh et al., 2019). Eight inversion systems used surface observations from the global measurement network (Schuldt et al., 2023, 2024). Six inversion systems (CAMS-FT24r1, CMS-Flux, GONGGA, COLA, GCASv2, NTFVAR) used satellite XCO_2 retrievals from GOSAT and/or OCO-2, scaled to the WMO CO_2 X2019 calibration scale, and this year three of these inversion systems (CMS-Flux, COLA, NTFVAR) used these XCO_2 datasets in addition to the in situ observational CO_2 mole fraction records.

The original products delivered by the inverse modellers were modified to facilitate comparison to the other elements of the budget, specifically on two accounts: (1) global total fossil fuel emissions including cement carbonation CO_2 uptake and (2) riverine CO_2 transport. We note that with these adjustments, the inverse results no longer represent the net atmosphere–surface exchange over land and ocean areas as sensed by atmospheric observations. Instead, for land, they become the net uptake of CO_2 by vegetation and soils that is not exported by fluvial systems, which is similar to the DGVM estimates. For oceans, they become the net uptake of anthropogenic CO_2, which similar to the GOBM estimates.

The inversion systems prescribe global fossil fuel emissions based on, for example, the GCP's Gridded Fossil Emissions Dataset version 2024.0 (GCP-GridFED; Jones et al., 2024a), which is an update to GCP-GridFEDv2021 presented by Jones et al. (2021b). GCP-GridFEDv2024.0 scales gridded estimates of CO_2 emissions from EDGAR v4.3.2 (Janssens-Maenhout et al., 2019) within national territories to match national emissions estimates provided by the GCB for the years 1959–2023, which were compiled following the methodology described in Sect. 2.1. Small differences between the systems due to, for instance, regridding to the transport model resolution or use of fossil fuel emissions that are different to those of GCP-GridFEDv2024.0 are adjusted in the latitudinal partitioning we present to ensure agreement with the estimate of E_{FOS} in this budget. We also note that the ocean fluxes used as prior by 8 out of 14 inversions are part of the suite of the ocean process model or fCO_2 products listed in Sect. 2.5. Although these fluxes are further adjusted by the atmospheric inversions (except for Jena CarboScope), it means the inversion estimates of the ocean fluxes are not completely independent of S_{OCEAN} assessed here.

To facilitate comparisons to the independent S_{OCEAN} and S_{LAND} values, we used the same adjustments for transport and outgassing of carbon transported from land to ocean, as done for the observation-based estimates of S_{OCEAN} (see the Supplement, Sect. S3).

The atmospheric inversions are evaluated using vertical profiles of atmospheric CO_2 concentrations (Fig. S5). More than 30 aircraft programmes over the globe, either regular programmes or repeated surveys over at least 9 months (except for SH programmes), have been used to assess system performance (with space–time observational coverage sparse in the SH and tropics and denser in NH mid-latitudes; Table S8). The 14 systems are compared to the independent aircraft CO_2 measurements between 2 and 7 km above sea level between 2001 and 2023. Results are shown in Fig. S5 and discussed in the Supplement, Sect. S5.2.

With a relatively small ensemble of systems that cover at least 1 full decade ($N = 10$) and which moreover share some a priori fluxes used with one another or with the process-based models, it is difficult to justify using their mean and standard deviation as metrics for uncertainty across the ensemble. We therefore report their full range (min–max) without their mean. More details on the atmospheric inversion methodology can be found in the Supplement, Sect. S5.

2.8 Atmospheric-oxygen-based estimate

Long-term atmospheric O_2 and CO_2 observations allow estimation of the global ocean and land carbon sinks due to the coupling of O_2 and CO_2 with distinct exchange ratios for fossil fuel emissions and land uptake and uncoupled O_2 and CO_2 ocean exchange (Keeling and Manning, 2014). The global ocean and net land carbon sinks were calculated following methods and constants used in Keeling and Manning (2014) but were modified to also include the effective O_2 source from metal refining (Battle et al., 2023). For the exchange ratio of the net land sink, a value of 1.05 is used, following Resplandy et al. (2019). For fossil fuels, the following values are used: gas, 1.95 ± 0.04; liquid, 1.44 ± 0.03; solid, 1.17 ± 0.03; cement, 0 ± 0; and gas flaring, 1.98 ± 0.07 (Keeling, 1988). Atmospheric O_2 is observed as $\delta(O_2/N_2)$ and combined with CO_2 mole fraction observations into atmospheric potential oxygen (APO; Stephens et al., 1998). The APO observations from 1990 to 2024 were taken from

a weighted average of flask records from three stations in the Scripps O_2 Program network (Alert, Canada (ALT); La Jolla, California (LJO); and Cape Grim, Australia (CGO), weighted as per Keeling and Manning (2014). Observed CO_2 was taken from the globally averaged marine surface annual mean growth rate from the NOAA/GML Global Greenhouse Gas Reference Network (Lan et al., 2024). The O_2 source from ocean warming is based on ocean heat content from updated data from NOAA/NCEI (Levitus et al., 2012). The effective O_2 source from metal refining is based on production data from Bray (2020), Flanagan (2021), and Tuck (2022). Uncertainty was determined through a Monte Carlo approach with 20 000 iterations, using uncertainties prescribed in Keeling and Manning (2014), including observational uncertainties from Keeling et al. (2007) and autoregressive errors in fossil fuel emissions (Ballantyne et al., 2015). The reported uncertainty is 1 standard deviation of the ensemble. The difference from the atmospheric O_2 estimate for GCB2023 is due to a revision to the Scripps O_2 Program CO_2 data. As with the atmospheric inversions, the O_2-based estimates also close the carbon balance ($B_{IM} = 0$) by design and provide another independent estimate of the ocean and land fluxes. Note that the O_2 method requires a correction for global air–sea O_2 flux; this has the largest uncertainty at annual timescales but which is still non-negligible for decadal estimates (Nevison et al., 2008).

2.9 Earth system models' estimate

Reconstructions and predictions from decadal prediction systems based on Earth system models (ESMs) provide a novel line of evidence in assessing the atmosphere–land and atmosphere–ocean carbon fluxes in the past decades and predicting their changes for the current year. The decadal prediction systems based on ESMs used here consist of three sets of simulations: (i) uninitialized freely evolving historical simulations (1850–2014); (ii) assimilation reconstruction incorporating observational data into the model (1960–2023); and (iii) initialized prediction simulations for the 1981–2024 period, starting every year from initial states obtained from the above assimilation simulations. The assimilations are designed to reconstruct the actual evolution of the Earth system by assimilating essential fields from data products. The assimilations' states, which are expected to be close to observations, are used to start the initialized prediction simulations used for the current-year (2024) global carbon budget. Similar initialized prediction simulations starting every year (1 November or 1 January) over the 1981–2023 period (i.e. hindcasts) are also performed for predictive skill quantification and for bias correction. More details on the illustration of a decadal prediction system based on an ESM can be found in Fig. 1 of Li et al. (2023).

By assimilating physical atmospheric and oceanic data products into the ESMs, the models are able to reproduce the historical variations in the atmosphere–sea CO_2 fluxes, atmosphere–land CO_2 fluxes, and atmospheric CO_2 growth rate (Li et al., 2016, 2019; Lovenduski et al., 2019a, b; Ilyina et al., 2021; Li et al., 2023). Furthermore, the ESM-based predictions have proven their skill in predicting the air–sea CO_2 fluxes for up to 6 years and the air–land CO_2 fluxes and atmospheric CO_2 growth for 2 years (Lovenduski et al., 2019a, b; Ilyina et al., 2021; Li et al., 2023). The reconstructions from the fully coupled model simulations ensure a closed budget within the Earth system, i.e. no budget imbalance term.

Five ESMs, i.e. CanESM5 (Swart et al., 2019; Sospedra-Alfonso et al., 2021), EC-Earth3-CC (Döscher et al., 2022; Bilbao et al., 2021; Bernardello et al., 2024), IPSL-CM6A-CO_2-LR (Boucher et al., 2020), MIROC-ES2L (Watanabe et al., 2020), and MPI-ESM1-2-LR (Mauritsen et al., 2019; Li et al., 2023), have performed the set of prediction simulations. Each ESM uses a different assimilation method and combination of data products incorporated in the system; more details on the models' configuration can be found in Tables 4 and S5. The ESMs use external forcings from the Coupled Model Intercomparison Project Phase 6 (CMIP6) historical (1960–2014) and SSP2-4.5 baseline and CovidMIP 2-year blip scenarios (2015–2024) (Eyring et al., 2016; Lamboll et al., 2021). The CO_2 emissions forcing from 2015–2024 is substituted by GCB-GridFED (v2024.0, Jones et al., 2024a) to provide a consistent CO_2 forcing. Reconstructions of atmosphere–ocean CO_2 fluxes (S_{OCEAN}) and atmosphere–land CO_2 fluxes ($S_{LAND} - E_{LUC}$) for the time period from 1960–2023 are assessed here. Predictions of the atmosphere–ocean CO_2 flux, atmosphere–land CO_2 flux, and atmospheric CO_2 growth for 2024 are calculated based on the predictions at a lead time of 1 year. The predictions are bias-corrected using the 1985–2014 climatology mean of GCB2022 (Friedlingstein et al., 2022b); more details on methods can be found in Boer et al. (2016) and Li et al. (2023). The ensemble size of initialized prediction simulations is 10, and the ensemble mean for each individual model is used here. The ESMs are used here to support the assessment of S_{OCEAN} and net atmosphere–land CO_2 flux ($S_{LAND} - E_{LUC}$) over the 1960–2023 period and to provide an estimate of the 2024 projection of G_{ATM}.

2.10 Processes not included in the global carbon budget

The contribution of anthropogenic CO and CH_4 to the global carbon budget is not fully accounted for in Eq. (1) and is described in the Supplement, Sect. S6.1. The contributions to CO_2 emissions of the decomposition of carbonates not accounted for are described in the Supplement, Sect. S6.2. The contribution of anthropogenic changes in river fluxes is conceptually included in Eq. (1) in S_{OCEAN} and in S_{LAND}, but it is not represented in the process models used to quantify these fluxes. This effect is discussed in the Supplement, Sect. S6.3. Similarly, the loss of additional sink capacity from reduced forest cover is missing in the combination of

approaches used here to estimate both land fluxes (E_{LUC} and S_{LAND}), and its potential effect is discussed and quantified in the Supplement, Sect. S6.4.

3 Results

For each component of the global carbon budget, we present results for three different time periods: the full historical period, from 1850 to 2023, the decades for which we have atmospheric concentration records from Mauna Loa (1960–2023); a specific focus on last year (2023); and the projection for the current year (2024). Subsequently, we assess the estimates of the budget components of recent decades against the top-down constraints from inverse modelling of atmospheric observations, the land–ocean partitioning derived from the atmospheric O_2 measurements, and the budget component estimates from the ESM assimilation simulations. Atmospheric inversions further allow for an assessment of the budget components with a regional breakdown of land and ocean sinks.

3.1 Fossil CO_2 emissions

3.1.1 Historical period 1850–2023

Cumulative fossil CO_2 emissions for 1850–2023 were 490 ± 25 GtC, including the cement carbonation sink (Fig. 3, Table 8, with all cumulative numbers rounded to the nearest 5 GtC). In this period, 46 % of global fossil CO_2 emissions came from coal, 35 % from oil, 15 % from natural gas, 3 % from decomposition of carbonates, and 1 % from flaring. In 1850, the UK contributed 62 % of global fossil CO_2 emissions. In 1893 the combined cumulative emissions of the current members of the European Union reached and subsequently surpassed the level of the UK. Since 1917 US cumulative emissions have been the largest. Over the entire period of 1850–2023, US cumulative emissions amounted to 120 GtC (24 % of the world total), the EU's to 80 GtC (16 %), China's to 75 GtC (15 %), and India's to 15 GtC (3 %).

In addition to the estimates of fossil CO_2 emissions that we provide here (see Sect. 2.1), there are three global datasets with long time series that include all sources of fossil CO_2 emissions: CDIAC-FF (Hefner and Marland, 2023), CEDS version 2024_07_08 (Hoesly et al., 2024), and PRIMAP-hist version 2.6 (Gütschow et al., 2016, 2024), although these datasets are not entirely independent of each other (Andrew, 2020a). CEDS has cumulative emissions over 1750–2022 at 480 GtC, CDIAC-FF at 481 GtC, GCP at 484 GtC, and PRIMAP-hist at 490 GtC. CDIAC-FF excludes emissions from lime production. CEDS estimates higher emissions from international shipping in recent years, while PRIMAP-hist has higher fugitive emissions than the other datasets. However, in general these four datasets are in relative agreement as to total historical global emissions of fossil CO_2.

3.1.2 Recent period 1960–2023

Global fossil CO_2 emissions, E_{FOS} (including the cement carbonation sink), have increased every decade from an average of 3.0 ± 0.2 GtC yr^{-1} for the decade of the 1960s to an average of 9.7 ± 0.5 GtC yr^{-1} during 2014–2023 (Table 7, Figs. 2 and 5). The growth rate in these emissions decreased between the 1960s and the 1990s, from 4.3 % yr^{-1} in the 1960s (1960–1969), 3.2 % yr^{-1} in the 1970s (1970–1979), and 1.6 % yr^{-1} in the 1980s (1980–1989) to 1.0 % yr^{-1} in the 1990s (1990–1999). After this period, the growth rate began increasing again in the 2000s at an average growth rate of 2.8 % yr^{-1}, decreasing to 0.6 % yr^{-1} for the last decade (2014–2023). China's emissions increased by +1.9 % yr^{-1} on average over the last 10 years, dominating the global trend, and India's emissions increased by +3.6 % yr^{-1}, while emissions decreased in EU27 (the 27 countries of the EU) by 2.1 % yr^{-1} and in the USA by 1.2 % yr^{-1}. Figure 6 illustrates the spatial distribution of fossil fuel emissions for the 2014–2023 period.

E_{FOS} reported here includes the uptake of CO_2 by cement via carbonation, which has increased with increasing stocks of cement products from an average of 20 MtC yr^{-1} (0.02 GtC yr^{-1}) in the 1960s to an average of 200 MtC yr^{-1} (0.2 GtC yr^{-1}) during 2014–2023 (Fig. 5).

3.1.3 Final year 2023

Global fossil CO_2 emissions were slightly higher, 1.4 %, in 2023 than in 2022, with an increase of 0.14 GtC to reach 10.1 ± 0.5 GtC (including the 0.21 GtC cement carbonation sink) in 2023 (Fig. 5), distributed among coal (41 %), oil (32 %), natural gas (21 %), cement (4 %), flaring (< 1 %), and others (< 1 %). Compared to 2022, the 2023 emissions from coal, oil, and gas increased by 1.4 %, 2.5 %, and 0.1 %, respectively, while emissions from cement decreased by 2 %. All annual growth rates presented are adjusted for the leap year, unless stated otherwise.

In 2023, the largest absolute contributions to global fossil CO_2 emissions were from China (31 %), the USA (13 %), India (8 %), and EU27 (7 %). These four regions account for 59 % of global fossil CO_2 emissions, while the rest of the world contributed 41 %, including international aviation and marine bunker fuels (3 % of the total). Growth rates for these countries/regions from 2022 to 2023 were 4.9 % (China), −3.3 % (USA), −8.4 % (EU27), and 8.2 % (India), with +0.7 % for the rest of the world, including international aviation and marine bunker fuels (+9.5 %). The per capita fossil CO_2 emissions in 2023 were 1.3 tC per person per year for the globe and were 3.9 (USA), 2.3 (China), 1.5 (EU27), and 0.6 (India) tC per person per year for the four highest emitters (Fig. 5).

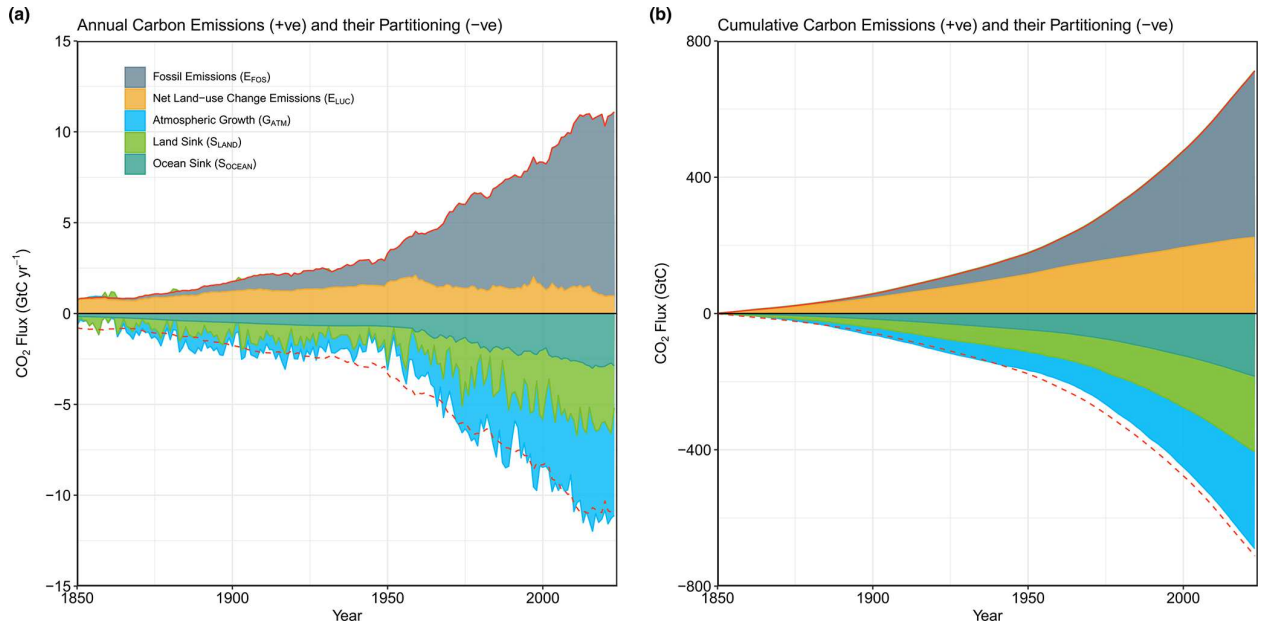

Figure 3. Combined components of the global carbon budget as a function of time, for fossil CO_2 emissions (E_{FOS}, including a small sink from cement carbonation; grey) and emissions from land-use change (E_{LUC}; yellow-brown), as well as their partitioning into the atmosphere (G_{ATM}; cyan), ocean (S_{OCEAN}; turquoise), and land (S_{LAND}; green). Panel **(a)** shows annual estimates of each flux (in GtC yr^{-1}) and panel **(b)** the cumulative flux (the sum of all prior annual fluxes, in GtC) since the year 1850. The partitioning is based on nearly independent estimates from observations (for G_{ATM}) and from process model ensembles constrained by data (for S_{OCEAN} and S_{LAND}) and does not exactly add up to the sum of the emissions, resulting in a budget imbalance (B_{IM}) which is represented by the difference between the bottom red line (mirroring total emissions) and the sum of carbon fluxes in the ocean, land, and atmosphere reservoirs. All data are in gigatonnes of carbon per year (GtC yr^{-1}) **(a)** and gigatonnes of carbon (GtC) **(b)**. The E_{FOS} estimate is based on a mosaic of different datasets and has an uncertainty of ±5 % (±1σ). The E_{LUC} estimate is from four bookkeeping models (Table 4) with an uncertainty of ±0.7 GtC yr^{-1}. The G_{ATM} estimates prior to 1959 are from Joos and Spahni (2008) with uncertainties equivalent to about ±0.1–0.15 GtC yr^{-1} and from Lan et al. (2024) since 1959 with uncertainties of about ±0.07 GtC yr^{-1} during 1959–1979 and ±0.02 GtC yr^{-1} since 1980. The S_{OCEAN} estimate is the average from Khatiwala et al. (2013) and DeVries (2014) with uncertainty of about ±30 % prior to 1959 and the average of an ensemble of models and an ensemble of fCO_2 products (Table 4) with uncertainties of about ±0.4 GtC yr^{-1} since 1959. The S_{LAND} estimate is the average of an ensemble of models (Table 4) with uncertainties of about ±1 GtC yr^{-1}. See the text for more details of each component and its uncertainties.

3.1.4 Year 2024 projection

Globally, we estimate that global fossil CO_2 emissions (including cement carbonation, −0.21 GtC) will grow by 0.8 % in 2024 (−0.2 % to +1.7 %) to 10.2 GtC (37.4 $GtCO_2$), a historical record high.[2] Carbon Monitor projects a comparable 2024 increase of 0.8 % (0.5 % to 1.1 %). GCB estimates of changes in 2024 emissions per fuel type, relative to 2023, are projected to be 0.1 % (range −1.0 % to 1.2 %) for coal, +0.9 % (range 0.3 % to 1.6 %) for oil, +2.5 % (range 1.3 % to 3.8 %) for natural gas, and −3.5 % (range −5.3 % to −1.6 %) for cement.

For China, projected fossil emissions in 2024 are expected to increase slightly by 0.1 % (range −1.7 % to 1.9 %) compared with 2023 emissions, bringing 2023 emissions for China to around 3.3 GtC yr^{-1} (11.9 $GtCO_2$ yr^{-1}). In contrast, the Carbon Monitor estimate projects a 2024 decrease of 0.8 % (range −1.3 % to −1.4 %). Our projected changes by fuel for China are +0.4 % for coal, −1.0 % for oil, +7.6 % for natural gas, and −9.4 % for cement.

For the USA, using the Energy Information Administration (EIA) emissions projection for 2024 combined with cement clinker data from USGS, we project a decrease of 0.9 % (range −2.1 % to 0.3 %) compared to 2023, bringing USA 2023 emissions to around 1.3 GtC yr^{-1} (4.9 $GtCO_2$ yr^{-1}). Conversely, Carbon Monitor projects a 2024 increase of 1.3 % (1.0 % to 1.6 %). Our projected changes by fuel are −5.7 % for coal, −0.7 % for oil, +1.1 % for natural gas, and −7.1 % for cement.

For the European Union, our projection for 2024 is for a decrease of 2.8 % (range −5.2 % to −0.3 %) relative to 2023, with 2024 emissions around 0.7 GtC yr^{-1} (2.4 $GtCO_2$ yr^{-1}). The Carbon Monitor projection for EU27 is slightly lower than that of the GCB, with a decrease of 4.5 % (−5.4 % to −3.6 %). Our projected changes by fuel are −11.3 % for

[2]Growth rates in this section use a leap year adjustment that corrects for the extra day in 2024.

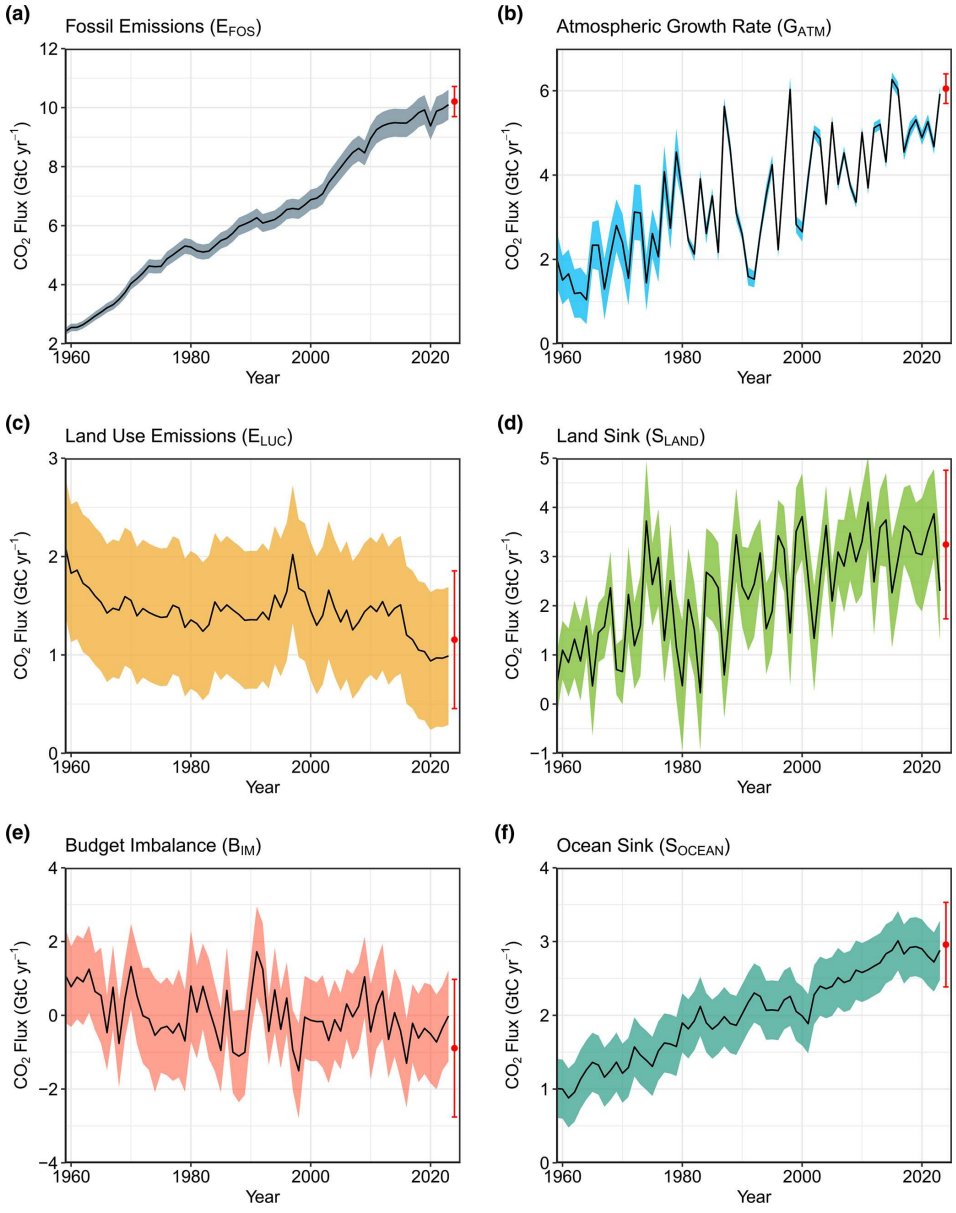

Figure 4. Components of the global carbon budget and their uncertainties as a function of time, presented individually for **(a)** fossil CO_2, including cement carbonation emissions (E_{FOS}); **(b)** the growth rate in atmospheric CO_2 concentration (G_{ATM}); **(c)** emissions from land-use change (E_{LUC}); **(d)** the land CO_2 sink (S_{LAND}); **(e)** the budget imbalance (B_{IM}) that is not accounted for by the other terms; and **(f)** the ocean CO_2 sink (S_{OCEAN}). Positive values of S_{LAND} and S_{OCEAN} represent a flux from the atmosphere to land or the ocean. All data are in GtC yr^{-1} with the uncertainty bounds representing ± 1 standard deviation in shaded colour. Data sources are as in Fig. 3. The red dots indicate our projections for the year 2024 and the red error bars the uncertainty in the 2024 projections (see Methods).

coal, −0.6 % for oil, +0.4 % for natural gas, and −3.1 % for cement.

For India, our projection for 2024 is an increase of 3.7 % (range of 3.3 % to 4.0 %) over 2023, with 2024 emissions around 0.9 GtC yr^{-1} (3.2 $GtCO_2$ yr^{-1}). The Carbon Monitor projection for India is an increase of 5.0 % (4.4 % to 5.5 %). Our projected changes by fuel are +3.3 % for coal, +3.3 % for oil, +11.8 % for natural gas, and +3.8 % for cement.

International aviation and shipping are projected to increase by 7.8 % in 2024, reaching 0.3 GtC yr^{-1} (1.2 $GtCO_2$ yr^{-1}), with international aviation projected to be up 14 % over 2023, continuing to recover from pandemic lows, and international shipping projected to rise by 3 %. The Carbon Monitor projects international aviation and shipping to only increase by 2.6 % in 2024.

For the rest of the world, the expected change for 2024 is an increase of 1.2 % (range −0.7 % to 3.2 %), with 2024

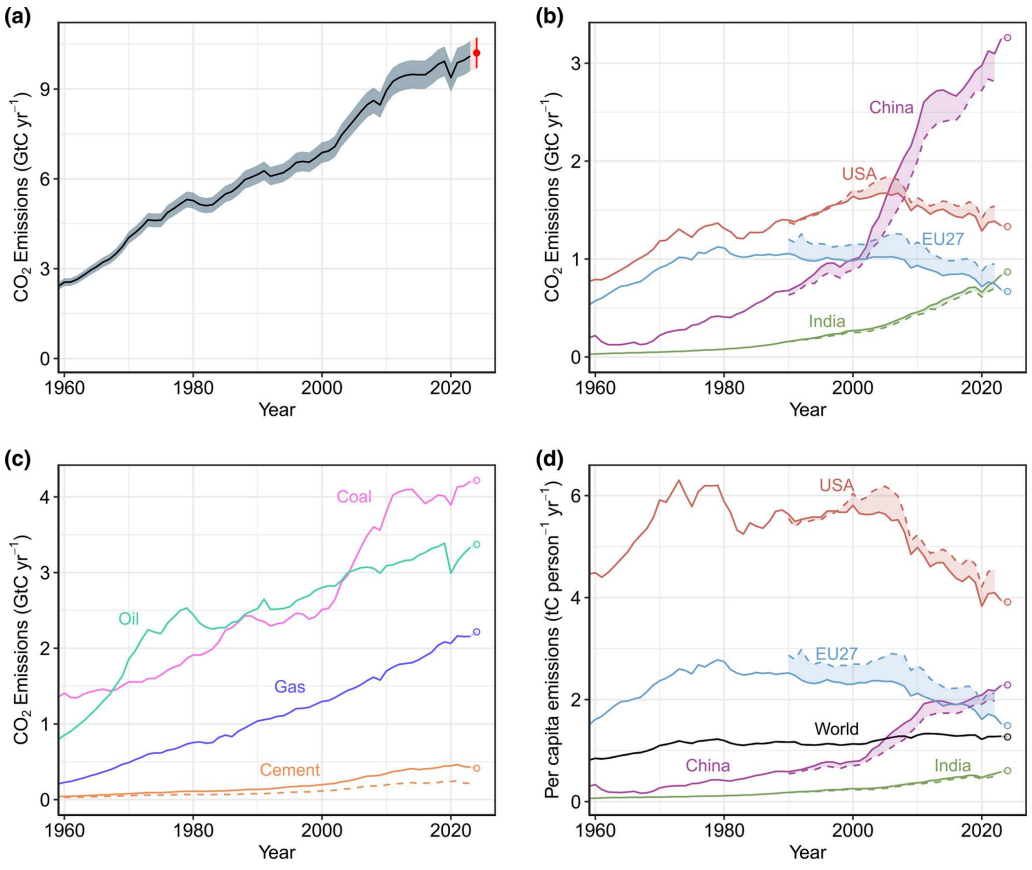

Figure 5. Fossil CO_2 emissions for **(a)** the globe, including an uncertainty of ±5 % (grey shading) and a projection through the year 2024 (red dot and uncertainty range); **(b)** territorial (solid lines) and consumption (dashed lines) emissions for the top three country emitters (USA, China, India) and for the European Union (EU27); **(c)** global emissions by fuel type, including coal, oil, gas, cement, and cement minus cement carbonation (dashed); and **(d)** per capita emissions for the world and for the large emitters as in panel **(b)**. Territorial emissions are primarily from a draft update of Hefner and Marland (2023), except for national data for most Annex I countries for 1990–2022, which are reported to the UNFCCC as detailed in the text, as well as some improvements in individual countries, and are extrapolated forward to 2023 using data from the Energy Institute. Consumption-based emissions are updated from Peters et al. (2011). See Sects. 2.1 and S1 for details of the calculations and data sources.

emissions around 4.0 GtC yr^{-1} (14.5 $GtCO_2$ yr^{-1}), which is similar to the Carbon Monitor projection of 1.5 % (range −1.2 % to 1.8 %). The fuel-specific projected 2024 growth rates for the rest of the world are +0.5 % for coal, +0.8 % for oil, +2.2 % for natural gas, and +2.0 % for cement.

For traceability, Table S6 provides a comparison of annual projections from the GCB since 2015 with the actual emissions assessed in the subsequent GCB annual report.

3.2 Emissions from land-use change

3.2.1 Historical period 1850–2023

Cumulative CO_2 emissions from land-use change (E_{LUC}) for 1850–2023 were 225 ± 65 GtC (Table 8; Figs. 3, 16). The cumulative emissions from E_{LUC} show a large spread among individual estimates of 150 GtC (H&C2023), 205 GtC (OSCAR), 250 GtC (LUCE), and 285 GtC (BLUE) for the four bookkeeping models and a similar wide estimate of 250 ± 85 GtC for the DGVMs (all cumulative numbers are rounded to the nearest 5 GtC). Vegetation biomass observations provide independent constraints on the E_{LUC} estimates (Li et al., 2017). Over the 1901–2012 period, the GCB bookkeeping models' cumulative E_{LUC} amounts to 165 [105, 210] GtC, which is similar to the observation-based estimate of 155 ± 50 GtC (Li et al., 2017).

3.2.2 Recent period 1960–2023

In contrast to growing fossil emissions, CO_2 emissions from land-use, land-use change, and forestry remained relatively constant (around 1.5 GtC yr^{-1}) over the 1960–1999 period. Since then, they have shown a statistically significant decrease of about 0.2 GtC per decade, reaching 1.1 ± 0.7 GtC yr^{-1} for the 2014–2023 period (Table 7), but with significant spread from 0.8 to 1.3 GtC yr^{-1}, across the four

bookkeeping models (Table 5, Fig. 7). Differently from the bookkeeping average, the DGVM average grows slightly larger over the 1980–2010 period and shows no sign of decreasing emissions in the recent decades, apart from in the most recent decade (Table 5, Fig. 7). This is, however, expected as DGVM-based estimates include the loss of additional sink capacity, which grows with time, while the bookkeeping estimates do not (Supplement, Sect. S6.4).

We separate net E_{LUC} into five component fluxes to gain further insight into the drivers of net emissions: deforestation, forest (re)growth, wood harvest and other forest management, peat drainage and peat fires, and all other transitions (Fig. 7c; Supplement, Sect. S2.1). We further decompose the deforestation and the forest (re)growth term into contributions from shifting cultivation vs. permanent forest cover changes (Fig. 7d). Averaged over the 2014–2023 period and over the four bookkeeping estimates, fluxes from deforestation amount to 1.7 [1.4, 2.3] GtC yr^{-1} (Table 5), of which 1.0 [0.8, 1.1] GtC yr^{-1} is from permanent deforestation. Fluxes from forest (re)growth amount to −1.2 [−1.5, −0.9] GtC yr^{-1} (Table 5), of which −0.5 [−0.7, −0.3] GtC yr^{-1} is from re-/afforestation and the remainder is from forest regrowth in shifting cultivation cycles. Emissions from wood harvest and other forest management (0.3 [0.0, 0.6] GtC yr^{-1}) and peat drainage and peat fires (0.2 [0.2, 0.3] GtC yr^{-1}) and the net flux from other transitions (0.1 [0.0, 0.1] GtC yr^{-1}) are substantially less important globally (Table 5). However, the small net flux from wood harvest and other forest management contains substantial gross fluxes that largely compensate for each other (see Fig. S8): 1.4 [0.9, 2.0] GtC yr^{-1} of emissions result from the decomposition of slash and the decay of wood products and −1.1 [−1.4, −0.8] GtC yr^{-1} of removals result from regrowth after wood harvesting.

The split into component fluxes clarifies the potential for emissions reduction and carbon dioxide removal: the emissions from permanent deforestation – the largest of our component fluxes – could be halted (largely) without compromising carbon uptake by forests, contributing substantially to emissions reduction. By contrast, reducing wood harvesting would have limited potential to reduce emissions as it would be associated with less forest regrowth; removals and emissions cannot be decoupled here on long timescales. A similar conclusion applies to removals and emissions from shifting cultivation, which we have therefore separated out. Carbon dioxide removal (CDR) in forests could instead be increased by permanently increasing the forest cover through re-/afforestation. Our estimate of about −0.5 GtC yr^{-1} removed on average each year during 2014–2023 by re-/afforestation is similar to independent estimates that were derived from NGHGIs for CDR in managed forests (through re-/afforestation and forest management) for 2013–2022 (−0.5 GtC yr^{-1}; Pongratz et al., 2024). Re-/afforestation constitutes the vast majority of all current CDR (Pongratz et al., 2024). Though transfers between non-atmospheric reservoirs cannot be compared directly to annual fluxes from the atmosphere and are thus not included in our estimate of E_{LUC}, CDR through these reservoirs such as in durable HWPs, biochar, or BECCS comprise much smaller amounts of carbon. A total of 218 MtC yr^{-1} has been estimated to be transferred to HWPs, averaged over 2013–2022 (Pongratz et al., 2024). The net flux of HWPs, considering the re-release of CO_2 through their decay, amounts to 91 MtC yr^{-1} over that period (Pongratz et al., 2024). Note that some double counting between the CDR through HWPs and the CDR through re-/afforestation exists if the HWPs are derived from newly forested areas. BECCS projects have been estimated to have stored 0.1 MtC yr^{-1} in geological projects worldwide in 2023 and biochar projects 0.2 MtC yr^{-1} (Pongratz et al., 2024). "Blue carbon", i.e. coastal wetland management such as restoration of mangrove forests, salt marshes, and seagrass meadows, though at the interface of land and ocean carbon fluxes, is counted towards the land-use sector as well. Currently, bookkeeping models do not include blue carbon; however, current CDR deployment in coastal wetlands is small globally, less than 0.003 MtC yr^{-1} (Powis et al., 2023).

The statistically significant decrease in E_{LUC} since the late 1990s, including the larger drop within the most recent decade, is due to the combination of decreasing emissions from deforestation (in particular permanent deforestation) and increasing removals from forest regrowth (with those from re-/afforestation stagnating globally in the last decade). Emissions in 2014–2023 are 28 % lower than in the late 1990s (1995–2004) and 20 % lower than in 2004–2013. The steep drop in E_{LUC} after 2015 is due to the combined effect from a peak in peat fire emissions in 2015 and a long-term decline in deforestation emissions in many countries over the 2010–2020 period, with the largest declines in the Democratic Republic of the Congo, Brazil, China, and Indonesia. Since the processes behind gross removals, foremost forest regrowth and soil recovery, are all slow, while gross emissions include a large instantaneous component, short-term changes in land-use dynamics, such as a temporary decrease in deforestation, influences gross emissions dynamics more than gross removal dynamics, which rather are a response to longer-term dynamics. Component fluxes often differ more across the four bookkeeping estimates than the net flux, which is expected due to different process representation; in particular, the treatment of shifting cultivation, which increases both gross emissions and removals, differs across models, but net and gross wood harvest fluxes also show high uncertainty. By contrast, models agree relatively well for emissions from permanent deforestation.

Overall, the highest land-use emissions occur in the tropical regions of all three continents. The top three emitters (both cumulatively 1959–2023 and on average over 2014–2023) are Brazil (in particular the Amazon arc of deforestation), Indonesia, and the Democratic Republic of the Congo, with these three countries contributing 0.7 GtC yr^{-1} or 60 %

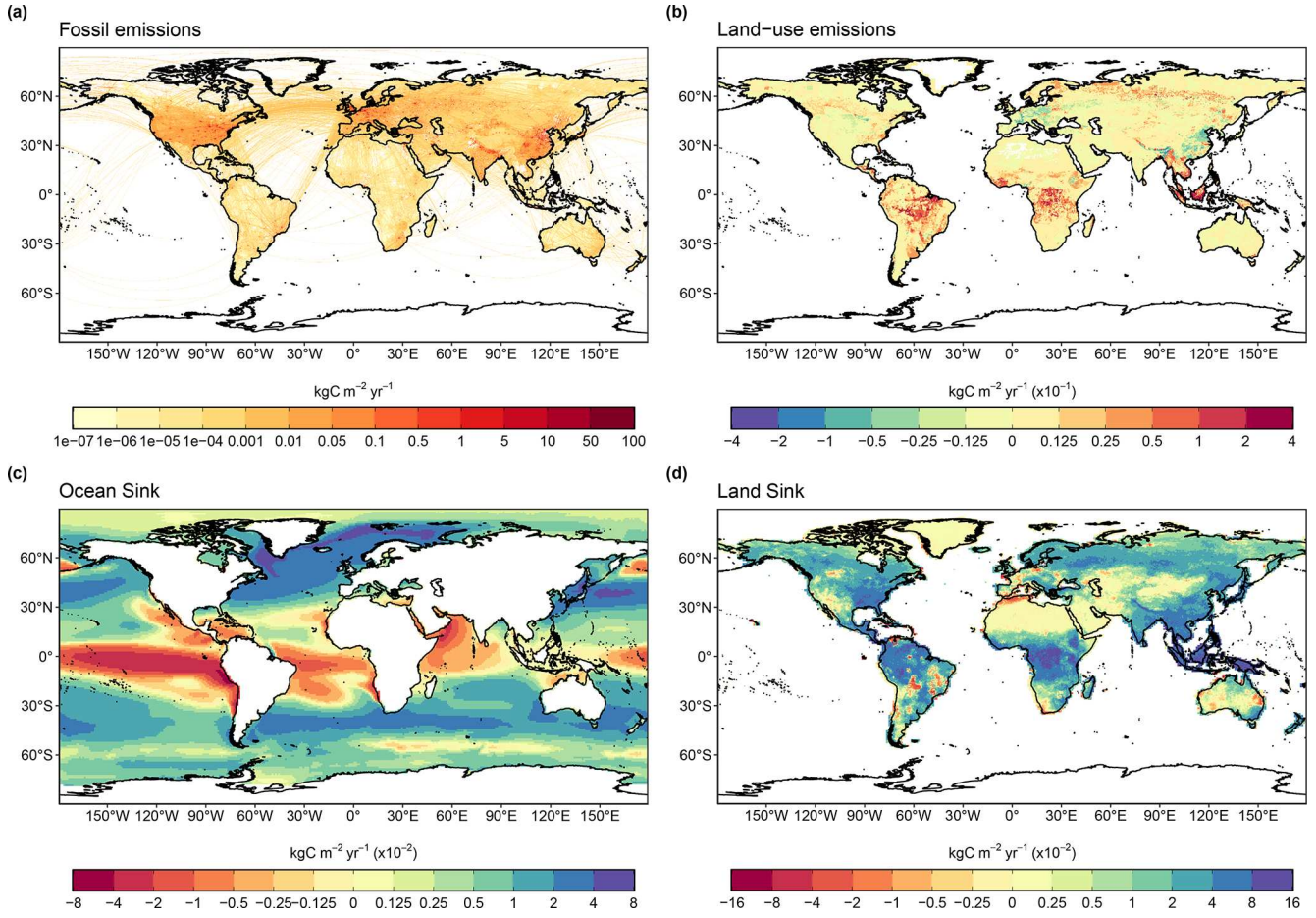

Figure 6. The 2014–2023 decadal mean components of the global carbon budget, presented for **(a)** fossil CO_2 emissions (E_{FOS}), **(b)** land-use change emissions (E_{LUC}), **(c)** the ocean CO_2 sink (S_{OCEAN}), and **(d)** the land CO_2 sink (S_{LAND}). Positive values for E_{FOS} and E_{LUC} represent a flux to the atmosphere, whereas positive values of S_{OCEAN} and S_{LAND} represent a flux from the atmosphere to the ocean or the land (carbon sink). In all panels, yellow and red colours represent a source (flux from the land and ocean to the atmosphere) and green and blue colours represent a sink (flux from the atmosphere into the land and ocean). All units are in kgC m^{-2} yr^{-1}. Note the different scales in each panel. E_{FOS} data shown are from GCP-GridFEDv2024.0 and do not include cement carbonation. The E_{LUC} map shows the average E_{LUC} from the four bookkeeping models and emissions from peat drainage and peat fires. BLUE and LUCE provide spatially explicit estimates at 0.25° resolution. Gridded E_{LUC} estimates for H&C2023 and OSCAR are derived by spatially distributing their national data based on the spatial patterns of BLUE gross fluxes in each country (see Schwingshackl et al., 2022, for more details about the methodology). S_{OCEAN} data shown are the average of GOBM and fCO_2-product means, using GOBM simulation A, no adjustment for bias, and drift applied to the gridded fields (see Sect. 2.5). S_{LAND} data shown are the average of the DGVMs (see Sect. 2.6).

of the global net land-use emissions (average over 2014–2023) (Figs. 6b, 7b). This is related to massive expansion of cropland, particularly in the last few decades in Latin America, Southeast Asia, and sub-Saharan Africa (Hong et al., 2021), with a substantial part for export of agricultural products (Pendrill et al., 2019). Emissions intensity is high in many tropical countries, particularly in Southeast Asia, due to high rates of land conversion in regions of carbon-dense and often still pristine, undegraded natural forests (Hong et al., 2021). Emissions are further increased by peat fires in equatorial Asia (GFED4.1s; van der Werf et al., 2017). Our estimates of high E_{LUC} in China have been revised down since the 1980s as compared to GCB2023, which is related to the update of the land-use forcing, now based on the cropland dataset by Yu et al. (2022) (see the Supplement, Sect. S2.2); this suggests lower cropland expansion and thus less deforestation than the previous datasets assumed. Uptake due to land-use change occurs in several regions of the world (Fig. 6b) particularly because of re-/afforestation. The highest CDR in the last decade is seen in China, where our estimates show an even larger uptake since 2010 compared to GCB2023, related to the updated land-use forcing in EU27, which is partly related to expanding forest area as a consequence of the forest transition in the 19th and 20th centuries and subsequent regrowth of forest (Mather, 2001; McGrath et al., 2015), and in the USA. Substantial uptake through

Table 5. Comparison of results from the bookkeeping method and budget residuals with results from the DGVMs, as well as additional estimates from atmospheric oxygen, atmospheric inversions and Earth system models (ESMs) for different periods, the last decade, and the last year available. All values are in GtC yr^{-1}. See Fig. 7 for explanation of the bookkeeping component fluxes. The DGVM uncertainties represent $\pm 1\sigma$ of the decadal or annual (for 2023) estimates from the individual DGVMs: for the inverse systems, the mean and range of available results are given. All values are rounded to the nearest 0.1 GtC, and therefore columns do not necessarily add to zero.

		Mean (GtC yr^{-1})						
		1960s	1970s	1980s	1990s	2000s	2014–2023	2023
Land-use change emissions (E_{LUC})	Bookkeeping (BK) net flux (1a)	1.6 ± 0.7	1.4 ± 0.7	1.4 ± 0.7	1.6 ± 0.7	1.4 ± 0.7	1.1 ± 0.7	1 ± 0.7
	BK – deforestation (total)	1.7 [1.3, 2.2]	1.6 [1.2, 2]	1.6 [1.3, 1.9]	1.8 [1.6, 2]	1.9 [1.6, 2.2]	1.7 [1.4, 2.3]	1.7 [1.3, 2.3]
	BK – forest regrowth (total)	−0.8 [−1.1, −0.6]	−0.9 [−1.1, −0.7]	−0.9 [−1, −0.7]	−0.9 [−1.1, −0.8]	−1.1 [−1.2, −0.9]	−1.2 [−1.5, −0.9]	−1.2 [−1.5, −0.9]
	BK – other transitions	0.3 [0.3, 0.4]	0.2 [0.2, 0.3]	0.2 [0.1, 0.3]	0.1 [0, 0.2]	0.1 [0, 0.1]	0.1 [0, 0.1]	0 [0, 0.1]
	BK – peat drainage and peat fires	0.2 [0.1, 0.2]	0.2 [0.1, 0.2]	0.2 [0.2, 0.2]	0.3 [0.2, 0.3]	0.2 [0.2, 0.3]	0.2 [0.2, 0.3]	0.2 [0.2, 0.3]
	BK – wood harvest and forest management	0.2 [−0.2, 0.6]	0.3 [−0.2, 0.6]	0.3 [−0.2, 0.7]	0.3 [−0.1, 0.6]	0.3 [−0.1, 0.6]	0.3 [0, 0.6]	0.3 [0, 0.7]
	DGVM net flux (1b)	1.5 ± 0.5	1.5 ± 0.5	1.5 ± 0.5	1.7 ± 0.5	1.7 ± 0.6	1.5 ± 0.6	1.2 ± 0.7
Terrestrial sink (S_{LAND})	Residual sink from global budget ($E_{FOS} + E_{LUC}$ (1a) $- G_{ATM} - S_{OCEAN}$) (2a)	1.7 ± 0.8	1.9 ± 0.8	1.6 ± 0.9	2.6 ± 0.9	2.8 ± 0.9	2.7 ± 0.9	2.3 ± 1
	DGVMs (2b)	1.2 ± 0.5	2 ± 0.8	1.8 ± 0.8	2.5 ± 0.6	2.8 ± 0.7	3.2 ± 0.9	2.3 ± 1
Net land fluxes ($S_{LAND} - E_{LUC}$)	GCB2024 (2b − 1a)	−0.4 ± 0.9	0.5 ± 1.1	0.4 ± 1.1	0.9 ± 0.9	1.4 ± 1	2.1 ± 1.1	1.3 ± 1.2
	Atmospheric O_2	–	–	–	1.3 ± 0.7	1 ± 0.7	1 ± 0.8	–
	DGVM net (2b − 1b)	−0.3 ± 0.5	0.5 ± 0.7	0.3 ± 0.6	0.8 ± 0.4	1.1 ± 0.4	1.7 ± 0.6	1.1 ± 0.8
	Inversions*	– [–, –]	– [–, –]	0.3 [0.3, 0.4] (2)	0.9 [0.6, 1.1] (3)	1.2 [0.6, 1.5] (4)	1.4 [0.3, 2.2] (10)	0.9 [−0.1, 2.7] (14)
	ESMs	0 [−0.7, 0.5]	1.5 [1.2, 2]	1 [0.5, 1.4]	1.7 [1.2, 2.4]	1.8 [0.4, 2.7]	2.2 [0.3, 3.6]	1.8 [−2.9, 3.7]

* Estimates are adjusted for the pre-industrial influence of river fluxes and for the cement carbonation sink and are adjusted to a common E_{FOS} (Sect. 2.7). The ranges given include varying numbers (in parentheses) of inversions in each decade (Table S4).

re-/afforestation also exists in other regions such as Brazil, Myanmar, or Russia, where, however, emissions from deforestation and other land-use changes dominate the net flux.

While the mentioned patterns are robust and supported by independent literature, we acknowledge that model spread is substantially larger on regional than on global levels, as has been shown for bookkeeping models (Bastos et al., 2021) as well as DGVMs (Obermeier et al., 2021). Assessments for individual regions are being performed as part of REgional Carbon Cycle Assessment and Processes (RECCAP-2; Ciais et al., 2022; Poulter et al., 2022) or already exist for selected regions (e.g. for Europe by Petrescu et al., 2020; for Brazil by Rosan et al. (2021); for eight selected countries/regions in comparison to inventory data by Schwingshackl et al., 2022). The revisions since GCB2023 reflect such uncertainties: the integration of a fourth bookkeeping model alters our estimates, though only to a limited extent given that the new model LUCE lies in between the other three models for the global E_{LUC} estimates. Larger changes are obvious at a regional level due to the revisions of the land-use forcing, with a general update to more recent FAO input for agricultural ar-

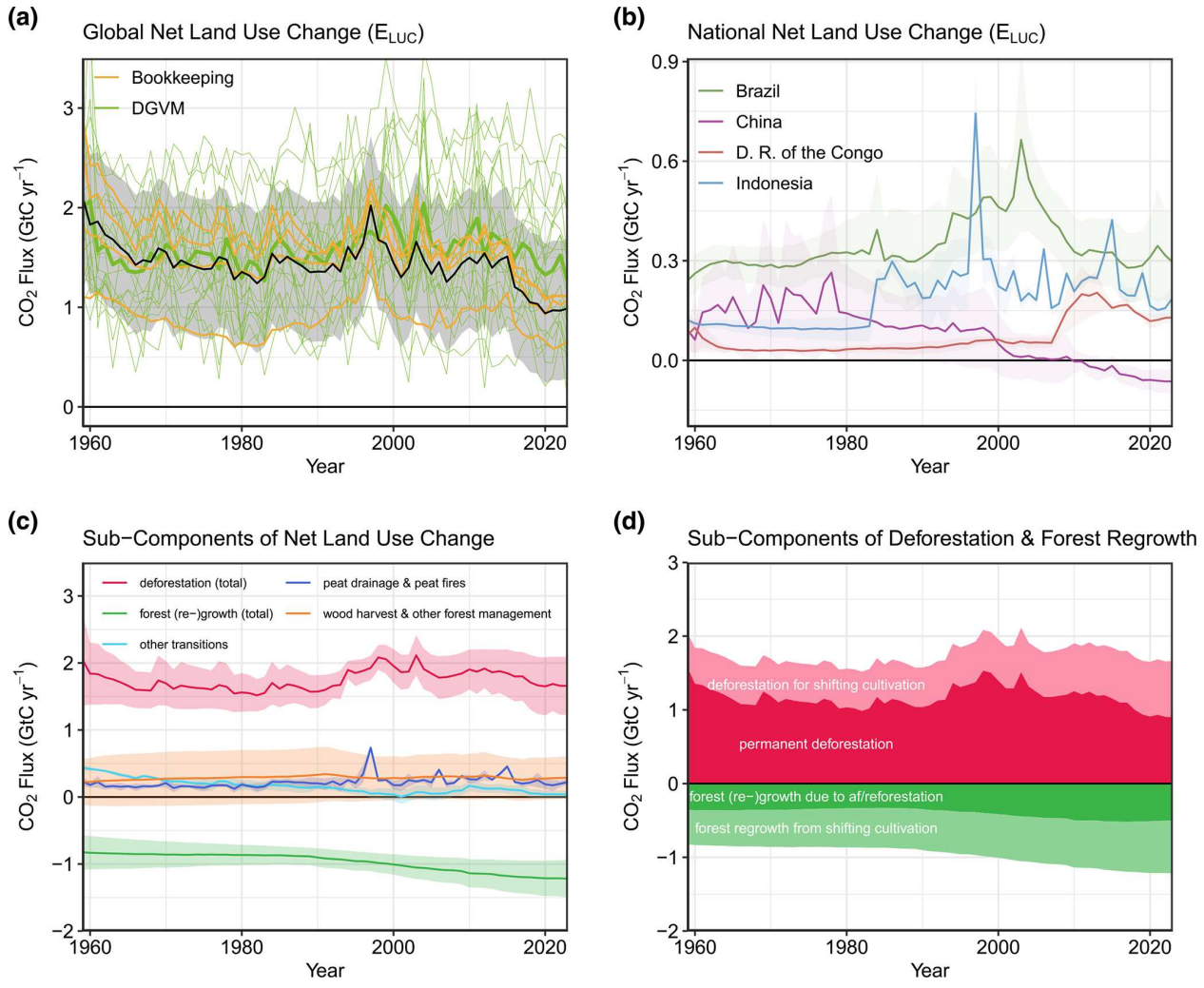

Figure 7. Net CO_2 exchanges between the atmosphere and the terrestrial biosphere related to land-use change. **(a)** Net CO_2 emissions from land-use change (E_{LUC}) with estimates from the four bookkeeping models (yellow lines) and the budget estimate (black with $\pm 1\sigma$ uncertainty), which is the average of the four bookkeeping models. Estimates from individual DGVMs (narrow green lines) and the DGVM ensemble mean (thick green line) are also shown. **(b)** Net CO_2 emissions from land-use change from the four countries/regions with the largest cumulative emissions since 1959. Values shown are the average of the four bookkeeping models, with shaded regions as $\pm 1\sigma$ uncertainty. **(c)** Subcomponents of E_{LUC}: (i) emissions from deforestation (including permanent deforestation and deforestation in shifting cultivation cycles), (ii) emissions from peat drainage and peat fires, (iii) removals from forest (re)growth (including forest (re)growth due to afforestation and reforestation and forest regrowth in shifting cultivation cycles), (iv) fluxes from wood harvest and other forest management (comprising slash and product decay following wood harvest, regrowth after wood harvest, and fire suppression), and (v) emissions and removals related to other land-use transitions. The sum of the five components is E_{LUC} shown in panel **(a)**. **(d)** Subcomponents of "deforestation (total)" and of "forest (re)growth (total)": (i) deforestation in shifting cultivation cycles, (ii) permanent deforestation, (iii) forest (re)growth due to afforestation and/or reforestation, and (iv) forest regrowth in shifting cultivation cycles.

eas and wood harvest, new MapBiomas input for Brazil and Indonesia, and the updated cropland dataset in China.

The NGHGI data under the LULUCF sector and the LULUCF estimates from FAOSTAT differ from the global models' definition of E_{LUC} (see Sect. 2.2.1). In the NGHGI reporting, the natural fluxes (S_{LAND}) are counted towards E_{LUC} when they occur on managed land (Grassi et al., 2018). To compare our results to the NGHGI approach, we perform a translation of our E_{LUC} estimates by adding S_{LAND} in managed forest from the DGVM simulations (following the methodology described in Grassi et al., 2023) to the bookkeeping E_{LUC} estimate (see the Supplement, Sect. S2.3). For the 2014–2023 period, we estimate that 1.8 GtC yr^{-1} of S_{LAND} occurred in managed forests. Adding this sink to E_{LUC} changes E_{LUC} from being a source of 1.1 GtC yr^{-1} to a sink of 0.7 GtC yr^{-1}, which is very similar to the NGHGI estimate that yields a sink of 0.8 GtC yr^{-1} (Fig. 8, Table S10). We further apply a mask of managed land to the

net atmosphere-to-land flux estimate from atmospheric inversions to obtain inverse estimates that are comparable to the NGHGI estimates and to the translated E_{LUC} estimates from bookkeeping models (see the Supplement, Sect. S2.3). The inversion-based net flux in managed land indicates a sink of 0.7 GtC yr^{-1} for 2014–2023, which agrees very well with the NGHGIs and the translated E_{LUC} estimates (Fig. 8, Table S10). Additionally, the interannual variability in the inversion estimates and that in the translated E_{LUC} estimates show remarkable agreement (Pearson correlation of 0.81 in 2000–2023), which supports the suggested translation approach.

The translation approach has been shown to also be generally applicable at the country level (Grassi et al., 2023; Schwingshackl et al., 2022). Country-level analysis suggests, for example, that the bookkeeping method estimates higher deforestation emissions than the national report in Indonesia but less CO_2 removal by afforestation than the national report in China. The fraction of the natural CO_2 sinks that the NGHGI estimates include differs substantially across countries, related to varying proportions of managed vs. total forest areas (Schwingshackl et al., 2022). By comparing E_{LUC} and NGHGI on the basis of the component fluxes used above, we find that our estimates very closely reproduce the NGHGI estimates for emissions from permanent deforestation, peat emissions, and other transitions (Fig. 8), although a difference in sign for the latter (small source in bookkeeping estimates, small sink in NGHGI) creates a notable difference between NGHGI and bookkeeping estimates. Fluxes due to forest (re)growth and other forest management, that is, (re)growth from re-/afforestation and the net flux from wood harvesting and other forest management and emissions and removals in shifting cultivation cycles, constitute a large sink in the NGHGI (-1.9 GtC yr^{-1} averaged over 2014–2023), since they also include S_{LAND} in managed forests. Summing up the bookkeeping estimates of (re)growth from re-/afforestation, the net flux from wood harvesting and other forest management, and the emissions and removals in shifting cultivation cycles and adding S_{LAND} in managed forests yields a flux of -2.0 GtC yr^{-1} (averaged over 2014–2023), which compares well with the NGHGI estimate. Though estimates between NGHGI, FAOSTAT, and the translated budget estimates still differ in value and need further analysis, the approach suggested by Grassi et al. (2023), which we adopt here, provides a feasible way to relate the global models' and NGHGI approaches to each other and thus link the anthropogenic carbon budget estimates of land CO_2 fluxes directly to the Global Stocktake as part of the UNFCCC Paris Agreement.

3.2.3 Final year 2023

The global CO_2 emissions from land-use change are estimated as 1.0 ± 0.7 GtC in 2023, which is similar to the 2022 estimate. However, confidence in the annual change remains

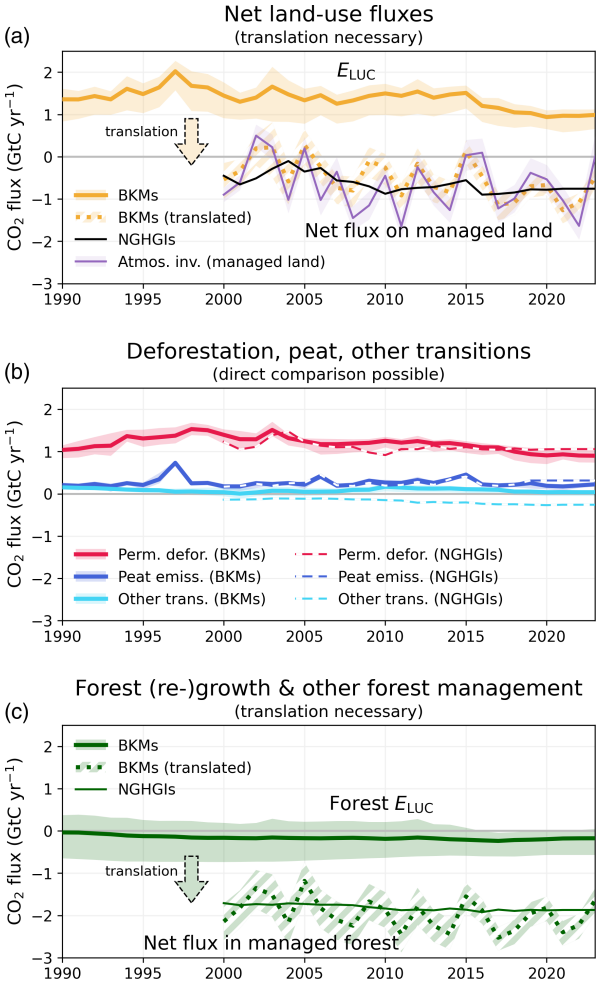

Figure 8. Comparison of land-use flux estimates from bookkeeping models (BKMs; following the GCB definition of E_{LUC}), national GHG inventories (NGHGIs; following IPCC guidelines and thus including all carbon fluxes on managed land), and atmospheric inversion systems (considering fluxes on managed land only). To compare BKM results with NGHGIs, a translation is necessary for some subcomponents. **(a)** Net land-use fluxes, for which a translation of BKMs is necessary; **(b)** permanent deforestation, peat drainage and peat fire, and other transition subcomponents, which can be directly compared; and **(c)** the forest (re)growth and other forest management subcomponent, for which a translation is necessary. The lines represent the mean of 4 BKMs and 14 atmospheric inversion estimates; shaded areas denote the full range across BKM estimates and the standard deviation for atmospheric inversions. The subcomponent forest (re)growth and other forest management includes removals from forest (re)growth (permanent), emissions and removals from wood harvest and other forest management, and emissions and removals in shifting cultivation cycles. The translation of BKM estimates to NGHGI estimates in **(a)** and **(c)** is done by adding the natural land sink in managed forests to the BKM estimates (see also Table S10). The GCB definition of E_{LUC} and the NGHGI definition of land-use fluxes are equally valid, each in its own context. For illustrative purposes we only show the translation of BKM estimates to the NGHGI definition.

low. Despite El Niño conditions, which in general lead to more fires in deforestation areas, peat fire emissions in Indonesia remained below average (GFED4.1s; updated from van der Werf et al., 2017). In South America, emissions from tropical deforestation and degradation fires have been about average, as effects of the El Niño in the Amazon, such as droughts, are not expected before 2024.

3.2.4 Year 2024 projection

In Southeast Asia, peat fire emissions have further dropped (from 27 TgC in 2023 to 2 TgC in 2024 through 31 December 2024; GFED4.1s – van der Werf et al., 2017), as have tropical deforestation and degradation fires (from 33 to 8 TgC) as the El Niño conditions ceased. By contrast, emissions from tropical deforestation and degradation fires in South America have risen from 121 TgC in 2023 to 334 TgC in 2024 up until 31 December, as the impacts of the El Niño unfolded, in particular drought conditions since 2023. The 2024 South American fire emissions are among the highest values in the record, which started in 1997. Part of the increase is due to elevated fire activity in the wetlands of the Pantanal. Disentangling the degree to which interannual variability in rainfall patterns and stronger environmental protection measures in both Indonesia after their 2015 high-fire-activity season and Brazil after the change in government play a role in fire trends is an important research topic. Cumulative 2024 fire emissions estimates through 31 December 2024 are 439 TgC for global deforestation and degradation fires and 2 TgC for peatland fires in Southeast Asia.

Based on these estimates, we expect E_{LUC} emissions of around 1.2 GtC (4.2 $GtCO_2$) in 2024, 0.17 GtC above the 2023 level. Note that although our extrapolation includes tropical deforestation and degradation fires, the degradation attributable to selective logging, edge effects, or fragmentation is not captured. Further, deforestation and fires in deforestation zones may become more disconnected, partly due to changes in legislation in some regions. For example, van Wees et al. (2021) found that the contribution from fires to forest loss decreased in the Amazon and in Indonesia over the period of 2003–2018.

3.3 CDR not based on vegetation

Besides the CDR through land use (Sect. 3.2), the atmosphere-to-geosphere flux of carbon resulting from carbon dioxide removal (CDR) activity in 2023 is estimated at 0.011 MtC yr^{-1}. This results primarily from 0.009 MtC yr^{-1} of enhanced-weathering projects and 0.001 MtC yr^{-1} of DACCS. While it represents a growth of 200 % in the anthropogenic sink from the 0.0036 MtC yr^{-1} estimate in 2022, it remains about a million times smaller than current fossil CO_2 emissions. Note that the lower estimate for DACCS is due to more accurate (lower) annual estimates now being available rather than to lower activity. Enhanced rock weathering has gone up relative to last year, as a result of both better coverage of projects and an actual increase in activity.

3.4 Total anthropogenic emissions

Cumulative anthropogenic CO_2 emissions (fossil and land use) for 1850–2023 totalled 710 ± 70 GtC (2605 ± 260 $GtCO_2$), of which 70 % (500 GtC) occurred since 1960 and 34 % (240 GtC) since 2000 (Tables 7 and 8). Total anthropogenic emissions more than doubled over the last 60 years, from 4.6 ± 0.7 GtC yr^{-1} for the decade of the 1960s to an average of 10.8 ± 0.9 GtC yr^{-1} during 2014–2023 and reaching 11.1 ± 0.9 GtC (40.6 ± 3.2 $GtCO_2$) in 2023. However, total anthropogenic CO_2 emissions have been stable over the last decade (zero growth rate over the 2014–2023 period), much slower than the 2.0 % growth rate over the previous decade (2004–2013).

During the historical period 1850–2023, 31 % of historical emissions were from land-use change and 69 % from fossil emissions. However, fossil emissions have grown significantly since 1960, while land-use changes have not, and consequently the contributions of land-use change to total anthropogenic emissions were smaller during recent periods, 18 % during the period 1960–2023 and down to 10 % over the last decade (2014–2023).

For 2024, we project global total anthropogenic CO_2 emissions from fossil and land-use changes to be around 11.4 GtC (41.6 $GtCO_2$), 2 % above the 2023 level. All values here include the cement carbonation sink (currently about 0.2 GtC yr^{-1}).

3.5 Atmospheric CO_2

3.5.1 Historical period 1850–2023

Atmospheric CO_2 concentration was approximately 278 parts per million (ppm) in 1750, reaching 300 ppm in the late 1900s, 350 ppm in the late 1980s, and 419.31 ± 0.1 ppm in 2023 (Lan et al., 2024; Fig. 1). The mass of carbon in the atmosphere increased by 51 % from 590 GtC in 1750 to 890 GtC in 2023. Current CO_2 concentrations in the atmosphere are unprecedented for the last 2 million years, and the current rate of atmospheric CO_2 increase is at least 10 times faster than at any other time during the last 800 000 years (Canadell et al., 2021).

3.5.2 Recent period 1960–2023

The growth rate in the atmospheric CO_2 level increased from 1.7 ± 0.07 GtC yr^{-1} in the 1960s to 5.2 ± 0.02 GtC yr^{-1} during 2014–2023, with important decadal variations (Table 7, Figs. 3 and 4). During the last decade (2014–2023), the growth rate in atmospheric CO_2 concentration continued to increase, albeit with large interannual variability (Fig. 4).

Table 6. Comparison of results for the ocean sink from the fCO_2 products, from global ocean biogeochemistry models (GOBMs); the best estimate for GCB2024 as calculated from fCO_2 products and GOBMs that is used in the budget (Table 7); and additional estimates from atmospheric oxygen, atmospheric inversions, and Earth system models (ESMs) for different periods, the last decade, and the last year available. All values are in GtC yr^{-1}. Uncertainties represent $\pm 1\sigma$ of the estimates from the GOBMs ($N > 10$), and the range of ensemble members is given for ensembles with $N < 10$ (fCO_2 products, inversions, ESMs). The uncertainty in the GCB2024 budget estimate is based on expert judgement (Sects. 2 and S1 to S4), and for oxygen it is the standard deviation of a Monte Carlo ensemble (Sect. 2.8).

	Mean (GtC yr^{-1})						
Product	1960s	1970s	1980s	1990s	2000s	2014–2023	2023
fCO_2 products	–	–	–	2.3 [1.9, 2.9]	2.5 [2.3, 2.7]	3.1 [2.9, 3.7]	3 [2.3, 4]
GOBMs	1 ± 0.2	1.3 ± 0.3	1.8 ± 0.3	2 ± 0.3	2.2 ± 0.3	2.6 ± 0.4	2.7 ± 0.4
GCB2024	1.2 ± 0.4	1.5 ± 0.4	1.9 ± 0.4	2.1 ± 0.4	2.3 ± 0.4	2.9 ± 0.4	2.9 ± 0.4
Atmospheric O_2	–	–	–	2 ± 0.5	2.8 ± 0.4	3.4 ± 0.5	–
Inversions	– [–, –]	– [–, –]	1.8 [1.8, 1.9] (2)	2.3 [2.1, 2.5] (3)	2.5 [2.3, 3.1] (4)	3.1 [2.4, 4.1] (10)	3 [1.8, 4.1] (14)
ESMs	0.7 [0.1, 1.1]	1 [0.4, 1.4]	1.4 [0.7, 1.7]	1.7 [1.1, 2]	1.9 [1.5, 2.2]	2.5 [2.2, 2.8]	2.5 [2.2, 3]

Table 7. Decadal mean in the five components of the anthropogenic CO_2 budget for different periods and the last year available. All values are in GtC yr^{-1}, and uncertainties are reported as $\pm 1\sigma$. Fossil CO_2 emissions include cement carbonation. The table also shows the budget imbalance (B_{IM}), which provides a measure of the discrepancies among the nearly independent estimates. A positive imbalance means the emissions are overestimated and/or the sinks are too small. All values are rounded to the nearest 0.1 GtC, and therefore columns do not necessarily add to zero.

		Mean (GtC yr^{-1})							
		1960s	1970s	1980s	1990s	2000s	2014–2023	2023	2024 (projection)
Total emissions ($E_{FOS} + E_{LUC}$)	Fossil CO_2 emissions (E_{FOS})*	3 ± 0.2	4.7 ± 0.2	5.5 ± 0.3	6.4 ± 0.3	7.8 ± 0.4	9.7 ± 0.5	10.1 ± 0.5	10.2 ± 0.5
	Land-use change emissions (E_{LUC})	1.6 ± 0.7	1.4 ± 0.7	1.4 ± 0.7	1.6 ± 0.7	1.4 ± 0.7	1.1 ± 0.7	1 ± 0.7	1.2 ± 0.7
	Total emissions	4.6 ± 0.7	6.1 ± 0.7	6.9 ± 0.8	7.9 ± 0.8	9.2 ± 0.8	10.8 ± 0.9	11.1 ± 0.9	11.4 ± 0.9
Partitioning	Growth rate in atmospheric CO_2 (G_{ATM})	1.7 ± 0.07	2.8 ± 0.07	3.4 ± 0.02	3.1 ± 0.02	4 ± 0.02	5.2 ± 0.02	5.9 ± 0.2	6.1 ± 0.3
	Ocean sink (S_{OCEAN})	1.2 ± 0.4	1.5 ± 0.4	1.9 ± 0.4	2.1 ± 0.4	2.3 ± 0.4	2.9 ± 0.4	2.9 ± 0.4	3 ± 0.6
	Terrestrial sink (S_{LAND})	1.2 ± 0.5	2 ± 0.8	1.8 ± 0.8	2.5 ± 0.6	2.8 ± 0.7	3.2 ± 0.9	2.3 ± 1	3.2 ± 1.5
Budget imbalance	$B_{IM} = E_{FOS} + E_{LUC} - (G_{ATM} + S_{OCEAN} + S_{LAND})$	0.5	−0.1	−0.2	0.1	0	−0.4	0	−0.9

* Fossil emissions excluding the cement carbonation sink amount to 3 ± 0.2, 4.7 ± 0.2, 5.5 ± 0.3, 6.4 ± 0.3, 7.9 ± 0.4, and 9.9 ± 0.5 GtC yr^{-1} for the decades of the 1960s to 2010s, respectively, and to 10.3 ± 0.5 GtC yr^{-1} for 2023 and 10.4 ± 0.5 GtC yr^{-1} for 2024.

The airborne fraction (AF) is defined as the ratio of the atmospheric CO_2 growth rate to total anthropogenic emissions:

$$AF = G_{ATM} / (E_{FOS} + E_{LUC}). \quad (2)$$

It provides a diagnostic of the relative strength of the land and ocean carbon sinks in removing part of the anthropogenic CO_2 perturbation. The evolution of AF over the last 60 years shows no significant trend, remaining at around 44 %, albeit showing a large interannual and decadal variability driven by the year-to-year variability in G_{ATM} (Fig. 10). The observed stability of the airborne fraction over the 1960–2023 period indicates that the ocean and land CO_2 sinks have been increasing in pace with the total anthropogenic emissions over that period, removing on average about 56 % of the emissions (see Sect. 3.6.2 and 3.7.2).

3.5.3 Final year 2023

The growth rate in atmospheric CO_2 concentration was 5.9 ± 0.2 GtC (2.79 ± 0.08 ppm) in 2023 (Fig. 4; Lan et al., 2024), well above the 2022 growth rate (4.6 ± 0.2 GtC) or the 2014–2023 average (5.2 ± 0.02 GtC), as to be expected during an El Niño year. The 2023 atmospheric CO_2 growth rate was the fourth largest over the 1959–2023 atmospheric ob-

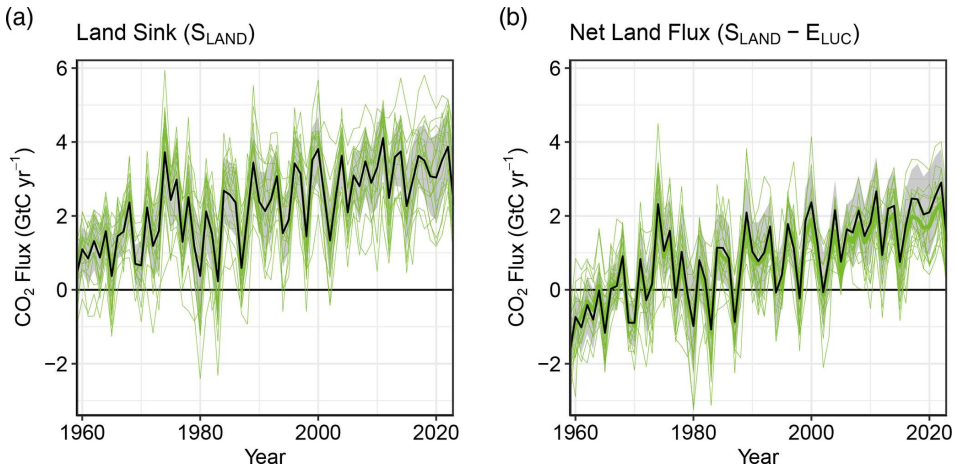

Figure 9. **(a)** The land CO_2 sink (S_{LAND}) estimated by individual DGVMs (green) as well as the budget estimate (black with $\pm 1\sigma$ uncertainty), which is the average of all DGVMs. **(b)** Net atmosphere–land CO_2 fluxes ($S_{LAND} - E_{LUC}$). The budget estimate of the net land flux (black with $\pm 1\sigma$ uncertainty) combines the DGVM estimate of S_{LAND} from panel **(a)** with the bookkeeping estimate of E_{LUC} from Fig. 7a. Uncertainties are similarly propagated in quadrature. DGVMs also provide estimates of E_{LUC} (see Fig. 7a), which can be combined with their own estimates of the land sink. Hence panel **(b)** also includes an estimate for the net land flux for individual DGVMs (thin green lines) and their multi-model mean (thick green line).

servational record, closely following 2015, 2016, and 1998, all strong El Niño years.

3.5.4 Year 2024 projection

The 2024 growth in atmospheric CO_2 concentration (G_{ATM}) is projected to be about 6.1 GtC (2.87 ppm), still high, which is common for the year after a strong El Niño year. This is the average of the GCB regression method (6.1 GtC, 2.85 ppm) and the ESM multi-model mean (6.1 GtC, 2.88 ppm). The 2024 atmospheric CO_2 concentration, averaged over the year, is expected to reach the level of 422.45 ppm, 52 % above the pre-industrial level.

3.6 Ocean sink

3.6.1 Historical period 1850–2023

Cumulated since 1850, the ocean sink adds up to 185 ± 35 GtC, with more than two-thirds of this amount (130 ± 25 GtC) being taken up by the global ocean since 1960. Over the historical period, the ocean sink increased in pace with the anthropogenic emissions exponential increase (Fig. 3). Since 1850, the ocean has removed 26 % of total anthropogenic emissions.

3.6.2 Recent period 1960–2023

The ocean CO_2 sink increased from 1.2 ± 0.4 GtC yr^{-1} in the 1960s to 2.9 ± 0.4 GtC yr^{-1} during 2014–2023 (Table 7), with interannual variations on the order of a few tenths of gigatonnes of carbon per year (Figs. 4, 11). The ocean-borne fraction ($S_{OCEAN}/(E_{FOS} + E_{LUC})$) has been remarkably constant at around 25 % on average (Fig. 10c), with variations around this mean illustrating the decadal variability in the ocean carbon sink. So far, there has been no indication of a decrease in the ocean-borne fraction from 1960 to 2022. The increase in the ocean sink is primarily driven by the increased atmospheric CO_2 concentration, with the strongest CO_2-induced signal in the North Atlantic and the Southern Ocean (Fig. 12a). The effect of climate change is much weaker, reducing the ocean sink globally by 0.17 ± 0.05 GtC yr^{-1} (−5.9 % of S_{OCEAN}) during 2014–2023 (all models simulate a weakening of the ocean sink by climate change, range −3.4 % to −10.7 %), and does not show clear spatial patterns across the GOBM ensemble (Fig. 12b). This is the combined effect of change and variability in all atmospheric forcing fields, previously attributed to wind and temperature changes (Le Quéré et al., 2010; Bunsen et al., 2024). The effect of warming is smaller than expected from offline calculation due to a stabilizing feedback from limited exchange between surface and deep waters (Bunsen et al., 2024).

The global net air–sea CO_2 flux is a residual of large natural and anthropogenic CO_2 fluxes into and out of the ocean, with distinct regional and seasonal variations (Figs. 6 and S1). Natural fluxes dominate on regional scales but are largely cancelled out when integrated globally (Gruber et al., 2009). Mid-latitudes in all basins and the high-latitude North Atlantic dominate the ocean CO_2 uptake where low temperatures and high wind speeds facilitate CO_2 uptake at the surface (Takahashi et al., 2009). In these regions, formation of mode, intermediate, and deep water masses transports anthropogenic carbon into the ocean interior, thus allowing for continued CO_2 uptake at the surface. Outgassing of natural

Table 8. Cumulative CO_2 for different time periods in gigatonnes of carbon (GtC). Fossil CO_2 emissions include cement carbonation. The budget imbalance (B_{IM}) provides a measure of the discrepancies among the nearly independent estimates. All values are rounded to the nearest 5 GtC, and therefore columns do not necessarily add to zero. Uncertainties are reported as follows: E_{FOS} is 5 % of cumulative emissions, E_{LUC} prior to 1959 is the 1σ spread from the DGVMs, E_{LUC} post-1959 is 0.7 × the number of years (where 0.7 GtC yr^{-1} is the uncertainty in the annual E_{LUC} flux estimate), G_{ATM} uncertainty is held constant at 5 GtC for all time periods, S_{OCEAN} uncertainty is 20 % of the cumulative sink (20 % relates to the annual uncertainty of 0.4 GtC yr^{-1}, which is ∼ 20 % of the current ocean sink), and S_{LAND} is the 1σ spread from the DGVM estimates.

		1750–2023	1850–2014	1850–2023	1960–2023	1850–2024
Emissions	Fossil CO_2 emissions (E_{FOS})	490 ± 25	400 ± 20	490 ± 25	410 ± 20	500 ± 25
	Land-use change emissions (E_{LUC})	255 ± 75	215 ± 60	225 ± 65	90 ± 45	225 ± 65
	Total emissions	745 ± 80	615 ± 65	710 ± 70	500 ± 50	725 ± 70
Partitioning	Growth rate in atmospheric CO_2 (G_{ATM})	305 ± 5	235 ± 5	285 ± 5	220 ± 5	290 ± 5
	Ocean sink (S_{OCEAN})	195 ± 40	160 ± 30	185 ± 35	130 ± 25	185 ± 35
	Terrestrial sink (S_{LAND})	245 ± 65	190 ± 55	220 ± 60	150 ± 40	225 ± 60
Budget imbalance	$B_{IM} = E_{FOS} + E_{LUC} - (G_{ATM} + S_{OCEAN} + S_{LAND})$	0	30	25	0	20

CO_2 occurs mostly in the tropics, especially in the equatorial upwelling region and to a lesser extent in the North Pacific and polar Southern Ocean, mirroring a well-established understanding of regional patterns of air–sea CO_2 exchange (e.g. Takahashi et al., 2009; Gruber et al., 2009). These patterns are also noticeable in the Surface Ocean CO_2 Atlas (SOCAT) dataset, where an ocean fCO_2 value above the atmospheric level indicates outgassing (Fig. S1). This map further illustrates the data sparsity in the Indian Ocean and the Southern Hemisphere in general.

The largest variability in the ocean sink occurs on decadal timescales (Fig. 11). The ensemble means of GOBMs and fCO_2 products show the same patterns of decadal variability, although with a larger amplitude of variability in the fCO_2 products than in the GOBMs. The ocean sink stagnated in the 1990s and strengthened between the early 2000s and the mid-2010s (Fig. 11; Le Quéré et al., 2007; Landschützer et al., 2015, 2016; DeVries et al., 2017; Hauck et al., 2020; McKinley et al., 2020; Gruber et al., 2023). More recently, the sink seems to have entered a phase of stagnation since 2016, largely in response to large interannual climate variability. Different explanations have been proposed for the decadal variability in the 1990s and 2000s, ranging from the ocean's response to changes in atmospheric wind systems (e.g. Le Quéré et al., 2007; Keppler and Landschützer, 2019), including variations in upper-ocean overturning circulation (DeVries et al., 2017), to the eruption of Mount Pinatubo in the 1990s (McKinley et al., 2020). The main origin of the decadal variability is a matter of debate, with a number of studies initially pointing to the Southern Ocean (see review in Canadell et al., 2021), but contributions from the North Atlantic and North Pacific (Landschützer et al., 2016; DeVries et al., 2019) or from a global signal (McKinley et al., 2020) have also been proposed.

On top of the decadal variability, interannual variability in the ocean carbon sink is driven by climate variability, with a first-order effect from a stronger ocean sink during large El Niño events (e.g. 1997–1998) (Fig. 11; Rödenbeck et al., 2014; Hauck et al., 2020; McKinley et al., 2017) leading to a reduction in CO_2 outgassing from the tropical Pacific. During 2010–2016, the ocean CO_2 sink appears to have intensified in line with the expected increase from atmospheric CO_2 (McKinley et al., 2020). This effect is similar in the fCO_2 products (Fig. 11, ocean sink 2016 minus 2010; GOBMs: $+0.42 \pm 0.11$ GtC yr^{-1}; fCO_2 products: $+0.44$ GtC yr^{-1}, range 0.18 to 0.72 GtC yr^{-1}). The reduction of -0.18 GtC yr^{-1} (range -0.41 to -0.03 GtC yr^{-1}) in the ocean CO_2 sink in 2017 is consistent with the return to normal conditions after the El Niño in 2015/16, which caused an enhanced sink in previous years. After an increasing S_{OCEAN} in 2018 and 2019, the GOBM and fCO_2-product ensemble means suggest a decrease in S_{OCEAN}, related to the triple La Niña event 2020–2022, followed by a rebound in 2023, linked to the onset of an El Niño event.

Although all individual GOBMs and fCO_2 products fall within the observational constraint, the ensemble means of GOBMs and fCO_2 products (adjusted for the riverine flux) show a mean offset increasing from 0.31 GtC yr^{-1} in the 1990s to 0.49 GtC yr^{-1} in the decade 2014–2023 and a slightly lower offset of 0.3 GtC yr^{-1} in 2023. In this version of the GCB, the S_{OCEAN} positive trend has diverged over time by a factor of 1.4 since 2002 (GOBMs: 0.25 ± 0.04 GtC yr^{-1}

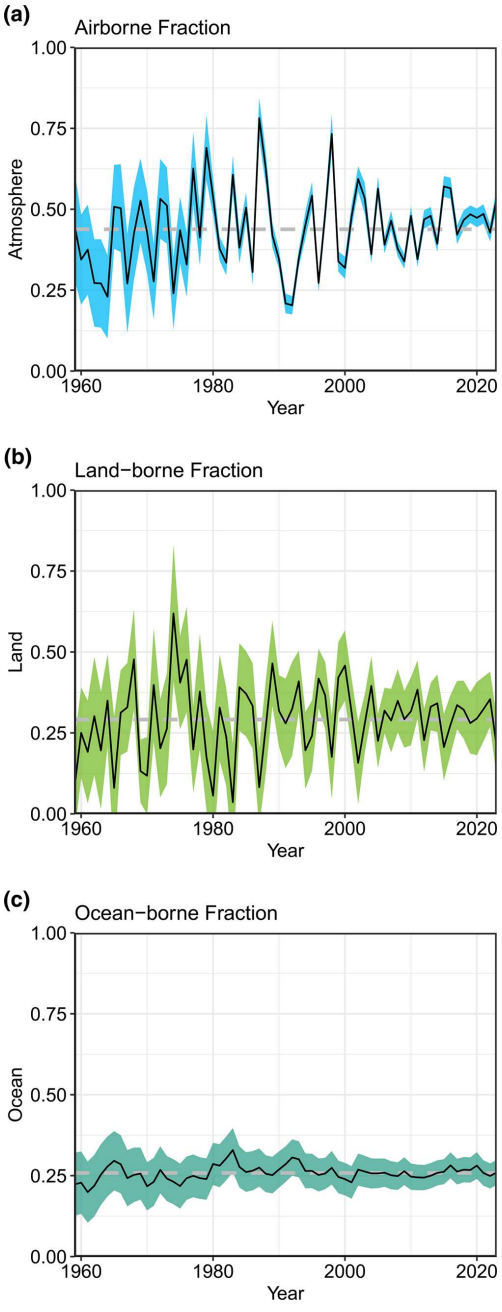

Figure 10. The partitioning of total anthropogenic CO_2 emissions ($E_{FOS} + E_{LUC}$) across the **(a)** atmosphere (airborne fraction), **(b)** land (land-borne fraction), and **(c)** ocean (ocean-borne fraction). Black lines represent the central estimate, and the coloured shading represents the uncertainty. The dashed grey lines represent the long-term average of the airborne (44 %), land-borne (30 %), and ocean-borne (25 %) fractions during 1960–2023 (with a B_{IM} of 1 %).

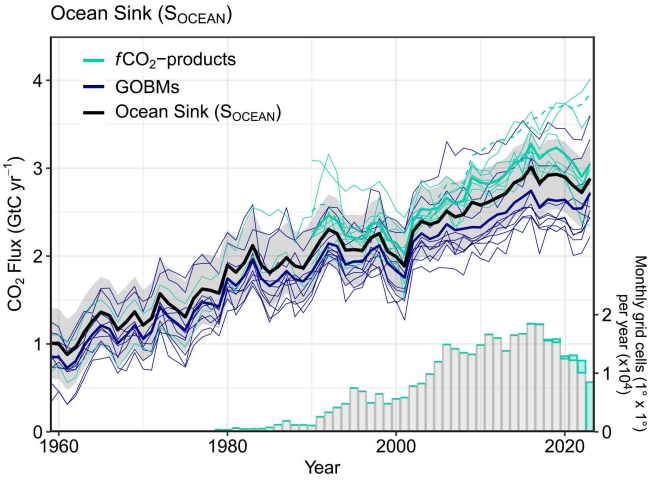

Figure 11. Comparison of the anthropogenic atmosphere–ocean CO_2 flux showing the budget values of S_{OCEAN} (black; with the uncertainty in grey shading), individual ocean models (royal blue), and the ocean fCO_2 products (cyan; with UExP-FFN-U, previously Watson et al. (2020), in a dashed line as it is not used for ensemble mean). Two fCO_2 products (Jena-MLS, LDEO-HPD) extend back to 1959. The fCO_2 products were adjusted for the pre-industrial ocean source of CO_2 from river input to the ocean by subtracting a source of 0.65 GtC yr^{-1} to make them comparable to S_{OCEAN} (see Sect. 2.5). The bar plot in the lower right illustrates the number of monthly gridded values in the SOCAT v2024 database (Bakker et al., 2024). Grey bars indicate the number of grid cells in SOCAT v2023, and coloured bars indicate the newly added grid cells in v2024.

per decade; fCO_2 products: 0.35 GtC yr^{-1} per decade (0.17 to 0.79 GtC yr^{-1} per decade); S_{OCEAN}: 0.30 GtC yr^{-1} per decade), but the uncertainty ranges overlap. This divergence is smaller than reported in previous GCB versions because of the updated lower sink estimates by the fCO_2 products for recent years. This also leads to agreement on the trend since 2010 (GOBMs: 0.18 ± 0.06 GtC yr^{-1} per decade; fCO_2 products: 0.18 GtC yr^{-1} per decade (-0.36 to 0.73 GtC yr^{-1} per decade); S_{OCEAN}: 0.18 GtC yr^{-1} per decade). A hybrid approach recently constrained the trend of 2000–2022 to 0.42 ± 0.06 GtC yr^{-1} per decade (Mayot et al., 2024), which aligns with the updated trends of S_{OCEAN} (0.39 GtC yr^{-1} per decade) and of the fCO_2 products (0.45 [0.28, 0.84] GtC yr^{-1} per decade), while the GOBMs result in a lower trend (0.32 ± 0.04 GtC yr^{-1} per decade) over the same period.

In the current dataset, the discrepancy between the two types of estimates stems from a persistently larger S_{OCEAN} in the fCO_2 products in the northern extra-tropics that has been the case since around 2002 and an intermittently larger S_{OCEAN} in the southern extra-tropics in the period 2008–2020 (Fig. 14). Note that the discrepancy in the mean flux, which was located in the Southern Ocean in GCB2022 and earlier, was reduced due to the choice of the regional river flux adjustment (Lacroix et al., 2020, instead of Aumont et al., 2001). This comes at the expense of a discrepancy in the mean S_{OCEAN} of about 0.2 GtC yr^{-1} in the tropics. Likely explanations for the discrepancy in the trends and decadal variability in the high latitudes are data sparsity and uneven

data distribution (Bushinsky et al., 2019; Gloege et al., 2021; Hauck et al., 2023a; Mayot et al., 2024). In particular, two fCO_2 products were shown to overestimate the Southern Ocean CO_2 flux trend by 50 % and 130 % based on current sampling in a model subsampling experiment (Hauck et al., 2023a), and the largest trends in the fCO_2 products occurred in a data-void region in the North Pacific (Mayot et al., 2024). In this respect it is highly worrisome that the coverage of fCO_2 observations continues to decline (Dong et al., 2024b) and is now down to that of the early 2000s (Fig. 11). Another likely contributor to the discrepancy between GOBMs and fCO_2 products constitutes model biases (as indicated by the comparison with Mayot et al. (2024); by the large model spread in the south, Fig. 14; and the larger model–data fCO_2 mismatch, Fig. S2).

The reported S_{OCEAN} estimate from GOBMs and fCO_2 products is $2.2 \pm 0.4\,GtC\,yr^{-1}$ over the period 1994 to 2007, which is in agreement with the ocean interior estimate of $2.2 \pm 0.4\,GtC\,yr^{-1}$, which in turn accounts for the climate effect on the natural CO_2 flux of $-0.4 \pm 0.24\,GtC\,yr^{-1}$ (Gruber et al., 2019) to match the definition of S_{OCEAN} used here (Hauck et al., 2020). This comparison depends critically on the estimate of the climate effect on the natural CO_2 flux, which is smaller from the GOBMs ($-0.1\,GtC\,yr^{-1}$) than in Gruber et al. (2019). Uncertainties in these two estimates would also overlap when using the GOBM estimate of the climate effect on the natural CO_2 flux. Similarly, the S_{OCEAN} estimates integrated over the decades 1994–2004 ($21.5\,GtC\,yr^{-1}$) and 2004–2014 ($25.6\,GtC\,yr^{-1}$) agree with the interior-ocean-based estimates of Müller et al. (2023; 21.4 ± 2.8 and $26.5 \pm 1.3\,GtC\,yr^{-1}$) but depend critically on assumptions of the climate effect on natural carbon, which, in turn, are based on the fCO_2 products in Müller et al. (2023).

3.6.3 Final year 2023

The estimated ocean CO_2 sink is $2.9 \pm 0.4\,GtC$ for 2023. This is a small increase of 0.16 GtC compared to 2022, in line with the expected sink strengthening from the 2023 El Niño conditions. GOBM and fCO_2-product ensemble mean estimates consistently result in an S_{OCEAN} increase in 2023 (GOBMs: $0.17 \pm 0.15\,GtC$; fCO_2 products: 0.14 [−0.04, 0.30] GtC). Eight GOBMs and six fCO_2 products show an increase in S_{OCEAN}, while only two GOBMs and two fCO_2 products show a minor decrease in S_{OCEAN} of less than 0.05 GtC (Fig. 11). The fCO_2 products have a larger uncertainty at the end of the reconstructed time series, potentially linked to uncertainties related to fewer available observations in the final year and the shift from La Niña to El Niño (see, for example, Watson et al., 2020; Pérez et al., 2024). Specifically, the fCO_2 products' estimate of the last year is regularly adjusted in the following release owing to the tail effect and incrementally increasing data availability. While the monthly grid cells covered may have a lag of only about a year (Fig. 11, lower right), the values within grid cells may change with a 1–5-year lag (see absolute number of observations plotted in previous GCB releases), potentially resulting in annual changes in the flux magnitude from fCO_2 products.

3.6.4 Year 2024 projection

Using a feed-forward neural network method (see Sect. 2.5.2), we project an ocean sink of 3.0 GtC for 2024, only 0.1 GtC higher than for the year 2023 and consistent with El Niño to neutral conditions in 2024. The set of ESM predictions supports this estimate with a 2024 ocean sink of around 3.0 [2.9, 3.1] GtC.

3.6.5 Evaluation of ocean models and fCO_2 products

The process-based model evaluation draws a generally positive picture, with GOBMs scattered around the observational values for Southern Ocean sea-surface salinity, the Southern Ocean stratification index, and the surface ocean Revelle factor (Sect. S3.3 and Table S11). However, the Atlantic Meridional Overturning Circulation at 26° N is underestimated by 8 out of 10 GOBMs and overestimated by 1 GOBM. It is planned to derive skill scores for the GOBMs in future releases based on these metrics.

The model simulations allow us to separate the anthropogenic carbon component (steady-state and non-steady-state, sim D − sim A) and to compare the model flux and dissolved inorganic carbon (DIC) inventory change directly to the interior-ocean estimate of Gruber et al. (2019) without further assumptions (Table S11). The GOBM ensemble average of anthropogenic carbon inventory changes in 1994–2007 amounts to $2.4\,GtC\,yr^{-1}$ and is thus lower than the $2.6 \pm 0.3\,GtC\,yr^{-1}$ estimated by Gruber et al. (2019) although within the uncertainty. Only three models fall within the range reported by Gruber et al. (2019). This suggests that the majority of the GOBMs may underestimate anthropogenic carbon uptake by 10 %–20 % and some models even more. Comparison to the decadal estimates of anthropogenic carbon accumulation (Müller et al., 2023) are close to the estimate based on interior-ocean data for the decade 2004–2014 (GOBMs, sim D minus sim A, $24.7 \pm 3.6\,GtC\,yr^{-1}$; Müller et al. (2023), $27.3 \pm 2.5\,GtC\,yr^{-1}$), but they do not reproduce the supposedly higher anthropogenic carbon accumulation in the earlier period 1994–2004 (GOBMs, sim D minus sim A, $21.1 \pm 3.0\,GtC\,yr^{-1}$; Müller et al. (2023), $29.3 \pm 2.5\,GtC\,yr^{-1}$). Analysis of Earth system models indicates that an underestimation by about 10 % may be due to biases in ocean carbon transport and mixing from the surface mixed layer to the ocean interior (Goris et al., 2018; Terhaar et al., 2021; Bourgeois et al., 2022; Terhaar et al., 2022), biases in the chemical buffer capacity (Revelle factor) of the ocean (Vaittinada Ayar et al., 2022; Terhaar et al., 2022), and partly a late starting date of the simulations (mirrored in atmospheric CO_2 chosen for the pre-industrial control simula-

tion, Table S2; Bronselaer et al., 2017; Terhaar et al., 2022, 2024). Interestingly, and in contrast to the uncertainties in the surface CO_2 flux, we find the largest mismatch in interior-ocean carbon accumulation in the tropics, with smaller contributions from the north and the south. The large discrepancy in accumulation in the tropics highlights the role of interior-ocean carbon redistribution for those inventories (Khatiwala et al., 2009; DeVries et al., 2023).

The evaluation of the ocean estimates with the fCO_2 observations from the SOCAT v2024 dataset for the period 1990–2023 shows an RMSE from annually detrended data of 0.2 to 2.4 µatm for the eight fCO_2 products over the globe (Fig. S2). The GOBM RMSEs are larger and range from 2.7 to 4.9 µatm. The RMSEs are generally larger at high latitudes compared to the tropics for both the fCO_2 products and the GOBMs. The fCO_2 products have RMSEs of 0.3 to 2.9 µatm in the tropics, 0.6 to 2.4 µatm in the north, and 0.8 to 2.4 µatm in the south. Note that the fCO_2 products are based on the SOCAT v2024 database; hence SOCAT is not an independent dataset for the evaluation of the fCO_2 products. The GOBM RMSEs are more spread across regions, ranging from 2.4 to 3.9 µatm in the tropics, 2.8 to 5.9 µatm in the north, and 2.7 to 6.0 µatm in the south. The higher RMSEs occur in regions with stronger climate variability, such as the northern and southern high latitudes (polewards of the subtropical gyres). Additionally, this year we evaluate the trends derived from a subset of fCO_2 products by subsampling four GOBMs used in Friedlingstein et al. (2023; covering the period up to the year 2022) following the approach of Hauck et al. (2023a) and evaluating the air–sea CO_2 flux trend for the 2001–2021 period, i.e. the period of strong divergence in the air–sea CO_2 exchange excluding the final year to remove the tail effect, against trend biases identified by the GOBM reconstruction. The results indicate a relationship between reconstruction bias and the strength of the decadal trends (see Fig. S3), indicating a tendency of the fCO_2-product ensemble to overestimate the air–sea CO_2 flux trends, in agreement with a recent study by Mayot et al. (2024).

3.7 Land sink

3.7.1 Historical period 1850–2023

Cumulated since 1850, the terrestrial carbon sink amounts to 220 ± 60 GtC, 31 % of total anthropogenic emissions, with more than two-thirds of this amount (150 ± 40 GtC) being taken up by the terrestrial ecosystems since 1960. Over the historical period, the land sink increased in pace with the anthropogenic emissions exponential increase (Fig. 3).

3.7.2 Recent period 1960–2023

The terrestrial CO_2 sink S_{LAND} increased from 1.2 ± 0.5 GtC yr^{-1} in the 1960s to 3.2 ± 0.9 GtC yr^{-1} during 2014–2023, with important interannual variations of up to 2 GtC yr^{-1} generally showing a decreased land sink during El Niño events (Fig. 9) that is responsible for the corresponding enhanced growth rate in atmospheric CO_2 concentration. The larger land CO_2 sink during 2014–2023 compared to the 1960s is reproduced by all the DGVMs in response to the increase in both atmospheric CO_2 and nitrogen deposition and the changes in climate, and it is consistent with the residual estimated from the other budget terms ($E_{FOS} + E_{LUC} - G_{ATM} - S_{OCEAN}$, Table 5).

Over the period of 1960 to the present, the increase in the global terrestrial CO_2 sink is largely attributed to the CO_2 fertilization effect (Prentice et al., 2001; Piao et al., 2009; Schimel et al., 2015) and increased nitrogen deposition (Huntzinger et al., 2017; O'Sullivan et al., 2019), directly stimulating plant photosynthesis and increased plant water use in water-limited systems with a small negative contribution of climate change (Fig. 12). There is a range of evidence to support a positive terrestrial carbon sink in response to increasing atmospheric CO_2, albeit with uncertain magnitude (Walker et al., 2021). As expected from theory, the greatest CO_2 effect is simulated in the tropical forest regions, associated with warm temperatures and long growing seasons (Hickler et al., 2008) (Fig. 12a). However, evidence from tropical intact forest plots indicates an overall decline in the land sink across Amazonia (1985–2011), attributed to enhanced mortality offsetting productivity gains (Brienen et al., 2015; Hubau et al., 2020). During 2014–2023 the land sink is positive in all regions (Fig. 6) with the exception of eastern Brazil, Bolivia, northern Venezuela, the southwestern USA, central Europe and Central Asia, northern and southern Africa, and eastern Australia, where the negative effects of climate variability and change (i.e. reduced rainfall and/or increased temperature) counterbalance CO_2 effects. This is clearly visible in Fig. 12, where the effects of CO_2 (Fig. 12a) and climate (Fig. 12b) as simulated by the DGVMs are isolated. The negative effect of climate can be seen across the globe and is particularly strong in most of South America, Central America, the southwestern USA, central Europe, the western Sahel, southern Africa, Southeast Asia and southern China, and eastern Australia (Fig. 12b). Globally, over the 2014–2023 period, climate change reduces the land sink by 0.87 ± 0.56 GtC yr^{-1} (27 % of S_{LAND}).

Most DGVMs have similar S_{LAND} values averaged over 2014–2023: 14 out of 20 models fall within the 1σ range of the residual land sink (1.8–3.7 GtC yr^{-1}) (see Table 5), and all models but 1 are within the 2σ range (0.8–4.6 GtC yr^{-1}). The ED model is an outlier, with a land sink estimate of 5.1 GtC yr^{-1} for the 2014–2023 period, driven by a strong CO_2 fertilization effect (6.3 GtC yr^{-1} in the CO_2-only (S1) simulation). There are no direct global observations of the land sink (S_{LAND}) or the CO_2 fertilization effect, and so we are not yet in a position to rule out models based on component fluxes if their net land sink ($S_{LAND} - E_{LUC}$) is within the observational uncertainty provided by atmospheric inversions or O_2 measurements (Table 5). Furthermore, DGVMs were compared against an analysis based on

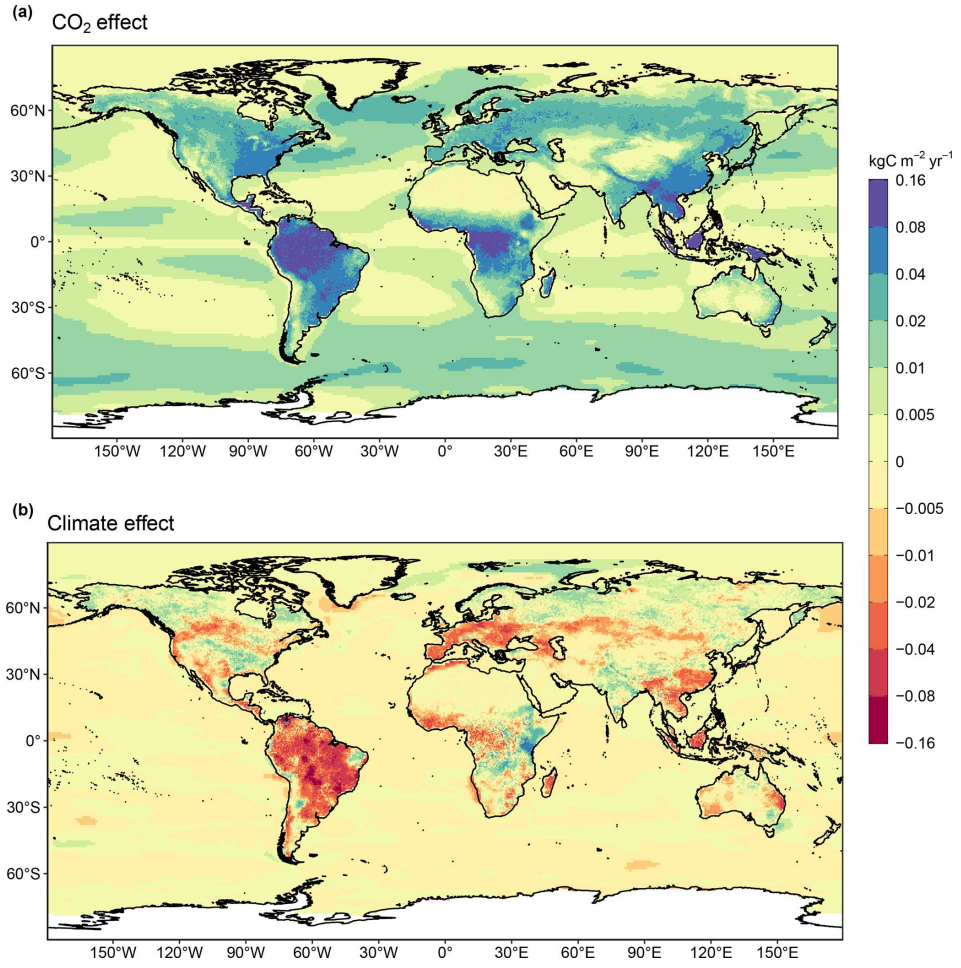

Figure 12. Attribution of the atmosphere–ocean (S_{OCEAN}) and atmosphere–land (S_{LAND}) CO_2 fluxes to **(a)** increasing atmospheric CO_2 concentrations and **(b)** changes in climate, averaged over the previous decade 2014–2023. All data shown are from the processed-based GOBMs and DGVMs. Note that the sum of ocean CO_2 and climate effects shown here will not equal the ocean sink shown in Fig. 6, which includes the fCO_2 products. See the Supplement, Sects. S3.2 and S4.1, for the attribution methodology. Units are in kgC m^{-2} yr^{-1} (note the non-linear colour scale). Positive values (blue) are CO_2 sinks; negative values (red) are CO_2 sources.

model–data fusion of the land carbon cycle (CARDAMOM) (Bloom and Williams, 2015; Bloom et al., 2016). Results suggest good correspondence between approaches at interannual timescales but divergence in the recent trend in S_{LAND}, with CARDAMOM simulating a stronger trend than the DGVM multi-model mean (Fig. 9).

Since 2020 the globe has experienced La Niña conditions, which would be expected to lead to an increased land carbon sink. This 3-year-long period of La Niña conditions came to an end by the second half of 2023 and transitioned to an El Niño that lasted until mid-2024. A clear transition from a maximum to a minimum in the global land sink is evident in S_{LAND} from 2022 to 2023, and we find that an El Niño-driven decrease in the tropical land sink is offset by a smaller increase in the high-latitude land sink. In the past years, several regions have experienced record-setting fire events (see also Sect. 3.8.3). While the global burned area has declined over the past decades mostly due to declining fire activity in savannas (Andela et al., 2017), forest fire emissions are rising and have the potential to counter the negative fire trend in savannas (Zheng et al., 2021). Noteworthy extreme fire events include the 2019–2020 Black Summer event in Australia (emissions of roughly 0.2 GtC; van der Velde et al., 2021); fires in Siberia in 2021, where emissions approached 0.4 GtC or 3 times the 1997–2020 average according to GFED4.1s; and fires in Canada in 2023 (Byrne et al., 2024a). While other regions, including the western USA and Mediterranean Europe, also experienced intense fire seasons in 2021, their emissions are substantially lower.

Despite these regional negative effects of climate change on S_{LAND}, the efficiency of land to remove anthropogenic CO_2 emissions has remained broadly constant over the last 6 decades, with a land-borne fraction ($S_{LAND}/(E_{FOS} + E_{LUC})$) of around 30 % (Fig. 10b).

3.7.3 Final year 2023

The terrestrial CO_2 sink from the DGVM ensemble S_{LAND} was 2.3 ± 1.0 GtC in 2023, 41 % below the 2022 La Niña-induced strong sink of 3.9 ± 1.0 GtC and also below the 2014–2023 average of 3.2 ± 0.9 GtC yr^{-1} (Fig. 4, Table 7). We estimate that the 2023 land sink was the lowest since 2015. The severe reduction in the land sink in 2023 is likely driven by the El Niño conditions, leading to a 58 % reduction in S_{LAND} in the tropics (30° N–30° S) from 2.8 GtC in 2022 to 1.2 GtC in 2023. This is combined with intense wildfires in Canada that led to a significant CO_2 source (see also Sect. 3.8.3). We note that the S_{LAND} DGVM estimate for 2023 of 2.3 ± 1.0 GtC is very similar to the 2.2 ± 1.0 GtC yr^{-1} estimate from the residual sink from the global budget ($E_{FOS} + E_{LUC} - G_{ATM} - S_{OCEAN}$, Table 5).

3.7.4 Year 2024 projection

Using a feed-forward neural network method, we project a land sink of 3.2 GtC for 2024, 0.9 GtC larger than the 2023 estimate. As for the ocean sink, we attribute this to the transition from the El Niño conditions in 2023 to a neutral state. The ESMs do not provide an additional estimate of S_{LAND} as they only simulate the net atmosphere–land carbon flux ($S_{LAND} - E_{LUC}$).

3.7.5 Evaluation of land models

The evaluation of the DGVMs shows generally higher agreement across models for runoff and to a lesser extent for gross primary production (GPP) and ecosystem respiration. These conclusions are supported by a more comprehensive analysis of DGVM performance in comparison with benchmark data (Sitch et al., 2024). A relative comparison of DGVM performance (Fig. S4) suggests several DGVMs (CABLE-POP, CLASSIC, OCN, ORCHIDEE) may outperform others in terms of multiple carbon and water cycle benchmarks. However, results from Seiler et al. (2022) also show how DGVM differences are often of similar magnitude compared with the range across observational datasets. All models score high enough over the metrics tests to support their use here. There are a few anomalously low scores for individual metrics from a single model, and these can direct the effort to improve models for use in future budgets.

3.8 Partitioning the carbon sinks

3.8.1 Global sinks and spread of estimates

In the period 2014–2023, the bottom-up view of global net ocean and land carbon sinks provided by the GCB, S_{OCEAN} for the ocean and $S_{LAND} - E_{LUC}$ for the land, agrees closely with the top-down global carbon sinks delivered by the atmospheric inversions. This is shown in Fig. 13, which visualizes the individual decadal mean atmosphere–land and atmosphere–ocean fluxes from each, along with the constraints on their sum offered by the global fossil CO_2 emissions flux minus the atmospheric growth rate ($E_{FOS} - G_{ATM}$, 4.4 ± 0.5 GtC yr^{-1}, Table 7, shown as diagonal line in Fig. 13). The GCB estimate for net atmosphere-to-surface flux ($S_{OCEAN} + S_{LAND} - E_{LUC}$) during 2014–2023 is 4.9 ± 1.2 GtC yr^{-1} (Table 7), with the difference from the diagonal representing the budget imbalance (B_{IM}) of 0.4 GtC yr^{-1}, discussed in Sect. 3.9. By virtue of the inversion methodology, the atmospheric inversion estimate of the net atmosphere-to-surface flux during 2014–2023 is 4.5 GtC yr^{-1}, with a < 0.1 GtC yr^{-1} imbalance and thus scatter across the diagonal, with inverse models trading land for ocean fluxes in their solution. The independent constraint on the net atmosphere-to-surface flux based on atmospheric O_2 by design also closes the balance and is 4.5 ± 0.9 GtC yr^{-1} over the 2014–2023 period (orange symbol in Fig. 13), while the ESM estimate for the net atmosphere-to-surface flux over that period averages to 4.7 [3.0, 5.8] GtC yr^{-1} (Tables 5 and 6).

The distributions based on the individual models and fCO_2 products reveal substantial spread but converge near the decadal means quoted in Tables 5 to 7. Sink estimates for S_{OCEAN} and from inverse systems are mostly non-Gaussian, while the ensemble of DGVMs appears more normally distributed, justifying the use of a multi-model mean and standard deviation for their errors in the budget. Noteworthy is that the tails of the distributions provided by the land and ocean bottom-up estimates would not agree with the global constraint provided by the fossil fuel emissions and the observed atmospheric CO_2 growth rate. This illustrates the power of the atmospheric joint constraint from G_{ATM} and the global CO_2 observation network it is derived from.

Net atmosphere-to-land flux

The GCB estimate of the net atmosphere-to-land flux ($S_{LAND} - E_{LUC}$), calculated as the difference between S_{LAND} from the DGVMs and E_{LUC} from the bookkeeping models, amounts to a 2.1 ± 1.1 GtC yr^{-1} sink during 2014–2023 (Table 5). Estimates of net atmosphere-to-land flux ($S_{LAND} - E_{LUC}$) from the DGVMs alone (1.7 ± 0.6 GtC yr^{-1}, Table 5, green symbols in Fig. 13) are slightly lower, although within the uncertainty in the GCB estimate and also within uncertainty in the global carbon budget constraint ($E_{FOS} - G_{ATM} - S_{OCEAN}$, 1.6 ± 0.6 GtC yr^{-1}, Table 7). Also, for 2014–2023, the inversions estimate that the net atmosphere-to-land flux is a 1.4 [0.3, 2.2] GtC yr^{-1} sink, slightly lower than the mean of the DGVM estimates (purple versus green symbols in Fig. 13). The independent constraint based on atmospheric O_2 is even lower, 1.0 ± 0.8 GtC yr^{-1} (orange symbol in Fig. 13), although its large uncertainty overlaps with the uncertainty range from other approaches. Lastly, the ESM estimate for the net atmosphere-to-land flux during 2014–

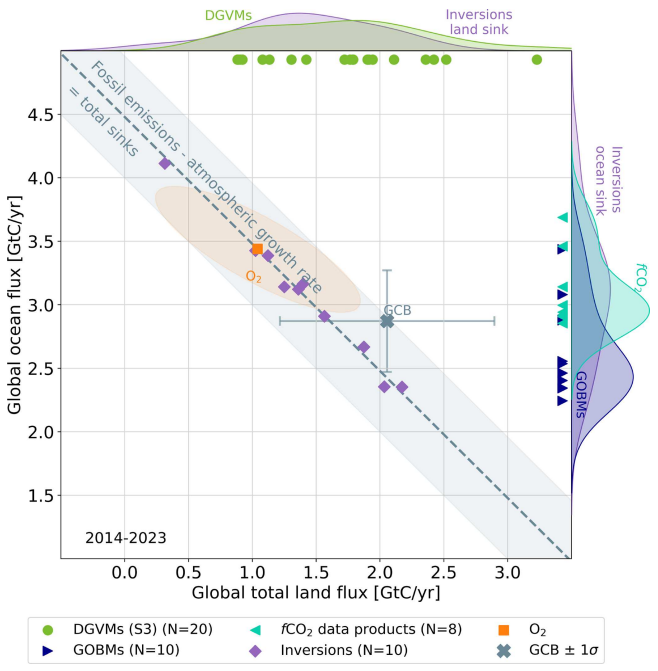

Figure 13. The 2014–2023 decadal mean global net atmosphere–ocean and atmosphere–land fluxes derived from the ocean models and fCO_2 products (y axis, right- and left-pointing blue triangles, respectively) and from the DGVMs (x axis, green symbols), and the same fluxes estimated from the atmospheric inversions (purple symbols). The shaded distributions show the densities of the ensembles of individual estimates. The grey central cross is the mean ($\pm 1\sigma$) of S_{OCEAN} and $S_{LAND} - E_{LUC}$ as assessed in this budget. The diagonal grey line represents the constraint on the global land + ocean net flux, i.e. global fossil fuel emissions minus the atmospheric growth rate from this budget ($E_{FOS} - G_{ATM}$). The orange square represents the same global net atmosphere–ocean and atmosphere–land fluxes as estimated from the atmospheric O_2 constraint (the ellipse drawn around the central atmospheric O_2 estimate is a contour representing the 1σ uncertainty in the land and ocean fluxes as a joint probability distribution). Positive values are CO_2 sinks. Note that the inverse estimates have been scaled for a minor difference between E_{FOS} and GridFEDv2024.0 (Jones et al., 2024a).

2023 is a 2.2 [0.3, 3.6] GtC yr^{-1} sink, more consistent with the GCB estimates of $S_{LAND} - E_{LUC}$ (Fig. 14, top row).

As discussed in Sect. 3.5.3, the atmospheric growth rate of CO_2 was very high in 2023, 5.9 GtC (2.79 ppm) the fourth largest on record. Both DGVMs and inversions assign this large CO_2 growth rate to a severe decrease in the net atmosphere-to-land flux, in particular in the tropics (Fig. 14). DGVMs simulate a 2023 global net atmosphere-to-land flux of 1.1 GtC yr^{-1}, a 55 % decline relative to the 2.4 GtC yr^{-1} sink in 2022, primarily driven by the severe reduction in S_{LAND} (−41 %; see Sect. 3.7.3). The tropics (30° N–30° S) are recording a dramatic decrease in the net atmosphere-to-land flux from 1.5 GtC yr^{-1} in 2022 to 0.1 GtC yr^{-1} in 2023. The atmospheric inversion shows a similar story, with the global net atmosphere-to-land flux declining from 2.6 GtC yr^{-1} in 2022 to 0.9 GtC yr^{-1} in 2023 (−64 %) and the tropics turning from a 1.0 GtC yr^{-1} sink in 2022 to a 0.4 GtC yr^{-1} source in 2023. Our results are broadly consistent with the Ke et al. (2024) study, which reported a global atmosphere-to-land flux of 0.4 ± 0.2 GtC yr^{-1} in 2023.

In addition to the large decline in the tropical land uptake, the northern extra-tropics experienced warmer-than-average conditions, in particular in the summer over North America and northern Eurasia. In Canada alone, 2023 led to enhanced CO_2 release due to fires of 0.5–0.8 GtC yr^{-1} (see Sect. 3.8.3). The atmospheric inversions do simulate a slight reduction in the atmosphere-to-land flux in the northern extra-tropics (north of 30° N), from 1.6 GtC yr^{-1} in 2022 to 1.4 GtC yr^{-1} in 2023, while the DGVMs fail to capture this pattern, with a simulated northern extra-tropics net atmosphere-to-land flux larger in 2023 than in 2022 (1.0 vs. 0.7 GtC yr^{-1}).

Net atmosphere-to-ocean flux

For the 2014–2023 period, the GOBMs (2.6 ± 0.4 GtC yr^{-1}) produce a lower estimate for S_{OCEAN} than the fCO_2 products, with 3.1 [2.9, 3.7] GtC yr^{-1}, which shows up in Fig. 13 as separate peaks in the distribution from the GOBMs (dark-blue symbols) and from the fCO_2 products (light-blue symbols). Atmospheric inversions (3.1 [2.4, 4.1] GtC yr^{-1}) suggest an ocean uptake more in line with the fCO_2 products for the recent decade (Table 7), although the inversions' range includes both the GOBM and the fCO_2-product estimates (Fig. 14, top row) and the inversions are not fully independent as 6 out of 10 inversions covering the last decade use fCO_2 products as ocean priors and one uses a GOBM (Table S4). The independent constraint based on atmospheric O_2 (3.4 ± 0.5 GtC yr^{-1}) is at the high end of the distribution of the other methods. However, as mentioned in Sect. 2.8, the O_2 method requires a correction for global air–sea O_2 flux, which induces a non-negligible uncertainty in the decadal estimates (about 0.5 GtC yr^{-1}). The large growth in the ocean carbon sink from O_2 is compatible with the GOBM and fCO_2-product estimates when accounting for their uncertainty ranges. Lastly, the ESM estimate, 2.5 [2.2, 2.8] GtC yr^{-1}, suggests a moderate ocean carbon sink, comparable to the GOBM estimate with regard to mean and spread. We caution that the riverine transport of carbon taken up on land and outgassing from the ocean, accounted for here, is a substantial (0.65 ± 0.3 GtC yr^{-1}) and uncertain term (Crisp et al., 2022; Gruber et al., 2023; DeVries et al., 2023) that separates the GOBM, ESM, and oxygen-based estimates on the one hand from the fCO_2 products and atmospheric inversions on the other hand.

3.8.2 Regional partitioning

Figure 14 shows the latitudinal partitioning of the global atmosphere-to-ocean flux (S_{OCEAN}) and atmosphere-to-land flux ($S_{LAND} - E_{LUC}$) and their sum ($S_{OCEAN} + S_{LAND} -$

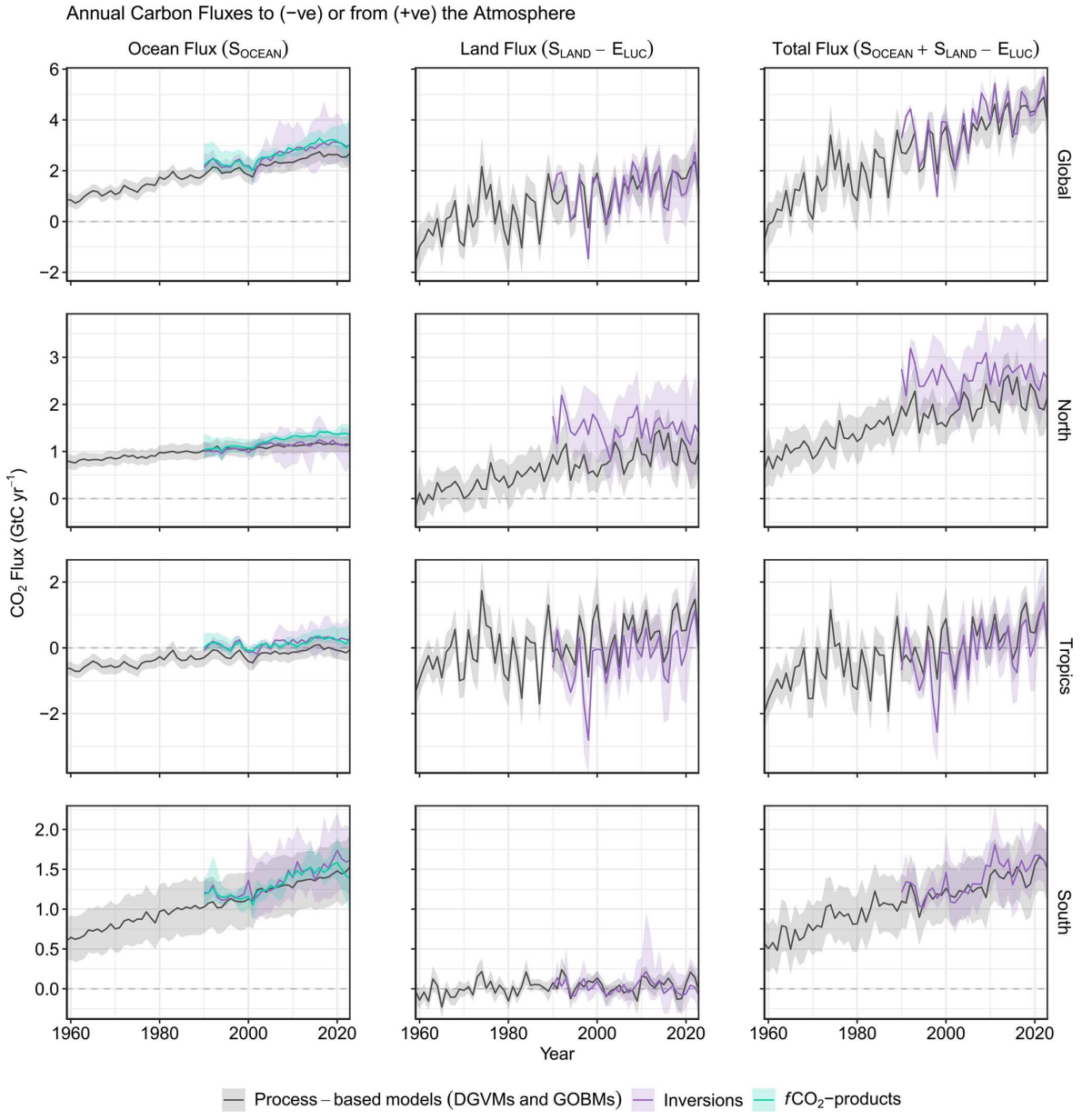

Figure 14. CO_2 fluxes between the atmosphere and the Earth's surface separated between land and oceans, globally and in three latitude bands. The ocean flux is S_{OCEAN}, and the land flux is the net atmosphere–land fluxes from the DGVMs. The latitude bands are (top row) global, (second row) north ($> 30°$ N), (third row) tropics (30° S–30° N), and (bottom row) south ($< 30°$ S), and the surface categories are over ocean (left column), over land (middle column), and total (right column). Estimates are shown for process-based models (DGVMs for land, GOBMs for oceans), inversion systems (land and ocean), and fCO_2 products (ocean only). Positive values are CO_2 sinks. Mean estimates from the combination of the process models for the land and oceans are shown (black line) with $\pm 1\sigma$ of the model ensemble (grey shading). For the total uncertainty in the process-based estimate of the total sink, uncertainties are summed in quadrature. Mean estimates from the atmospheric inversions are shown (purple lines) with their full spread (purple shading). Mean estimates from the fCO_2 products are shown for the ocean domain (light-blue lines) with full model spread (light-blue shading). The global S_{OCEAN} (upper left) and the sum of S_{OCEAN} in all three regions represent the anthropogenic atmosphere-to-ocean flux based on the assumption that the pre-industrial ocean sink was $0\,GtC\,yr^{-1}$ when riverine fluxes are not considered. This assumption does not hold at the regional level, where pre-industrial fluxes can be significantly different from zero. Hence, the regional panels for S_{OCEAN} represent a combination of natural and anthropogenic fluxes. Bias correction and area weighting were only applied to global S_{OCEAN}; hence the sum of the regions is slightly different from the global estimate ($< 0.07\,GtC\,yr^{-1}$).

E_{LUC}) according to the estimates from GOBMs and ocean fCO_2 products (S_{OCEAN}), DGVMs ($S_{LAND} - E_{LUC}$), and atmospheric inversions (S_{OCEAN} and $S_{LAND} - E_{LUC}$).

North

Despite being one of the most densely observed and studied regions of our globe, annual mean carbon sink estimates in the northern extra-tropics (north of 30° N) continue to differ. The atmospheric inversions suggest an atmosphere-to-surface sink ($S_{OCEAN} + S_{LAND} - E_{LUC}$) for 2014–2023 of 2.6 [2.0, 3.4] GtC yr^{-1}, which is slightly higher than the process models' estimate of 2.2 ± 0.4 GtC yr^{-1} (Fig. 14). The GOBMs (1.2 ± 0.2 GtC yr^{-1}), fCO_2 products (1.4 [1.3, 1.5] GtC yr^{-1}), and inversion systems (1.2 [0.9, 1.4] GtC yr^{-1}) produce largely consistent estimates of the ocean sink. However, the larger flux in the fCO_2 products may be related to data sparsity (Mayot et al., 2024). Thus, the difference mainly arises from the net land flux ($S_{LAND} - E_{LUC}$) estimate, which is 1.0 ± 0.4 GtC yr^{-1} in the DGVMs compared to 1.5 [0.6, 2.3] GtC yr^{-1} in the atmospheric inversions (Fig. 14, second row).

Discrepancies in the northern land fluxes conform with persistent issues surrounding the quantification of the drivers of the global net land CO_2 flux (Arneth et al., 2017; Huntzinger et al., 2017; O'Sullivan et al., 2022) and the distribution of atmosphere-to-land fluxes between the tropics and high northern latitudes (Baccini et al., 2017; Schimel et al., 2015; Stephens et al., 2007; Ciais et al., 2019; Gaubert et al., 2019).

In the northern extra-tropics, the process models, inversions, and fCO_2 products consistently suggest that most of the interannual variability stems from the land (Fig. 14). Inversions generally agree on the magnitude of interannual variations (IAVs) over land, more so than DGVMs (0.29–0.32 vs. 0.14–0.63 GtC yr^{-1}, averaged over 1990–2023).

Tropics

In the tropics (30° S–30° N), both the atmospheric inversions and the process models estimate a net carbon balance ($S_{OCEAN} + S_{LAND} - E_{LUC}$) that has been relatively close to neutral over the past decade (inversions: 0.3 [−0.4, 0.9] GtC yr^{-1}; process models: 0.6 ± 0.6 GtC yr^{-1}). The GOBMs (-0.03 ± 0.3 GtC yr^{-1}), fCO_2 products (0.3 [0.1, 0.6] GtC yr^{-1}), and inversion systems (0.3 [−0.1, 0.8] GtC yr^{-1}) indicate a neutral to positive tropical ocean flux (see Fig. S1 for spatial patterns). DGVMs indicate a net land sink ($S_{LAND} - E_{LUC}$) of 0.6 ± 0.4 GtC yr^{-1}, whereas the inversion systems indicate a neutral net land flux although with large model spread (−0.0 [−0.9, 0.8] GtC yr^{-1}, Fig. 14, third row).

The tropical lands are the origin of most of the atmospheric CO_2 interannual variability (Ahlström et al., 2015) consistently among the process models and inversions (Fig. 14). The interannual variability in the tropics is similar among the ocean fCO_2 products (0.06–0.16 GtC yr^{-1}) and the GOBMs (0.07–0.16 GtC yr^{-1}, Fig. S2). The DGVMs and inversions indicate that atmosphere-to-land CO_2 fluxes are more variable than atmosphere-to-ocean CO_2 fluxes in the tropics, with interannual variability of 0.37–1.33 and 0.86–0.96 GtC yr^{-1} for DGVMs and inversions, respectively.

South

In the southern extra-tropics (south of 30° S), the atmospheric inversions suggest a net atmosphere-to-surface sink ($S_{OCEAN} + S_{LAND} - E_{LUC}$) for 2014–2023 of 1.5 [1.2, 1.9] GtC yr^{-1}, identical to the process models' estimate of 1.5 ± 0.4 GtC yr^{-1} (Fig. 14). An approximately neutral net land flux ($S_{LAND} - E_{LUC}$) for the southern extra-tropics is estimated by both the DGVMs (0.05 ± 0.1 GtC yr^{-1}) and the inversion systems (−0.03 [−0.11, 0.08] GtC yr^{-1}). This means nearly all carbon uptake is due to oceanic sinks south of 30° S. The Southern Ocean flux in the fCO_2 products (1.5 [1.3, 1.7] GtC yr^{-1}) and inversion estimates (1.6 [1.2, 1.9] GtC yr^{-1}) is marginally higher than in the GOBMs (1.4 ± 0.4 GtC yr^{-1}) (Fig. 14, bottom row). This agreement is subject to the choice of the river flux adjustment (Lacroix et al., 2020; Hauck et al., 2023b). Nevertheless, the time series of atmospheric inversions and fCO_2 products diverge from those of the GOBMs. A substantial overestimation of the trends in the fCO_2 products could be explained by sparse and unevenly distributed observations, especially in wintertime (Fig. S1; Hauck et al., 2023a; Gloege et al., 2021). Model biases may contribute as well, with biases in mode water formation, stratification, and the chemical buffer capacity known to play a role in Earth system models (Terhaar et al., 2021; Bourgeois et al., 2022; Terhaar et al., 2022).

The interannual variability in the southern extra-tropics is low because of the dominance of ocean areas with low variability compared to land areas. The split between land ($S_{LAND} - E_{LUC}$) and ocean (S_{OCEAN}) shows a substantial contribution to variability in the south coming from the land, with no consistency between the DGVMs and the inversions or among inversions. This is expected due to the difficulty of precisely separating the land and oceanic fluxes when viewed from the perspective of atmospheric observations alone. The S_{OCEAN} interannual variability was found to be higher in the fCO_2 products (0.04–0.20 GtC yr^{-1}) compared to GOBMs (0.04–0.06 GtC yr^{-1}) in 1990–2023 (Fig. S2). Inversions give an interannual variability of 0.10 to 0.13 GtC yr^{-1}. Model subsampling experiments recently illustrated that fCO_2 products may overestimate decadal variability in the Southern Ocean carbon sink by 30 % and the trend since 2000 by 50 %–130 % due to data sparsity, based on fCO_2 products with strong variability (Gloege et al., 2021; Hauck et al., 2023a). The trend benchmark test using the method of Hauck et al. (2023a) and a subset of six fCO_2 products confirms the sensitivity of the decadal trends

in fCO_2 products to reconstruction biases, particularly in the Southern Ocean, indicating an overestimation of the ensemble mean trend. However, we also find compensatory positive biases in the ensemble, so the ensemble mean bias is smaller than the bias from some individual fCO_2 products.

RECCAP-2 regions

Aligning with the RECCAP-2 initiative (Ciais et al., 2022; Poulter et al., 2022; DeVries et al., 2023), we provide a breakdown of this GCB paper estimate of the E_{LUC}, S_{LAND}, net land ($S_{LAND} - E_{LUC}$), and S_{OCEAN} fluxes over the 10 land and 5 ocean RECCAP-2 regions, averaged over the period 2014–2023 (Fig. 15). The DGVMs and inversions suggest a positive net land sink in all regions, except for South America and Africa, where the inversions indicate a small net source of -0.1 [-0.8, 0.3] GtC yr^{-1} and -0.3 [-0.7, -0.1] GtC yr^{-1}, respectively, compared to a small sink of 0.1 ± 0.3 GtC yr^{-1} and 0.3 ± 0.1 GtC yr^{-1} for the DGVMs. However, for South America, there is substantial uncertainty in both products (ensembles span zero). For the DGVMs, this is driven by uncertainty in both S_{LAND} (0.5 ± 0.4 GtC yr^{-1}) and E_{LUC} (0.4 ± 0.2 GtC yr^{-1}). The bookkeeping models also suggest an E_{LUC} source of around 0.4 GtC yr^{-1} in South America and Africa, in line with the DGVM estimates. Bookkeeping models and DGVMs similarly estimate a source of 0.3–0.4 GtC yr^{-1} in Southeast Asia, with DGVMs suggesting a small net land sink (0.1 ± 0.1 GtC yr^{-1}). This is similar to the inversion mean estimate of a 0.1 [-0.3, 0.8] GtC yr^{-1} sink, although the inversion spread is substantial. The inversions suggest the largest net land sinks are located in North America (0.5 [-0.1, 1.0] GtC yr^{-1}), Russia (0.6 [0.1, 0.9] GtC yr^{-1}), and East Asia (0.4 [-0.2, 1.3] GtC yr^{-1}). This agrees well with the DGVMs in North America (0.4 ± 0.1 GtC yr^{-1}), which indicate a large natural land sink (S_{LAND}) of 0.6 ± 0.2 GtC yr^{-1}, being slightly reduced by land-use-related carbon losses (0.2 ± 0.1 GtC yr^{-1}). The DGVMs suggest a smaller net land sink in Russia compared to inversions (0.3 ± 0.2 GtC yr^{-1}) and a similar net sink in East Asia (0.2 ± 0.1 GtC yr^{-1}).

There is generally a higher level of agreement in the estimates of regional S_{OCEAN} between the different data streams (GOBMs, fCO_2 products, and atmospheric inversions) on a decadal scale compared to the agreement between the different land flux estimates. All data streams agree that the largest contribution to S_{OCEAN} stems from the Southern Ocean due to a combination of high flux density and large surface area, but with important contributions also from the Atlantic (high flux density) and Pacific (large area) basins. In the Southern Ocean, GOBMs suggest a sink of 1.0 ± 0.3 GtC yr^{-1}, in line with the fCO_2 products (1.0 [0.8, 1.3] GtC yr^{-1}) and atmospheric inversions (1.0 [0.7, 1.4] GtC yr^{-1}). There is similar agreement in the Pacific Ocean, with GOBMs, fCO_2 products, and atmospheric inversions indicating a sink of 0.6 ± 0.2 GtC yr^{-1}, 0.7 [0.6, 1.0] GtC yr^{-1}, and 0.6 [0.1, 1.0] GtC yr^{-1}, respectively. However, in the Atlantic Ocean, GOBMs simulate a sink of 0.5 ± 0.1 GtC yr^{-1}, noticeably lower than both the fCO_2 products (0.8 [0.7, 1.0] GtC yr^{-1}) and atmospheric inversions (0.7 [0.4, 1.1] GtC yr^{-1}). It is important to note the fCO_2 products and atmospheric inversions have a substantial and uncertain river flux adjustment in the Atlantic Ocean (0.3 GtC yr^{-1}) that also leads to a mean offset between GOBMs and fCO_2 products and inversions in the latitude band of the tropics (Fig. 14). The Indian Ocean, due to its smaller size, and the Arctic Ocean, due to its size and sea-ice cover that prevents air–sea gas exchange, are responsible for smaller but non-negligible S_{OCEAN} fluxes (Indian Ocean: 0.3 [0.2, 0.3] GtC yr^{-1}, 0.3 [0.3, 0.4] GtC yr^{-1}, and 0.4 [0.3, 0.6] GtC yr^{-1} for GOBMs, fCO_2 products, and atmospheric inversions, respectively; Arctic Ocean: 0.1 [0.1, 0.1] GtC yr^{-1}, 0.2 [0.1, 0.2] GtC yr^{-1}, and 0.1 [0.1, 0.2] GtC yr^{-1} for GOBMs, fCO_2 products, and atmospheric inversions, respectively). Note that the S_{OCEAN} numbers presented here deviate from numbers reported in RECCAP-2 where the net air–sea CO_2 flux is reported (i.e. without river flux adjustment for fCO_2 products and inversions and with river flux adjustment subtracted from GOBMs in most chapters or comparing unadjusted datasets with discussion of uncertain regional riverine fluxes as major uncertainty, e.g. Sarma et al., 2023; DeVries et al., 2023).

Tropical vs. northern land uptake

A continuing conundrum is the partitioning of the global atmosphere–land flux between the Northern Hemisphere land and the tropical land (Stephens et al., 2007; Pan et al., 2011; Gaubert et al., 2019). It is of importance because each region has its own history of land-use change, climate drivers, and the impact of increasing atmospheric CO_2 and nitrogen deposition. Quantifying the magnitude of each sink is a prerequisite to understanding how each individual driver impacts the tropical and mid- to high-latitude carbon balance.

We define the north–south (N–S) difference as net atmosphere–land flux north of 30° N minus the net atmosphere–land flux south of 30° N. For the inversions, the N–S difference is 1.50 [0.05, 3.0] GtC yr^{-1} across this year's inversion ensemble. An apparent clustering of six satellite-driven solutions towards a common NH land sink noted in GCB2023 is no longer clear.

In the ensemble of DGVMs the N–S difference is 0.4 ± 0.5 GtC yr^{-1}, a much narrower range than the one from atmospheric inversions. Only 3 out of 20 DGVMs have a N–S difference larger than 1.0 GtC yr^{-1}, compared to half of the inversion systems simulating a difference at least this large. The smaller spread across DGVMs compared to across inversions is to be expected as there is no correlation between northern and tropical land sinks in the DGVMs as opposed to the inversions where the sum of the two regions being well constrained by atmospheric observations leads to an anti-correlation between these two regions. This atmospheric N–

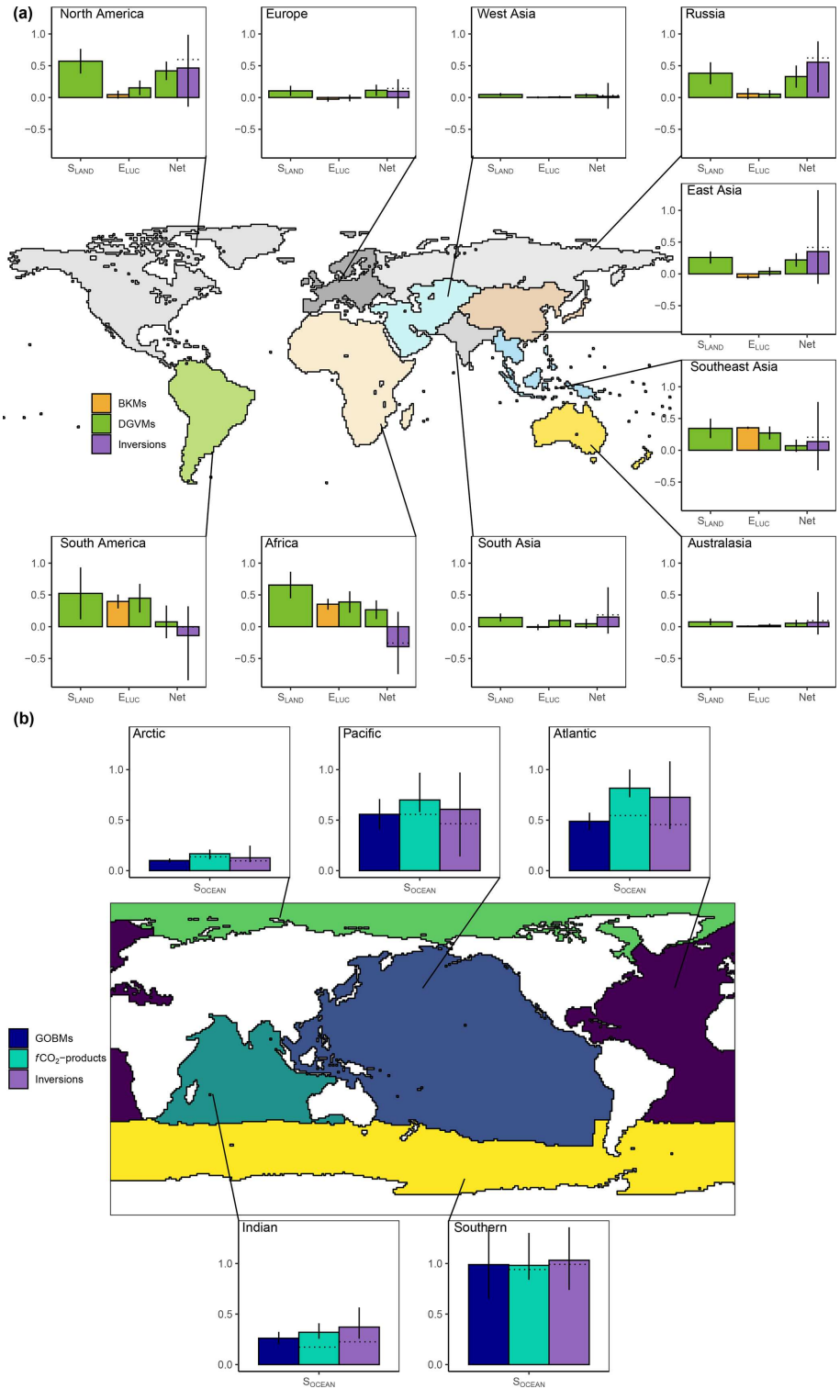

Figure 15. Decadal mean **(a)** land and **(b)** ocean fluxes for RECCAP-2 regions over 2014–2023. For land fluxes, S_{LAND} is estimated by the DGVMs (green bars), with the error bar as $\pm 1\sigma$ spread among models. A positive S_{LAND} is a net transfer of carbon from the atmosphere to the land. E_{LUC} fluxes are shown for both DGVMs (green) and bookkeeping models (orange), again with the uncertainty calculated as the $\pm 1\sigma$ spread. Note that a positive E_{LUC} flux indicates a loss of carbon from the land. The net land flux is shown for both DGVMs (green) and atmospheric inversions (purple), including the full model spread for inversions. The net ocean sink (S_{OCEAN}) is estimated by GOBMs (royal blue), $f\mathrm{CO}_2$ products (cyan), and atmospheric inversions (purple). Uncertainty is estimated as the $\pm 1\sigma$ spread for GOBMs and as the full model spread for the other two datasets. The dotted lines show the $f\mathrm{CO}_2$ products and inversion results without river flux adjustment. Positive values are CO_2 sinks.

S gradient could be used as an additional way to evaluate tropical and NH uptake in DGVMs if their fluxes were combined with multiple transport models. Vice versa, the much smaller spread in the N–S difference between the DGVMs could help in scrutinizing the inverse systems further. For example, a large northern land sink and a tropical land source in an inversion would suggest large sensitivity to CO_2 fertilization (the dominant factor driving the land sinks) for northern ecosystems, which would not be mirrored by tropical ecosystems. Such a combination could be hard to reconcile with the process understanding gained from the DGVM ensembles and independent measurements (e.g. free-air CO_2 enrichment (FACE) experiments).

3.8.3 Fire emissions in 2024

Fire emissions so far in 2024 have been above the average of recent decades, chiefly due to synchronous large emissions fluxes from North America and South America. Figure S9 shows global and regional emissions estimates for the period of 1 January–30 September in each year 2003–2024. Estimates are derived from two global fire emissions products: the Global Fire Emissions Database (GFED, version 4.1s; van der Werf et al., 2017) and the Global Fire Assimilation System (GFAS, operated by the Copernicus Atmosphere Monitoring Service; Kaiser et al., 2012). The two products estimate that global emissions from fires were 1.6–2.2 GtC yr^{-1} during January–September 2024. These estimates are 11 %–32 % above the 2014–2023 average for the same months (1.5–1.7 GtC yr^{-1}). In the GFED4.1s product, the year-to-date emissions in 2024 were at their highest since 2003, exceeding even the large emissions estimate of 2023, whereas the GFAS product showed lower emissions in 2024 than in 2023 and in six other years since 2003.

The pattern of high fire emissions from Canada in 2023, which were record-breaking (Jones et al., 2024b; Byrne et al., 2024a), continued into 2024. In January–September 2024, emissions from Canada (0.2–0.3 GtC yr^{-1}) were half as great as in the same months of 2023 (0.5–0.8 GtC yr^{-1}) but still 2.1–2.3 times the average of January–September periods in 2014–2023 (and 4–6 times greater than the average of those months in 2003–2022 (excluding the record-breaking year in 2023); Fig. S9). The continued anomaly in Canada propagated to the Northern Hemisphere, where emissions of 0.5–0.6 GtC yr^{-1} were 26 %–44 % above the average of 2014–2023.

In January–September 2024, fire emissions from South America (0.4–0.6 GtC yr^{-1}) were 94 %–164 % above the average of the January–September periods in 2014–2023, marking 2024 out as a year with synchronous high fire emissions across the Americas. Emissions from Brazil in January–September 2024 (0.2–0.3 GtC yr^{-1}) were 91 %–118 % above the average of January–September periods of 2014–2023 and were at a level not seen since the major drought year of 2010 (Fig. S9; Aragão et al., 2018; Silva Junior et al., 2019). In 2023, deforestation fire activity in the Brazilian Amazon was below the average levels recorded in national recording systems and is attributed to renewed environmental policy implementation; however the fall in Amazon deforestation fire activity was largely offset by above-average wildfires related to historic drought (Mataveli et al., 2024). According to the National Center for Monitoring and Early Warning of Natural Disasters (CEMADEN), drought conditions continued into 2024 and the current drought is the most intense and widespread that Brazil has experienced since records began in 1950 (CEMADEN, 2024), prompting large wildfire anomalies across the Amazon, Cerrado, and Pantanal regions (INPE, 2024).

Emissions anomalies in Africa strongly influence global totals because the continent typically contributed 41 %–47 % of global fire emissions during 2014–2023 (average of January–September periods). GFAS suggests that fire emissions in Africa through September 2024 (0.6 GtC yr^{-1}) were slightly below the average of 2014–2023, whereas GFED4.1s suggests that fire emissions through September 2024 were slightly above the average of 2014–2023 (0.8 GtC yr^{-1}).

Tropical fire emissions through September 2024 (1.1–1.6 GtC yr^{-1}) accounted for 69 %–74 % of the global total emissions, which is close to the average of the 2014–2023 period (1.1–1.2 GtC yr^{-1}; 72 %–75 %). This marks a return to a more typical distribution of fire emissions between the tropics and extra-tropics after the tropical contribution fell to just 55 %–59 % during January–September 2023 (Fig. S9).

We caution that the fire emissions fluxes presented here should not be compared directly with other fluxes of the budget (e.g. S_{LAND} or E_{LUC}) due to incompatibilities between the observable fire emissions fluxes and what is quantified in the S_{LAND} and E_{LUC} components of the budget. The fire emissions estimates from global fire products relate to all fire types that can be observed in Earth observations (Giglio et al., 2018; Randerson et al., 2012; Kaiser et al., 2012), including (i) fires occurring as part of natural disturbance–recovery cycles that would also have occurred in the pre-industrial period (Yue et al., 2016; Keeley and Pausas, 2019; Zou et al., 2019); (ii) fires occurring above and beyond natural disturbance–recovery cycle due to changes in climate, CO_2, and N fertilization and to an increased frequency of extreme drought and heatwave events (Abatzoglou et al., 2019; Jones et al., 2022; Zheng et al., 2021; Burton et al., 2024); and (iii) fires occurring in relation to land use and land-use change, such as deforestation fires and agricultural fires (van der Werf et al., 2010; Magi et al., 2012). In the context of the global carbon budget, only the portion of fire emissions associated with (ii) should be included in the S_{LAND} component, and fire emissions associated with (iii) should already be accounted for in the E_{LUC} component. Emissions associated with (i) should not be included in the global carbon budget. It is not currently possible to derive specific estimates for fluxes (i), (ii), and (iii) using global fire emissions products such as GFED or GFAS. In addition, the fire emis-

sions estimates from global fire emissions products represent a gross flux of carbon to the atmosphere, whereas the S_{LAND} component of the budget is a net flux that should also include post-fire recovery fluxes. Even if emissions from fires of type (ii) could be separated from those of type (i), these fluxes may be partially or wholly offset in subsequent years by post-fire fluxes as vegetation recovers, sequestering carbon from the atmosphere to the terrestrial biosphere (Yue et al., 2016; Jones et al., 2024c). Increases in forest fire emissions and severity (emissions per unit area) globally during the past 2 decades have highlighted the increasing potential for fire emissions fluxes to outweigh post-fire recovery fluxes, though long-term monitoring of vegetation recovery is required to quantify the net effect on terrestrial C storage (Jones et al., 2024c).

3.9 Closing the global carbon cycle

3.9.1 Partitioning of cumulative emissions and sink fluxes

Emissions during the period 1850–2023 amounted to 710 ± 70 GtC and were partitioned among the atmosphere (285 ± 5 GtC; 40 %), ocean (185 ± 35 GtC; 26 %), and land (220 ± 60 GtC; 32 %). The cumulative land sink is almost equal to the cumulative land-use emissions (225 ± 65 GtC), making the global land nearly neutral over the whole 1850–2023 period (Fig. 3).

The use of nearly independent estimates for the individual terms of the global carbon budget shows a cumulative budget imbalance of 25 GtC (3 % of total emissions) during 1850–2023 (Fig. 3, Table 8), which, if correct, suggests that emissions could be slightly too high by the same proportion or that the combined land and ocean sinks are slightly underestimated (by about 6 %), although these are well within the uncertainty range of each component of the budget. Nevertheless, part of the imbalance could originate from the estimation of significant increase in E_{FOS} and E_{LUC} between the mid-1920s and the mid-1960s which is unmatched by a similar growth in atmospheric CO_2 concentration as recorded in ice cores (Fig. 3). However, the known loss of additional sink capacity of 30–40 GtC (over the 1850–2020 period) due to reduced forest cover has not been accounted for in our method and would exacerbate the budget imbalance (see Sects. 2.10 and S6.4).

For the more recent 1960–2023 period where direct atmospheric CO_2 measurements are available, total emissions ($E_{FOS} + E_{LUC}$) amounted to 500 ± 50 GtC, of which 410 ± 20 GtC (82 %) was caused by fossil CO_2 emissions and 90 ± 45 GtC (18 %) by land-use change (Table 8). The total emissions were partitioned among the atmosphere (220 ± 5 GtC; 45 %), ocean (130 ± 26 GtC; 25 %), and land (150 ± 40 GtC; 30 %), with a near-zero (< 1 GtC) unattributed budget imbalance. All components except land-use change emissions have significantly grown since 1960,

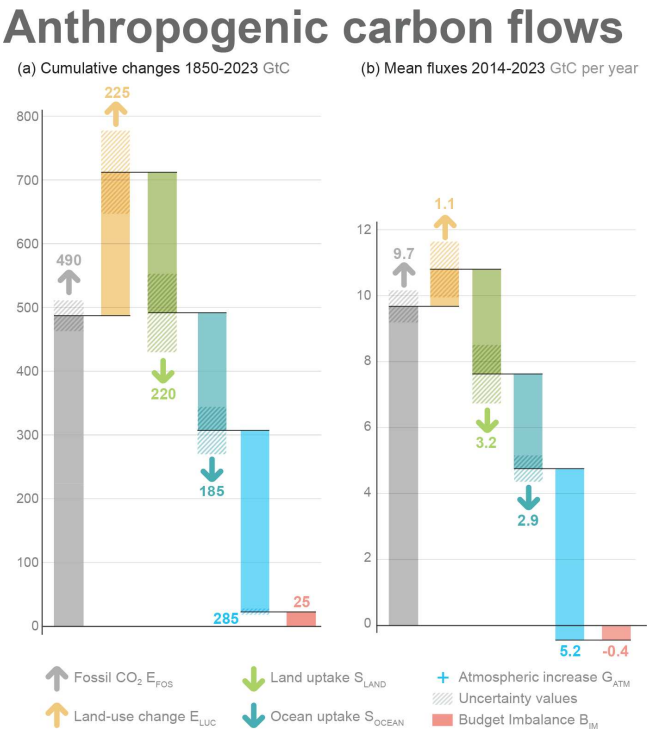

Figure 16. Cumulative changes over the 1850–2023 period **(a)** and average fluxes over the 2014–2023 period **(b)** for the anthropogenic perturbation of the global carbon cycle. See the caption of Fig. 3 for key information and the Methods section in the text for full details. This figure was produced by Nigel Hawtin.

with important interannual variability in the growth rate in atmospheric CO_2 concentration and in the land CO_2 sink (Fig. 4) and some decadal variability in all terms (Table 7). Differences with previous budget releases are documented in Fig. S6.

The global carbon budget averaged over the last decade (2014–2023) is shown in Figs. 2 and 16 (right panel) and Table 7. For this period, 90 % of the total emissions ($E_{FOS} + E_{LUC}$) were from fossil CO_2 emissions (E_{FOS}) and 10 % from land-use change (E_{LUC}). The total emissions were partitioned among the atmosphere (48 %), ocean (26 %), and land (30 %), with a small negative budget imbalance (~ 4 %, 0.4 GtC yr^{-1}). For single years, the budget imbalance can be larger (Fig. 4). For 2023, the combination of our estimated sources (11.1 ± 0.9 GtC yr^{-1}) and sinks (11.1 ± 0.9 GtC yr^{-1}) leads to a B_{IM} of -0.02 GtC, suggesting a near-perfect closure of the global carbon budget.

3.9.2 Trend and variability in the carbon budget imbalance

The carbon budget imbalance (B_{IM}; Eq. 1, Fig. 4) quantifies the mismatch between the estimated total emissions and the estimated changes in the atmosphere, land, and ocean reservoirs. The budget imbalance from 1960 to 2023 is very small

(0.5 GtC over the period, i.e. < 0.01 GtC yr^{-1} on average) and shows no trend over the full time series (Fig. 4e). The process models (GOBMs and DGVMs) and fCO_2 products have been selected to match observational constraints in the 1990s, but no further constraints have been applied to their representation of trend and variability. Therefore, the near-zero mean of and trend in the budget imbalance are seen as evidence of a coherent community understanding of the emissions and their partitioning on those timescales (Fig. 4). However, the budget imbalance shows substantial variability on the order of ± 1 GtC yr^{-1}, particularly over semi-decadal timescales, although most of the variability is within the uncertainty in the estimates. The positive carbon imbalance during the 1960s and early 1990s indicates that either the emissions were overestimated or the sinks were underestimated during these periods. The reverse is true for the 1970s and to a lesser extent for the 1980s and 2014–2023 period (Fig. 4, Table 7).

We cannot attribute the cause of the variability in the budget imbalance with our analysis; we only note that the budget imbalance is unlikely to be explained by errors or biases in the emissions alone because of its component of large semi-decadal variability, a variability that is atypical of emissions and has not changed in the past 60 years despite a near tripling in emissions (Fig. 4). Errors in S_{LAND} and S_{OCEAN} are more likely to be the main cause for the budget imbalance, especially on interannual to semi-decadal timescales. For example, underestimation of the S_{LAND} by DGVMs has been reported following the eruption of Mount Pinatubo in 1991, possibly due to missing responses to changes in diffuse radiation (Mercado et al., 2009). Although since GCB2021 we have accounted for aerosol effects on solar radiation quantity and quality (diffuse vs. direct), most DGVMs only used the former as input (i.e. total solar radiation) (Table S1). Thus, the ensemble mean may not capture the full effects of volcanic eruptions, i.e. those associated with high-light-scattering sulfate aerosols, on the land carbon sink (O'Sullivan et al., 2021). DGVMs are suspected to overestimate the land sink in response to the wet decade of the 1970s (Sitch et al., 2008). Quasi-decadal variability in the ocean sink has also been reported, with all methods agreeing on a smaller-than-expected ocean CO_2 sink in the 1990s and a larger-than-expected sink in the 2000s (Fig. 11; Landschützer et al., 2016; DeVries et al., 2019; Hauck et al., 2020; McKinley et al., 2020; Gruber et al., 2023), and the climate-driven variability could be substantial but is not well constrained (DeVries et al., 2023; Müller et al., 2023). Errors in sink estimates could also be driven by errors in the climatic forcing data, particularly precipitation for S_{LAND} and wind for S_{OCEAN}. Also, the B_{IM} shows substantial departure from zero on yearly timescales (Fig. 4e), highlighting unresolved variability in the carbon cycle, likely in the land sink (S_{LAND}), given its large year-to-year variability (Figs. 4d and 9).

Both the budget imbalance (B_{IM}, Table 7) and the residual land sink from the global budget ($E_{FOS} + E_{LUC} - G_{ATM} - S_{OCEAN}$, Table 5) include an error term due to the inconsistencies that arise from combining E_{LUC} from bookkeeping models with S_{LAND} from DGVMs, most notably the loss of additional sink capacity (see Sects. 2.10 and S6.4). Other differences include better accounting of land-use change practices and processes in bookkeeping models than in DGVMs and of the bookkeeping model error of having present-day observed carbon densities fixed in the past. That the budget imbalance shows no clear trend towards larger values over time is an indication that these inconsistencies probably play a minor role compared to other errors in S_{LAND} or S_{OCEAN}.

Although the budget imbalance is near zero for recent decades, this could be due to a compensation of errors. We cannot exclude the possibility of an overestimation of CO_2 emissions, particularly from land-use change, given their large uncertainty, as has been suggested elsewhere (Piao et al., 2018), and/or an underestimate of the sinks. A larger DGVM estimate of the atmosphere–land CO_2 flux ($S_{LAND} - E_{LUC}$) over the extra-tropics would reconcile model results with inversion estimates for fluxes in the total land during the past decade (Fig. 14, Table 5). Likewise, a larger S_{OCEAN} is also possible given the higher estimates from the fCO_2 products, inversions, and oxygen-based estimates (see Sect. 3.6.2, Figs. 11 and 14); the underestimation of interior-ocean anthropogenic carbon accumulation in the GOBMs (Sect. 3.6.5; Müller et al., 2023); known biases of ocean models (e.g. Terhaar et al., 2022, 2024); the role of potential temperature bias and skin effects in fCO_2 products (Watson et al., 2020; Dong et al., 2022; Bellenger et al., 2023; Fig. 11); and regionally larger estimates based, for example, on eddy covariance measurements and aircraft data (Dong et al., 2024a; Long et al., 2021; Jin et al., 2024). More integrated use of observations in the global carbon budget, either on their own or for further constraining model results, should help resolve some of the budget imbalance (Peters et al., 2017a).

4 Tracking progress towards mitigation targets

The average growth in global fossil CO_2 emissions peaked at nearly $+3\,\%$ yr^{-1} during the 2000s, driven by the rapid growth in emissions in China. In the last decade, however, the global growth rate has slowly declined, reaching a low of $+0.6\,\%$ yr^{-1} over 2014–2023. While this slowdown in global fossil CO_2 emissions growth is welcome, global fossil CO_2 emissions continue to grow, and we are far from the rapid emission decreases needed to be consistent with the temperature goals of the Paris Agreement.

Since the 1990s, the average growth rate of fossil CO_2 emissions has continuously declined across the group of developed countries of the Organisation for Economic Co-operation and Development (OECD), with emissions peak-

ing in around 2005 and declining at 1.4 % yr^{-1} in the decade 2014–2023, compared to a decline of 0.9 % yr^{-1} during the 2004–2013 period (Table 9). In the decade 2014–2023, territorial fossil CO_2 emissions decreased significantly (at the 95 % confidence level) in 23 countries/economies whose economies grew significantly (also at the 95 % confidence level): Belgium, Czechia, Denmark, Estonia, Finland, France, Gabon, Germany, Jordan, Luxembourg, the Netherlands, Aotearoa / New Zealand, Norway, Portugal, South Korea, Romania, Slovenia, Somalia, Spain, Sweden, Switzerland, the United Kingdom, and the USA (updated from Le Quéré et al., 2019). Altogether, these 23 countries emitted 2.2 GtC yr^{-1} (8.2 $GtCO_2$ yr^{-1}) on average over the last decade, about 23 % of world CO_2 fossil emissions. For comparison, 17 countries showed a significant decrease in territorial fossil CO_2 emissions over the previous decade (2004–2013).

Decomposing emission changes into the components of growth, a Kaya decomposition, helps give an initial understanding of the drivers of the changes (Peters et al., 2017b). The reduction in growth in global fossil CO_2 emissions in the last decade is due to slightly weaker economic growth, accelerating declines in CO_2 emissions per unit energy, and sustained declines in energy per unit GDP (Fig. 17). These trends are a supposition of the trends at the national level. Fossil CO_2 emission declines in the USA and EU27 are primarily driven by slightly weaker economic growth since the global financial crisis (GFC) in 2008–2009, sustained declines in energy per GDP, and sustained declines in CO_2 emissions per unit energy with a slight acceleration in the USA in the last decade. In contrast, fossil CO_2 emissions continue to grow in non-OECD countries, although the growth rate has slowed from 4.9 % yr^{-1} during the 2004–2013 decade to 1.8 % yr^{-1} in the last decade (Table 9). Representing 47 % of non-OECD emissions in 2023, a large part of this slowdown is due to China, which has seen emissions growth decline from 7.5 % yr^{-1} in the 2004–2013 decade to 1.9 % yr^{-1} in the last decade. Excluding China, non-OECD emissions grew at 3 % yr^{-1} in the 2004–2013 decade compared to 1.7 % yr^{-1} in the last decade. China had weaker economic growth in the 2000s compared to the 2010s, and the rate of reduction in the energy intensity of economic production has weakened significantly since 2015, with accelerating declines in CO_2 emissions per unit energy (Fig. 17). India has had strong economic growth that has not been offset by declines in energy per GDP or declines in CO_2 emissions per unit energy, driving up fossil CO_2 emissions. Despite the high deployment of renewables in some countries (e.g. China, India), fossil energy sources continue to grow to meet growing energy demand (Le Quéré et al., 2019). In the rest of the world, economic growth has slowed considerably in the last decade but has only been partly offset by declines in energy or carbon intensity, leading to growing emissions.

Globally, fossil CO_2 emissions growth is slowing, and this is due in part to the emergence of climate policy (Eskander and Fankhauser, 2020; Le Quéré et al., 2019) and technological change, which are leading to a shift from coal to gas and growth in renewable energies and reduced expansion of coal capacity. At the aggregated global level, decarbonization has shown a strong and growing signal in the last decade, with smaller contributions from lower economic growth and declines in energy per GDP (Fig. 17). Altogether, global fossil CO_2 emissions are still growing (average of 0.6 % yr^{-1} over the 2014–2023 decade), and they are far from the reductions needed to meet the ambitious climate goals of the UNFCCC Paris Agreement.

Lastly, we update the remaining carbon budget (RCB) based on two studies, the IPCC AR6 (Canadell et al., 2021) and the revision of the IPCC AR6 estimates (Forster et al., 2024; Lamboll et al., 2023). We update the RCB assessed by the IPCC AR6 (Canadell et al., 2021), accounting for the 2020–2024 estimated emissions from fossil fuel combustion (E_{FOS}) and land-use changes (E_{LUC}). From January 2025, the IPCC AR6 RCB (50 % likelihood) for limiting global warming to 1.5, 1.7, and 2 °C is estimated to amount to 85, 180, and 315 GtC (305, 655, 1155 $GtCO_2$). The Forster et al. (2024) study proposed a significantly lower RCB than IPCC AR6, with the largest reduction being due to an update of the climate emulator (MAGICC) used to estimate the warming contribution of non-CO_2 agents and due to the warming (i.e. emissions) that occurred over the 2020–2023 period. We update the Forster et al. (2024) budget, accounting for the 2024 estimated emissions from fossil fuel combustion (E_{FOS}) and land-use changes (E_{LUC}). From January 2025, the Forster et al. (2024) RCB (50 % likelihood) for limiting global warming to 1.5, 1.7, and 2 °C is estimated to amount to 45, 140, and 290 GtC (160, 510, 1060 $GtCO_2$), significantly smaller than the updated IPCC AR6 estimate. Both the original IPCC AR6 and the Forster et al. (2024) estimates include the Earth system uncertainty in the climate response to cumulative CO_2 emissions, which is reflected through the percent likelihood of exceeding the given temperature threshold, an additional uncertainty of ± 220 $GtCO_2$ due to alternative non-CO_2 emission scenarios, and other sources of uncertainties (see Canadell et al., 2021). The two sets of estimates overlap when considering all uncertainties.

Here, we take the average of our 2024 update of both the IPCC AR6 and the Forster et al. (2024) estimates, giving a remaining carbon budget (50 % likelihood) for limiting global warming to 1.5, 1.7, and 2 °C of 65, 160, and 305 GtC (235, 585, 1110 $GtCO_2$), respectively, starting from January 2025. We emphasize the large uncertainties, particularly when close to the global warming limit of 1.5 °C. These 1.5, 1.7, and 2 °C remaining carbon budgets correspond to about 6, 14, and 27 years, respectively, from the beginning of 2025, at the 2024 level of total anthropogenic CO_2 emissions. Reaching net-zero CO_2 emissions by 2050 entails cutting total anthropogenic CO_2 emissions by about 0.4 GtC (1.6 $GtCO_2$), 3.9 % of 2024 emissions, each year on average, comparable to the decrease in E_{FOS} observed in 2020 during

Table 9. Average annual growth rate in fossil CO_2 emissions over the most recent decade (2014–2023) and the previous decade (2004–2013). The data for the world include the cement carbonation sink. IAS denotes emissions from international aviation and shipping. The rest of the world is the world minus China, the USA, EU27, India, and IAS.

	World	China	USA	EU27	India	OECD	Non-OECD	IAS	Rest of the world
2004–2013	2.4 %	7.5 %	−1.4 %	−1.8 %	6.4 %	−0.9 %	4.9 %	2.6 %	1.9 %
2014–2023	0.6 %	1.9 %	−1.2 %	−2.1 %	3.6 %	−1.4 %	1.8 %	−1.6 %	0.4 %

Figure 17. Kaya decomposition of the main drivers of fossil CO_2 emissions, considering population, GDP per person, energy per GDP, and CO_2 emissions per energy unit, for China **(a)**, the USA **(b)**, EU27 **(c)**, India **(d)**, the rest of the world **(e)**, and world **(f)**. Black dots are the annual fossil CO_2 emissions growth rate; coloured bars are the contributions from the different drivers to this growth rate. A general trend is that population and GDP growth put upward pressure on emissions (positive values), while energy per GDP and, more recently, CO_2 emissions per energy unit put downward pressure on emissions (negative values). Both the COVID-19-induced drop during 2020 and the recovery in 2021 led to a stark contrast to previous years, with different drivers in each region.

the COVID-19 pandemic. However, this would lead to cumulative emissions over 2025–2050 of 145 GtC (530 $GtCO_2$), well above the remaining carbon budget of 65 GtC to limit global warming to 1.5 °C but still within the remaining budget of 160 GtC to limit warming to 1.7 °C (in phase with the "well below 2 °C" ambition of the Paris Agreement). Even reaching net-zero CO_2 globally by 2040, which would require annual emissions cuts of 0.7 GtC (2.5 $GtCO_2$) on average, would still exceed the remaining carbon budget for 1.5 °C, with 90 GtC (325 $GtCO_2$) of cumulative emissions over 2025–2040, unless the global emissions trajectory becomes net negative (i.e. more anthropogenic CO_2 sinks than emissions) after 2040.

5 Discussion

Each year when the global carbon budget is published, each flux component is updated for all previous years to consider corrections that are the result of further scrutiny and verification of the underlying data in the primary input datasets. Annual estimates may be updated with improvements in data quality and timeliness (e.g. to eliminate the need for extrapolation of forcing data such as land-use data). Of all terms in the global budget, only the fossil CO_2 emissions and the growth rate in atmospheric CO_2 concentration are based primarily on empirical inputs supporting annual estimates in this carbon budget. The carbon budget imbalance, still an imperfect measure, provides a strong indication of the limitations in observations, in understanding and representing processes in models, and/or in the integration of the carbon budget components.

The persistent unexplained variability in the carbon budget imbalance limits our ability to verify reported emissions (Peters et al., 2017a) and suggests we do not yet have a complete understanding of the underlying carbon cycle dynamics on annual to decadal timescales. Resolving most of this unexplained variability should be possible through different and complementary approaches. First, as intended with our annual updates, the imbalance as an error term should be reduced by improvements of individual components of the global carbon budget that follow from improving the underlying data and statistics and by improving the models through the resolution of some of the key uncertainties detailed in Table 10. Second, additional clues to the origin and processes responsible for the variability in the budget imbalance could be obtained through closer scrutiny of carbon variability in light of other Earth system data (e.g. heat balance, water balance) and the use of a wider range of biogeochemical observations to better understand the land–ocean partitioning of the carbon imbalance, such as the constraint from atmospheric oxygen included this year. Finally, additional information could also be obtained through better inclusion of process knowledge at the regional level and through the introduction of inferred fluxes such as those based on satellite XCO_2 retrievals. The limit of the resolution of the carbon budget imbalance is still unclear but most certainly has not yet been reached given the possibilities for improvements that lie ahead.

Estimates of global fossil CO_2 emissions from different datasets are in relatively good agreement when the different system boundaries of these datasets are considered (Andrew, 2020a). But while estimates of E_{FOS} are derived from reported activity data requiring much fewer complex transformations than some other components of the budget, uncertainties remain, and one reason for the apparently low variation between datasets is precisely the reliance on the same underlying reported energy data. The budget excludes some sources of fossil CO_2 emissions, which available evidence suggests are relatively small ($< 1\,\%$). We have added emissions from lime production in China and the USA, but these are still absent in most other non-Annex I countries and before 1990 in other Annex I countries.

Estimates of E_{LUC} suffer from a range of intertwined issues, including the poor quality of historical land-cover and land-use change maps, the rudimentary representation of management processes in most models, and the confusion in methodologies and boundary conditions used across methods (e.g. Arneth et al., 2017; Pongratz et al., 2014; see also the Supplement, Sect. S6.4, on the loss of sink capacity; Bastos et al., 2021). Uncertainties in current and historical carbon stocks in soils and vegetation also add uncertainty to the E_{LUC} estimates. Unless a major effort to resolve these issues is made, little progress is expected in the resolution of E_{LUC}. This is particularly concerning given the growing importance of E_{LUC} for climate mitigation strategies and the large issues in the quantification of the cumulative emissions over the historical period that arise from large uncertainties in E_{LUC}.

By adding the DGVM estimates of CO_2 fluxes due to environmental change from countries' managed forest areas (part of S_{LAND} in this budget) to the budget E_{LUC} estimate, we successfully reconciled the large gap between our E_{LUC} estimate and the land-use flux from NGHGIs using the approach described in Grassi et al. (2021) for future scenarios and in Grassi et al. (2023) using data from the Global Carbon Budget 2021. The updated data presented here can be used for potential adjustments in the policy context, e.g. to help assess the collective countries' progress towards the goal of the Paris Agreement and to avoid double accounting for the sink in managed forests. In the absence of this adjustment, collective progress would hence appear better than it is (Grassi et al., 2021). The application of this adjustment is also recommended in the UNFCCC Synthesis Report for the first Global Stocktake (UNFCCC, 2022) whenever a comparison between LULUCF fluxes reported by countries and the global emissions estimates of the IPCC is conducted. However, this adjustment should be seen as a short-term and pragmatic fix based on existing data rather than as a definitive solution to bridge the differences between global models and national inventories. Additional steps are needed to

Table 10. Major known sources of uncertainties in each component of the global carbon budget, defined as input data or processes that have a demonstrated effect of at least $\pm 0.3\,\mathrm{GtC\,yr^{-1}}$.

Source of uncertainty	Timescale (years)	Location	Evidence
Fossil CO_2 emissions (E_{FOS}; Sect. 2.1)			
Energy statistics	annual to decadal	global but mainly China and major developing countries	Korsbakken et al. (2016), Guan et al. (2012)
Carbon content of coal	annual to decadal	global but mainly China and major developing countries	Liu et al. (2015)
System boundary	annual to decadal	all countries	Andrew (2020a)
Net land-use change flux (E_{LUC}; Sect. 2.2)			
Land-cover and land-use change statistics	continuous	global, in particular the tropics	Houghton et al. (2012), Gasser et al. (2020), Ganzenmüller et al. (2022), Yu et al. (2022)
Sub-grid-scale transitions	annual to decadal	global	Wilkenskjeld et al. (2014), Bastos et al. (2021)
Vegetation biomass	annual to decadal	global, in particular the tropics	Houghton et al. (2012), Bastos et al. (2021)
Forest degradation (fire, selective logging)	annual to decadal	the tropics, Amazon	Aragão et al. (2018), Qin et al. (2021), Lapola et al. (2023)
Wood and crop harvest	annual to decadal	global, SE Asia	Arneth et al. (2017), Erb et al. (2018)
Peat burning	multi-decadal trend	global	van der Werf et al. (2010, 2017)
Loss of additional sink capacity	multi-decadal trend	global	Pongratz et al. (2014), Gasser et al. (2020), Obermeier et al. (2021), Dorgeist et al. (2024)
Environmental effects	multi-decadal trend	global	Gasser et al. (2020), Dorgeist et al. (2024)
Atmospheric growth rate (G_{ATM}; Sect. 2.4) – no demonstrated uncertainties larger than $\pm 0.3\,\mathrm{GtC\,yr^{-1}}$; the uncertainties in G_{ATM} estimated as $\pm 0.2\,\mathrm{GtC\,yr^{-1}}$, although the conversion of the growth rate into a global annual flux assuming instantaneous mixing throughout the atmosphere introduces additional errors that have not yet been quantified			
Ocean sink (S_{OCEAN}; Sect. 2.5)			
Sparsity in surface fCO_2 observations	mean, decadal variability and trend	global, in particular the Southern Hemisphere	Gloege et al. (2021), Denvil-Sommer et al. (2021), Hauck et al. (2023a), Dong et al. (2024b)
Riverine carbon outgassing and its anthropogenic perturbation	annual to decadal	global, in particular partitioning between the tropics and the south	Aumont et al. (2001), Lacroix et al. (2020), Crisp et al. (2022)
Models underestimate interior-ocean anthropogenic carbon storage	annual to decadal	global	Friedlingstein et al. (2022a), this study, DeVries et al. (2023), Müller et al. (2023)
Near-surface temperature and salinity gradients	mean on all timescales	global	Watson et al. (2020), Dong et al. (2022), Bellenger et al. (2023), Dong et al. (2024a)

Table 10. Continued.

Source of uncertainty	Timescale (years)	Location	Evidence
Land sink (S_{LAND}; Sect. 2.6)			
Strength of CO_2 fertilization	multi-decadal trend	global	Wenzel et al. (2016), Walker et al. (2021)
Response to variability in temperature and rainfall	annual to decadal	global, in particular the tropics	Cox et al. (2013), Jung et al. (2017), Humphrey et al. (2018, 2021)
Nutrient limitation and supply	annual to decadal	global	Zaehle et al. (2014)
Carbon allocation and tissue turnover rates	annual to decadal	global	De Kauwe et al. (2014), O'Sullivan et al. (2022)
Tree mortality	annual	global, in particular the tropics	Hubau et al. (2020), Brienen et al. (2020)
Response to diffuse radiation	annual	global	Mercado et al. (2009), O'Sullivan et al. (2021)
Estimation under constant pre-industrial land cover	multi-decadal trend	global	Gasser et al. (2020), Dorgeist et al. (2024)

understand and reconcile the remaining differences, some of which are relevant at the country level (Grassi et al., 2023; Schwingshackl et al., 2022).

The comparison of GOBMs, fCO_2 products, and inversions highlights a substantial discrepancy in the temporal evolution of S_{OCEAN} in the Southern Ocean and northern high latitudes (Fig. 14; Hauck et al., 2023a) and in the mean S_{OCEAN} in the tropics. A large part of the uncertainty in the mean fluxes stems from the regional distribution of the river flux adjustment term. The current distribution simulates the largest share of the outgassing occurring in the tropics (Lacroix et al., 2020). The long-standing sparse data coverage of fCO_2 observations in the Southern Hemisphere compared to the Northern Hemisphere (e.g. Takahashi et al., 2009) continues to exist (Bakker et al., 2016, 2024; Fig. S1) and to lead to substantially higher uncertainty in the S_{OCEAN} estimate for the Southern Hemisphere (Watson et al., 2020; Gloege et al., 2021; Hauck et al., 2023a). This discrepancy, which also hampers model improvement, points to the need for increased high-quality fCO_2 observations especially in the Southern Ocean. At the same time, model uncertainty is illustrated by the large spread of individual GOBM estimates (indicated by shading in Fig. 14) and highlights the need for model improvement. The issue of diverging trends in S_{OCEAN} from different methods is smaller this year because the trend in the fCO_2 products was revised downwards with the data available in this GCB release, but it remains a matter of concern. Recent and ongoing work suggests that the fCO_2 products may overestimate the trend (Hauck et al., 2023a; see the Supplement, Sect. S3.4), though the full fCO_2-product ensemble remains to be tested. A data-constrained model approach suggests that the GOBMs underestimate the amplitude of decadal variability but that the fCO_2 products overestimate the trend (Mayot et al., 2024). At the same time, evidence is accumulating that GOBMs likely underestimate the mean flux (Sect. 3.6.2; Terhaar et al., 2022; DeVries et al., 2023; Müller et al., 2023; Dong et al., 2024a). The independent constraint from atmospheric oxygen measurements gives a larger sink for the past decade and a steeper trend. However, the estimate is consistent within uncertainties with S_{OCEAN}, with the relatively large ocean sink in the fCO_2 products and some of the GOBMs. The assessment of the net land–atmosphere exchange from DGVMs and atmospheric inversions also shows substantial discrepancy, particularly for the estimate of the net land flux over the northern extra-tropics. This discrepancy highlights the difficulty of quantifying complex processes (CO_2 fertilization, nitrogen deposition and fertilizers, climate change and variability, land management, etc.) that collectively determine the net land CO_2 flux. Resolving the differences in the Northern Hemisphere land sink will require the consideration and inclusion of larger quantities of observations.

We provide metrics for the evaluation of the ocean and land models and the atmospheric inversions (Figs. S2 to S4, Table S11). These metrics expand the use of observations in the global carbon budget, helping (1) to support improvements in the ocean and land carbon models that produce the sink estimates and (2) to constrain the representation of key underlying processes in the models and to allocate the regional partitioning of the CO_2 fluxes. The introduction of process-based metrics targeted to evaluate the simulation of S_{OCEAN} in the ocean biogeochemistry models is an important addition to the evaluation based on ocean carbon observations. This is an initial step towards the introduction of a

broader range of observations and more stringent model evaluation that we hope will support continued improvements in the annual estimates of the global carbon budget.

We have previously established that a sustained decrease of −1 % in global emissions could be detected at the 66 % likelihood level after a decade only (Peters et al., 2017a). Similarly, a change in behaviour of the land and/or ocean carbon sink would take as long to detect and much longer if it emerges more slowly. To continue reducing the carbon imbalance on annual to decadal timescales, regionalizing the carbon budget and integrating multiple variables are powerful ways to shorten the detection limit and ensure the research community can rapidly identify issues of concern in the evolution of the global carbon cycle under the current rapid and unprecedented changing environmental conditions.

6 Conclusions

The estimation of global CO_2 emissions and sinks is a major effort by the carbon cycle research community that requires a careful compilation and synthesis of measurements, statistical estimates, and model results. The delivery of an annual carbon budget serves two purposes. First, there is a large demand for up-to-date information on the state of the anthropogenic perturbation of the climate system and its underpinning causes. A broad stakeholder community relies on the datasets associated with the annual carbon budget including scientists, policymakers, businesses, journalists, and non-governmental organizations engaged in adapting to and mitigating human-driven climate change. Second, over recent decades we have seen unprecedented changes in human and biophysical environments (e.g. changes in the growth of fossil fuel emissions, impact of COVID-19 pandemic, Earth's warming, and strength of the carbon sinks), which call for frequent assessments of the state of the planet, a better quantification of the causes of changes in the contemporary global carbon cycle, and an improved capacity to anticipate the evolution of the global carbon cycle in the future. Building this scientific understanding to meet the extraordinary climate mitigation challenge requires frequent, robust, transparent, and traceable datasets and methods that can be scrutinized and replicated. Via living data, this paper helps to keep track of new budget updates.

7 Data availability

The data presented here are made available in the belief that their wide dissemination will lead to greater understanding and new scientific insights of how the carbon cycle works, how humans are altering it, and how we can mitigate the resulting human-driven climate change. Full contact details and information on how to cite the data shown here are given at the top of each page in the accompanying database and are summarized in Table 2.

The accompanying database includes three Excel files organized in the following spreadsheets.

The file Global_Carbon_Budget_2024v1.0.xlsx includes the following:

1. a summary,
2. the global carbon budget (1959–2023),
3. the historical global carbon budget (1750–2023),
4. global CO_2 emissions from fossil fuels and cement production by fuel type and the per capita emissions (1850–2023),
5. CO_2 emissions from land-use change from the individual bookkeeping models (1959–2023),
6. the ocean CO_2 sink from the individual global ocean biogeochemistry models and fCO_2 products (1959–2023),
7. the terrestrial CO_2 sink from the individual DGVMs (1959–2023),
8. the cement carbonation CO_2 sink (1959–2023).

The file National_Fossil_Carbon_Emissions _2024v1.0.xlsx includes the following:

1. summary,
2. territorial country CO_2 emissions from fossil fuels and cement production (1850–2023),
3. consumption country CO_2 emissions from fossil fuels and cement production and emissions transfer from the international trade of goods and services (1990–2020) using CDIAC/UNFCCC data as reference,
4. emissions transfers (consumption minus territorial emissions, 1990–2020),
5. country definitions.

The file National_LandUseChange_Carbon_Emissions _2024v1.0.xlsx includes the following:

1. a summary,
2. territorial country CO_2 emissions from land-use change (1850–2023) from three bookkeeping models.

All three spreadsheets are published by the Integrated Carbon Observation System (ICOS) Carbon Portal and are available at https://doi.org/10.18160/GCP-2024 (Friedlingstein et al., 2024). National emissions data are also available at https://doi.org/10.5281/zenodo.13981696 (Andrew and Peters, 2024), from the Global Carbon Atlas (http://www.globalcarbonatlas.org/, Global Carbon Project, 2024) and from Our World in Data (2024, https://ourworldindata.org/co2-emissions).

Supplement. The supplement related to this article is available online at https://doi.org/10.5194/essd-17-965-2025-supplement.

Author contributions. PF, MO, MWJ, RMA, JH, PL, CLQ, HL, ITL, AO, GPP, WP, JP, CS, and SSi designed the study, conducted the analysis, and wrote the paper with input from JGC, PCi, and RBJ. RMA, GPP, and JIK produced the fossil CO_2 emissions and their uncertainties and analysed the emissions data. MH and GMa provided fossil fuel emissions data. JP, TGa, ZQ, and CS provided the bookkeeping land-use change emissions with synthesis by JP and CS. SSm provided the estimates of non-vegetation CDR fluxes. LB, MC, ÖG, NG, TI, TJ, LR, JS, RS, and HTs provided an update of the global ocean biogeochemical models; LMD, ARF, DJF, MG, LG, YI, AJ, CR, AR, JZ, and PC provided an update of the ocean fCO_2 data products, with synthesis on both streams by JH, PL, and NMa. SRA, NRB, MB, CFB, HCB, KC, KE, WE, RAF, TGk, SKL, NL, NMe, NMM, SN, LO, TO, DP, AJS, ST, BT, CN, and RW provided ocean fCO_2 measurements for the year 2023, with synthesis by AO and TS. AA, VA, PCa, THC, JD, CDR, AF, JHe, AKJ, EK, JK, PCM, LM, TN, MO, QS, HTi, XYa, WY, XYu, and SZ provided an update of the dynamic global vegetation models, with synthesis by SSi and MO. HL, RSA, OT, and ET provided estimates of land and ocean sinks from Earth system models, as well as a projection of the atmospheric growth rate for 2024. NC, FC, ARJ, FJ, ZJ, JL, SM, YN, PIP, CR, DY, and NZ provided an updated atmospheric inversion. WP, FC, and ITL developed the protocol and produced the synthesis and evaluation of the atmospheric inversions. RMA provided projections of the 2024 fossil emissions and atmospheric CO_2 growth rate. PL provided the predictions of the 2024 ocean and land sinks. LPC, GCH, KKG, TMR, GRvdW, WX, and ZY provided forcing data for land-use change. FT and GG provided data for the land-use change NGHGI harmonization. RFK provided key atmospheric CO_2 data. EJM and RFK provided the atmospheric oxygen constraint on surface net carbon sinks. MWJ provided the historical atmospheric CO_2 concentration and growth rate. MO and NB produced the aerosol diffuse radiative forcing for the DGVMs. IH provided the climate forcing data for the DGVMs. PCM provided the evaluation of the DGVMs. MWJ provided the emissions prior for use in the inversion systems. XD provided seasonal emissions data for the most recent years for the emissions prior. PF, MO, and MWJ coordinated the effort and revised all figures, tables, text, and numbers to ensure the update was clear in relation to the 2023 edition and in line with https://globalcarbonatlas.org/ (last access: 21 January 2025).

Competing interests. At least one of the (co-)authors is a member of the editorial board of *Earth System Science Data*. The peer-review process was guided by an independent editor, and the authors also have no other competing interests to declare.

Disclaimer. The views expressed in this paper are the authors' only and do not necessarily reflect those of FAO.

Publisher's note: Copernicus Publications remains neutral with regard to jurisdictional claims made in the text, published maps, institutional affiliations, or any other geographical representation in this paper. While Copernicus Publications makes every effort to include appropriate place names, the final responsibility lies with the authors.

Acknowledgements. We thank all the people and institutions who provided the data used in the Global Carbon Budget 2024 and the Global Carbon Project members for their input throughout the development of this publication. We thank Nigel Hawtin for producing Figs. 2 and 16. We thank Alex Vermeulen and Hannah Ritchie for hosting the global carbon budget datasets on the ICOS portal and the Our World in Data website, respectively. We thank Ram Alkama, Ian G. C. Ashton, Dorothee Bakker, Raffaele Bernardello, Ida Bagus Mandhara Brasika, Sebastian Brune, Fatemeh Cheginig, Emeric Claudel, Jason Cole, Lushanya Dayathilake, Pengyue Du, Christian Ethé, Stefanie Falk, Kristina Frölich, Lonneke Goddijn-Murphy, Ian Harman, Thomas Holding, Drew Holzworth, Rajesh Janardanan, Daniel Kennedy, Erik Kluzek, Fabrice Lacroix, Vladimir Lapin, Peter Lawrence, Sam Levis, Yi Liu, Damian Loher, Zoé Lloret, Adrien Martinez, Hideyuki Nakano, Lorna Nayagam, Naiqing Pan, Shufen Pan, Tristan Quaife, Simone Rossi, Paridhi Rustogi, Jamie D. Shutler, Richard Sims, Victoria Spada, Sean Swenson, Phillip Townsend, Katsuya Toyama, Shogo L. Urakawa, Anthony P. Walker, Jing Wang, Andrew J. Watson, S. Lachlan Whyborn, David K. Woolf, and Yakun Zhu for their involvement in the development, use, and analysis of the models and data products used here. We thank Kim Currie, Siyabulela Hamnca, Boris Herrmann, Arne Körtzinger, C. Lo Monaco, Team Malizia, Pedro Monteiro, and Mutshutshu Tsanwani, who contributed to the provision of surface ocean CO_2 observations for the year 2023 (see Table S7). We also thank Stephen D. Jones of the Ocean Thematic Centre of the EU Integrated Carbon Observation System (ICOS) Research Infrastructure, Eugene Burger of NOAA's Pacific Marine Environmental Laboratory, and Alex Kozyr of NOAA's National Centers for Environmental Information for their contribution to surface ocean CO_2 data and metadata management. We thank the scientists, institutions, and funding agencies responsible for the collection and quality control of the data in SOCAT as well as the International Ocean Carbon Coordination Project (IOCCP), the Surface Ocean – Lower Atmosphere Study (SOLAS), and the Integrated Marine Biosphere Research (IMBeR) programme for their support. We thank Nadine Goris and Lavinia Patara for support in calculating observational ocean evaluation metrics. We thank Fortunat Joos, Samar Khatiwala, and Timothy DeVries for providing historical atmospheric and ocean data. We thank the data providers ObsPack GLOBALVIEWplus v9.0 and NRT v9.2 for atmospheric CO_2 observations. Ingrid T. Luijkx and Wouter Peters thank the CarbonTracker Europe team at Wageningen University, including Remco de Kok, Joram Hooghiem, Linda Kooijmans, and Auke van der Woude. Ian Harris thanks the Japan Meteorological Agency (JMA) for producing the Japanese 55-year Reanalysis (JRA-55). Reinel Sospedra-Alfonso thanks William J. Merryfield, Woosung Lee, Jason Cole, and Victoria Spada for their help in setting up and producing CanESM5 runs. Olivier Torres thanks Patricia Cadule, Juliette Mignot, Didier Swingedouw, and Laurent Bopp for contributions to the IPSL-CM6A-CO_2-LR simulations. Yosuke Niwa thanks CSIRO, EC, EMPA, FMI, IPEN, JMA, LSCE, NCAR, NIES, NILU, NIWA, NOAA, SIO, and TU/NIPR for providing data for NISMON-CO_2. Zhe Jin thanks Xiangjun Tian, Yi-

long Wang, Hongqin Zhang, Min Zhao, Tao Wang, Jinzhi Ding, and Shilong Piao for their contributions to the GONGGA inversion system. Paul I. Palmer thanks Lian Fang and acknowledges ongoing support from the National Centre for Earth Observation. Ning Zeng thanks Zhiqiang Liu, Yun Liu, Eugenia Kalnay, and Gassem Asrar for their contributions to the COLA system. Fei Jiang acknowledges the High-Performance Computing Center (HPCC) of Nanjing University for performing the inversions on its blade cluster system and thanks Weimin Ju for updating the a priori fluxes of the terrestrial ecosystems. Meike Becker and Are Olsen thank Sparebanken Vest/Agenda Vestlandet for their support for the observations on the *Statsraad Lehmkuhl*. Wiley Evans and Katie Campbell thank the Tula Foundation for funding support. Thanos Gkritzalis and the VLIZ ICOS team are thankful to the crew of the research vessel *Simon Stevin* for all the support and help they provide. Bronte Tilbrook and Craig Neill thank Australia's Integrated Marine Observing System (IMOS) for sourcing CO_2 data. FAOSTAT is funded by FAO member states through their contributions to the FAO Regular Programme; data contributions by national experts are greatly acknowledged. Finally, we thank all funders who have supported the individual and joint contributions to this work (see details below), as well as the two reviewers of this paper and the many researchers who have provided feedback.

Financial support. This research was supported by the following sources of funding: the Argentinian-Uruguayan Joint Technical Commission of the Maritime Front (Comisión Técnica Mixta del Frente Marítimo, CTMFM) (Argentina); the Instituto Nacional de Investigación y Dessarrollo Pesquero (Argentina); Australia's Integrated Marine Observing System (IMOS), which is enabled by the National Collaborative Research Infrastructure Strategy (NCRIS) (Australia); Australian Community Climate and Earth System Simulator National Research Infrastructure (ACCESS-NRI) (Australia); the Australian National Environmental Science Program, Climate Systems Hub (Australia); the Research Foundation – Flanders (ICOS Flanders, grant no. I001821N) (Belgium); the Tula Foundation (Canada); the National Key Research and Development Program (grant nos. 2021YFD2200405, 2023YFF0805400, and 2023YFB3907404) (China); the Jiangsu Provincial Science Fund for Distinguished Young Scholars (grant no. BK20231530) (China); the National Natural Science Foundation (grant no. 42141020) (China); the Carbon Neutrality and Energy System Transformation (CNEST) programme led by Tsinghua University, granted by the National Key Research and Development Program of China (grant no. 2023YFE0113000) (China); the Second Tibetan Plateau Scientific Expedition and Research Program (grant no. 2022QZKK0101) (China); the CAS Project for Young Scientists in Basic Research (grant no. YSBR-037) (China); the Copernicus Atmosphere Monitoring Service, implemented by ECMWF (grant no. CAMS2 55) (European Commission); the Copernicus Marine Environment Monitoring Service, implemented by MOi (grant no. CMEMS-TAC-MOB) (European Commission); Horizon 2020 4C (grant no. 821003) (European Commission); Horizon 2020 ESM2025 – Earth System Models for the Future (grant no. 101003536) (European Commission); Horizon 2020 GEORGE (grant no. 101094716) (European Commission); Horizon 2020 EYE-CLIMA (grant no. 101081395) (European Commission); ERC-2022-STG OceanPeak (grant no. 101077209) (European Commission); Horizon 2020 OceanICU Improving Carbon Understanding (grant no. 101083922) (European Commission); Horizon 2020 RESCUE project (grant no. 101056939) (European Commission); Horizon 2020 COMFORT project (grant no. 820989) (European Commission); Climate Space RECCAP-2 (European Space Agency); Ocean Carbon for Climate (European Space Agency); EO-LINCS (European Space Agency); the OceanSODA project (grant no. 4000112091/14/I-LG) (European Space Agency); Institut National des Sciences de l'Univers (INSU) (France); Institut Polaire français, Paul-Émile Victor (IPEV) (France); Observatoire des sciences de l'univers Ecce Terra (OSU at Sorbonne Université) (France); Institut de recherché français sur les ressources marines (IFREMER) (France); the French Oceanographic Fleet (FOF) (France); ICOS France (France); Institut de Recherche pour le Développement (IRD) (France); Agence Nationale de la Recherche – France 2030 (PEPR TRACCS programme under grant no. ANR-22-EXTR-0009) (France); Institut de l'Océan and the Institut des Sciences du Calcul et des Données of Sorbonne Université (IDEX SUPER 11-IDEX-0004, project team FORMAL) (France); the Federal Ministry of Education and Research, collaborative project C-SCOPE (project no. 03F0877A) (Germany); the Helmholtz Association ATMO programme (Germany); the Initiative and Networking Fund of the Helmholtz Association (grant no. VH-NG-19-33) (Germany); ICOS Germany (Germany); the Federal Ministry of Education and Research (BMBF), project STEPSEC (grant no. 01LS2102A) (Germany); Helmholtz Young Investigator Group Marine Carbon and Ecosystem Feedbacks in the Earth System (MarESys, grant no. VH-NG-1301) (Germany); Deutsche Forschungsgemeinschaft (DFG) under Germany's Excellence Strategy – EXC 2037 "Climate, Climatic Change, and Society" (project no. 390683824) (Germany); the Arctic Challenge for Sustainability II project (ArCS II; grant no. JP-MXD1420318865) (Japan); the Environment Research and Technology Development Fund (grants no. JPMEERF24S12205, JPMEERF24S12206, and JPMEERF24S12200) (Japan); CREST, Japan Science and Technology Agency (grant no. JPMJCR23J4) (Japan); the Global Environmental Research Coordination System, Ministry of the Environment (grant no. E2252) (Japan); the Meteorological Agency (Japan); the Ministry of Education, Culture, Sports, Science and Technology, MEXT Program for The Advanced Studies of Climate Change Projection (SENTAN) (grant nos. JPMXD0722680395 and JPMXD0722681344) (Japan); the NIES GOSAT project (Japan); the Research Council of Norway (N-ICOS-2, grant no. 296012) (Norway); the Research Council of Norway (grant no. 270061) (Norway); the Swiss National Science Foundation (grant no. 200020-200511) (Switzerland); the Natural Environmental Research Council, National Centre for Earth Observation (grant no. NE/R016518/1) (UK); the Natural Environment Research Council, UK EO Climate Information Service (grant no. NE/X019071/1) (UK); the Natural Environment Research Council (grant nos. NE/V01417X/1, NE/Y005260/1, and NE/V013106/1) (UK); the Natural Environment Research Council, National Centre for Atmospheric Science (UK); the Royal Society (grant no. RP\R1\191063) (UK); the National Center for Atmospheric Research (NSF cooperative agreement no. 1852977) (USA); the NOAA Ocean Acidification Program (grant no. 100018228) (USA); the NOAA Global Ocean Monitoring and Observing Program (grant no. 100018302) (USA); NOAA (cooperative agreement nos. NA22OAR4320151 and NA20OAR4310340

and grant no. 1305M322PNRMJ0338) (USA); NASA (grant nos. 80NSSC22K0150 and 80NM0018D0004); the National Science Foundation (grant nos. NSF-2019625, NSF-831361857, NSF-1903722, and NSF-1852977) (USA); the NASA Terrestrial Ecology Program (USA); NASA Carbon Monitoring System programme (80NSSC21K1059) (USA); the NASA Land Cover and Land Use Change Program (80NSSC24K0920) (USA); the US Department of Energy, Office of Science, Office of Biological and Environmental Research (USA); the Department for Education SciDAC (grant no. DESC0012972) (USA); IDS (grant no. 80NSSC17K0348) (USA); and Schmidt Sciences, LLC (USA).

We were also supported by the following computing facilities: the Australian Community Climate and Earth System Simulator National Research Infrastructure (ACCESS-NRI) (Australia); the Deutsches Klimarechenzentrum (DKRZ) granted by its Scientific Steering Committee (WLA) under project ID bm0891 (Germany); HPC cluster Aether at the University of Bremen, financed by DFG within the scope of the Excellence Initiative (Germany); HPC resources of TGCC under the allocation A0150102201 awarded by GENCI and of CCRT under grant no. CCRT2024-p24cheva awarded by CEA/DRF (France); HPC resources of Météo-France (France); JAMSTEC's ES4 supercomputer system (Japan); the NIES supercomputer system (Japan); UNINETT Sigma2, national infrastructure for high-performance computing and data storage in Norway (NN2980K and NS2980K) (Norway); the UK CEDA JASMIN supercomputer (UK); the UEA (University of East Anglia) high-performance computing cluster (UK); the Derecho supercomputer (https://doi.org/10.5065/D6RX99HX), provided by the Computational and Information Systems Laboratory (CISL) at NCAR (USA); the Oak Ridge Leadership Computing Facility at the Oak Ridge National Laboratory (USA); and, for ISAM simulations, Cheyenne, NCAR HPC resources managed by CISL (https://doi.org/10.5065/D6RX99HX) (USA).

Review statement. This paper was edited by Kirsten Elger and reviewed by H. Damon Matthews and Andrew Lenton.

References

Abatzoglou, J. T., Williams, A. P., and Barbero, R.: Global Emergence of Anthropogenic Climate Change in Fire Weather Indices, Geophys. Res. Lett., 46, 326–336, https://doi.org/10.1029/2018GL080959, 2019.

Ahlström, A., Raupach, M. R., Schurgers, G., Smith, B., Arneth, A., Jung, M., Reichstein, M., Canadell, J. G., Friedlingstein, P., Jain, A. K., Kato, E., Poulter, B., Sitch, S., Stocker, B. D., Viovy, N., Wang, Y. P., Wiltshire, A., Zaehle, S., and Zeng, N.: The dominant role of semi-arid ecosystems in the trend and variability of the land CO_2 sink, 348, 895–899, https://doi.org/10.1126/science.aaa1668, 2015.

Andela, N., Morton, D. C., Giglio, L., Chen, Y., van der Werf, G. R., Kasibhatla, P. S., DeFries, R. S., Collatz, G. J., Hantson, S., Kloster, S., Bachelet, D., Forrest, M., Lasslop, G., Li, F., Mangeon, S., Melton, J. R., Yue, C., and Randerson, J. T.: A human-driven decline in global burned area, Science, 356, 1356–1362, https://doi.org/10.1126/science.aal4108, 2017.

Andrew, R. M.: A comparison of estimates of global carbon dioxide emissions from fossil carbon sources, Earth Syst. Sci. Data, 12, 1437–1465, https://doi.org/10.5194/essd-12-1437-2020, 2020a.

Andrew, R. M.: Timely estimates of India's annual and monthly fossil CO_2 emissions, Earth Syst. Sci. Data, 12, 2411–2421, https://doi.org/10.5194/essd-12-2411-2020, 2020b.

Andrew, R. M. and Peters, G. P.: The Global Carbon Project's fossil CO_2 emissions dataset (2024v17), Zenodo [data set], https://doi.org/10.5281/zenodo.13981696, 2024.

Aragão, L. E. O. C., Anderson, L. O., Fonseca, M. G., Rosan, T. M., Vedovato, L. B., Wagner, F. H., Silva, C. V. J., Silva Junior, C. H. L., Arai, E., Aguiar, A. P., Barlow, J., Berenguer, E., Deeter, M. N., Domingues, L. G., Gatti, L., Gloor, M., Malhi, Y., Marengo, J. A., Miller, J. B., Phillips, O. L., and Saatchi, S.: 21st Century drought-related fires counteract the decline of Amazon deforestation carbon emissions, Nat. Commun., 9, 536, https://doi.org/10.1038/s41467-017-02771-y, 2018.

Archer, D., Eby, M., Brovkin, V., Ridgwell, A., Cao, L., Mikolajewicz, U., Caldeira, K., Matsumoto, K., Munhoven, G., Montenegro, A., and Tokos, K.: Atmospheric Lifetime of Fossil Fuel Carbon Dioxide, Annu. Rev. Earth Pl. Sc., 37, 117–134, https://doi.org/10.1146/annurev.earth.031208.100206, 2009.

Arneth, A., Sitch, S., Pongratz, J., Stocker, B. D., Ciais, P., Poulter, B., Bayer, A. D., Bondeau, A., Calle, L., Chini, L. P., Gasser, T., Fader, M., Friedlingstein, P., Kato, E., Li, W., Lindeskog, M., Nabel, J. E. M. S., Pugh, T. A. M., Robertson, E., Viovy, N., Yue, C., and Zaehle, S.: Historical carbon dioxide emissions caused by land-use changes are possibly larger than assumed, Nat. Geosci., 10, 79–84, https://doi.org/10.1038/ngeo2882, 2017.

Asaadi, A., Arora, V. K., Melton, J. R., and Bartlett, P.: An improved parameterization of leaf area index (LAI) seasonality in the Canadian Land Surface Scheme (CLASS) and Canadian Terrestrial Ecosystem Model (CTEM) modelling framework, Biogeosciences, 15, 6885–6907, https://doi.org/10.5194/bg-15-6885-2018, 2018.

Aumont, O., Orr, J. C., Monfray, P., Ludwig, W., Amiotte-Suchet, P., and Probst, J.-L.: Riverine-driven interhemispheric transport of carbon, Global Biogeochem. Cy., 15, 393–405, https://doi.org/10.1029/1999GB001238, 2001.

Aumont, O., Ethé, C., Tagliabue, A., Bopp, L., and Gehlen, M.: PISCES-v2: an ocean biogeochemical model for carbon and ecosystem studies, Geosci. Model Dev., 8, 2465–2513, https://doi.org/10.5194/gmd-8-2465-2015, 2015.

Babiker, M., G. Berndes, K. Blok, B. Cohen, A. Cowie, O. Geden, V. Ginzburg, A. Leip, P. Smith, M. Sugiyama, F. Yamba, Al Khourdajie, A., Arneth, A., Lima de Azevedo, I. M., Bataille, C., Beerling, D., Bezner Kerr, R., Bradley, J., Buck, H. J., Cabeza, L. F., Calvin, K., Campbell, D., Carnicer Cols, J., Daioglou, V., Harmsen, M., Höglund-Isaksson, L., House, J. I., Keller, D., de Kleijne, K., Kugelberg, S., Makarov, I., Meza, F., Minx, J. C., Morecroft, M., Nabuurs, G. J., Neufeldt, H., Novikova, A., Nugroho, S. B., Oschlies, A., Parmesan, C., Peters, G. P., Poore, J., Portugal-Pereira, J., Postigo, J. C., Pradhan, P., Renforth, P., Rivera-Ferre, M. G., Roe, S., Singh, P. K., Slade, R., Smith, S. M., Tirado von der Pahlen, M. C., and Toribio Ramirez, D.: Cross sectoral perspectives, in: Climate Change 2022: Mitigation of Climate Change. Contribution of Working Group III to the Sixth Assessment Report of the Intergovernmental Panel on Climate Change, edited by: Shukla, P. R., Skea,

J., Slade, R., Al Khourdajie, A., van Diemen, R., McCollum, D., Pathak, M., Some, S., Vyas, P., Fradera, R., Belkacemi, M., Hasija, A., Lisboa, G., Luz, S., and Malley, J., Cambridge University Press, Cambridge, UK and New York, NY, USA, https://doi.org/10.1017/9781009157926.014, 2022.

Baccini, A., Walker, W., Carvalho, L., Farina, M., Sulla-Menashe, D., and Houghton, R. A.: Tropical forests are a net carbon source based on aboveground measurements of gain and loss, Science, 358, 230–234, https://doi.org/10.1126/science.aam5962, 2017.

Bakker, D. C. E., Pfeil, B., Landa, C. S., Metzl, N., O'Brien, K. M., Olsen, A., Smith, K., Cosca, C., Harasawa, S., Jones, S. D., Nakaoka, S., Nojiri, Y., Schuster, U., Steinhoff, T., Sweeney, C., Takahashi, T., Tilbrook, B., Wada, C., Wanninkhof, R., Alin, S. R., Balestrini, C. F., Barbero, L., Bates, N. R., Bianchi, A. A., Bonou, F., Boutin, J., Bozec, Y., Burger, E. F., Cai, W.-J., Castle, R. D., Chen, L., Chierici, M., Currie, K., Evans, W., Featherstone, C., Feely, R. A., Fransson, A., Goyet, C., Greenwood, N., Gregor, L., Hankin, S., Hardman-Mountford, N. J., Harlay, J., Hauck, J., Hoppema, M., Humphreys, M. P., Hunt, C. W., Huss, B., Ibánhez, J. S. P., Johannessen, T., Keeling, R., Kitidis, V., Körtzinger, A., Kozyr, A., Krasakopoulou, E., Kuwata, A., Landschützer, P., Lauvset, S. K., Lefèvre, N., Lo Monaco, C., Manke, A., Mathis, J. T., Merlivat, L., Millero, F. J., Monteiro, P. M. S., Munro, D. R., Murata, A., Newberger, T., Omar, A. M., Ono, T., Paterson, K., Pearce, D., Pierrot, D., Robbins, L. L., Saito, S., Salisbury, J., Schlitzer, R., Schneider, B., Schweitzer, R., Sieger, R., Skjelvan, I., Sullivan, K. F., Sutherland, S. C., Sutton, A. J., Tadokoro, K., Telszewski, M., Tuma, M., van Heuven, S. M. A. C., Vandemark, D., Ward, B., Watson, A. J., and Xu, S.: A multidecade record of high-quality fCO_2 data in version 3 of the Surface Ocean CO_2 Atlas (SOCAT), Earth Syst. Sci. Data, 8, 383–413, https://doi.org/10.5194/essd-8-383-2016, 2016.

Bakker, D. C. E., Alin, S. R., Bates, N., Becker, M., Gkritzalis, T., Jones, S. D., Kozyr, A., Lauvset, S. K., Metzl, N., Nakaoka, S.-I., O'Brien, K. M., Olsen, A., Pierrot, D., Steinhoff, T., Sutton, A. J., Takao, S., Tilbrook, B., Wada, C., Wanninkhof, R., Akl, J., Arbilla, L. A., Arruda, R., Azetsu-Scott, K., Barbero, L., Beatty, C. M., Berghoff, C. F., Bittig, H. C., Burger, E. F., Campbell, K., Cardin, V., Collins, A., Coppola, L., Cronin, M., Cross, J. N., Currie, K. I., Emerson, S. R., Enright, M. P., Enyo, K., Evans, W., Feely, R. A., Flohr, A., Gehrung, M. Glockzin, M., González-Dávila, M., Hamnca, S., Hartman, S., Howden, S. D., Kam, K., Kamb, L., Körtzinger, A., Kosugi, N., Lefèvre, N., Lo Monaco, C., Macovei, V. A., Maenner Jones, S., Manalang, D., Martz, T. R., Mdokwana, B., Monacci, N. M., Monteiro, P. M. S., Mordy, C., Morell, J. M., Murata, A., Neill, C., Noh, J.-H., Nojiri, Y., Ohman, M., Olivier, L., Ono, T., Petersen, W., Plueddemann, A. J., Prytherch, J., Rehder, G., Rutgersson, A., Santana-Casiano, J. M., Schlitzer, R., Send, U., Skjelvan, I., Sullivan, K. F., T'Jampens, M., Tadokoro, K., Telszewski, M., Theetaert, H., Tsanwani, M., Vandemark, D., van Ooijen, E., Veccia, M. H., Voynova, Y. G., Wang, H., Weller, R. A., and Woosley, R. J.: Surface Ocean CO_2 Atlas Database Version 2024 (SOCATv2024) (NCEI Accession 0293257), NOAA National Centers for Environmental Information [data set], https://doi.org/10.25921/9wpn-th28, 2024.

Ballantyne, A. P., Alden, C. B., Miller, J. B., Tans, P. P., and White, J. W. C.: Increase in observed net carbon dioxide uptake by land and oceans during the past 50 years, Nature, 488, 70–72, https://doi.org/10.1038/nature11299, 2012.

Ballantyne, A. P., Andres, R., Houghton, R., Stocker, B. D., Wanninkhof, R., Anderegg, W., Cooper, L. A., DeGrandpre, M., Tans, P. P., Miller, J. B., Alden, C., and White, J. W. C.: Audit of the global carbon budget: estimate errors and their impact on uptake uncertainty, Biogeosciences, 12, 2565–2584, https://doi.org/10.5194/bg-12-2565-2015, 2015.

Bastos, A., Hartung, K., Nützel, T. B., Nabel, J. E. M. S., Houghton, R. A., and Pongratz, J.: Comparison of uncertainties in land-use change fluxes from bookkeeping model parameterisation, Earth Syst. Dynam., 12, 745–762, https://doi.org/10.5194/esd-12-745-2021, 2021.

Battle, M. O., Raynor, R., Kesler, S., and Keeling, R.: Technical Note: The impact of industrial activity on the amount of atmospheric O_2, Atmos. Chem. Phys. Discuss. [preprint], https://doi.org/10.5194/acp-2022-765, 2023.

Bellenger, H., Bopp, L., Ethé, C., Ho, D., Duvel, J. P., Flavoni, S., Guez, L., Kataoka, T., Perrot, X., Parc, L., and Watanabe, M.: Sensitivity of the Global Ocean Carbon Sink to the Ocean Skin in a Climate Model, J. Geophys. Res.-Oceans, 128, e2022JC019479, https://doi.org/10.1029/2022JC019479, 2023.

Bennington, V., Gloege, L., and McKinley, G. A.: Variability in the Global Ocean Carbon Sink From 1959 to 2020 by Correcting Models with Observations, Geophys. Res. Lett., 49, e2022GL098632, https://doi.org/10.1029/2022GL098632, 2022.

Bernardello, R., Sicardi, V., Lapin, V., Ortega, P., Ruprich-Robert, Y., Tourigny, E., and Ferrer, E.: Ocean biogeochemical reconstructions to estimate historical ocean CO_2 uptake, Earth Syst. Dynam., 15, 1255–1275, https://doi.org/10.5194/esd-15-1255-2024, 2024.

Berthet, S., Séférian, R., Bricaud, C., Chevallier, M., Voldoire, A., and Ethé, C.: Evaluation of an Online Grid-Coarsening Algorithm in a Global Eddy-Admitting Ocean Biogeochemical Model, J. Adv. Model Earth Sy., 11, 1759–1783, https://doi.org/10.1029/2019MS001644, 2019.

Betts, R. A., Jones, C. D., Knight, J. R., Keeling, R. F., and Kennedy, J. J.: El Niño and a record CO_2 rise, Nat. Clim. Change, 6, 806–810, https://doi.org/10.1038/nclimate3063, 2016.

Bilbao, R., Wild, S., Ortega, P., Acosta-Navarro, J., Arsouze, T., Bretonnière, P.-A., Caron, L.-P., Castrillo, M., Cruz-García, R., Cvijanovic, I., Doblas-Reyes, F. J., Donat, M., Dutra, E., Echevarría, P., Ho, A.-C., Loosveldt-Tomas, S., Moreno-Chamarro, E., Pérez-Zanon, N., Ramos, A., Ruprich-Robert, Y., Sicardi, V., Tourigny, E., and Vegas-Regidor, J.: Assessment of a full-field initialized decadal climate prediction system with the CMIP6 version of EC-Earth, Earth Syst. Dynam., 12, 173–196, https://doi.org/10.5194/esd-12-173-2021, 2021.

Bloom, A. A. and Williams, M.: Constraining ecosystem carbon dynamics in a data-limited world: integrating ecological "common sense" in a model–data fusion framework, Biogeosciences, 12, 1299–1315, https://doi.org/10.5194/bg-12-1299-2015, 2015.

Bloom, A. A., Exbrayat, J.-F., van der Velde, I. R., Feng, L., and Williams, M.: The decadal state of the terrestrial carbon cycle: Global retrievals of terrestrial carbon allocation, pools, and residence times, P. Natl. Acad. Sci. USA, 113, 1285–1290, https://doi.org/10.1073/pnas.1515160113, 2016.

Boer, G. J., Smith, D. M., Cassou, C., Doblas-Reyes, F., Danabasoglu, G., Kirtman, B., Kushnir, Y., Kimoto, M., Meehl, G. A.,

Msadek, R., Mueller, W. A., Taylor, K. E., Zwiers, F., Rixen, M., Ruprich-Robert, Y., and Eade, R.: The Decadal Climate Prediction Project (DCPP) contribution to CMIP6, Geosci. Model Dev., 9, 3751–3777, https://doi.org/10.5194/gmd-9-3751-2016, 2016.

Boucher, O., Servonnat, J., Albright, A. L., Aumont, O., Balkanski, Y., Bastrikov, V., Bekki, S., Bonnet, R., Bony, S., Bopp, L., Braconnot, P., Brockmann, P., Cadule, P., Caubel, A., Cheruy, F., Codron, F., Cozic, A., Cugnet, D., D'Andrea, F., Davini, P., de Lavergne, C., Denvil, S., Deshayes, J., Devilliers, M., Ducharne, A., Dufresne, J.-L., Dupont, E., Éthé, C., Fairhead, L., Falletti, L., Flavoni, S., Foujols, M.-A., Gardoll, S., Gastineau, G., Ghattas, J., Grandpeix, J.-Y., Guenet, B., Guez, E., Lionel, Guilyardi, E., Guimberteau, M., Hauglustaine, D., Hourdin, F., Idelkadi, A., Joussaume, S., Kageyama, M., Khodri, M., Krinner, G., Lebas, N., Levavasseur, G., Lévy, C., Li, L., Lott, F., Lurton, T., Luyssaert, S., Madec, G., Madeleine, J.-B., Maignan, F., Marchand, M., Marti, O., Mellul, L., Meurdesoif, Y., Mignot, J., Musat, I., Ottlé, C., Peylin, P., Planton, Y., Polcher, J., Rio, C., Rochetin, N., Rousset, C., Sepulchre, P., Sima, A., Swingedouw, D., Thiéblemont, R., Traore, A. K., Vancoppenolle, M., Vial, J., Vialard, J., Viovy, N., and Vuichard, N.: Presentation and Evaluation of the IPSL-CM6A-LR Climate Model, J. Adv. Model. Earth Sy., 12, e2019MS002010, https://doi.org/10.1029/2019MS002010, 2020.

Bourgeois, T., Goris, N., Schwinger, J., and Tjiputra, J. F.: Stratification constrains future heat and carbon uptake in the Southern Ocean between 30° S and 55° S, Nat. Commun., 13, 340, https://doi.org/10.1038/s41467-022-27979-5, 2022.

Bray, E.: 2017 Minerals Yearbook: Aluminum [Advance Release], Tech. rep., U.S. Geological Survey, https://d9-wret.s3-us-west-2.amazonaws.com/assets/palladium/production/atoms/files/myb1-2017-alumi.pdf (last access: 21 January 2025), 2020.

Brienen, R. J. W., Phillips, O. L., Feldpausch, T. R., Gloor, E., Baker, T. R., Lloyd, J., Lopez-Gonzalez, G., Monteagudo-Mendoza, A., Malhi, Y., Lewis, S. L., Vásquez Martinez, R., Alexiades, M., Álvarez Dávila, E., Alvarez-Loayza, P., Andrade, A., Aragão, L. E. O. C., Araujo-Murakami, A., Arets, E. J. M. M., Arroyo, L., Aymard C., G. A., Bánki, O. S., Baraloto, C., Barroso, J., Bonal, D., Boot, R. G. A., Camargo, J. L. C., Castilho, C. V., Chama, V., Chao, K. J., Chave, J., Comiskey, J. A., Cornejo Valverde, F., da Costa, L., de Oliveira, E. A., Di Fiore, A., Erwin, T. L., Fauset, S., Forsthofer, M., Galbraith, D. R., Grahame, E. S., Groot, N., Hérault, B., Higuchi, N., Honorio Coronado, E. N., Keeling, H., Killeen, T. J., Laurance, W. F., Laurance, S., Licona, J., Magnussen, W. E., Marimon, B. S., Marimon-Junior, B. H., Mendoza, C., Neill, D. A., Nogueira, E. M., Núñez, P., Pallqui Camacho, N. C., Parada, A., Pardo-Molina, G., Peacock, J., Peña-Claros, M., Pickavance, G. C., Pitman, N. C. A., Poorter, L., Prieto, A., Quesada, C. A., Ramírez, F., Ramírez-Angulo, H., Restrepo, Z., Roopsind, A., Rudas, A., Salomão, R. P., Schwarz, M., Silva, N., Silva-Espejo, J. E., Silveira, M., Stropp, J., Talbot, J., ter Steege, H., Teran-Aguilar, J., Terborgh, J., Thomas-Caesar, R., Toledo, M., Torello-Raventos, M., Umetsu, R. K., van der Heijden, G. M. F., van der Hout, P., Guimarães Vieira, I. C., Vieira, S. A., Vilanova, E., Vos, V. A., and Zagt, R. J.: Long-term decline of the Amazon carbon sink, Nature, 519, 344–348, https://doi.org/10.1038/nature14283, 2015.

Brienen, R. J. W., Caldwell, L., Duchesne, L., Voelker, S., Barichivich, J., Baliva, M., Ceccantini, G., Di Filippo, A., Helama, S., Locosselli, G. M., Lopez, L., Piovesan, G., Schöngart, J., Villalba, R., and Gloor, E.: Forest carbon sink neutralized by pervasive growth-lifespan trade-offs, Nat. Commun., 11, 4241, https://doi.org/10.1038/s41467-020-17966-z, 2020.

Bronselaer, B., Winton, M., Russell, J., Sabine, C. L., and Khatiwala, S.: Agreement of CMIP5 Simulated and Observed Ocean Anthropogenic CO_2 Uptake, Geophys. Res. Lett., 44, 12298–12305, https://doi.org/10.1002/2017GL074435, 2017.

Bruno, M. and Joos, F.: Terrestrial carbon storage during the past 200 years: A Monte Carlo Analysis of CO_2 data from ice core and atmospheric measurements, Global Biogeochem. Cy., 11, 111–124, https://doi.org/10.1029/96GB03611, 1997.

Burrows, S. M., Maltrud, M., Yang, X., Zhu, Q., Jeffery, N., Shi, X., Ricciuto, D., Wang, S., Bisht, G., Tang, J., Wolfe, J., Harrop, B. E., Singh, B., Brent, L., Baldwin, S., Zhou, T., Cameron-Smith, P., Keen, N., Collier, N., Xu, M., Hunke, E. C., Elliott, S. M., Turner, A. K., Li, H., Wang, H., Golaz, J.-C., Bond-Lamberty, B., Hoffman, F. M., Riley, W. J., Thornton, P. E., Calvin, K., and Leung, L. R.: The DOE E3SM v1.1 Biogeochemistry Configuration: Description and Simulated Ecosystem-Climate Responses to Historical Changes in Forcing, J. Adv. Model. Earth Sy., 12, e2019MS001766, https://doi.org/10.1029/2019MS001766, 2020.

Bunsen, F., Nissen, C., and Hauck, J.: The Impact of Recent Climate Change on the Global Ocean Carbon Sink, Geophys. Res. Lett., 51, e2023GL107030, https://doi.org/10.1029/2023GL107030, 2024.

Burton, C., Betts, R., Cardoso, M., Feldpausch, T. R., Harper, A., Jones, C. D., Kelley, D. I., Robertson, E., and Wiltshire, A.: Representation of fire, land-use change and vegetation dynamics in the Joint UK Land Environment Simulator vn4.9 (JULES), Geosci. Model Dev., 12, 179–193, https://doi.org/10.5194/gmd-12-179-2019, 2019.

Burton, C., Lampe, S., Kelley, D. I., Thiery, W., Hantson, S., Christidis, N., Gudmundsson, L., Forrest, M., Burke, E., Chang, J., Huang, H., Ito, A., Kou-Giesbrecht, S., Lasslop, G., Li, W., Nieradzik, L., Li, F., Chen, Y., Randerson, J., Reyer, C. P. O., and Mengel, M.: Global burned area increasingly explained by climate change, Nat. Clim. Change, 14, 1186–1192, https://doi.org/10.1038/s41558-024-02140-w, 2024.

Bushinsky, S. M., Landschützer, P., Rödenbeck, C., Gray, A. R., Baker, D., Mazloff, M. R., Resplandy, L., Johnson, K. S., and Sarmiento, J. L.: Reassessing Southern Ocean Air-Sea CO_2 Flux Estimates With the Addition of Biogeochemical Float Observations, Global Biogeochem. Cy., 33, 1370–1388, https://doi.org/10.1029/2019GB006176, 2019.

Byrne, B., Liu, J., Bowman, K. W., Pascolini-Campbell, M., Chatterjee, A., Pandey, S., Miyazaki, K., van der Werf, G. R., Wunch, D., Wennberg, P. O., Roehl, C. M., and Sinha, S.: Carbon emissions from the 2023 Canadian wildfires, Nature, 633, 835–839, https://doi.org/10.1038/s41586-024-07878-z, 2024a.

Byrne, B., Liu, J., Bowman, K. W., Yin, Y., Yun, J., Ferreira, G. D., Ogle, S. M., Baskaran, L., He, L., Li, X., Xiao, J., and Davis, K. J.: Regional Inversion Shows Promise in Capturing Extreme-Event-Driven CO_2 Flux Anomalies but Is Limited by Atmospheric CO_2 Observational Coverage, J. Geophys. Res.-Atmos.,

129, e2023JD040006, https://doi.org/10.1029/2023JD040006, 2024b.

Canadell, J. G., Le Quéré, C., Raupach, M. R., Field, C. B., Buitenhuis, E. T., Ciais, P., Conway, T. J., Gillett, N. P., Houghton, R. A., and Marland, G.: Contributions to accelerating atmospheric CO_2 growth from economic activity, carbon intensity, and efficiency of natural sinks, P. Natl. Acad. Sci. USA, 104, 18866–18870, https://doi.org/10.1073/pnas.0702737104, 2007.

Canadell, J. G., Monteiro, P. M. S., Costa, M. H., Cotrim da Cunha, L., Cox, P. M., Eliseev, A. V., Henson, S., Ishii, M., Jaccard, S., Koven, C., Lohila, A., Patra, P. K., Piao, S., Rogelj, J., Syampungani, S., Zaehle, S., and Zickfeld, K.: Global Carbon and other Biogeochemical Cycles and Feedbacks. In: Climate Change 2021: The Physical Science Basis. Contribution of Working Group I to the Sixth Assessment Report of the Intergovernmental Panel on Climate Change, edited by: Masson-Delmotte, V., Zhai, P., Pirani, A., Connors, S. L., Péan, C., Berger, S., Caud, N., Chen, Y., Goldfarb, L., Gomis, M. I., Huang, M., Leitzell, K., Lonnoy, E., Matthews, J. B. R., Maycock, T. K., Waterfield, T., Yelekçi, O., Yu, R., and Zhou, B., Cambridge University Press, Cambridge, United Kingdom and New York, NY, USA, 673–816, https://doi.org/10.1017/9781009157896.007, 2021.

Cao, Z., Myers, R. J., Lupton, R. C., Duan, H., Sacchi, R., Zhou, N., Reed Miller, T., Cullen, J. M., Ge, Q., and Liu, G.: The sponge effect and carbon emission mitigation potentials of the global cement cycle, Nat. Commun., 11, 3777, https://doi.org/10.1038/s41467-020-17583-w, 2020.

Centro Nacional de Monitoramento e Alertas de Desastres Naturais (CEMADEN): Monitoramento de secas e impactos no Brasil – Agosto 2024, https://www.gov.br/cemaden/pt-br/assuntos/monitoramento/monitoramento-de-seca-para-o-brasil/monitoramento-de-secas-e-impactos-no-brasil-agosto-2024 (last access: 21 January 2025), 2024.

Chandra, N., Patra, P. K., Niwa, Y., Ito, A., Iida, Y., Goto, D., Morimoto, S., Kondo, M., Takigawa, M., Hajima, T., and Watanabe, M.: Estimated regional CO_2 flux and uncertainty based on an ensemble of atmospheric CO_2 inversions, Atmos. Chem. Phys., 22, 9215–9243, https://doi.org/10.5194/acp-22-9215-2022, 2022.

Chau, T. T. T., Gehlen, M., and Chevallier, F.: A seamless ensemble-based reconstruction of surface ocean pCO_2 and air–sea CO_2 fluxes over the global coastal and open oceans, Biogeosciences, 19, 1087–1109, https://doi.org/10.5194/bg-19-1087-2022, 2022.

Chevallier, F., Fisher, M., Peylin, P., Serrar, S., Bousquet, P., Bréon, F.-M., Chédin, A., and Ciais, P.: Inferring CO_2 sources and sinks from satellite observations: Method and application to TOVS data, J. Geophys. Res., 110, D24309, https://doi.org/10.1029/2005JD006390, 2005.

Ciais, P., Sabine, C., Bala, G., Bopp, L., Brovkin, V., Canadell, J. G., Chhabra, A., DeFries, R., Galloway, J., Heimann, M., Jones, C., Le Quéré, C., Myneni, R., Piao, S., Thornton, P., Willem, J., Friedlingstein, P., and Munhoven, G.: Carbon and Other Biogeochemical Cycles, in: Climate Change 2013: The Physical Science Basis, Contribution of Working Group I to the Fifth Assessment Report of the Intergovernmental Panel on Climate Change, edited by: Intergovernmental Panel on Climate Change, Cambridge University Press, Cambridge, United Kingdom and New York, NY, USA, https://doi.org/10.1017/CBO9781107415324.015, 2013.

Ciais, P., Tan, J., Wang, X., Roedenbeck, C., Chevallier, F., Piao, S.-L., Moriarty, R., Broquet, G., Le Quéré, C., Canadell, J. G., Peng, S., Poulter, B., Liu, Z., and Tans, P.: Five decades of northern land carbon uptake revealed by the interhemispheric CO_2 gradient, Nature, 568, 221–225, https://doi.org/10.1038/s41586-019-1078-6, 2019.

Ciais, P., Bastos, A., Chevallier, F., Lauerwald, R., Poulter, B., Canadell, J. G., Hugelius, G., Jackson, R. B., Jain, A., Jones, M., Kondo, M., Luijkx, I. T., Patra, P. K., Peters, W., Pongratz, J., Petrescu, A. M. R., Piao, S., Qiu, C., Von Randow, C., Regnier, P., Saunois, M., Scholes, R., Shvidenko, A., Tian, H., Yang, H., Wang, X., and Zheng, B.: Definitions and methods to estimate regional land carbon fluxes for the second phase of the REgional Carbon Cycle Assessment and Processes Project (RECCAP-2), Geosci. Model Dev., 15, 1289–1316, https://doi.org/10.5194/gmd-15-1289-2022, 2022.

Collier, N., Hoffman, F. M., Lawrence, D. M., Keppel-Aleks, G., Koven, C. D., Riley, W. J., Mu, M., and Randerson, J. T.: The International Land Model Benchmarking (ILAMB) System: Design, Theory, and Implementation, J. Adv. Model. Earth Sy., 10, 2731–2754, https://doi.org/10.1029/2018MS001354, 2018.

Conchedda, G. and Tubiello, F. N.: Drainage of organic soils and GHG emissions: validation with country data, Earth Syst. Sci. Data, 12, 3113–3137, https://doi.org/10.5194/essd-12-3113-2020, 2020.

Cox, P. M., Pearson, D., Booth, B. B., Friedlingstein, P., Huntingford, C., Jones, C. D., and Luke, C. M.: Sensitivity of tropical carbon to climate change constrained by carbon dioxide variability, Nature, 494, 341–344, https://doi.org/10.1038/nature11882, 2013.

Crisp, D., Dolman, H., Tanhua, T., McKinley, G. A., Hauck, J., Bastos, A., Sitch, S., Eggleston, S., and Aich, V.: How Well Do We Understand the Land-Ocean-Atmosphere Carbon Cycle?, Rev. Geophys., 60, e2021RG000736, https://doi.org/10.1029/2021RG000736, 2022.

De Kauwe, M. G., Medlyn, B. E., Zaehle, S., Walker, A. P., Dietze, M. C., Wang, Y.-P., Luo, Y., Jain, A. K., El-Masri, B., Hickler, T., Wårlind, D., Weng, E., Parton, W. J., Thornton, P. E., Wang, S., Prentice, I. C., Asao, S., Smith, B., McCarthy, H. R., Iversen, C. M., Hanson, P. J., Warren, J. M., Oren, R., and Norby, R. J.: Where does the carbon go? A model–data intercomparison of vegetation carbon allocation and turnover processes at two temperate forest free-air CO_2 enrichment sites, New Phytol., 203, 883–899, https://doi.org/10.1111/nph.12847, 2014.

Delire, C., Séférian, R., Decharme, B., Alkama, R., Calvet, J.-C., Carrer, D., Gibelin, A.-L., Joetzjer, E., Morel, X., Rocher, M., and Tzanos, D.: The Global Land Carbon Cycle Simulated With ISBA-CTRIP: Improvements Over the Last Decade, J. Adv. Model. Earth Sy., 12, e2019MS001886, https://doi.org/10.1029/2019MS001886, 2020.

Denman, K. L., Brasseur, G., Chidthaisong, A., Ciais, P., Cox, P. M., Dickinson, R. E., Hauglustaine, D., Heinze, C., Holland, E., Jacob, D., Lohmann, U., Ramachandran, S., Leite da Silva Dias, P., Wofsy, S. C., and Zhang, X.: Couplings Between Changes in the Climate System and Biogeochemistry, in: Climate Change 2007: The Physical Science Basis. Contribution of Working Group I to the Fourth Assessment Report of the Intergovernmental Panel on Climate Change, edited by: Solomon, S., Qin, D., Manning, M., Marquis, M., Averyt, K., Tignor, M. M. B., Miller, H. L., and

Chen, Z. L., Cambridge University Press, Cambridge, UK and New York, USA, 499–587, ISBN 9780521705967, 2007.

Denvil-Sommer, A., Gehlen, M., and Vrac, M.: Observation system simulation experiments in the Atlantic Ocean for enhanced surface ocean pCO_2 reconstructions, Ocean Sci., 17, 1011–1030, https://doi.org/10.5194/os-17-1011-2021, 2021.

DeVries, T.: The oceanic anthropogenic CO_2 sink: Storage, air-sea fluxes, and transports over the industrial era, Global Biogeochem. Cy., 28, 631–647, https://doi.org/10.1002/2013GB004739, 2014.

DeVries, T., Holzer, M., and Primeau, F.: Recent increase in oceanic carbon uptake driven by weaker upper-ocean overturning, Nature, 542, 215–218, https://doi.org/10.1038/nature21068, 2017.

DeVries, T., Quéré, C. L., Andrews, O., Berthet, S., Hauck, J., Ilyina, T., Landschützer, P., Lenton, A., Lima, I. D., Nowicki, M., Schwinger, J., and Séférian, R.: Decadal trends in the ocean carbon sink, P. Natl. Acad. Sci. USA, 116, 11646–11651, https://doi.org/10.1073/pnas.1900371116, 2019.

DeVries, T., Yamamoto, K., Wanninkhof, R., Gruber, N., Hauck, J., Müller, J. D., Bopp, L., Carroll, D., Carter, B., Chau, T.-T.-T., Doney, S. C., Gehlen, M., Gloege, L., Gregor, L., Henson, S., Kim, J. H., Iida, Y., Ilyina, T., Landschützer, P., Le Quéré, C., Munro, D., Nissen, C., Patara, L., Pérez, F. F., Resplandy, L., Rodgers, K. B., Schwinger, J., Séférian, R., Sicardi, V., Terhaar, J., Triñanes, J., Tsujino, H., Watson, A., Yasunaka, S., and Zeng, J.: Magnitude, trends, and variability of the global ocean carbon sink from 1985–2018, Global Biogeochem. Cy., 37, e2023GB007780, https://doi.org/10.1029/2023GB007780, 2023.

Döscher, R., Acosta, M., Alessandri, A., Anthoni, P., Arsouze, T., Bergman, T., Bernardello, R., Boussetta, S., Caron, L.-P., Carver, G., Castrillo, M., Catalano, F., Cvijanovic, I., Davini, P., Dekker, E., Doblas-Reyes, F. J., Docquier, D., Echevarria, P., Fladrich, U., Fuentes-Franco, R., Gröger, M., v. Hardenberg, J., Hieronymus, J., Karami, M. P., Keskinen, J.-P., Koenigk, T., Makkonen, R., Massonnet, F., Ménégoz, M., Miller, P. A., Moreno-Chamarro, E., Nieradzik, L., van Noije, T., Nolan, P., O'Donnell, D., Ollinaho, P., van den Oord, G., Ortega, P., Prims, O. T., Ramos, A., Reerink, T., Rousset, C., Ruprich-Robert, Y., Le Sager, P., Schmith, T., Schrödner, R., Serva, F., Sicardi, V., Sloth Madsen, M., Smith, B., Tian, T., Tourigny, E., Uotila, P., Vancoppenolle, M., Wang, S., Wårlind, D., Willén, U., Wyser, K., Yang, S., Yepes-Arbós, X., and Zhang, Q.: The EC-Earth3 Earth system model for the Coupled Model Intercomparison Project 6, Geosci. Model Dev., 15, 2973–3020, https://doi.org/10.5194/gmd-15-2973-2022, 2022.

Doney, S. C., Lima, I., Feely, R. A., Glover, D. M., Lindsay, K., Mahowald, N., Moore, J. K., and Wanninkhof, R.: Mechanisms governing interannual variability in upper-ocean inorganic carbon system and air–sea CO_2 fluxes: Physical climate and atmospheric dust, Deep-Sea Res. Pt. II, 56, 640–655, https://doi.org/10.1016/j.dsr2.2008.12.006, 2009.

Dong, Y., Bakker, D. C. E., Bell, T. G., Huang, B., Landschützer, P., Liss, P. S., and Yang, M.: Update on the Temperature Corrections of Global Air-Sea CO_2 Flux Estimates, Global Biogeochem. Cy, 36, e2022GB007360, https://doi.org/10.1029/2022GB007360, 2022.

Dong, Y., Bakker, D. C. E., Bell, T. G., Yang, M., Landschützer, P., Hauck, J., Rödenbeck, C., Kitidis, V., Bushinsky, S. M., and Liss, P. S.: Direct observational evidence of strong CO_2 uptake in the Southern Ocean. Sci. Adv., 10, eadn5781, https://doi.org/10.1126/sciadv.adn5781, 2024a.

Dong, Y., Bakker, D. C. E., and Landschützer, P.: Accuracy of ocean CO_2 uptake estimates at a risk by a reduction in the data collection. Geophys. Res. Lett., 51, e2024GL108502, https://doi.org/10.1029/2024GL108502, 2024b.

Dorgeist, L., Schwingshackl, C., Bultan, S., and Pongratz, J.: A consistent budgeting of terrestrial carbon fluxes, Nat. Commun., 15, 7426, https://doi.org/10.1038/s41467-024-51126-x, 2024.

EIA: Short-Term Energy Outlook: September 2023, U.S. Energy Information Administration [data set], http://www.eia.gov/forecasts/steo/outlook.cfm (last access: 21 January 2025), 2023.

Embury, O., Merchant, C. J., Good, S. A., Rayner, N. A., Høyer, J. L., Atkinson, C., Block, T., Alerskans, E., Pearson, K. J., Worsfold, M., and McCarroll, N., and Donlon, C.: Satellite-based time-series of sea-surface temperature since 1980 for climate applications, Sci. Data, 11, 326, https://doi.org/10.1038/s41597-024-03147-w, 2024.

Emmons, L. K., Walters, S., Hess, P. G., Lamarque, J.-F., Pfister, G. G., Fillmore, D., Granier, C., Guenther, A., Kinnison, D., Laepple, T., Orlando, J., Tie, X., Tyndall, G., Wiedinmyer, C., Baughcum, S. L., and Kloster, S.: Description and evaluation of the Model for Ozone and Related chemical Tracers, version 4 (MOZART-4), Geosci. Model Dev., 3, 43–67, https://doi.org/10.5194/gmd-3-43-2010, 2010.

Erb, K.-H., Kastner, T., Luyssaert, S., Houghton, R. A., Kuemmerle, T., Olofsson, P., and Haberl, H.: Bias in the attribution of forest carbon sinks, Nat. Clim. Change, 3, 854–856, https://doi.org/10.1038/nclimate2004, 2013.

Erb, K.-H., Kastner, T., Plutzar, C., Bais, A. L. S., Carvalhais, N., Fetzel, T., Gingrich, S., Haberl, H., Lauk, C., Niedertscheider, M., Pongratz, J., Thurner, M., and Luyssaert, S.: Unexpectedly large impact of forest management and grazing on global vegetation biomass, Nature, 553, 73–76, https://doi.org/10.1038/nature25138, 2018.

Eskander, S. M. S. U. and Fankhauser, S.: Reduction in greenhouse gas emissions from national climate legislation, Nat. Clim. Change, 10, 750–756, https://doi.org/10.1038/s41558-020-0831-z, 2020.

Etheridge, D. M., Steele, L. P., Langenfelds, R. L., Francey, R. J., Barnola, J.-M., and Morgan, V. I.: Natural and anthropogenic changes in atmospheric CO_2 over the last 1000 years from air in Antarctic ice and firn, J. Geophys. Res., 101, 4115–4128, https://doi.org/10.1029/95JD03410, 1996.

Eyring, V., Bony, S., Meehl, G. A., Senior, C. A., Stevens, B., Stouffer, R. J., and Taylor, K. E.: Overview of the Coupled Model Intercomparison Project Phase 6 (CMIP6) experimental design and organization, Geosci. Model Dev., 9, 1937–1958, https://doi.org/10.5194/gmd-9-1937-2016, 2016.

FAO: Impact of the Ukraine-Russia conflict on global food security and related matters under the mandate of the Food and Agriculture Organization of the United Nations (FAO), Hundred and Seventieth Session of the Council, https://www.fao.org/3/nj164en/nj164en.pdf (last access: 21 January 2025), 2023a.

FAO: FAOSTAT Climate Change: Agrifood systems emissions, Emissions from Drained, http://www.fao.org/faostat/en/#data/GV (last access: 12 January 2025), 2023b.

Fay, A. R., Gregor, L., Landschützer, P., McKinley, G. A., Gruber, N., Gehlen, M., Iida, Y., Laruelle, G. G., Rödenbeck, C., Roobaert, A., and Zeng, J.: SeaFlux: harmonization of air–sea CO_2 fluxes from surface pCO_2 data products using a standardized approach, Earth Syst. Sci. Data, 13, 4693–4710, https://doi.org/10.5194/essd-13-4693-2021, 2021.

Feng, L., Palmer, P. I., Parker, R. J., Deutscher, N. M., Feist, D. G., Kivi, R., Morino, I., and Sussmann, R.: Estimates of European uptake of CO_2 inferred from GOSAT X_{CO_2} retrievals: sensitivity to measurement bias inside and outside Europe, Atmos. Chem. Phys., 16, 1289–1302, https://doi.org/10.5194/acp-16-1289-2016, 2016.

Flanagan, D.: 2017 Minerals Yearbook: Copper [Advance Release], Tech. rep., U.S. Geological Survey, https://pubs.usgs.gov/myb/vol1/2017/myb1-2017-copper.pdf (last access: 21 January 2025), 2021.

Ford, D., Blannin, J., Watts, J., Watson, A., Landschützer, P., Jersild, A. and Shutler, J.: A comprehensive analysis of air-sea CO_2 flux uncertainties constructed from surface ocean data products, Global Biogeochem. Cy., 38, e2024GB008188, https://doi.org/10.1029/2024GB008188, 2024.

Forster, P. M., Smith, C., Walsh, T., Lamb, W. F., Lamboll, R., Hall, B., Hauser, M., Ribes, A., Rosen, D., Gillett, N. P., Palmer, M. D., Rogelj, J., von Schuckmann, K., Trewin, B., Allen, M., Andrew, R., Betts, R. A., Borger, A., Boyer, T., Broersma, J. A., Buontempo, C., Burgess, S., Cagnazzo, C., Cheng, L., Friedlingstein, P., Gettelman, A., Gütschow, J., Ishii, M., Jenkins, S., Lan, X., Morice, C., Mühle, J., Kadow, C., Kennedy, J., Killick, R. E., Krummel, P. B., Minx, J. C., Myhre, G., Naik, V., Peters, G. P., Pirani, A., Pongratz, J., Schleussner, C.-F., Seneviratne, S. I., Szopa, S., Thorne, P., Kovilakam, M. V. M., Majamäki, E., Jalkanen, J.-P., van Marle, M., Hoesly, R. M., Rohde, R., Schumacher, D., van der Werf, G., Vose, R., Zickfeld, K., Zhang, X., Masson-Delmotte, V., and Zhai, P.: Indicators of Global Climate Change 2023: annual update of key indicators of the state of the climate system and human influence, Earth Syst. Sci. Data, 16, 2625–2658, https://doi.org/10.5194/essd-16-2625-2024, 2024.

Friedlingstein, P., Houghton, R. A., Marland, G., Hackler, J., Boden, T. A., Conway, T. J., Canadell, J. G., Raupach, M. R., Ciais, P., and Le Quéré, C.: Update on CO_2 emissions, Nat. Geosci., 3, 811–812, https://doi.org/10.1038/ngeo1022, 2010.

Friedlingstein, P., Andrew, R. M., Rogelj, J., Peters, G. P., Canadell, J. G., Knutti, R., Luderer, G., Raupach, M. R., Schaeffer, M., van Vuuren, D. P., and Le Quéré, C.: Persistent growth of CO_2 emissions and implications for reaching climate targets, Nat. Geosci., 7, 709–715, https://doi.org/10.1038/ngeo2248, 2014.

Friedlingstein, P., Jones, M. W., O'Sullivan, M., Andrew, R. M., Hauck, J., Peters, G. P., Peters, W., Pongratz, J., Sitch, S., Le Quéré, C., Bakker, D. C. E., Canadell, J. G., Ciais, P., Jackson, R. B., Anthoni, P., Barbero, L., Bastos, A., Bastrikov, V., Becker, M., Bopp, L., Buitenhuis, E., Chandra, N., Chevallier, F., Chini, L. P., Currie, K. I., Feely, R. A., Gehlen, M., Gilfillan, D., Gkritzalis, T., Goll, D. S., Gruber, N., Gutekunst, S., Harris, I., Haverd, V., Houghton, R. A., Hurtt, G., Ilyina, T., Jain, A. K., Joetzjer, E., Kaplan, J. O., Kato, E., Klein Goldewijk, K., Korsbakken, J. I., Landschützer, P., Lauvset, S. K., Lefèvre, N., Lenton, A., Lienert, S., Lombardozzi, D., Marland, G., McGuire, P. C., Melton, J. R., Metzl, N., Munro, D. R., Nabel, J. E. M. S., Nakaoka, S.-I., Neill, C., Omar, A. M., Ono, T., Peregon, A., Pierrot, D., Poulter, B., Rehder, G., Resplandy, L., Robertson, E., Rödenbeck, C., Séférian, R., Schwinger, J., Smith, N., Tans, P. P., Tian, H., Tilbrook, B., Tubiello, F. N., van der Werf, G. R., Wiltshire, A. J., and Zaehle, S.: Global Carbon Budget 2019, Earth Syst. Sci. Data, 11, 1783–1838, https://doi.org/10.5194/essd-11-1783-2019, 2019.

Friedlingstein, P., O'Sullivan, M., Jones, M. W., Andrew, R. M., Hauck, J., Olsen, A., Peters, G. P., Peters, W., Pongratz, J., Sitch, S., Le Quéré, C., Canadell, J. G., Ciais, P., Jackson, R. B., Alin, S., Aragão, L. E. O. C., Arneth, A., Arora, V., Bates, N. R., Becker, M., Benoit-Cattin, A., Bittig, H. C., Bopp, L., Bultan, S., Chandra, N., Chevallier, F., Chini, L. P., Evans, W., Florentie, L., Forster, P. M., Gasser, T., Gehlen, M., Gilfillan, D., Gkritzalis, T., Gregor, L., Gruber, N., Harris, I., Hartung, K., Haverd, V., Houghton, R. A., Ilyina, T., Jain, A. K., Joetzjer, E., Kadono, K., Kato, E., Kitidis, V., Korsbakken, J. I., Landschützer, P., Lefèvre, N., Lenton, A., Lienert, S., Liu, Z., Lombardozzi, D., Marland, G., Metzl, N., Munro, D. R., Nabel, J. E. M. S., Nakaoka, S.-I., Niwa, Y., O'Brien, K., Ono, T., Palmer, P. I., Pierrot, D., Poulter, B., Resplandy, L., Robertson, E., Rödenbeck, C., Schwinger, J., Séférian, R., Skjelvan, I., Smith, A. J. P., Sutton, A. J., Tanhua, T., Tans, P. P., Tian, H., Tilbrook, B., van der Werf, G., Vuichard, N., Walker, A. P., Wanninkhof, R., Watson, A. J., Willis, D., Wiltshire, A. J., Yuan, W., Yue, X., and Zaehle, S.: Global Carbon Budget 2020, Earth Syst. Sci. Data, 12, 3269–3340, https://doi.org/10.5194/essd-12-3269-2020, 2020.

Friedlingstein, P., Jones, M. W., O'Sullivan, M., Andrew, R. M., Bakker, D. C. E., Hauck, J., Le Quéré, C., Peters, G. P., Peters, W., Pongratz, J., Sitch, S., Canadell, J. G., Ciais, P., Jackson, R. B., Alin, S. R., Anthoni, P., Bates, N. R., Becker, M., Bellouin, N., Bopp, L., Chau, T. T. T., Chevallier, F., Chini, L. P., Cronin, M., Currie, K. I., Decharme, B., Djeutchouang, L. M., Dou, X., Evans, W., Feely, R. A., Feng, L., Gasser, T., Gilfillan, D., Gkritzalis, T., Grassi, G., Gregor, L., Gruber, N., Gürses, Ö., Harris, I., Houghton, R. A., Hurtt, G. C., Iida, Y., Ilyina, T., Luijkx, I. T., Jain, A., Jones, S. D., Kato, E., Kennedy, D., Klein Goldewijk, K., Knauer, J., Korsbakken, J. I., Körtzinger, A., Landschützer, P., Lauvset, S. K., Lefèvre, N., Lienert, S., Liu, J., Marland, G., McGuire, P. C., Melton, J. R., Munro, D. R., Nabel, J. E. M. S., Nakaoka, S.-I., Niwa, Y., Ono, T., Pierrot, D., Poulter, B., Rehder, G., Resplandy, L., Robertson, E., Rödenbeck, C., Rosan, T. M., Schwinger, J., Schwingshackl, C., Séférian, R., Sutton, A. J., Sweeney, C., Tanhua, T., Tans, P. P., Tian, H., Tilbrook, B., Tubiello, F., van der Werf, G. R., Vuichard, N., Wada, C., Wanninkhof, R., Watson, A. J., Willis, D., Wiltshire, A. J., Yuan, W., Yue, C., Yue, X., Zaehle, S., and Zeng, J.: Global Carbon Budget 2021, Earth Syst. Sci. Data, 14, 1917–2005, https://doi.org/10.5194/essd-14-1917-2022, 2022a.

Friedlingstein, P., O'Sullivan, M., Jones, M. W., Andrew, R. M., Gregor, L., Hauck, J., Le Quéré, C., Luijkx, I. T., Olsen, A., Peters, G. P., Peters, W., Pongratz, J., Schwingshackl, C., Sitch, S., Canadell, J. G., Ciais, P., Jackson, R. B., Alin, S. R., Alkama, R., Arneth, A., Arora, V. K., Bates, N. R., Becker, M., Bellouin, N., Bittig, H. C., Bopp, L., Chevallier, F., Chini, L. P., Cronin, M., Evans, W., Falk, S., Feely, R. A., Gasser, T., Gehlen, M., Gkritzalis, T., Gloege, L., Grassi, G., Gruber, N., Gürses, Ö., Harris, I., Hefner, M., Houghton, R. A., Hurtt, G. C., Iida, Y., Ilyina, T., Jain, A. K., Jersild, A., Kadono, K., Kato, E., Kennedy, D., Klein Goldewijk, K., Knauer, J., Korsbakken, J. I., Landschützer, P.,

Lefèvre, N., Lindsay, K., Liu, J., Liu, Z., Marland, G., Mayot, N., McGrath, M. J., Metzl, N., Monacci, N. M., Munro, D. R., Nakaoka, S.-I., Niwa, Y., O'Brien, K., Ono, T., Palmer, P. I., Pan, N., Pierrot, D., Pocock, K., Poulter, B., Resplandy, L., Robertson, E., Rödenbeck, C., Rodriguez, C., Rosan, T. M., Schwinger, J., Séférian, R., Shutler, J. D., Skjelvan, I., Steinhoff, T., Sun, Q., Sutton, A. J., Sweeney, C., Takao, S., Tanhua, T., Tans, P. P., Tian, X., Tian, H., Tilbrook, B., Tsujino, H., Tubiello, F., van der Werf, G. R., Walker, A. P., Wanninkhof, R., Whitehead, C., Willstrand Wranne, A., Wright, R., Yuan, W., Yue, C., Yue, X., Zaehle, S., Zeng, J., and Zheng, B.: Global Carbon Budget 2022, Earth Syst. Sci. Data, 14, 4811–4900, https://doi.org/10.5194/essd-14-4811-2022, 2022b.

Friedlingstein, P., O'Sullivan, M., Jones, M. W., Andrew, R. M., Bakker, D. C. E., Hauck, J., Landschützer, P., Le Quéré, C., Luijkx, I. T., Peters, G. P., Peters, W., Pongratz, J., Schwingshackl, C., Sitch, S., Canadell, J. G., Ciais, P., Jackson, R. B., Alin, S. R., Anthoni, P., Barbero, L., Bates, N. R., Becker, M., Bellouin, N., Decharme, B., Bopp, L., Brasika, I. B. M., Cadule, P., Chamberlain, M. A., Chandra, N., Chau, T.-T.-T., Chevallier, F., Chini, L. P., Cronin, M., Dou, X., Enyo, K., Evans, W., Falk, S., Feely, R. A., Feng, L., Ford, D. J., Gasser, T., Ghattas, J., Gkritzalis, T., Grassi, G., Gregor, L., Gruber, N., Gürses, Ö., Harris, I., Hefner, M., Heinke, J., Houghton, R. A., Hurtt, G. C., Iida, Y., Ilyina, T., Jacobson, A. R., Jain, A., Jarníková, T., Jersild, A., Jiang, F., Jin, Z., Joos, F., Kato, E., Keeling, R. F., Kennedy, D., Klein Goldewijk, K., Knauer, J., Korsbakken, J. I., Körtzinger, A., Lan, X., Lefèvre, N., Li, H., Liu, J., Liu, Z., Ma, L., Marland, G., Mayot, N., McGuire, P. C., McKinley, G. A., Meyer, G., Morgan, E. J., Munro, D. R., Nakaoka, S.-I., Niwa, Y., O'Brien, K. M., Olsen, A., Omar, A. M., Ono, T., Paulsen, M., Pierrot, D., Pocock, K., Poulter, B., Powis, C. M., Rehder, G., Resplandy, L., Robertson, E., Rödenbeck, C., Rosan, T. M., Schwinger, J., Séférian, R., Smallman, T. L., Smith, S. M., Sospedra-Alfonso, R., Sun, Q., Sutton, A. J., Sweeney, C., Takao, S., Tans, P. P., Tian, H., Tilbrook, B., Tsujino, H., Tubiello, F., van der Werf, G. R., van Ooijen, E., Wanninkhof, R., Watanabe, M., Wimart-Rousseau, C., Yang, D., Yang, X., Yuan, W., Yue, X., Zaehle, S., Zeng, J., and Zheng, B.: Global Carbon Budget 2023, Earth Syst. Sci. Data, 15, 5301–5369, https://doi.org/10.5194/essd-15-5301-2023, 2023.

Friedlingstein, P., O'Sullivan, M., Jones, M. W., Andrew, R. M., Hauck, J., Landschützer, P., Le Quéré, C., Li, H., Luijkx, I. T., Olsen, A., Peters, G. P., Peters, W., Pongratz, J., Schwingshackl, C., Sitch, S., Canadell, J. G., Ciais, P., Jackson, R. B., Alin, S. R., Arneth, A., Arora, V., Bates, N. R., Becker, M., Bellouin, N., Berghoff, C. F., Bittig, H. C., Bopp, L., Cadule, P., Campbell, K., Chamberlain, M. A., Chandra, N., Chevallier, F., Chini, L. P., Colligan, T., Decayeux, J., Djeutchouang, L. M., Dou, X., Duran Rojas, C., Enyo, K., Evans, W., Fay, A. R., Feely, R. A., Ford, D. J., Foster, A., Gasser, T., Gehlen, M., Gkritzalis, T., Grassi, G., Gregor, L., Gruber, N., Gürses, Ö., Harris, I., Hefner, M., Heinke, J., Hurtt, G. C., Iida, Y., Ilyina, T., Jacobson, A. R., Jain, A. K., Jarníková, T., Jersild, A., Jiang, F., Jin, Z., Kato, E., Keeling, R. F., Klein Goldewijk, K., Knauer, J., Korsbakken, J. I., Lauvset, S. K., Lefèvre, N., Liu, Z., Liu, J., Ma, L., Maksyutov, S., Marland, G., Mayot, N., McGuire, P. C., Metzl, N., Monacci, N. M., Morgan, E. J., Nakaoka, S., Neill, C., Niwa, Y., Nützel, T., Olivier, L., Ono, T., Palmer, P. I., Pierrot, D., Qin, Z., Resplandy, L., Roobaert, A., Rosan, T. M., Rödenbeck, C., Schwinger, J., Smallman, T. L., Smith, S. M., Sospedra-Alfonso, R., Steinhoff, T., Sun, Q., Sutton, A. J., Séférian, R., Takao, S., Tatebe, H., Tian, H., Tilbrook, B., Torres, O., Tourigny, E., Tsujino, H., Tubiello, F., van der Werf, G., Wanninkhof, R., Wang, X., Yang, D., Yang, X., Yu, Z., Yuan, W., Yue, X., Zaehle, S., Zeng, N., Zeng, J.: Supplemental data of the Global Carbon Budget 2024, ICOS-ERIC Carbon Portal, ICOS-ERIC Carbon Portal [data set], https://doi.org/10.18160/GCP-2024, 2024.

Ganzenmüller, R., Bultan, S., Winkler, K., Fuchs, R., Zabel, F., and Pongratz, J.: Land-use change emissions based on high-resolution activity data substantially lower than previously estimated, Environ. Res. Lett., 17, 064050, https://doi.org/10.1088/1748-9326/ac70d8, 2022.

Gasser, T., Crepin, L., Quilcaille, Y., Houghton, R. A., Ciais, P., and Obersteiner, M.: Historical CO_2 emissions from land use and land cover change and their uncertainty, Biogeosciences, 17, 4075–4101, https://doi.org/10.5194/bg-17-4075-2020, 2020.

Gaubert, B., Stephens, B. B., Basu, S., Chevallier, F., Deng, F., Kort, E. A., Patra, P. K., Peters, W., Rödenbeck, C., Saeki, T., Schimel, D., Van der Laan-Luijkx, I., Wofsy, S., and Yin, Y.: Global atmospheric CO_2 inverse models converging on neutral tropical land exchange, but disagreeing on fossil fuel and atmospheric growth rate, Biogeosciences, 16, 117–134, https://doi.org/10.5194/bg-16-117-2019, 2019.

GCP: The Global Carbon Budget 2007, http://www.globalcarbonproject.org/carbonbudget/archive.htm (last access: 21 January 2025), 2007.

Giglio, L., Schroeder, W., and Justice, C. O.: The collection 6 MODIS active fire detection algorithm and fire products, Remote Sens. Environ., 178, 31–41, https://doi.org/10.1016/j.rse.2016.02.054, 2016.

Global Carbon Project: Global Carbon Atlas, Global Carbon Project [data set], https://globalcarbonatlas.org/ (last access: 21 January 2025), 2024.

Gloege, L., McKinley, G. A., Landschützer, P., Fay, A. R., Frölicher, T. L., Fyfe, J. C., Ilyina, T., Jones, S., Lovenduski, N. S., Rodgers, K. B., Schlunegger, S., and Takano, Y.: Quantifying Errors in Observationally Based Estimates of Ocean Carbon Sink Variability, Global Biogeochem. Cy., 35, e2020GB006788, https://doi.org/10.1029/2020GB006788, 2021.

Gloege, L., Yan, M., Zheng, T., and McKinley, G. A.: Improved Quantification of Ocean Carbon Uptake by Using Machine Learning to Merge Global Models and pCO_2 Data, J. Adv. Model. Earth Sy., 14, e2021MS002620, https://doi.org/10.1029/2021MS002620, 2022.

Goris, N., Tjiputra, J. F., Olsen, A., Schwinger, J., Lauvset, S. K., and Jeansson, E.: Constraining Projection-Based Estimates of the Future North Atlantic Carbon Uptake, J. Climate, 31, 3959–3978, https://doi.org/10.1175/JCLI-D-17-0564.1, 2018.

Grassi, G., House, J., Kurz, W. A., Cescatti, A., Houghton, R. A., Peters, G. P., Sanz, M. J., Viñas, R. A., Alkama, R., Arneth, A., Bondeau, A., Dentener, F., Fader, M., Federici, S., Friedlingstein, P., Jain, A. K., Kato, E., Koven, C. D., Lee, D., Nabel, J. E. M. S., Nassikas, A. A., Perugini, L., Rossi, S., Sitch, S., Viovy, N., Wiltshire, A., and Zaehle, S.: Reconciling global-model estimates and country reporting of anthropogenic forest CO_2 sinks, Nat. Clim. Change, 8, 914–920, https://doi.org/10.1038/s41558-018-0283-x, 2018.

Grassi, G., Stehfest, E., Rogelj, J., van Vuuren, D., Cescatti, A., House, J., Nabuurs, G.-J., Rossi, S., Alkama, R., Viñas, R. A., Calvin, K., Ceccherini, G., Federici, S., Fujimori, S., Gusti, M., Hasegawa, T., Havlik, P., Humpenöder, F., Korosuo, A., Perugini, L., Tubiello, F. N., and Popp, A.: Critical adjustment of land mitigation pathways for assessing countries' climate progress, Nat. Clim. Change, 11, 425–434, https://doi.org/10.1038/s41558-021-01033-6, 2021.

Grassi, G., Schwingshackl, C., Gasser, T., Houghton, R. A., Sitch, S., Canadell, J. G., Cescatti, A., Ciais, P., Federici, S., Friedlingstein, P., Kurz, W. A., Sanz Sanchez, M. J., Abad Viñas, R., Alkama, R., Bultan, S., Ceccherini, G., Falk, S., Kato, E., Kennedy, D., Knauer, J., Korosuo, A., Melo, J., McGrath, M. J., Nabel, J. E. M. S., Poulter, B., Romanovskaya, A. A., Rossi, S., Tian, H., Walker, A. P., Yuan, W., Yue, X., and Pongratz, J.: Harmonising the land-use flux estimates of global models and national inventories for 2000–2020, Earth Syst. Sci. Data, 15, 1093–1114, https://doi.org/10.5194/essd-15-1093-2023, 2023.

Gregor, L., Lebehot, A. D., Kok, S., and Scheel Monteiro, P. M.: A comparative assessment of the uncertainties of global surface ocean CO_2 estimates using a machine-learning ensemble (CSIR-ML6 version 2019a) – have we hit the wall?, Geosci. Model Dev., 12, 5113–5136, https://doi.org/10.5194/gmd-12-5113-2019, 2019.

Gregor, L., Shutler, J., and Gruber, N.: High-resolution variability of the ocean carbon sink. Global Biogeochem. Cy., 38, e2024GB008127, https://doi.org/10.1029/2024GB008127, 2024.

Gruber, N., Bakker, D. C. E., DeVries, T., Gregor, L., Hauck, J., Landschützer, P., McKinley, G. A., and Müller, J. D.: Trends and variability in the ocean carbon sink, Nat. Rev. Earth Environ., 4, 119–134, https://doi.org/10.1038/s43017-022-00381-x, 2023.

Gruber, N., Clement, D., Carter, B. R., Feely, R. A., van Heuven, S., Hoppema, M., Ishii, M., Key, R. M., Kozyr, A., Lauvset, S. K., Lo Monaco, C., Mathis, J. T., Murata, A., Olsen, A., Perez, F. F., Sabine, C. L., Tanhua, T., and Wanninkhof, R.: The oceanic sink for anthropogenic CO_2 from 1994 to 2007, Science, 363, 1193–1199, https://doi.org/10.1126/science.aau5153, 2019.

Guan, D., Liu, Z., Geng, Y., Lindner, S., and Hubacek, K.: The gigatonne gap in China's carbon dioxide inventories, Nat. Clim. Change, 2, 672–675, https://doi.org/10.1038/nclimate1560, 2012.

Gulev, S. K., Thorne, P. W., Ahn, J., Dentener, F. J., Domingues, C. M., Gerland, S., Gong, D. S., Kaufman, S., Nnamchi, H. C., Quaas, J., Rivera, J. A., Sathyendranath, S., Smith, S. L., Trewin, B., von Shuckmann, K., and Vose, R. S.: Changing State of the Climate System, in: Climate Change 2021: The Physical Science Basis. Contribution of Working Group I to the Sixth Assessment Report of the Intergovernmental Panel on Climate Change, edited by: Masson-Delmotte, V., Zhai, P., Pirani, A., Connors, S. L., Péan, C., Berger, S., Caud, N., Chen, Y., Goldfarb, L., Gomis, M. I., Huang, M., Leitzell, K., Lonnoy, E., Matthews, J. B. R., Maycock, T. K., Waterfield, T., Yelekçi, O., Yu, R., and Zhou, B., Cambridge University Press, Cambridge, United Kingdom and New York, NY, USA, 287–422, https://doi.org/10.1017/9781009157896.004, 2021.

Guo, R., Wang, J., Bing, L., Tong, D., Ciais, P., Davis, S. J., Andrew, R. M., Xi, F., and Liu, Z.: Global CO_2 uptake by cement from 1930 to 2019, Earth Syst. Sci. Data, 13, 1791–1805, https://doi.org/10.5194/essd-13-1791-2021, 2021.

Gürses, Ö., Oziel, L., Karakuş, O., Sidorenko, D., Völker, C., Ye, Y., Zeising, M., Butzin, M., and Hauck, J.: Ocean biogeochemistry in the coupled ocean–sea ice–biogeochemistry model FESOM2.1–REcoM3, Geosci. Model Dev., 16, 4883–4936, https://doi.org/10.5194/gmd-16-4883-2023, 2023.

Gütschow, J., Jeffery, M. L., Gieseke, R., Gebel, R., Stevens, D., Krapp, M., and Rocha, M.: The PRIMAP-hist national historical emissions time series, Earth Syst. Sci. Data, 8, 571–603, https://doi.org/10.5194/essd-8-571-2016, 2016.

Gütschow, J., Busch, D., and Pflüger, M.: The PRIMAP-hist national historical emissions time series (1750–2023) v2.6, Zenodo [data set], https://doi.org/10.5281/zenodo.13752654, 2023.

Gütschow, J., Busch, D., and Pflüger, M.: The PRIMAP-hist national historical emissions time series (1750–2023) v2.6, Zenodo [data set], https://doi.org/10.5281/zenodo.13752654, 2024.

Hall, B. D., Crotwell, A. M., Kitzis, D. R., Mefford, T., Miller, B. R., Schibig, M. F., and Tans, P. P.: Revision of the World Meteorological Organization Global Atmosphere Watch (WMO/GAW) CO_2 calibration scale, Atmos. Meas. Tech., 14, 3015–3032, https://doi.org/10.5194/amt-14-3015-2021, 2021.

Hansis, E., Davis, S. J., and Pongratz, J.: Relevance of methodological choices for accounting of land use change carbon fluxes, Global Biogeochem. Cy., 29, 1230–1246, https://doi.org/10.1002/2014GB004997, 2015.

Hauck, J., Zeising, M., Le Quéré, C., Gruber, N., Bakker, D. C. E., Bopp, L., Chau, T. T. T., Gürses, Ö., Ilyina, T., Landschützer, P., Lenton, A., Resplandy, L., Rödenbeck, C., Schwinger, J., and Séférian, R.: Consistency and Challenges in the Ocean Carbon Sink Estimate for the Global Carbon Budget, Front. Mar. Sci., 7, 571720, https://doi.org/10.3389/fmars.2020.571720, 2020.

Hauck, J., Nissen, C., Landschützer, P., Rödenbeck, C., Bushinsky, S., and Olsen, A.: Sparse observations induce large biases in estimates of the global ocean CO_2 sink: an ocean model subsampling experiment, Philos. T. R. Soc. Math. Phys. Eng. Sci., 381, 20220063, https://doi.org/10.1098/rsta.2022.0063, 2023a.

Hauck, J., Gregor, L., Nissen, C., Patara, L., Hague, M., Mongwe, P., Bushinsky, S., Doney, S. C., Gruber, N., Le Quéré, C., Manizza, M., Mazloff, M., Monteiro, P. M. S., and Terhaar, J.: The Southern Ocean Carbon Cycle 1985–2018: Mean, Seasonal Cycle, Trends, and Storage. Global Biogeochem. C., 37, e2023GB007848, https://doi.org/10.1029/2023GB007848, 2023b.

Haverd, V., Smith, B., Nieradzik, L., Briggs, P. R., Woodgate, W., Trudinger, C. M., Canadell, J. G., and Cuntz, M.: A new version of the CABLE land surface model (Subversion revision r4601) incorporating land use and land cover change, woody vegetation demography, and a novel optimisation-based approach to plant coordination of photosynthesis, Geosci. Model Dev., 11, 2995–3026, https://doi.org/10.5194/gmd-11-2995-2018, 2018.

Heinke, J., Rolinski, S., and Müller, C.: Modelling the role of livestock grazing in C and N cycling in grasslands with LPJmL5.0-grazing, Geosci. Model Dev., 16, 2455–2475, https://doi.org/10.5194/gmd-16-2455-2023, 2023.

Hefner, M. W. and Marland, G.: CDIAC at AppState: Carbon dioxide information analysis center, https://energy.appstate.edu/research/work-areas/cdiac-appstate (last access: 21 January 2025), 2023.

Hickler, T., Smith, B., Prentice, I. C., Mjöfors, K., Miller, P., Arneth, A., and Sykes, M. T.: CO_2 fertilization in temperate FACE experiments not representative of boreal and tropical forests, Glob. Change Biol., 14, 1531–1542, https://doi.org/10.1111/j.1365-2486.2008.01598.x, 2008.

Hoesly, R., Smith, S. J., Prime, N., Ahsan, H., Suchyta, H., O'Rourke, P., Crippa, M., Klimont, Z., Guizzardi, D., Behrendt, J., Feng, L., Harkins, C., McDonald, B., Mott, A., McDuffie, A., Nicholson, M., and Wang, S.: CEDS v_2024_07_08 Release Emission Data, Zenodo [data set], https://doi.org/10.5281/zenodo.12803196, 2024.

Hong, C., Burney, J. A., Pongratz, J., Nabel, J. E. M. S., Mueller, N. D., Jackson, R. B., and Davis, S. J.: Global and regional drivers of land-use emissions in 1961–2017, Nature, 589, 554–561, https://doi.org/10.1038/s41586-020-03138-y, 2021.

Houghton, R. A. and Castanho, A.: Annual emissions of carbon from land use, land-use change, and forestry from 1850 to 2020, Earth Syst. Sci. Data, 15, 2025–2054, https://doi.org/10.5194/essd-15-2025-2023, 2023.

Houghton, R. A., House, J. I., Pongratz, J., van der Werf, G. R., DeFries, R. S., Hansen, M. C., Le Quéré, C., and Ramankutty, N.: Carbon emissions from land use and land-cover change, Biogeosciences, 9, 5125–5142, https://doi.org/10.5194/bg-9-5125-2012, 2012.

Huang, B., Thorne, P. W., Banzon, V. F., Boyer, T., Chepurin, G., Lawrimore, J. H., Menne, M. J., Smith, T. M., Vose, R. S., and Zhang, H.-M.: NOAA Extended Reconstructed Sea Surface Temperature (ERSST), Version 5, NOAA National Centers for Environmental Information [data set], https://doi.org/10.7289/V5T72FNM, 2017.

Hubau, W., Lewis, S. L., Phillips, O. L., Affum-Baffoe, K., Beeckman, H., Cuní-Sanchez, A., Daniels, A. K., Ewango, C. E. N., Fauset, S., Mukinzi, J. M., Sheil, D., Sonké, B., Sullivan, M. J. P., Sunderland, T. C. H., Taedoumg, H., Thomas, S. C., White, L. J. T., Abernethy, K. A., Adu-Bredu, S., Amani, C. A., Baker, T. R., Banin, L. F., Baya, F., Begne, S. K., Bennett, A. C., Benedet, F., Bitariho, R., Bocko, Y. E., Boeckx, P., Boundja, P., Brienen, R. J. W., Brncic, T., Chezeaux, E., Chuyong, G. B., Clark, C. J., Collins, M., Comiskey, J. A., Coomes, D. A., Dargie, G. C., de Haulleville, T., Kamdem, M. N. D., Doucet, J.-L., Esquivel-Muelbert, A., Feldpausch, T. R., Fofanah, A., Foli, E. G., Gilpin, M., Gloor, E., Gonmadje, C., Gourlet-Fleury, S., Hall, J. S., Hamilton, A. C., Harris, D. J., Hart, T. B., Hockemba, M. B. N., Hladik, A., Ifo, S. A., Jeffery, K. J., Jucker, T., Yakusu, E. K., Kearsley, E., Kenfack, D., Koch, A., Leal, M. E., Levesley, A., Lindsell, J. A., Lisingo, J., Lopez-Gonzalez, G., Lovett, J. C., Makana, J.-R., Malhi, Y., Marshall, A. R., Martin, J., Martin, E. H., Mbayu, F. M., Medjibe, V. P., Mihindou, V., Mitchard, E. T. A., Moore, S., Munishi, P. K. T., Bengone, N. N., Ojo, L., Ondo, F. E., Peh, K. S.-H., Pickavance, G. C., Poulsen, A. D., Poulsen, J. R., Qie, L., Reitsma, J., Rovero, F., Swaine, M. D., Talbot, J., Taplin, J., Taylor, D. M., Thomas, D. W., Toirambe, B., Mukendi, J. T., Tuagben, D., Umunay, P. M., van der Heijden, G. M. F., Verbeeck, H., Vleminckx, J., Willcock, S., Wöll, H., Woods, J. T., and Zemagho, L.: Asynchronous carbon sink saturation in African and Amazonian tropical forests, Nature, 579, 80–87, https://doi.org/10.1038/s41586-020-2035-0, 2020.

Humphrey, V., Zscheischler, J., Ciais, P., Gudmundsson, L., Sitch, S., and Seneviratne, S. I.: Sensitivity of atmospheric CO_2 growth rate to observed changes in terrestrial water storage, Nature, 560, 628–631, https://doi.org/10.1038/s41586-018-0424-4, 2018.

Humphrey, V., Berg, A., Ciais, P., Gentine, P., Jung, M., Reichstein, M., Seneviratne, S. I., and Frankenberg, C.: Soil moisture–atmosphere feedback dominates land carbon uptake variability, Nature, 592, 65–69, https://doi.org/10.1038/s41586-021-03325-5, 2021.

Huntzinger, D. N., Michalak, A. M., Schwalm, C., Ciais, P., King, A. W., Fang, Y., Schaefer, K., Wei, Y., Cook, R. B., Fisher, J. B., Hayes, D., Huang, M., Ito, A., Jain, A. K., Lei, H., Lu, C., Maignan, F., Mao, J., Parazoo, N., Peng, S., Poulter, B., Ricciuto, D., Shi, X., Tian, H., Wang, W., Zeng, N., and Zhao, F.: Uncertainty in the response of terrestrial carbon sink to environmental drivers undermines carbon-climate feedback predictions, Sci. Rep., 7, 4765, https://doi.org/10.1038/s41598-017-03818-2, 2017.

Iida, Y., Takatani, Y., Kojima, A., and Ishii, M.: Global trends of ocean CO_2 sink and ocean acidification: an observation-based reconstruction of surface ocean inorganic carbon variables, J. Oceanogr., 77, 323–358, https://doi.org/10.1007/s10872-020-00571-5, 2021.

Ilyina, T., Li, H., Spring, A., Müller, W. A., Bopp, L., Chikamoto, M. O., Danabasoglu, G., Dobrynin, M., Dunne, J., Fransner, F., Friedlingstein, P., Lee, W., Lovenduski, N. S., Merryfield, W. j., Mignot, J., Park, J. Y., Séférian, R., Sospedra-Alfonso, R., Watanabe, M., and Yeager, S.: Predictable Variations of the Carbon Sinks and Atmospheric CO_2 Growth in a Multi-Model Framework, Geophys. Res. Lett., 48, e2020GL090695, https://doi.org/10.1029/2020GL090695, 2021.

IMF: International Monetary Fund: World Economic Outlook, http://www.imf.org (last access: 21 January 2025), 2024.

Instituto Nacional de Pesquisas Espaciais (INPE): Portal TerraBrasilis, http://terrabrasilis.dpi.inpe.br/en/home-page/ (last access: 21 January 2025), 2024.

Ito, A. and Inatomi, M.: Use of a process-based model for assessing the methane budgets of global terrestrial ecosystems and evaluation of uncertainty, Biogeosciences, 9, 759–773, https://doi.org/10.5194/bg-9-759-2012, 2012.

Jackson, R. B., Canadell, J. G., Le Quéré, C., Andrew, R. M., Korsbakken, J. I., Peters, G. P., and Nakicenovic, N.: Reaching peak emissions, Nat. Clim. Change, 6, 7–10, https://doi.org/10.1038/nclimate2892, 2016.

Jackson, R. B., Le Quéré, C., Andrew, R. M., Canadell, J. G., Korsbakken, J. I., Liu, Z., Peters, G. P., and Zheng, B.: Global energy growth is outpacing decarbonization, Environ. Res. Lett., 13, 120401, https://doi.org/10.1088/1748-9326/aaf303, 2018.

Jackson, R. B., Friedlingstein, P., Andrew, R. M., Canadell, J. G., Le Quéré, C., and Peters, G. P.: Persistent fossil fuel growth threatens the Paris Agreement and planetary health, Environ. Res. Lett., 14, 121001, https://doi.org/10.1088/1748-9326/ab57b3, 2019.

Jackson, R. B., Friedlingstein, P., Quéré, C. L., Abernethy, S., Andrew, R. M., Canadell, J. G., Ciais, P., Davis, S. J., Deng, Z., Liu, Z., Korsbakken, J. I., and Peters, G. P.: Global fossil carbon emissions rebound near pre-COVID-19 levels, Environ. Res. Lett., 17, 031001, https://doi.org/10.1088/1748-9326/ac55b6, 2022.

Jacobson, A. R., Schuldt, K. N., Tans, P., Andrews, A., Miller, J. B., Oda, T., Basu, S., Mund, J., Weir, B., Ott, L., Aalto, T., Abshire, J. B., Aikin, K., Aoki, S., Apadula, F., Arnold, S., Baier, B., Bar-

tyzel, J., Beyersdorf, A., Biermann, T., Biraud, S. C., Boenisch, H., Brailsford, G., Brand, W. A., Chen, G., Chen, H., Chmura, L., Clark, S., Colomb, A., Commane, R., Conil, S., Couret, C., Cox, A., Cristofanelli, P., Cuevas, E., Curcoll, R., Daube, B., Davis, K. J., De Wekker, S., Della Coletta, J., Delmotte, M., DiGangi, E., DiGangi, J. P., di Sarra, A. G., Dlugokencky, E., Elkins, J. W., Emmenegger, L., Fang, S., Fischer, M. L., Forster, G., Frumau, A., Galkowski, M., Gatti, L. V., Gehrlein, T., Gerbig, C., Gheusi, F., Gloor, E., Gomez-Trueba, V., Goto, D., Griffis, T., Hammer, S., Hanson, C., Haszpra, L., Hatakka, J., Heimann, M., Heliasz, M., Hensen, A., Hermansen, O., Hintsa, E., Holst, J., Ivakhov, V., Jaffe, D. A., Jordan, A., Joubert, W., Karion, A., Kawa, S. R., Kazan, V., Keeling, R. F., Keronen, P., Kneuer, T., Kolari, P., Komínková, K., Kort, E., Kozlova, E., Krummel, P., Kubistin, D., Labuschagne, C., Lam, D. H. Y., Lan, X., Langenfelds, R. L., Laurent, O., Laurila, T., Lauvaux, T., Lavric, J., Law, B. E., Lee, J., Lee, O. S. M., Lehner, I., Lehtinen, K., Leppert, R., Leskinen, A., Leuenberger, M., Levin, I., Levula, J., Lin, J., Lindauer, M., Loh, Z., Lopez, M., Luijkx, I. T., Lunder, C. R., Machida, T., Mammarella, I., Manca, G., Manning, A., Manning, A., Marek, M. V., Martin, M. Y., Matsueda, H., McKain, K., Meijer, H., Meinhardt, F., Merchant, L., Mihalopoulos, N., Miles, N. L., Miller, C. E., Mitchell, L., Mölder, M., Montzka, S., Moore, F., Moossen, H., Morgan, E., Morgui, J.-A., Morimoto, S., Müller-Williams, J., Munger, J. W., Munro, D., Myhre, C. L., Nakaoka, S.-I., Necki, J., Newman, S., Nichol, S., Niwa, Y., Obersteiner, F., O'Doherty, S., Paplawsky, B., Peischl, J., Peltola, O., Piacentino, S., Pichon, J.-M., Pickers, P., Piper, S., Pitt, J., Plass-Dülmer, C., Platt, S. M., Prinzivalli, S., Ramonet, M., Ramos, R., Reyes-Sanchez, E., Richardson, S. J., Riris, H., Rivas, P. P., Ryerson, T., Saito, K., Sargent, M., Sasakawa, M., Scheeren, B., Schuck, T., Schumacher, M., Seifert, T., Sha, M. K., Shepson, P., Shook, M., Sloop, C. D., Smith, P., Stanley, K., Steinbacher, M., Stephens, B., Sweeney, C., Thoning, K., Timas, H., Torn, M., Tørseth, K., Trisolino, P., Turnbull, J., van den Bulk, P., van Dinther, D., Vermeulen, A., Viner, B., Vitkova, G., Walker, S., Watson, A., Wofsy, S. C., Worsey, J., Worthy, D., Young, D., Zaehle, S., Zahn, A., and Zimnoch, M.: CarbonTracker CT2022, NOAA GML [data set], https://doi.org/10.25925/Z1GJ-3254, 2023a.

Jacobson, A. R., Schuldt, K. N., Tans, P., Andrews, A., Miller, J. B., Oda, T., Basu, S., Mund, J., Weir, B., Ott, L., Aalto, T., Abshire, J. B., Aikin, K., Aoki, S., Apadula, F., Arnold, S., Baier, B., Bartyzel, J., Beyersdorf, A., Biermann, T., Biraud, S. C., Boenisch, H., Brailsford, G., Brand, W. A., Chen, G., Chen, H., Chmura, L., Clark, S., Colomb, A., Commane, R., Conil, S., Couret, C., Cox, A., Cristofanelli, P., Cuevas, E., Curcoll, R., Daube, B., Davis, K. J., De Wekker, S., Della Coletta, J., Delmotte, M., DiGangi, E., DiGangi, J. P., di Sarra, A. G., Dlugokencky, E., Elkins, J. W., Emmenegger, L., Fang, S., Fischer, M. L., Forster, G., Frumau, A., Galkowski, M., Gatti, L. V., Gehrlein, T., Gerbig, C., Gheusi, F., Gloor, E., Gomez-Trueba, V., Goto, D., Griffis, T., Hammer, S., Hanson, C., Haszpra, L., Hatakka, J., Heimann, M., Heliasz, M., Hensen, A., Hermansen, O., Hintsa, E., Holst, J., Ivakhov, V., Jaffe, D. A., Jordan, A., Joubert, W., Karion, A., Kawa, S. R., Kazan, V., Keeling, R. F., Keronen, P., Kneuer, T., Kolari, P., Komínková, K., Kort, E., Kozlova, E., Krummel, P., Kubistin, D., Labuschagne, C., Lam, D. H. Y., Lan, X., Langenfelds, R. L., Laurent, O., Laurila, T., Lauvaux, T., Lavric, J., Law, B. E., Lee, J., Lee, O. S. M., Lehner, I., Lehtinen, K., Leppert, R., Leskinen, A., Leuenberger, M., Levin, I., Levula, J., Lin, J., Lindauer, M., Loh, Z., Lopez, M., Luijkx, I. T., Lunder, C. R., Machida, T., Mammarella, I., Manca, G., Manning, A., Manning, A., Marek, M. V., Martin, M. Y., Matsueda, H., McKain, K., Meijer, H., Meinhardt, F., Merchant, L., Mihalopoulos, N., Miles, N. L., Miller, C. E., Mitchell, L., Mölder, M., Montzka, S., Moore, F., Moossen, H., Morgan, E., Morgui, J.-A., Morimoto, S., Müller-Williams, J., Munger, J. W., Munro, D., Myhre, C. L., Nakaoka, S.-I., Necki, J., Newman, S., Nichol, S., Niwa, Y., Obersteiner, F., O'Doherty, S., Paplawsky, B., Peischl, J., Peltola, O., Piacentino, S., Pichon, J.-M., Pickers, P., Piper, S., Pitt, J., Plass-Dülmer, C., Platt, S. M., Prinzivalli, S., Ramonet, M., Ramos, R., Reyes-Sanchez, E., Richardson, S. J., Riris, H., Rivas, P. P., Ryerson, T., Saito, K., Sargent, M., Sasakawa, M., Scheeren, B., Schuck, T., Schumacher, M., Seifert, T., Sha, M. K., Shepson, P., Shook, M., Sloop, C. D., Smith, P., Stanley, K., Steinbacher, M., Stephens, B., Sweeney, C., Thoning, K., Timas, H., Torn, M., Tørseth, K., Trisolino, P., Turnbull, J., van den Bulk, P., van Dinther, D., Vermeulen, A., Viner, B., Vitkova, G., Walker, S., Watson, A., Wofsy, S. C., Worsey, J., Worthy, D., Young, D., Zaehle, S., Zahn, A., and Zimnoch, M.: CarbonTracker CT-NRT.v2023-3, NOAA GML [data set], https://doi.org/10.25925/7TAF-J322, 2023b.

Jain, A. K., Meiyappan, P., Song, Y., and House, J. I.: CO_2 emissions from land-use change affected more by nitrogen cycle, than by the choice of land-cover data, Glob. Change Biol., 19, 2893–2906, https://doi.org/10.1111/gcb.12207, 2013.

Janssens-Maenhout, G., Crippa, M., Guizzardi, D., Muntean, M., Schaaf, E., Dentener, F., Bergamaschi, P., Pagliari, V., Olivier, J. G. J., Peters, J. A. H. W., van Aardenne, J. A., Monni, S., Doering, U., Petrescu, A. M. R., Solazzo, E., and Oreggioni, G. D.: EDGAR v4.3.2 Global Atlas of the three major greenhouse gas emissions for the period 1970–2012, Earth Syst. Sci. Data, 11, 959–1002, https://doi.org/10.5194/essd-11-959-2019, 2019.

Jiang, F., Wang, H., Chen, J. M., Ju, W., Tian, X., Feng, S., Li, G., Chen, Z., Zhang, S., Lu, X., Liu, J., Wang, H., Wang, J., He, W., and Wu, M.: Regional CO_2 fluxes from 2010 to 2015 inferred from GOSAT XCO_2 retrievals using a new version of the Global Carbon Assimilation System, Atmos. Chem. Phys., 21, 1963–1985, https://doi.org/10.5194/acp-21-1963-2021, 2021.

Jin, Y., Keeling, R. F., Stephens, B. B., Long, M. C., Patra, P. K., Rödenbeck, C., Morgan, E. J., Kort, E. A., and Sweeney, C.: Improved atmospheric constraints on Southern Ocean CO_2 exchange, P. Natl. Acad. Sci. USA, 121, e2309333121, https://doi.org/10.1073/pnas.2309333121, 2024.

Jin, Z., Wang, T., Zhang, H., Wang, Y., Ding, J., and Tian, X.: Constraint of satellite CO_2 retrieval on the global carbon cycle from a Chinese atmospheric inversion system, Sci. China Earth Sci., 66, 609–618, https://doi.org/10.1007/s11430-022-1036-7, 2023.

Jones, M. W., Abatzoglou, J. T., Veraverbeke, S., Andela, N., Lasslop, G., Forkel, M., Smith, A. J. P., Burton, C., Betts, R. A., van der Werf, G. R., Sitch, S., Canadell, J. G., Santín, C., Kolden, C., Doerr, S. H., and Le Quéré, C.: Global and Regional Trends and Drivers of Fire Under Climate Change, Rev. Geophys., 60, e2020RG000726, https://doi.org/10.1029/2020RG000726, 2022.

Jones, M. W., Andrew, R. M., Peters, G. P., Janssens-Maenhout, G., De-Gol, A. J., Ciais, P., Patra, P. K., Chevallier, F., and Le Quéré, C.: Gridded fossil CO_2 emissions and related O_2 combustion

consistent with national inventories 1959–2018, Sci. Data, 8, 2, https://doi.org/10.1038/s41597-020-00779-6, 2021b.

Jones, M. W., Andrew, R. M., Peters, G. P., Janssens-Maenhout, G., De-Gol, A. J., Dou, X., Liu, Z., Pickers, P., Ciais, P., Patra, P. K., Chevallier, F., and Le Quéré, C.: Gridded fossil CO_2 emissions and related O_2 combustion consistent with national inventories, Zenodo [data set], https://doi.org/10.5281/zenodo.13909046, 2024a.

Jones, M. W., Kelley, D. I., Burton, C. A., Di Giuseppe, F., Barbosa, M. L. F., Brambleby, E., Hartley, A. J., Lombardi, A., Mataveli, G., McNorton, J. R., Spuler, F. R., Wessel, J. B., Abatzoglou, J. T., Anderson, L. O., Andela, N., Archibald, S., Armenteras, D., Burke, E., Carmenta, R., Chuvieco, E., Clarke, H., Doerr, S. H., Fernandes, P. M., Giglio, L., Hamilton, D. S., Hantson, S., Harris, S., Jain, P., Kolden, C. A., Kurvits, T., Lampe, S., Meier, S., New, S., Parrington, M., Perron, M. M. G., Qu, Y., Ribeiro, N. S., Saharjo, B. H., San-Miguel-Ayanz, J., Shuman, J. K., Tanpipat, V., van der Werf, G. R., Veraverbeke, S., and Xanthopoulos, G.: State of Wildfires 2023–2024, Earth Syst. Sci. Data, 16, 3601–3685, https://doi.org/10.5194/essd-16-3601-2024, 2024b.

Jones, M. W., Veraverbeke, S., Andela, N., Doerr, S. H., Kolden, C., Mataveli, G., Pettinari, M. L., Le Quéré, C., Rosan, T. M., van der Werf, G. R. and van Wees, D.: Global rise in forest fire emissions linked to climate change in the extratropics, Science, 386, eadl5889, https://doi.org/10.1126/science.adl5889, 2024c.

Joos, F. and Spahni, R.: Rates of change in natural and anthropogenic radiative forcing over the past 20,000 years, P. Natl. Acad. Sci. USA, 105, 1425–1430, https://doi.org/10.1073/pnas.0707386105, 2008.

Jung, M., Reichstein, M., Schwalm, C. R., Huntingford, C., Sitch, S., Ahlström, A., Arneth, A., Camps-Valls, G., Ciais, P., Friedlingstein, P., Gans, F., Ichii, K., Jain, A. K., Kato, E., Papale, D., Poulter, B., Raduly, B., Rödenbeck, C., Tramontana, G., Viovy, N., Wang, Y.-P., Weber, U., Zaehle, S., and Zeng, N.: Compensatory water effects link yearly global land CO_2 sink changes to temperature, Nature, 541, 516–520, https://doi.org/10.1038/nature20780, 2017.

Kaiser, J. W., Heil, A., Andreae, M. O., Benedetti, A., Chubarova, N., Jones, L., Morcrette, J.-J., Razinger, M., Schultz, M. G., Suttie, M., and van der Werf, G. R.: Biomass burning emissions estimated with a global fire assimilation system based on observed fire radiative power, Biogeosciences, 9, 527–554, https://doi.org/10.5194/bg-9-527-2012, 2012.

Kato, E., Kinoshita, T., Ito, A., Kawamiya, M., and Yamagata, Y.: Evaluation of spatially explicit emission scenario of land-use change and biomass burning using a process-based biogeochemical model, J. Land Use Sci., 8, 104–122, https://doi.org/10.1080/1747423X.2011.628705, 2013.

Ke, P., Ciais, P., Sitch, S., Li, W., Bastos, A., Liu, Z., Xu, Y., Gui, X., Bian, J., Goll, D. S., Xi, Y., Li, W., O'Sullivan, M., Goncalves de Souza, J., Friedlingstein, P., and Chevallier, F.: Low latency carbon budget analysis reveals a large decline of the land carbon sink in 2023, Natl. Sci. Rev., 11, nwae367, https://doi.org/10.1093/nsr/nwae367, 2024.

Keeley, J. E. and Pausas, J. G.: Distinguishing disturbance from perturbations in fire-prone ecosystems, Int. J. Wildland Fire, 28, 282–287, https://doi.org/10.1071/WF18203, 2019.

Keeling, C. D., Bacastow, R. B., Bainbridge, A. E., Ekdahl, C. A., Guenther, P. R., Waterman, L. S., and Chin, J. F. S.: Atmospheric carbon dioxide variations at Mauna Loa Observatory, Hawaii, Tellus A, 28, 538–551, https://doi.org/10.1111/j.2153-3490.1976.tb00701.x, 1976.

Keeling, R. F.: Development of an Interferometric Oxygen Analyzer for Precise Measurement of the Atmospheric O_2 Mole Fraction, PhD thesis, Harvard University, Cambridge, Massachusetts, https://bluemoon.ucsd.edu/publications/ralph/34_PhDthesis.pdf (last access: 21 January 2025), 1988.

Keeling, R. F. and Manning, A. C.: 5.15 – Studies of Recent Changes in Atmospheric O_2 Content, in: Treatise on Geochemistry, 2nd Edn., edited by: Holland, H. D. and Turekian, K. K., Elsevier, Oxford, 385–404, https://doi.org/10.1016/B978-0-08-095975-7.00420-4, 2014.

Keeling, R. F., Manning, A. C., Paplawsky, W. J., and Cox, A. C.: On the long-term stability of reference gases for atmospheric O_2/N_2 and CO_2 measurements, Tellus B, 59, 3–14, https://doi.org/10.1111/j.1600-0889.2006.00196.x, 2007.

Keppler, L. and Landschützer, P.: Regional Wind Variability Modulates the Southern Ocean Carbon Sink, Sci. Rep., 9, 7384, https://doi.org/10.1038/s41598-019-43826-y, 2019.

Khatiwala, S., Primeau, F., and Hall, T.: Reconstruction of the history of anthropogenic CO_2 concentrations in the ocean, Nature, 462, 346–349, https://doi.org/10.1038/nature08526, 2009.

Khatiwala, S., Tanhua, T., Mikaloff Fletcher, S., Gerber, M., Doney, S. C., Graven, H. D., Gruber, N., McKinley, G. A., Murata, A., Ríos, A. F., and Sabine, C. L.: Global ocean storage of anthropogenic carbon, Biogeosciences, 10, 2169–2191, https://doi.org/10.5194/bg-10-2169-2013, 2013.

Korsbakken, J. I., Peters, G. P., and Andrew, R. M.: Uncertainties around reductions in China's coal use and CO_2 emissions, Nat. Clim. Change, 6, 687–690, https://doi.org/10.1038/nclimate2963, 2016.

Krinner, G., Viovy, N., de Noblet-Ducoudré, N., Ogée, J., Polcher, J., Friedlingstein, P., Ciais, P., Sitch, S., and Prentice, I. C.: A dynamic global vegetation model for studies of the coupled atmosphere-biosphere system: DVGM for coupled climate studies, Global Biogeochem. Cy., 19, GB1015, https://doi.org/10.1029/2003GB002199, 2005.

Krol, M., Houweling, S., Bregman, B., van den Broek, M., Segers, A., van Velthoven, P., Peters, W., Dentener, F., and Bergamaschi, P.: The two-way nested global chemistry-transport zoom model TM5: algorithm and applications, Atmos. Chem. Phys., 5, 417–432, https://doi.org/10.5194/acp-5-417-2005, 2005.

Lacroix, F., Ilyina, T., and Hartmann, J.: Oceanic CO_2 outgassing and biological production hotspots induced by pre-industrial river loads of nutrients and carbon in a global modeling approach, Biogeosciences, 17, 55–88, https://doi.org/10.5194/bg-17-55-2020, 2020.

Lacroix, F., Ilyina, T., Mathis, M., Laruelle, G. G., and Regnier, P.: Historical increases in land-derived nutrient inputs may alleviate effects of a changing physical climate on the oceanic carbon cycle, Glob. Change Biol., 27, 5491–5513, https://doi.org/10.1111/gcb.15822, 2021.

Lamboll, R. D., Nicholls, Z. R. J., Smith, C. J., Kikstra, J. S., Byers, E., and Rogelj, J.: Assessing the size and uncertainty of remaining carbon budgets, Nat. Clim. Change, 13, 1360–1367, https://doi.org/10.1038/s41558-023-01848-5, 2023.

Lamboll, R. D., Jones, C. D., Skeie, R. B., Fiedler, S., Samset, B. H., Gillett, N. P., Rogelj, J., and Forster, P. M.: Modifying emis-

sions scenario projections to account for the effects of COVID-19: protocol for CovidMIP, Geosci. Model Dev., 14, 3683–3695, https://doi.org/10.5194/gmd-14-3683-2021, 2021.

Lan, X., Tans, P. and Thoning, K.: NOAA Greenhouse Gas Marine Boundary Layer Reference – CO_2, NOAA Global Monitoring Laboratory [data set], https://doi.org/10.15138/DVNP-F961, 2023.

Lan, X., Tans, P., and Thoning, K. W.: Trends in globally-averaged CO_2 determined from NOAA Global Monitoring Laboratory measurements, Version 2024-09, National Oceanic and Atmospheric Administration, Global Monitoring Laboratory (NOAA/GML) [data set], https://gml.noaa.gov/ccgg/trends/global.html (last access: 21 January 2025), 2024.

Landschützer, P., Gruber, N., Haumann, F. A., Rödenbeck, C., Bakker, D. C. E., van Heuven, S., Hoppema, M., Metzl, N., Sweeney, C., Takahashi, T., Tilbrook, B., and Wanninkhof, R.: The reinvigoration of the Southern Ocean carbon sink, Science, 349, 1221–1224, https://doi.org/10.1126/science.aab2620, 2015.

Landschützer, P., Gruber, N., and Bakker, D. C. E.: Decadal variations and trends of the global ocean carbon sink: decadal air-sea CO_2 flux variability, Global Biogeochem. Cy., 30, 1396–1417, https://doi.org/10.1002/2015GB005359, 2016.

Lapola, D. M., Pinho, P., Barlow, J., Aragão, L. E. O. C., Berenguer, E., Carmenta, R., Liddy, H. M., Seixas, H., Silva, C. V. J., Silva-Junior, C. H. L., Alencar, A. A. C., Anderson, L. O., Armenteras, D., Brovkin, V., Calders, K., Chambers, J., Chini, L., Costa, M. H., Faria, B. L., Fearnside, P. M., Ferreira, J., Gatti, L., Gutierrez-Velez, V. H., Han, Z., Hibbard, K., Koven, C., Lawrence, P., Pongratz, J., Portela, B. T. T., Rounsevell, M., Ruane, A. C., Schaldach, R., da Silva, S. S., von Randow, C., and Walker, W. S.: The drivers and impacts of Amazon forest degradation, Science, 379, eabp8622, https://doi.org/10.1126/science.abp8622, 2023.

Law, R. M., Ziehn, T., Matear, R. J., Lenton, A., Chamberlain, M. A., Stevens, L. E., Wang, Y.-P., Srbinovsky, J., Bi, D., Yan, H., and Vohralik, P. F.: The carbon cycle in the Australian Community Climate and Earth System Simulator (ACCESS-ESM1) – Part 1: Model description and pre-industrial simulation, Geosci. Model Dev., 10, 2567–2590, https://doi.org/10.5194/gmd-10-2567-2017, 2017.

Lawrence, D. M., Fisher, R. A., Koven, C. D., Oleson, K. W., Swenson, S. C., Bonan, G., Collier, N., Ghimire, B., van Kampenhout, L., Kennedy, D., Kluzek, E., Lawrence, P. J., Li, F., Li, H., Lombardozzi, D., Riley, W. J., Sacks, W. J., Shi, M., Vertenstein, M., Wieder, W. R., Xu, C., Ali, A. A., Badger, A. M., Bisht, G., van den Broeke, M., Brunke, M. A., Burns, S. P., Buzan, J., Clark, M., Craig, A., Dahlin, K., Drewniak, B., Fisher, J. B., Flanner, M., Fox, A. M., Gentine, P., Hoffman, F., Keppel-Aleks, G., Knox, R., Kumar, S., Lenaerts, J., Leung, L. R., Lipscomb, W. H., Lu, Y., Pandey, A., Pelletier, J. D., Perket, J., Randerson, J. T., Ricciuto, D. M., Sanderson, B. M., Slater, A., Subin, Z. M., Tang, J., Thomas, R. Q., Val Martin, M., and Zeng, X.: The Community Land Model Version 5: Description of New Features, Benchmarking, and Impact of Forcing Uncertainty, J. Adv. Model Earth, Sy., 11, 4245–4287, https://doi.org/10.1029/2018MS001583, 2019.

Le Quéré, C., Rödenbeck, C., Buitenhuis, E. T., Conway, T. J., Langenfelds, R., Gomez, A., Labuschagne, C., Ramonet, M., Nakazawa, T., Metzl, N., Gillett, N., and Heimann, M.: Saturation of the Southern Ocean CO_2 Sink Due to Recent Climate Change, Science, 316, 1735–1738, https://doi.org/10.1126/science.1136188, 2007.

Le Quéré, C., Raupach, M. R., Canadell, J. G., Marland, G., Bopp, L., Ciais, P., Conway, T. J., Doney, S. C., Feely, R. A., Foster, P., Friedlingstein, P., Gurney, K., Houghton, R. A., House, J. I., Huntingford, C., Levy, P. E., Lomas, M. R., Majkut, J., Metzl, N., Ometto, J. P., Peters, G. P., Prentice, I. C., Randerson, J. T., Running, S. W., Sarmiento, J. L., Schuster, U., Sitch, S., Takahashi, T., Viovy, N., van der Werf, G. R., and Woodward, F. I.: Trends in the sources and sinks of carbon dioxide, Nat. Geosci., 2, 831–836, https://doi.org/10.1038/ngeo689, 2009.

Le Quéré, C., Takahashi, T., Buitenhuis, E. T., Rödenbeck, C., and Sutherland, S. C.: Impact of climate change and variability on the global oceanic sink of CO_2, Global Biogeochem. Cy., 24, GB4007, https://doi.org/10.1029/2009GB003599, 2010.

Le Quéré, C., Andres, R. J., Boden, T., Conway, T., Houghton, R. A., House, J. I., Marland, G., Peters, G. P., van der Werf, G. R., Ahlström, A., Andrew, R. M., Bopp, L., Canadell, J. G., Ciais, P., Doney, S. C., Enright, C., Friedlingstein, P., Huntingford, C., Jain, A. K., Jourdain, C., Kato, E., Keeling, R. F., Klein Goldewijk, K., Levis, S., Levy, P., Lomas, M., Poulter, B., Raupach, M. R., Schwinger, J., Sitch, S., Stocker, B. D., Viovy, N., Zaehle, S., and Zeng, N.: The global carbon budget 1959–2011, Earth Syst. Sci. Data, 5, 165–185, https://doi.org/10.5194/essd-5-165-2013, 2013.

Le Quéré, C., Peters, G. P., Andres, R. J., Andrew, R. M., Boden, T. A., Ciais, P., Friedlingstein, P., Houghton, R. A., Marland, G., Moriarty, R., Sitch, S., Tans, P., Arneth, A., Arvanitis, A., Bakker, D. C. E., Bopp, L., Canadell, J. G., Chini, L. P., Doney, S. C., Harper, A., Harris, I., House, J. I., Jain, A. K., Jones, S. D., Kato, E., Keeling, R. F., Klein Goldewijk, K., Körtzinger, A., Koven, C., Lefèvre, N., Maignan, F., Omar, A., Ono, T., Park, G.-H., Pfeil, B., Poulter, B., Raupach, M. R., Regnier, P., Rödenbeck, C., Saito, S., Schwinger, J., Segschneider, J., Stocker, B. D., Takahashi, T., Tilbrook, B., van Heuven, S., Viovy, N., Wanninkhof, R., Wiltshire, A., and Zaehle, S.: Global carbon budget 2013, Earth Syst. Sci. Data, 6, 235–263, https://doi.org/10.5194/essd-6-235-2014, 2014.

Le Quéré, C., Moriarty, R., Andrew, R. M., Peters, G. P., Ciais, P., Friedlingstein, P., Jones, S. D., Sitch, S., Tans, P., Arneth, A., Boden, T. A., Bopp, L., Bozec, Y., Canadell, J. G., Chini, L. P., Chevallier, F., Cosca, C. E., Harris, I., Hoppema, M., Houghton, R. A., House, J. I., Jain, A. K., Johannessen, T., Kato, E., Keeling, R. F., Kitidis, V., Klein Goldewijk, K., Koven, C., Landa, C. S., Landschützer, P., Lenton, A., Lima, I. D., Marland, G., Mathis, J. T., Metzl, N., Nojiri, Y., Olsen, A., Ono, T., Peng, S., Peters, W., Pfeil, B., Poulter, B., Raupach, M. R., Regnier, P., Rödenbeck, C., Saito, S., Salisbury, J. E., Schuster, U., Schwinger, J., Séférian, R., Segschneider, J., Steinhoff, T., Stocker, B. D., Sutton, A. J., Takahashi, T., Tilbrook, B., van der Werf, G. R., Viovy, N., Wang, Y.-P., Wanninkhof, R., Wiltshire, A., and Zeng, N.: Global carbon budget 2014, Earth Syst. Sci. Data, 7, 47–85, https://doi.org/10.5194/essd-7-47-2015, 2015a.

Le Quéré, C., Moriarty, R., Andrew, R. M., Canadell, J. G., Sitch, S., Korsbakken, J. I., Friedlingstein, P., Peters, G. P., Andres, R. J., Boden, T. A., Houghton, R. A., House, J. I., Keeling, R. F., Tans, P., Arneth, A., Bakker, D. C. E., Barbero, L., Bopp, L., Chang, J., Chevallier, F., Chini, L. P., Ciais, P., Fader, M., Feely, R. A., Gkritzalis, T., Harris, I., Hauck, J., Ilyina, T., Jain, A. K., Kato,

E., Kitidis, V., Klein Goldewijk, K., Koven, C., Landschützer, P., Lauvset, S. K., Lefèvre, N., Lenton, A., Lima, I. D., Metzl, N., Millero, F., Munro, D. R., Murata, A., Nabel, J. E. M. S., Nakaoka, S., Nojiri, Y., O'Brien, K., Olsen, A., Ono, T., Pérez, F. F., Pfeil, B., Pierrot, D., Poulter, B., Rehder, G., Rödenbeck, C., Saito, S., Schuster, U., Schwinger, J., Séférian, R., Steinhoff, T., Stocker, B. D., Sutton, A. J., Takahashi, T., Tilbrook, B., van der Laan-Luijkx, I. T., van der Werf, G. R., van Heuven, S., Vandemark, D., Viovy, N., Wiltshire, A., Zaehle, S., and Zeng, N.: Global Carbon Budget 2015, Earth Syst. Sci. Data, 7, 349–396, https://doi.org/10.5194/essd-7-349-2015, 2015b.

Le Quéré, C., Andrew, R. M., Canadell, J. G., Sitch, S., Korsbakken, J. I., Peters, G. P., Manning, A. C., Boden, T. A., Tans, P. P., Houghton, R. A., Keeling, R. F., Alin, S., Andrews, O. D., Anthoni, P., Barbero, L., Bopp, L., Chevallier, F., Chini, L. P., Ciais, P., Currie, K., Delire, C., Doney, S. C., Friedlingstein, P., Gkritzalis, T., Harris, I., Hauck, J., Haverd, V., Hoppema, M., Klein Goldewijk, K., Jain, A. K., Kato, E., Körtzinger, A., Landschützer, P., Lefèvre, N., Lenton, A., Lienert, S., Lombardozzi, D., Melton, J. R., Metzl, N., Millero, F., Monteiro, P. M. S., Munro, D. R., Nabel, J. E. M. S., Nakaoka, S., O'Brien, K., Olsen, A., Omar, A. M., Ono, T., Pierrot, D., Poulter, B., Rödenbeck, C., Salisbury, J., Schuster, U., Schwinger, J., Séférian, R., Skjelvan, I., Stocker, B. D., Sutton, A. J., Takahashi, T., Tian, H., Tilbrook, B., van der Laan-Luijkx, I. T., van der Werf, G. R., Viovy, N., Walker, A. P., Wiltshire, A. J., and Zaehle, S.: Global Carbon Budget 2016, Earth Syst. Sci. Data, 8, 605–649, https://doi.org/10.5194/essd-8-605-2016, 2016.

Le Quéré, C., Andrew, R. M., Friedlingstein, P., Sitch, S., Pongratz, J., Manning, A. C., Korsbakken, J. I., Peters, G. P., Canadell, J. G., Jackson, R. B., Boden, T. A., Tans, P. P., Andrews, O. D., Arora, V. K., Bakker, D. C. E., Barbero, L., Becker, M., Betts, R. A., Bopp, L., Chevallier, F., Chini, L. P., Ciais, P., Cosca, C. E., Cross, J., Currie, K., Gasser, T., Harris, I., Hauck, J., Haverd, V., Houghton, R. A., Hunt, C. W., Hurtt, G., Ilyina, T., Jain, A. K., Kato, E., Kautz, M., Keeling, R. F., Klein Goldewijk, K., Körtzinger, A., Landschützer, P., Lefèvre, N., Lenton, A., Lienert, S., Lima, I., Lombardozzi, D., Metzl, N., Millero, F., Monteiro, P. M. S., Munro, D. R., Nabel, J. E. M. S., Nakaoka, S., Nojiri, Y., Padin, X. A., Peregon, A., Pfeil, B., Pierrot, D., Poulter, B., Rehder, G., Reimer, J., Rödenbeck, C., Schwinger, J., Séférian, R., Skjelvan, I., Stocker, B. D., Tian, H., Tilbrook, B., Tubiello, F. N., van der Laan-Luijkx, I. T., van der Werf, G. R., van Heuven, S., Viovy, N., Vuichard, N., Walker, A. P., Watson, A. J., Wiltshire, A. J., Zaehle, S., and Zhu, D.: Global Carbon Budget 2017, Earth Syst. Sci. Data, 10, 405–448, https://doi.org/10.5194/essd-10-405-2018, 2018a.

Le Quéré, C., Andrew, R. M., Friedlingstein, P., Sitch, S., Hauck, J., Pongratz, J., Pickers, P. A., Korsbakken, J. I., Peters, G. P., Canadell, J. G., Arneth, A., Arora, V. K., Barbero, L., Bastos, A., Bopp, L., Chevallier, F., Chini, L. P., Ciais, P., Doney, S. C., Gkritzalis, T., Goll, D. S., Harris, I., Haverd, V., Hoffman, F. M., Hoppema, M., Houghton, R. A., Hurtt, G., Ilyina, T., Jain, A. K., Johannessen, T., Jones, C. D., Kato, E., Keeling, R. F., Goldewijk, K. K., Landschützer, P., Lefèvre, N., Lienert, S., Liu, Z., Lombardozzi, D., Metzl, N., Munro, D. R., Nabel, J. E. M. S., Nakaoka, S., Neill, C., Olsen, A., Ono, T., Patra, P., Peregon, A., Peters, W., Peylin, P., Pfeil, B., Pierrot, D., Poulter, B., Rehder, G., Resplandy, L., Robertson, E., Rocher, M., Rödenbeck, C., Schuster, U., Schwinger, J., Séférian, R., Skjelvan, I., Steinhoff, T., Sutton, A., Tans, P. P., Tian, H., Tilbrook, B., Tubiello, F. N., van der Laan-Luijkx, I. T., van der Werf, G. R., Viovy, N., Walker, A. P., Wiltshire, A. J., Wright, R., Zaehle, S., and Zheng, B.: Global Carbon Budget 2018, Earth Syst. Sci. Data, 10, 2141–2194, https://doi.org/10.5194/essd-10-2141-2018, 2018b.

Le Quéré, C., Korsbakken, J. I., Wilson, C., Tosun, J., Andrew, R., Andres, R. J., Canadell, J. G., Jordan, A., Peters, G. P., and van Vuuren, D. P.: Drivers of declining CO_2 emissions in 18 developed economies, Nat. Clim. Change, 9, 213–217, https://doi.org/10.1038/s41558-019-0419-7, 2019.

Le Quéré, C., Peters, G. P., Friedlingstein, P., Andrew, R. M., Canadell, J. G., Davis, S. J., Jackson, R. B., and Jones, M. W.: Fossil CO_2 emissions in the post-COVID-19 era, Nat. Clim. Change, 11, 197–199, https://doi.org/10.1038/s41558-021-01001-0, 2021.

Levitus, S., Antonov, J. I., Boyer, T. P., Baranova, O. K., Garcia, H. E., Locarnini, R. A., Mishonov, A. V., Reagan, J. R., Seidov, D., Yarosh, E. S., and Zweng, M. M.: World ocean heat content and thermosteric sea level change (0–2000 m), 1955–2010, Geophys. Res. Lett., 39, L10603, https://doi.org/10.1029/2012GL051106, 2012.

Li, H., Ilyina, T., Müller, W. A., and Sienz, F.: Decadal predictions of the North Atlantic CO_2 uptake, Nat. Commun., 7, 11076, https://doi.org/10.1038/ncomms11076, 2016.

Li, H., Ilyina, T., Müller, W. A., and Landschützer, P.: Predicting the variable ocean carbon sink, Sci. Adv., 5, eaav6471, https://doi.org/10.1126/sciadv.aav6471, 2019.

Li, H., Ilyina, T., Loughran, T., Spring, A., and Pongratz, J.: Reconstructions and predictions of the global carbon budget with an emission-driven Earth system model, Earth Syst. Dynam., 14, 101–119, https://doi.org/10.5194/esd-14-101-2023, 2023.

Li, W., Ciais, P., Peng, S., Yue, C., Wang, Y., Thurner, M., Saatchi, S. S., Arneth, A., Avitabile, V., Carvalhais, N., Harper, A. B., Kato, E., Koven, C., Liu, Y. Y., Nabel, J. E. M. S., Pan, Y., Pongratz, J., Poulter, B., Pugh, T. A. M., Santoro, M., Sitch, S., Stocker, B. D., Viovy, N., Wiltshire, A., Yousefpour, R., and Zaehle, S.: Land-use and land-cover change carbon emissions between 1901 and 2012 constrained by biomass observations, Biogeosciences, 14, 5053–5067, https://doi.org/10.5194/bg-14-5053-2017, 2017.

Liao, E., Resplandy, L., Liu, J., and Bowman, K. W.: Amplification of the Ocean Carbon Sink During El Niños: Role of Poleward Ekman Transport and Influence on Atmospheric CO_2, Global Biogeochem. Cy., 34, e2020GB006574, https://doi.org/10.1029/2020GB006574, 2020.

Lienert, S. and Joos, F.: A Bayesian ensemble data assimilation to constrain model parameters and land-use carbon emissions, Biogeosciences, 15, 2909–2930, https://doi.org/10.5194/bg-15-2909-2018, 2018.

Liu, J., Baskaran, L., Bowman, K., Schimel, D., Bloom, A. A., Parazoo, N. C., Oda, T., Carroll, D., Menemenlis, D., Joiner, J., Commane, R., Daube, B., Gatti, L. V., McKain, K., Miller, J., Stephens, B. B., Sweeney, C., and Wofsy, S.: Carbon Monitoring System Flux Net Biosphere Exchange 2020 (CMS-Flux NBE 2020), Earth Syst. Sci. Data, 13, 299–330, https://doi.org/10.5194/essd-13-299-2021, 2021.

Liu, Z., Guan, D., Wei, W., Davis, S. J., Ciais, P., Bai, J., Peng, S., Zhang, Q., Hubacek, K., Marland, G., Andres, R. J., Crawford-

Brown, D., Lin, J., Zhao, H., Hong, C., Boden, T. A., Feng, K., Peters, G. P., Xi, F., Liu, J., Li, Y., Zhao, Y., Zeng, N., and He, K.: Reduced carbon emission estimates from fossil fuel combustion and cement production in China, Nature, 524, 335–338, https://doi.org/10.1038/nature14677, 2015.

Liu, Z., Zeng, N., Liu, Y., Kalnay, E., Asrar, G., Wu, B., Cai, Q., Liu, D., and Han, P.: Improving the joint estimation of CO_2 and surface carbon fluxes using a constrained ensemble Kalman filter in COLA (v1.0), Geosci. Model Dev., 15, 5511–5528, https://doi.org/10.5194/gmd-15-5511-2022, 2022.

Long, M. C., Stephens, B. B., McKain, K., Sweeney, C., Keeling, R. F., Kort, E. A., Morgan, E. J., Bent, J. D., Chandra, N., Chevallier, F., Commane, R., Daube, B. C., Krummel, P. B., Loh, Z., Luijkx, I. T., Munro, D., Patra, P., Peters, W., Ramonet, M., Rödenbeck, C., Stavert, A., Tans, P., and Wofsy, S. C.: Strong Southern Ocean carbon uptake evident in airborne observations. Science, 374, 1275–1280, https://doi.org/10.1126/science.abi4355, 2021.

Lovenduski, N. S., Bonan, G. B., Yeager, S. G., Lindsay, K., and Lombardozzi, D. L.: High predictability of terrestrial carbon fluxes from an initialized decadal prediction system, Environ. Res. Lett., 14, 124074, https://doi.org/10.1088/1748-9326/ab5c55, 2019a.

Lovenduski, N. S., Yeager, S. G., Lindsay, K., and Long, M. C.: Predicting near-term variability in ocean carbon uptake, Earth Syst. Dynam., 10, 45–57, https://doi.org/10.5194/esd-10-45-2019, 2019b.

Lutz, F., Herzfeld, T., Heinke, J., Rolinski, S., Schaphoff, S., von Bloh, W., Stoorvogel, J. J., and Müller, C.: Simulating the effect of tillage practices with the global ecosystem model LPJmL (version 5.0-tillage), Geosci. Model Dev., 12, 2419–2440, https://doi.org/10.5194/gmd-12-2419-2019, 2019.

Ma, L., Hurtt, G., Ott, L., Sahajpal, R., Fisk, J., Lamb, R., Tang, H., Flanagan, S., Chini, L., Chatterjee, A., and Sullivan, J.: Global evaluation of the Ecosystem Demography model (ED v3.0), Geosci. Model Dev., 15, 1971–1994, https://doi.org/10.5194/gmd-15-1971-2022, 2022.

Magi, B. I., Rabin, S., Shevliakova, E., and Pacala, S.: Separating agricultural and non-agricultural fire seasonality at regional scales, Biogeosciences, 9, 3003–3012, https://doi.org/10.5194/bg-9-3003-2012, 2012.

Maksyutov, S., Oda, T., Saito, M., Janardanan, R., Belikov, D., Kaiser, J. W., Zhuravlev, R., Ganshin, A., Valsala, V. K., Andrews, A., Chmura, L., Dlugokencky, E., Haszpra, L., Langenfelds, R. L., Machida, T., Nakazawa, T., Ramonet, M., Sweeney, C., and Worthy, D.: Technical note: A high-resolution inverse modelling technique for estimating surface CO_2 fluxes based on the NIES-TM–FLEXPART coupled transport model and its adjoint, Atmos. Chem. Phys., 21, 1245–1266, https://doi.org/10.5194/acp-21-1245-2021, 2021.

Masarie, K. A. and Tans, P. P.: Extension and integration of atmospheric carbon dioxide data into a globally consistent measurement record, J. Geophys. Res., 100, 11593, https://doi.org/10.1029/95JD00859, 1995.

Mataveli, G., Jones, M. W., Carmenta, R., Sanchez, A., Dutra, D. J., Chaves, M., de Oliveira, G., Anderson, L. O., and Aragão, L. E.: Deforestation falls but rise of wildfires continues degrading Brazilian Amazon forests. Glob. Change Biol., 30, e17202, https://doi.org/10.1111/gcb.17202, 2024.

Mather, A. S.: The transition from deforestation to reforestation in Europe, in: Agricultural technologies and tropical deforestation, edited by: Angelsen, A. and Kaimowitz, D., CABI in association with centre for international Forestry Research, 35–52, 2001.

Mauritsen, T., Bader, J., Becker, T., Behrens, J., Bittner, M., Brokopf, R., Brovkin, V., Claussen, M., Crueger, T., Esch, M., Fast, I., Fiedler, S., Fläschner, D., Gayler, V., Giorgetta, M., Goll, D. S., Haak, H., Hagemann, S., Hedemann, C., Hohenegger, C., Ilyina, T., Jahns, T., Jimenéz-de-la-Cuesta, D., Jungclaus, J., Kleinen, T., Kloster, S., Kracher, D., Kinne, S., Kleberg, D., Lasslop, G., Kornblueh, L., Marotzke, J., Matei, D., Meraner, K., Mikolajewicz, U., Modali, K., Möbis, B., Müller, W. A., Nabel, J. E. M. S., Nam, C. C. W., Notz, D., Nyawira, S.-S., Paulsen, H., Peters, K., Pincus, R., Pohlmann, H., Pongratz, J., Popp, M., Raddatz, T. J., Rast, S., Redler, R., Reick, C. H., Rohrschneider, T., Schemann, V., Schmidt, H., Schnur, R., Schulzweida, U., Six, K. D., Stein, L., Stemmler, I., Stevens, B., von Storch, J.-S., Tian, F., Voigt, A., Vrese, P., Wieners, K.-H., Wilkenskjeld, S., Winkler, A., and Roeckner, E.: Developments in the MPI-M Earth System Model version 1.2 (MPI-ESM1.2) and Its Response to Increasing CO_2, J. Adv. Model Earth Sy., 11, 998–1038, https://doi.org/10.1029/2018MS001400, 2019.

Mayot, N., Buitenhuis, E. T., Wright, R. M., Hauck, J., Bakker, D. C. E., and Le Quéré, C.: Constraining the trend in the ocean CO_2 sink during 2000–2022, Nat. Commun., 15, 8429, https://doi.org/10.1038/s41467-024-52641-7, 2024.

McGrath, M. J., Luyssaert, S., Meyfroidt, P., Kaplan, J. O., Bürgi, M., Chen, Y., Erb, K., Gimmi, U., McInerney, D., Naudts, K., Otto, J., Pasztor, F., Ryder, J., Schelhaas, M.-J., and Valade, A.: Reconstructing European forest management from 1600 to 2010, Biogeosciences, 12, 4291–4316, https://doi.org/10.5194/bg-12-4291-2015, 2015.

McKinley, G. A., Fay, A. R., Lovenduski, N. S., and Pilcher, D. J.: Natural Variability and Anthropogenic Trends in the Ocean Carbon Sink, Annu. Rev. Mar. Sci., 9, 125–150, https://doi.org/10.1146/annurev-marine-010816-060529, 2017.

McKinley, G. A., Fay, A. R., Eddebbar, Y. A., Gloege, L., and Lovenduski, N. S.: External Forcing Explains Recent Decadal Variability of the Ocean Carbon Sink, AGU Adv., 1, e2019AV000149, https://doi.org/10.1029/2019AV000149, 2020.

Meiyappan, P., Jain, A. K., and House, J. I.: Increased influence of nitrogen limitation on CO_2 emissions from future land use and land use change, Global Biogeochem. Cy., 29, 1524–1548, https://doi.org/10.1002/2015GB005086, 2015.

Melton, J. R., Arora, V. K., Wisernig-Cojoc, E., Seiler, C., Fortier, M., Chan, E., and Teckentrup, L.: CLASSIC v1.0: the open-source community successor to the Canadian Land Surface Scheme (CLASS) and the Canadian Terrestrial Ecosystem Model (CTEM) – Part 1: Model framework and site-level performance, Geosci. Model Dev., 13, 2825–2850, https://doi.org/10.5194/gmd-13-2825-2020, 2020.

Mercado, L. M., Bellouin, N., Sitch, S., Boucher, O., Huntingford, C., Wild, M., and Cox, P. M.: Impact of changes in diffuse radiation on the global land carbon sink, Nature, 458, 1014–1017, https://doi.org/10.1038/nature07949, 2009.

Moorcroft, P. R., Hurtt, G. C., and Pacala, S. W.: A Method for Scaling Vegetation Dynamics: The Ecosystem Demography Model, Ecol. Monogr., 71, 557–586, https://doi.org/10.1890/0012-9615(2001)071[0557:AMFSVD]2.0.CO;2, 2001.

Müller, J. and Joos, F.: Committed and projected future changes in global peatlands – continued transient model simulations since the Last Glacial Maximum, Biogeosciences, 18, 3657–3687, https://doi.org/10.5194/bg-18-3657-2021, 2021.

Müller, J. D., Gruber, N., Carter, B., Feely, R., Ishii, M., Lange, N., Lauvset, S. K., Murata, A., Olsen, A., Pérez, F. F., Sabine, C., Tanhua, T., Wanninkhof, R., and Zhu, D.: Decadal Trends in the Oceanic Storage of Anthropogenic Carbon From 1994 to 2014, AGU Adv., 4, e2023AV000875, https://doi.org/10.1029/2023AV000875, 2023.

Nassar, R., Jones, D. B. A., Suntharalingam, P., Chen, J. M., Andres, R. J., Wecht, K. J., Yantosca, R. M., Kulawik, S. S., Bowman, K. W., Worden, J. R., Machida, T., and Matsueda, H.: Modeling global atmospheric CO_2 with improved emission inventories and CO_2 production from the oxidation of other carbon species, Geosci. Model Dev., 3, 689–716, https://doi.org/10.5194/gmd-3-689-2010, 2010.

Nayagam, L., Maksyutov, S., Oda, T., Janardanan, R., Trisolino, P., Zeng J., Kaiser, J. W., and Matsunaga, T.: A top-down estimation of subnational CO_2 budget using a global high-resolution inverse model with data from regional surface networks, Environ. Res. Lett., 19, 0140312024, https://doi.org/10.1088/1748-9326/ad0f74, 2024.

NCEP: National Centers for Environmental Prediction. ONI Index. Cold & Warm Episodes by Season, NCEP [data set], https://origin.cpc.ncep.noaa.gov/products/analysis_monitoring/ensostuff/ONI_v5.php (last access: 21 January 2025), 2024.

Nevison, C. D., Mahowald, N. M., Doney, S. C., Lima, I. D., and Cassar, N.: Impact of variable air-sea O_2 and CO_2 fluxes on atmospheric potential oxygen (APO) and land-ocean carbon sink partitioning, Biogeosciences, 5, 875–889, https://doi.org/10.5194/bg-5-875-2008, 2008.

Niwa, Y., Langenfelds, R., Krummel, P., Loh, Z., Worthy, D., Hatakka, J., Aalto, T., Ramonet, M., Delmotte, M., Schmidt, M., Gheusi, F., Mihalopoulos, N., Morgui, J. A., Andrews, A., Dlugokencky, E., Lee, J., Sweeney, C., Thoning, K., Tans, P., De Wekker, S., Fischer, M. L., Jaffe, D., McKain, K., Viner, B., Miller, J. B., Karion, A., Miller, C., Sloop, C. D., Saito, K., Aoki, S., Morimoto, S., Goto, D., Steinbacher, M., Myhre, C. L., Hermanssen, O., Stephens, B., Keeling, R., Afshar, S., Paplawsky, B., Cox, A., Walker, S., Schuldt, K., Mukai, H., Machida, T., Sasakawa, M., Nomura, S., Ito, A., Iida, Y., and Jones, M. W.: Long-term global CO_2 fluxes estimated by NICAM-based Inverse Simulation for Monitoring CO_2 (NISMON-CO_2) (ver.2022.1), National Institute for Environmental Studies Japan [data set], https://doi.org/10.17595/20201127.001, 2020.

Niwa, Y., Ishijima, K., Ito, A., and Iida, Y.: Toward a long-term atmospheric CO_2 inversion for elucidating natural carbon fluxes: technical notes of NISMON-CO_2 v2021.1, Prog. Earth Planet Sc., 9, 42, https://doi.org/10.1186/s40645-022-00502-6, 2022.

O'Sullivan, M., Spracklen, D. V., Batterman, S. A., Arnold, S. R., Gloor, M., and Buermann, W.: Have Synergies Between Nitrogen Deposition and Atmospheric CO_2 Driven the Recent Enhancement of the Terrestrial Carbon Sink?, Global Biogeochem. Cy., 33, 163–180, https://doi.org/10.1029/2018GB005922, 2019.

O'Sullivan, M., Zhang, Y., Bellouin, N., Harris, I., Mercado, L. M., Sitch, S., Ciais, P., and Friedlingstein, P.: Aerosol–light interactions reduce the carbon budget imbalance, Environ. Res. Lett., 16, 124072, https://doi.org/10.1088/1748-9326/ac3b77, 2021.

O'Sullivan, M., Friedlingstein, P., Sitch, S., Anthoni, P., Arneth, A., Arora, V. K., Bastrikov, V., Delire, C., Goll, D. S., Jain, A., Kato, E., Kennedy, D., Knauer, J., Lienert, S., Lombardozzi, D., McGuire, P. C., Melton, J. R., Nabel, J. E. M. S., Pongratz, J., Poulter, B., Séférian, R., Tian, H., Vuichard, N., Walker, A. P., Yuan, W., Yue, X., and Zaehle, S.: Process-oriented analysis of dominant sources of uncertainty in the land carbon sink, Nat. Commun., 13, 4781, https://doi.org/10.1038/s41467-022-32416-8, 2022.

Our World in Data: CO_2 Emissions, https://ourworldindata.org/co2-emissions (last access: 21 January 2025), 2024.

Palmer, P. I., Feng, L., Baker, D., Chevallier, F., Bösch, H., and Somkuti, P.: Net carbon emissions from African biosphere dominate pan-tropical atmospheric CO_2 signal, Nat. Commun., 10, 3344, https://doi.org/10.1038/s41467-019-11097-w, 2019.

Pan, Y., Birdsey, R. A., Fang, J., Houghton, R., Kauppi, P. E., Kurz, W. A., Phillips, O. L., Shvidenko, A., Lewis, S. L., Canadell, J. G., Ciais, P., Jackson, R. B., Pacala, S. W., McGuire, A. D., Piao, S., Rautiainen, A., Sitch, S., and Hayes, D.: A Large and Persistent Carbon Sink in the World's Forests, Science, 333, 988–993, https://doi.org/10.1126/science.1201609, 2011.

Patra, P. K., Takigawa, M., Watanabe, S., Chandra, N., Ishijima, K., and Yamashita, Y.: Improved Chemical Tracer Simulation by MIROC4.0-based Atmospheric Chemistry-Transport Model (MIROC4-ACTM), SOLA, 14, 91–96, https://doi.org/10.2151/sola.2018-016, 2018.

Peiro, H., Crowell, S., and Moore III, B.: Optimizing 4 years of CO_2 biospheric fluxes from OCO-2 and in situ data in TM5: fire emissions from GFED and inferred from MOPITT CO data, Atmos. Chem. Phys., 22, 15817–15849, https://doi.org/10.5194/acp-22-15817-2022, 2022.

Pendrill, F., Persson, U. M., Godar, J., Kastner, T., Moran, D., Schmidt, S., and Wood, R.: Agricultural and forestry trade drives large share of tropical deforestation emissions, Global Environ. Change, 56, 1–10, https://doi.org/10.1016/j.gloenvcha.2019.03.002, 2019.

Pérez, F. F., Becker, M., Goris, N., Gehlen, M., López-Mozos, M., Tjiputra, J., Olsen, A., Müller, J. D., Huertas, I. E., Chau, T. T. T., Cainzos, V., Velo, A., Benard, G., Hauck, J., Gruber, N., and Wanninkhof, R.: An Assessment of CO_2 Storage and Sea-Air Fluxes for the Atlantic Ocean and Mediterranean Sea Between 1985 and 2018, Global Biogeochem. Cy., 38, e2023GB007862, https://doi.org/10.1029/2023GB007862, 2024.

Peters, G. P., Minx, J. C., Weber, C. L., and Edenhofer, O.: Growth in emission transfers via international trade from 1990 to 2008, P. Natl. Acad. Sci. USA, 108, 8903–8908, https://doi.org/10.1073/pnas.1006388108, 2011.

Peters, G. P., Marland, G., Le Quéré, C., Boden, T., Canadell, J. G., and Raupach, M. R.: Rapid growth in CO_2 emissions after the 2008–2009 global financial crisis, Nat. Clim. Change, 2, 2–4, https://doi.org/10.1038/nclimate1332, 2012.

Peters, G. P., Andrew, R. M., Boden, T., Canadell, J. G., Ciais, P., Le Quéré, C., Marland, G., Raupach, M. R., and Wilson, C.: The challenge to keep global warming below 2 °C, Nat. Clim. Change, 3, 4–6, https://doi.org/10.1038/nclimate1783, 2013.

Peters, G. P., Le Quéré, C., Andrew, R. M., Canadell, J. G., Friedlingstein, P., Ilyina, T., Jackson, R. B., Joos, F., Korsbakken, J. I., McKinley, G. A., Sitch, S., and Tans, P.: Towards real-time

verification of CO_2 emissions, Nat. Clim. Change, 7, 848–850, https://doi.org/10.1038/s41558-017-0013-9, 2017a.

Peters, G. P., Andrew, R. M., Canadell, J. G., Fuss, S., Jackson, R. B., Korsbakken, J. I., Le Quéré, C., and Nakicenovic, N.: Key indicators to track current progress and future ambition of the Paris Agreement, Nat. Clim. Change, 7, 118–122, https://doi.org/10.1038/nclimate3202, 2017b.

Peters, G. P., Andrew, R. M., Canadell, J. G., Friedlingstein, P., Jackson, R. B., Korsbakken, J. I., Le Quéré, C., and Peregon, A.: Carbon dioxide emissions continue to grow amidst slowly emerging climate policies, Nat. Clim. Change, 10, 3–6, https://doi.org/10.1038/s41558-019-0659-6, 2020.

Petrescu, A. M. R., Peters, G. P., Janssens-Maenhout, G., Ciais, P., Tubiello, F. N., Grassi, G., Nabuurs, G.-J., Leip, A., Carmona-Garcia, G., Winiwarter, W., Höglund-Isaksson, L., Günther, D., Solazzo, E., Kiesow, A., Bastos, A., Pongratz, J., Nabel, J. E. M. S., Conchedda, G., Pilli, R., Andrew, R. M., Schelhaas, M.-J., and Dolman, A. J.: European anthropogenic AFOLU greenhouse gas emissions: a review and benchmark data, Earth Syst. Sci. Data, 12, 961–1001, https://doi.org/10.5194/essd-12-961-2020, 2020.

Pfeil, B., Olsen, A., Bakker, D. C. E., Hankin, S., Koyuk, H., Kozyr, A., Malczyk, J., Manke, A., Metzl, N., Sabine, C. L., Akl, J., Alin, S. R., Bates, N., Bellerby, R. G. J., Borges, A., Boutin, J., Brown, P. J., Cai, W.-J., Chavez, F. P., Chen, A., Cosca, C., Fassbender, A. J., Feely, R. A., González-Dávila, M., Goyet, C., Hales, B., Hardman-Mountford, N., Heinze, C., Hood, M., Hoppema, M., Hunt, C. W., Hydes, D., Ishii, M., Johannessen, T., Jones, S. D., Key, R. M., Körtzinger, A., Landschützer, P., Lauvset, S. K., Lefèvre, N., Lenton, A., Lourantou, A., Merlivat, L., Midorikawa, T., Mintrop, L., Miyazaki, C., Murata, A., Nakadate, A., Nakano, Y., Nakaoka, S., Nojiri, Y., Omar, A. M., Padin, X. A., Park, G.-H., Paterson, K., Perez, F. F., Pierrot, D., Poisson, A., Ríos, A. F., Santana-Casiano, J. M., Salisbury, J., Sarma, V. V. S. S., Schlitzer, R., Schneider, B., Schuster, U., Sieger, R., Skjelvan, I., Steinhoff, T., Suzuki, T., Takahashi, T., Tedesco, K., Telszewski, M., Thomas, H., Tilbrook, B., Tjiputra, J., Vandemark, D., Veness, T., Wanninkhof, R., Watson, A. J., Weiss, R., Wong, C. S., and Yoshikawa-Inoue, H.: A uniform, quality controlled Surface Ocean CO_2 Atlas (SOCAT), Earth Syst. Sci. Data, 5, 125–143, https://doi.org/10.5194/essd-5-125-2013, 2013.

Piao, S., Ciais, P., Friedlingstein, P., de Noblet-Ducoudré, N., Cadule, P., Viovy, N., and Wang, T.: Spatiotemporal patterns of terrestrial carbon cycle during the 20th century, Global Biogeochem. Cy., 23, GB4026, https://doi.org/10.1029/2008GB003339, 2009.

Piao, S., Huang, M., Liu, Z., Wang, X., Ciais, P., Canadell, J. G., Wang, K., Bastos, A., Friedlingstein, P., Houghton, R. A., Le Quéré, C., Liu, Y., Myneni, R. B., Peng, S., Pongratz, J., Sitch, S., Yan, T., Wang, Y., Zhu, Z., Wu, D., and Wang, T.: Lower land-use emissions responsible for increased net land carbon sink during the slow warming period, Nat. Geosci., 11, 739–743, https://doi.org/10.1038/s41561-018-0204-7, 2018.

Pongratz, J., Reick, C. H., Houghton, R. A., and House, J. I.: Terminology as a key uncertainty in net land use and land cover change carbon flux estimates, Earth Syst. Dynam., 5, 177–195, https://doi.org/10.5194/esd-5-177-2014, 2014.

Pongratz, J., Smith, S. M., Schwingshackl, C., Dayathilake, L., Gasser, T., Grassi, G., and Pilli, R.: Chapter 7: Current levels of CDR, in: The State of Carbon Dioxide Removal 2024, edited by: Smith, S. M., Geden, O., Gidden, M. J., Lamb, W. F., Nemet, G. F., Minx, J. C., Buck, H., Burke, J., Cox, E., Edwards, M. R., Fuss, S., Johnstone, I., Müller-Hansen, F., Pongratz, J., Probst, B. S., Roe, S., Schenuit, F., Schulte, I., and Vaughan, N. E., 2nd Edn., https://doi.org/10.17605/OSF.IO/F85QJ, 2024.

Poulter, B., Frank, D. C., Hodson, E. L., and Zimmermann, N. E.: Impacts of land cover and climate data selection on understanding terrestrial carbon dynamics and the CO_2 airborne fraction, Biogeosciences, 8, 2027–2036, https://doi.org/10.5194/bg-8-2027-2011, 2011.

Poulter, B., Bastos, A., Canadell, J., Ciais, P., Gruber, N., Hauck, J., Jackson, R., Ishii, M., Müller, J., Patra, P., and Tian, H.: Inventorying Earth's Land and Ocean Greenhouse Gases, Eos, 103, https://doi.org/10.1029/2022EO179084, 2022.

Powis, C. M., Smith, S. M., Minx, J. C., and Gasser, T.: Quantifying global carbon dioxide removal deployment, Environ. Res. Lett., 18, 024022, https://doi.org/10.1088/1748-9326/acb450, 2023.

Prentice, I. C., Farquhar, G. D., Fasham, M. J. R., Goulden, M. L., Heimann, M., Jaramillo, V. J., Kheshgi, H. S., Le Quéré, C., Scholes, R. J., and Wallace, D. W. R.: The Carbon Cycle and Atmospheric Carbon Dioxide, in Climate Change 2001: The Scientific Basis. Contribution of Working Group I to the Third Assessment Report of the Intergovernmental Panel on Climate Change, edited by: Houghton, J. T., Ding, Y., Griggs, D. J., Noguer, M., van der Linden, P. J., Dai, X., Maskell, K., and Johnson, C. A., Cambridge University Press, Cambridge, United Kingdom and New York, NY, USA, 183–237, ISBN 978-0521014953, 2001.

Price, J. T. and Warren, R.: Literature Review of the Potential of "Blue Carbon" Activities to Reduce Emissions, https://avoid-net-uk.cc.ic.ac.uk/wp-content/uploads/delightful-downloads/2016/03/Literature-review-of-the-potential-of-blue-carbon-activities-to-reduce-emissions-AVOID2-WPE2.pdf (last access: 21 January 2025), 2016.

Qin, Y., Xiao, X., Wigneron, J.-P., Ciais, P., Brandt, M., Fan, L., Li, X., Crowell, S., Wu, X., Doughty, R., Zhang, Y., Liu, F., Sitch, S., and Moore, B.: Carbon loss from forest degradation exceeds that from deforestation in the Brazilian Amazon, Nat. Clim. Change, 11, 442–448, https://doi.org/10.1038/s41558-021-01026-5, 2021.

Qin, Z., Zhu, Y., Canadell, J. G., Chen, M., Li, T., Mishra, U. and Yuan, W.: Global spatially explicit carbon emissions from land-use change over the past six decades (1961–2020), One Earth, 7, 835–847, https://doi.org/10.1016/j.oneear.2024.04.002, 2024.

Qiu, C., Ciais, P., Zhu, D., Guenet, B., Peng, S., Petrescu, A. M. R., Lauerwald, R., Makowski, D., Gallego-Sala, A. V., Charman, D. J., and Brewer, S. C.: Large historical carbon emissions from cultivated northern peatlands, Sci. Adv., 7, eabf1332, https://doi.org/10.1126/sciadv.abf1332, 2021.

Randerson, J. T., Chen, Y., van der Werf, G. R., Rogers, B. M., and Morton, D. C.: Global burned area and biomass burning emissions from small fires: BURNED AREA FROM SMALL FIRES, J. Geophys. Res.-Biogeo., 117, G04012, https://doi.org/10.1029/2012JG002128, 2012.

Raupach, M. R., Marland, G., Ciais, P., Le Quéré , C., Canadell, J. G., Klepper, G., and Field, C. B.: Global and regional drivers of accelerating CO_2 emissions, P. Natl. Acad. Sci. USA, 104, 10288–10293, https://doi.org/10.1073/pnas.0700609104, 2007.

Regnier, P., Resplandy, L., Najjar, R. G., and Ciais, P.: The land-to-ocean loops of the global carbon cycle, Nature, 603, 401–410, https://doi.org/10.1038/s41586-021-04339-9, 2022.

Reick, C. H., Gayler, V., Goll, D., Hagemann, S., Heidkamp, M., Nabel, J. E. M. S., Raddatz, T., Roeckner, E., Schnur, R., 110 and Wilkenskjeld, S.: JSBACH 3 – The land component of the MPI Earth System Model: documentation of version 3.2, https://doi.org/10.17617/2.3279802, 2021.

Remaud, M., Chevallier, F., Cozic, A., Lin, X., and Bousquet, P.: On the impact of recent developments of the LMDz atmospheric general circulation model on the simulation of CO_2 transport, Geosci. Model Dev., 11, 4489–4513, https://doi.org/10.5194/gmd-11-4489-2018, 2018.

Resplandy, L., Keeling, R. F., Eddebbar, Y., Brooks, M., Wang, R., Bopp, L., Long, M. C., Dunne, J. P., Koeve, W., and Oschlies, A.: Quantification of ocean heat uptake from changes in atmospheric O_2 and CO_2 composition, Sci. Rep., 9, 20244, https://doi.org/10.1038/s41598-019-56490-z, 2019.

Rödenbeck, C., Bakker, D. C. E., Metzl, N., Olsen, A., Sabine, C., Cassar, N., Reum, F., Keeling, R. F., and Heimann, M.: Interannual sea–air CO_2 flux variability from an observation-driven ocean mixed-layer scheme, Biogeosciences, 11, 4599–4613, https://doi.org/10.5194/bg-11-4599-2014, 2014.

Rödenbeck, C., Zaehle, S., Keeling, R., and Heimann, M.: History of El Niño impacts on the global carbon cycle 1957–2017: a quantification from atmospheric CO_2 data, Philos. T. Roy. Soc. B, 373, 20170303, https://doi.org/10.1098/rstb.2017.0303, 2018.

Rödenbeck, C., DeVries, T., Hauck, J., Le Quéré, C., and Keeling, R. F.: Data-based estimates of interannual sea–air CO_2 flux variations 1957–2020 and their relation to environmental drivers, Biogeosciences, 19, 2627–2652, https://doi.org/10.5194/bg-19-2627-2022, 2022.

Rosan, T. M., Klein Goldewijk, K., Ganzenmüller, R., O'Sullivan, M., Pongratz, J., Mercado, L. M., Aragao, L. E. O. C., Heinrich, V., Randow, C. V., Wiltshire, A., Tubiello, F. N., Bastos, A., Friedlingstein, P., and Sitch, S.: A multi-data assessment of land use and land cover emissions from Brazil during 2000–2019, Environ. Res. Lett., 16, 074004, https://doi.org/10.1088/1748-9326/ac08c3, 2021.

Sakamoto, K., Nakano, H., Urakawa, S., Toyoda, T., Kawakami, Y., Tsujino, H., and Yamanaka, G.: Reference manual for the Meteorological Research Institute Community Ocean Model version 5 (MRI.COMv5), Technical Reports of the Meteorological Research Institute, No. 87, https://doi.org/10.11483/mritechrepo.87, 2023.

Sarma, V. V. S. S., Sridevi, B., Metzl, N., Patra, P. K., Lachkar, Z., Chakraborty, K., Goyet, C., Levy, M., Mehari, M., and Chandra, N.: Air-Sea Fluxes of CO_2 in the Indian Ocean Between 1985 and 2018: A Synthesis Based on Observation-Based Surface CO_2, Hindcast and Atmospheric Inversion Models, Global Biogeochem. Cy., 37, e2023GB007694, https://doi.org/10.1029/2023GB007694, 2023.

Schaphoff, S., von Bloh, W., Rammig, A., Thonicke, K., Biemans, H., Forkel, M., Gerten, D., Heinke, J., Jägermeyr, J., Knauer, J., Langerwisch, F., Lucht, W., Müller, C., Rolinski, S., and Waha, K.: LPJmL4 – a dynamic global vegetation model with managed land – Part 1: Model description, Geosci. Model Dev., 11, 1343–1375, https://doi.org/10.5194/gmd-11-1343-2018, 2018.

Schimel, D., Alves, D., Enting, I. G., Heimann, M., Joos, F., Raynaud, D., Wigley, T., Prater, M., Derwent, R., Ehhalt, D., Fraser, P., Sanhueza, E., Zhou, X., Jonas, P., Charlson, R., Rodhe, H., Sadasivan, S., Shine, K. P., Fouquart, Y., Ramaswamy, V., Solomon, S., Srinivasan, J., Albritton, D., Derwent, R., Isaksen, I., Lal, M., and Wuebbles, D.: Radiative Forcing of Climate Change, in: Climate Change 1995: The Science of Climate Change, Contribution of Working Group I to the Second Assessment Report of the Intergovernmental Panel on Climate Change, edited by: Houghton, J. T., Meira Rilho, L. G., Callander, B. A., Harris, N., Kattenberg, A., and Maskell, K., Cambridge University Press, Cambridge, United Kingdom and New York, NY, USA, ISBN 978-0521559621, 1995.

Schuh, A. E., Jacobson, A. R., Basu, S., Weir, B., Baker, D., Bowman, K., Chevallier, F., Crowell, S., Davis, K. J., Deng, F., Denning, S., Feng, L., Jones, D., Liu, J., and Palmer, P. I.: Quantifying the Impact of Atmospheric Transport Uncertainty on CO_2 Surface Flux Estimates, Global Biogeochem. Cy., 33, 484–500, https://doi.org/10.1029/2018GB006086, 2019.

Schuldt, K. N., Mund, J., Aalto, T., Abshire, J. B., Aikin, K., Allen, G., Andrews, A., Apadula, F., Arnold, S., Baier, B., Bakwin, P., Bartyzel, J., Bentz, G., Bergamaschi, P., Beyersdorf, A., Biermann, T., Biraud, S. C., Blanc, P.-E., Boenisch, H., Bowling, D., Brailsford, G., Brand, W. A., Brunner, D., Bui, T. P., Bäni, L., Calzolari, F., Chang, C. S., Chen, H., Chen, G., Chmura, L., Clark, S., Climadat, S., Colomb, A., Commane, R., Conen, F., Conil, S., Couret, C., Cristofanelli, P., Cuevas, E., Curcoll, R., Daube, B., Davis, K. J., De Mazière, M., De Wekker, S., Dean-Day, J. M., Della Coletta, J., Delmotte, M., Di Iorio, T., DiGangi, E., DiGangi, J. P., Elkins, J. W., Elsasser, M., Emmenegger, L., Fang, S., Fischer, M. L., Forster, G., France, J., Frumau, A., Fuente-Lastra, M., Galkowski, M., Gatti, L. V., Gehrlein, T., Gerbig, C., Gheusi, F., Gloor, E., Goto, D., Griffis, T., Hammer, S., Hanisco, T. F., Hanson, C., Haszpra, L., Hatakka, J., Heimann, M., Heliasz, M., Heltai, D., Henne, S., Hensen, A., Hermans, C., Hermansen, O., Hintsa, E., Hoheisel, A., Holst, J., Iraci, L. T., Ivakhov, V., Jaffe, D. A., Jordan, A., Joubert, W., Karion, A., Kawa, S. R., Kazan, V., Keeling, R. F., Keronen, P., Kim, J., Klausen, J., Kneuer, T., Kolari, P., Kominkova, K., Kort, E., Kozlova, E., Krummel, P. B., Kubistin, D., Kulawik, S. S., Kumps, N., Labuschagne, C., Lam, D. H., Lan, X., Langenfelds, R. L., Lanza, A., Laurent, O., Laurila, T., Lauvaux, T., Lavric, J., Law, B. E., Lee, J., Lehner, I., Lehtinen, K., Leppert, R., Leskinen, A., Leuenberger, M., Leung, W. H., Levin, I., Levula, J., Lin, J., Lindauer, M., Lindroth, A., Loh, Z. M., Lopez, M., Lunder, C. R., Löfvenius, M. O., Machida, T., Mammarella, I., Manca, G., Manning, A., Manning, A., Marek, M. V., Marklund, P., Marrero, J. E., Martin, D., Martin, M. Y., Martins, G. A., Matsueda, H., McKain, K., Meijer, H., Meinhardt, F., Merchant, L., Metzger, J.-M., Mihalopoulos, N., Miles, N. L., Miller, J. B., Miller, C. E., Mitchell, L., Monteiro, V., Montzka, S., Moore, F., Moossen, H., Morgan, E., Morgui, J.-A., Morimoto, S., Munger, J. W., Munro, D., Mutuku, M., Myhre, C. L., Mölder, M., Müller-Williams, J., Necki, J., Newman, S., Nichol, S., Nisbet, E., Niwa, Y., Njiru, D. M., Noe, S. M., Nojiri, Y., O'Doherty, S., Obersteiner, F., Paplawsky, B., Parworth, C. L., Peischl, J., Peltola, O., Peters, W., Philippon, C., Piacentino, S., Pichon, J. M., Pickers, P., Piper, S., Pitt, J., Plass-Dülmer, C., Platt, S. M., Prinzivalli, S., Ramonet, M., Ramos, R., Reyes-

Sanchez, E., Richardson, S. J., Rigouleau, L.-J., Riris, H., Rivas, P. P., Rothe, M., Roulet, Y.-A., Ryerson, T., Ryoo, J.-M., Sargent, M., Sasakawa, M., Scheeren, B., Schmidt, M., Schuck, T., Schumacher, M., Seibel, J., Seifert, T., Sha, M. K., Shepson, P., Shook, M., Sloop, C. D., Smith, P. D., Spain, G., St. Clair, J. M., Steger, D., Steinbacher, M., Stephens, B., Sweeney, C., Sørensen, L. L., Taipale, R., Takatsuji, S., Tans, P., Thoning, K., Timas, H., Torn, M., Trisolino, P., Turnbull, J., Vermeulen, A., Viner, B., Vitkova, G., Walker, S., Watson, A., Weiss, R., Weyrauch, D., Wofsy, S. C., Worsey, J., Worthy, D., Xueref-Remy, I., Yates, E. L., Young, D., Yver-Kwok, C., Zaehle, S., Zahn, A., Zellweger, C., Zimnoch, M., de Souza, R. A., di Sarra, A. G., van Dinther, D., and van den Bulk, P.: Multi-laboratory compilation of atmospheric carbon dioxide data for the period 1957–2022; obspack_co2_1_GLOBALVIEWplus_v9.0_2023-09-09, NOAA Earth System Research Laboratory, Global Monitoring Laboratory [data set], https://doi.org/10.25925/20230801, 2023.

Schuldt, K. N., Jacobson, A. R., Aalto, T., Andrews, A., Apadula, F., Arnold, S., Bakwin, P., Bartyzel, J., Bergamaschi, P., Biermann, T., Biraud, S. C., Blanc, P.-E., Bäni, L., Calzolari, F., Chen, H., Chmura, L., Colomb, A., Condori, L., Conen, F., Conil, S., Couret, C., Cristofanelli, P., Cuevas, E., De Mazière, M., De Wekker, S., Della Coletta, J., Delmotte, M., Di Iorio, T., Elsasser, M., Emmenegger, L., Fischer, M. L., Forster, G., Frumau, A., Fuente-Lastra, M., Galkowski, M., Gheusi, F., Hammer, S., Hatakka, J., Heliasz, M., Heltai, D., Hensen, A., Hermans, C., Hermansen, O., Hoheisel, A., Holst, J., Jaffe, D. A., Karion, A., Kazan, V., Keronen, P., Kneuer, T., Kolari, P., Kominkova, K., Krummel, P. B., Kubistin, D., Kumps, N., Lan, X., Langenfelds, R. L., Lanza, A., Laurent, O., Laurila, T., Lee, J., Lehner, I., Lehtinen, K., Leskinen, A., Leuenberger, M., Levin, I., Levula, J., Lindauer, M., Lindroth, A., Loh, Z. M., Lopez, M., Lunder, C. R., Löfvenius, M. O., Mammarella, I., Manca, G., Manning, A., Manning, A., Marek, M. V., Marklund, P., McKain, K., Meijer, H., Meinhardt, F., Metzger, J.-M., Miller, C. E., Miller, J. B., Myhre, C. L., Mölder, M., Müller-Williams, J., Necki, J., O'Doherty, S., Peltola, O., Philippon, C., Piacentino, S., Pichon, J. M., Pickers, P., Pitt, J., Plass-Dülmer, C., Platt, S. M., Ramonet, M., Ramos, R., Reyes-Sanchez, E., Rigouleau, L.-J., Rivas, P. P., Roulet, Y.-A., Scheeren, B., Schmidt, M., Schumacher, M., Sha, M. K., Sloop, C. D., Smith, P. D., Steger, D., Steinbacher, M., Sweeney, C., Sørensen, L. L., Taipale, R., Tans, P., Thoning, K., Trisolino, P., Turnbull, J., Vermeulen, A., Viner, B., Vitkova, G., Weyrauch, D., Worthy, D., Xueref-Remy, I., Young, D., Yver-Kwok, C., Zimnoch, M., di Sarra, A. G., van Dinther, D., and van den Bulk, P.: Multi-laboratory compilation of atmospheric carbon dioxide data for the period 2023–2024; obspack_co2_1_ NRT_ v9.2_ 2024-03-25; NOAA Earth System Research Laboratory, Global Monitoring Laboratory [data set], https://doi.org/10.25925/20240215, 2024.

Schwinger, J., Goris, N., Tjiputra, J. F., Kriest, I., Bentsen, M., Bethke, I., Ilicak, M., Assmann, K. M., and Heinze, C.: Evaluation of NorESM-OC (versions 1 and 1.2), the ocean carbon-cycle stand-alone configuration of the Norwegian Earth System Model (NorESM1), Geosci. Model Dev., 9, 2589–2622, https://doi.org/10.5194/gmd-9-2589-2016, 2016.

Schwingshackl, C., Obermeier, W. A., Bultan, S., Grassi, G., Canadell, J. G., Friedlingstein, P., Gasser, T., Houghton, R. A., Kurz, W. A., Sitch, S., and Pongratz, J.: Differences in land-based mitigation estimates reconciled by separating natural and land-use CO_2 fluxes at the country level, One Earth, 5, 1367–1376, https://doi.org/10.1016/j.oneear.2022.11.009, 2022.

Séférian, R., Nabat, P., Michou, M., Saint-Martin, D., Voldoire, A., Colin, J., Decharme, B., Delire, C., Berthet, S., Chevallier, M., Sénési, S., Franchisteguy, L., Vial, J., Mallet, M., Joetzjer, E., Geoffroy, O., Guérémy, J.-F., Moine, M.-P., Msadek, R., Ribes, A., Rocher, M., Roehrig, R., Salas-y-Mélia, D., Sanchez, E., Terray, L., Valcke, S., Waldman, R., Aumont, O., Bopp, L., Deshayes, J., Éthé, C., and Madec, G.: Evaluation of CNRM Earth System Model, CNRM-ESM2-1: Role of Earth System Processes in Present-Day and Future Climate, J. Adv. Model. Earth Sy., 11, 4182–4227, https://doi.org/10.1029/2019MS001791, 2019.

Seiler, C., Melton, J. R., Arora, V. K., Sitch, S., Friedlingstein, P., Anthoni, P., Goll, D., Jain, A. K., Joetzjer, E., Lienert, S., Lombardozzi, D., Luyssaert, S., Nabel, J. E. M. S., Tian, H., Vuichard, N., Walker, A. P., Yuan, W., and Zaehle, S.: Are Terrestrial Biosphere Models Fit for Simulating the Global Land Carbon Sink?, J. Adv. Model. Earth Sy., 14, e2021MS002946, https://doi.org/10.1029/2021MS002946, 2022.

Sellar, A. A., Jones, C. G., Mulcahy, J. P., Tang, Y., Yool, A., Wiltshire, A., O'Connor, F. M., Stringer, M., Hill, R., Palmieri, J., Woodward, S., Mora, L., Kuhlbrodt, T., Rumbold, S. T., Kelley, D. I., Ellis, R., Johnson, C. E., Walton, J., Abraham, N. L., Andrews, M. B., Andrews, T., Archibald, A. T., Berthou, S., Burke, E., Blockley, E., Carslaw, K., Dalvi, M., Edwards, J., Folberth, G. A., Gedney, N., Griffiths, P. T., Harper, A. B., Hendry, M. A., Hewitt, A. J., Johnson, B., Jones, A., Jones, C. D., Keeble, J., Liddicoat, S., Morgenstern, O., Parker, R. J., Predoi, V., Robertson, E., Siahaan, A., Smith, R. S., Swaminathan, R., Woodhouse, M. T., Zeng, G., and Zerroukat, M.: UKESM1: Description and Evaluation of the U.K. Earth System Model, J. Adv. Model. Earth Sy., 11, 4513–4558, https://doi.org/10.1029/2019MS001739, 2019.

Shu, S., Jain, A. K., Koven, C. D., and Mishra, U.: Estimation of Permafrost SOC Stock and Turnover Time Using a Land Surface Model With Vertical Heterogeneity of Permafrost Soils, Global Biogeochem. Cy., 34, e2020GB006585, https://doi.org/10.1029/2020GB006585, 2020.

Silva Junior, C. H., Anderson, L. O., Silva, A. L., Almeida, C. T., Dalagnol, R., Pletsch, M. A., Penha, T. V., Paloschi, R. A., and Aragão, L. E.: Fire responses to the 2010 and 2015/2016 Amazonian droughts, Front. Earth Sci., 7, p. 97, https://doi.org/10.3389/feart.2019.00097, 2019.

Sitch, S., Huntingford, C., Gedney, N., Levy, P. E., Lomas, M., Piao, S. L., Betts, R., Ciais, P., Cox, P., Friedlingstein, P., Jones, C. D., Prentice, I. C., and Woodward, F. I.: Evaluation of the terrestrial carbon cycle, future plant geography and climate-carbon cycle feedbacks using five Dynamic Global Vegetation Models (DGVMs): Uncertainty In Land Carbon Cycle Feedbacks, Glob. Change Biol., 14, 2015–2039, https://doi.org/10.1111/j.1365-2486.2008.01626.x, 2008.

Sitch, S., O'Sullivan, M., Robertson, E., Friedlingstein, P., Albergel, C., Anthoni, P., Arneth, A., Arora, V. K., Bastos, A., Bastrikov, V., Bellouin, N., Canadell, J. G., Chini, L., Ciais, P., Falk, S., Harris, I., Hurtt, G., Ito, A., Jain, A. K., Jones, M. W., Joos, F., Kato, E., Kennedy, D., Klein Goldewijk, K., Kluzek, E., Knauer, J., Lawrence, P. J., Lombardozzi, D., Melton, J. R., Nabel, J. E. M. S., Pan, N., Peylin, P., Pongratz, J., Poulter, B., Rosan, T. M., Sun, Q., Tian, H., Walker, A. P.,

Weber, U., Yuan, W., Yue, X., and Zaehle, S.: Trends and Drivers of Terrestrial Sources and Sinks of Carbon Dioxide: An Overview of the TRENDY Project, Global Biogeochem. Cy., 38, e2024GB008102, https://doi.org/10.1029/2024GB008102, 2024.

Smallman, T. L., Milodowski, D. T., Neto, E. S., Koren, G., Ometto, J., and Williams, M.: Parameter uncertainty dominates C-cycle forecast errors over most of Brazil for the 21st century, Earth Syst. Dynam., 12, 1191–1237, https://doi.org/10.5194/esd-12-1191-2021, 2021.

Smith, B., Wårlind, D., Arneth, A., Hickler, T., Leadley, P., Siltberg, J., and Zaehle, S.: Implications of incorporating N cycling and N limitations on primary production in an individual-based dynamic vegetation model, Biogeosciences, 11, 2027–2054, https://doi.org/10.5194/bg-11-2027-2014, 2014.

Smith, S. M., Geden, O., Gidden, M. J., Lamb, W. F., Nemet, G. F., Minx, J. C., Buck, H., Burke, J., Cox, E., Edwards, M. R., Fuss, S., Johnstone, I., Müller-Hansen, F., Pongratz, J., Probst, B. S., Roe, S., Schenuit, F., Schulte, I., Vaughan, N. E. (Eds.): The State of Carbon Dioxide Removal 2024 – 2nd Edn., https://doi.org/10.17605/OSF.IO/F85QJ, 2024.

Sospedra-Alfonso, R., Merryfield, W. J., Boer, G. J., Kharin, V. V., Lee, W.-S., Seiler, C., and Christian, J. R.: Decadal climate predictions with the Canadian Earth System Model version 5 (CanESM5), Geosci. Model Dev., 14, 6863–6891, https://doi.org/10.5194/gmd-14-6863-2021, 2021.

Steele, L. P., Dlugokencky, E. J., Lang, P. M., Tans, P. P., Martin, R. C., and Masarie, K. A.: Slowing down of the global accumulation of atmospheric methane during the 1980s, Nature 358, 313–316, https://doi.org/10.1038/358313a0, 1992.

Stephens, B. B., Keeling, R. F., Heimann, M., Six, K. D., Murnane, R., and Caldeira, K.: Testing global ocean carbon cycle models using measurements of atmospheric O_2 and CO_2 concentration, Global Biogeochem. Cy., 12, 213–230, https://doi.org/10.1029/97GB03500, 1998.

Stephens, B. B., Gurney, K. R., Tans, P. P., Sweeney, C., Peters, W., Bruhwiler, L., Ciais, P., Ramonet, M., Bousquet, P., Nakazawa, T., Aoki, S., Machida, T., Inoue, G., Vinnichenko, N., Lloyd, J., Jordan, A., Heimann, M., Shibistova, O., Langenfelds, R. L., Steele, L. P., Francey, R. J., and Denning, A. S.: Weak Northern and Strong Tropical Land Carbon Uptake from Vertical Profiles of Atmospheric CO_2, Science, 316, 1732–1735, https://doi.org/10.1126/science.1137004, 2007.

Stocker, T., Qin, D., and Platner, G.-K.: Climate Change 2013: The Physical Science Basis. Contribution of Working Group I to the Fifth Assessment Report of the Intergovernmental Panel on Climate Change, Intergovernmental Panel on Climate Change, Cambridge University Press, Cambridge, ISBN 9789291691388, 2013.

Swart, N. C., Cole, J. N. S., Kharin, V. V., Lazare, M., Scinocca, J. F., Gillett, N. P., Anstey, J., Arora, V., Christian, J. R., Hanna, S., Jiao, Y., Lee, W. G., Majaess, F., Saenko, O. A., Seiler, C., Seinen, C., Shao, A., Sigmond, M., Solheim, L., von Salzen, K., Yang, D., and Winter, B.: The Canadian Earth System Model version 5 (CanESM5.0.3), Geosci. Model Dev., 12, 4823–4873, https://doi.org/10.5194/gmd-12-4823-2019, 2019.

Takahashi, T., Sutherland, S. C., Wanninkhof, R., Sweeney, C., Feely, R. A., Chipman, D. W., Hales, B., Friederich, G., Chavez, F., Sabine, C., Watson, A., Bakker, D. C. E., Schuster, U., Metzl, N., Yoshikawa-Inoue, H., Ishii, M., Midorikawa, T., Nojiri, Y., Körtzinger, A., Steinhoff, T., Hoppema, M., Olafsson, J., Arnarson, T. S., Tilbrook, B., Johannessen, T., Olsen, A., Bellerby, R., Wong, C. S., Delille, B., Bates, N. R., and de Baar, H. J. W.: Climatological mean and decadal change in surface ocean pCO_2, and net sea–air CO_2 flux over the global oceans, Deep-Sea Res. Pt. II, 56, 554–577, https://doi.org/10.1016/j.dsr2.2008.12.009, 2009.

Terhaar, J., Frölicher, T. L., and Joos, F.: Southern Ocean anthropogenic carbon sink constrained by sea surface salinity, Sci. Adv., 7, eabd5964, https://doi.org/10.1126/sciadv.abd5964, 2021.

Terhaar, J., Frölicher, T. L., and Joos, F.: Observation-constrained estimates of the global ocean carbon sink from Earth system models, Biogeosciences, 19, 4431–4457, https://doi.org/10.5194/bg-19-4431-2022, 2022.

Terhaar, J., Goris, N., Müller, J. D., DeVries, T., Gruber, N., Hauck, J., Perez, F. F., and Séférian, R.: Assessment of Global Ocean Biogeochemistry Models for Ocean Carbon Sink Estimates in RECCAP2 and Recommendations for Future Studies, J. Adv. Model. Earth Sy., 16, e2023MS003840, https://doi.org/10.1029/2023MS003840, 2024.

Tian, H., Chen, G., Lu, C., Xu, X., Hayes, D. J., Ren, W., Pan, S., Huntzinger, D. N., and Wofsy, S. C.: North American terrestrial CO_2 uptake largely offset by CH_4 and N_2O emissions: toward a full accounting of the greenhouse gas budget, Climatic Change, 129, 413–426, https://doi.org/10.1007/s10584-014-1072-9, 2015.

Tsujino, H., Nakano, H., Sakamoto, K., Urakawa, L. S., Toyama, K., Kosugi, N., Kitamura, Y., Ishii, M., Nishikawa, S., Nishikawa, H., Sugiyama, T., and Ishikawa, Y.: Impact of increased horizontal resolution of an ocean model on carbon circulation in the North Pacific Ocean, J. Adv. Model. Earth Sy., 16, e2023MS003720, https://doi.org/10.1029/2023MS003720, 2024.

Tubiello, F. N., Conchedda, G., Wanner, N., Federici, S., Rossi, S., and Grassi, G.: Carbon emissions and removals from forests: new estimates, 1990–2020, Earth Syst. Sci. Data, 13, 1681–1691, https://doi.org/10.5194/essd-13-1681-2021, 2021.

Tuck, C.: 2022 Mineral Commodity Summary: Iron Ore, Tech. rep., U.S. Geological Survey, https://pubs.usgs.gov/periodicals/mcs2022/mcs2022-iron-ore.pdf (last access: 21 January 2025), 2022.

UNFCCC: Synthesis report for the technical assessment component of the first global stocktake, https://unfccc.int/documents/461466 (last access: 21 January 2025), 2022.

van der Laan-Luijkx, I. T., van der Velde, I. R., van der Veen, E., Tsuruta, A., Stanislawska, K., Babenhauserheide, A., Zhang, H. F., Liu, Y., He, W., Chen, H., Masarie, K. A., Krol, M. C., and Peters, W.: The CarbonTracker Data Assimilation Shell (CTDAS) v1.0: implementation and global carbon balance 2001–2015, Geosci. Model Dev., 10, 2785–2800, https://doi.org/10.5194/gmd-10-2785-2017, 2017.

van der Velde, I. R., van der Werf, G. R., Houweling, S., Maasakkers, J. D., Borsdorff, T., Landgraf, J., Tol, P., van Kempen, T. A., van Hees, R., Hoogeveen, R., Veefkind, J. P., and Aben, I.: Vast CO_2 release from Australian fires in 2019–2020 constrained by satellite, Nature, 597, 366–369, https://doi.org/10.1038/s41586-021-03712-y, 2021.

van der Werf, G. R., Randerson, J. T., Giglio, L., Collatz, G. J., Mu, M., Kasibhatla, P. S., Morton, D. C., DeFries, R. S., Jin, Y., and van Leeuwen, T. T.: Global fire emissions and the contribution of deforestation, savanna, forest, agricultural, and peat fires (1997–2009), Atmos. Chem. Phys., 10, 11707–11735, https://doi.org/10.5194/acp-10-11707-2010, 2010.

van der Werf, G. R., Randerson, J. T., Giglio, L., van Leeuwen, T. T., Chen, Y., Rogers, B. M., Mu, M., van Marle, M. J. E., Morton, D. C., Collatz, G. J., Yokelson, R. J., and Kasibhatla, P. S.: Global fire emissions estimates during 1997–2016, Earth Syst. Sci. Data, 9, 697–720, https://doi.org/10.5194/essd-9-697-2017, 2017.

van Wees, D., van der Werf, G. R., Randerson, J. T., Andela, N., Chen, Y., and Morton, D. C.: The role of fire in global forest loss dynamics, Glob. Change Biol., 27, 2377–2391, https://doi.org/10.1111/gcb.15591, 2021.

Vaittinada Ayar, P., Bopp, L., Christian, J. R., Ilyina, T., Krasting, J. P., Séférian, R., Tsujino, H., Watanabe, M., Yool, A., and Tjiputra, J.: Contrasting projections of the ENSO-driven CO_2 flux variability in the equatorial Pacific under high-warming scenario, Earth Syst. Dynam., 13, 1097–1118, https://doi.org/10.5194/esd-13-1097-2022, 2022.

von Bloh, W., Schaphoff, S., Müller, C., Rolinski, S., Waha, K., and Zaehle, S.: Implementing the nitrogen cycle into the dynamic global vegetation, hydrology, and crop growth model LPJmL (version 5.0), Geosci. Model Dev., 11, 2789–2812, https://doi.org/10.5194/gmd-11-2789-2018, 2018.

Vuichard, N., Messina, P., Luyssaert, S., Guenet, B., Zaehle, S., Ghattas, J., Bastrikov, V., and Peylin, P.: Accounting for carbon and nitrogen interactions in the global terrestrial ecosystem model ORCHIDEE (trunk version, rev 4999): multi-scale evaluation of gross primary production, Geosci. Model Dev., 12, 4751–4779, https://doi.org/10.5194/gmd-12-4751-2019, 2019.

Walker, A. P., Quaife, T., Bodegom, P. M., De Kauwe, M. G., Keenan, T. F., Joiner, J., Lomas, M. R., MacBean, N., Xu, C., Yang, X., and Woodward, F. I.: The impact of alternative trait-scaling hypotheses for the maximum photosynthetic carboxylation rate (Vcmax) on global gross primary production, New Phytol., 215, 1370–1386, https://doi.org/10.1111/nph.14623, 2017.

Walker, A. P., De Kauwe, M. G., Bastos, A., Belmecheri, S., Georgiou, K., Keeling, R. F., McMahon, S. M., Medlyn, B. E., Moore, D. J. P., Norby, R. J., Zaehle, S., Anderson-Teixeira, K. J., Battipaglia, G., Brienen, R. J. W., Cabugao, K. G., Cailleret, M., Campbell, E., Canadell, J. G., Ciais, P., Craig, M. E., Ellsworth, D. S., Farquhar, G. D., Fatichi, S., Fisher, J. B., Frank, D. C., Graven, H., Gu, L., Haverd, V., Heilman, K., Heimann, M., Hungate, B. A., Iversen, C. M., Joos, F., Jiang, M., Keenan, T. F., Knauer, J., Körner, C., Leshyk, V. O., Leuzinger, S., Liu, Y., MacBean, N., Malhi, Y., McVicar, T. R., Penuelas, J., Pongratz, J., Powell, A. S., Riutta, T., Sabot, M. E. B., Schleucher, J., Sitch, S., Smith, W. K., Sulman, B., Taylor, B., Terrer, C., Torn, M. S., Treseder, K. K., Trugman, A. T., Trumbore, S. E., van Mantgem, P. J., Voelker, S. L., Whelan, M. E., and Zuidema, P. A.: Integrating the evidence for a terrestrial carbon sink caused by increasing atmospheric CO_2, New Phytol., 229, 2413–2445, https://doi.org/10.1111/nph.16866, 2021.

Watanabe, M., Tatebe, H., Koyama, H., Hajima, T., Watanabe, M., and Kawamiya, M.: Importance of El Niño reproducibility for reconstructing historical CO_2 flux variations in the equatorial Pacific, Ocean Sci., 16, 1431–1442, https://doi.org/10.5194/os-16-1431-2020, 2020.

Watson, A. J., Schuster, U., Shutler, J. D., Holding, T., Ashton, I. G. C., Landschützer, P., Woolf, D. K., and Goddijn-Murphy, L.: Revised estimates of ocean-atmosphere CO_2 flux are consistent with ocean carbon inventory, Nat. Commun., 11, 4422, https://doi.org/10.1038/s41467-020-18203-3, 2020.

Watson, R. T., Rohde, H., Oeschger, H., and Siegenthaler, U.: Greenhouse Gases and Aerosols, in: Climate Change: The IPCC Scientific Assessment. Intergovernmental Panel on Climate Change (IPCC), edited by: Houghton, J. T., Jenkins, G. J., and Ephraums, J. J., Cambridge University Press, Cambridge, ISBN 978-0521403603, 1990.

Wenzel, S., Cox, P. M., Eyring, V., and Friedlingstein, P.: Projected land photosynthesis constrained by changes in the seasonal cycle of atmospheric CO_2, Nature, 538, 499–501, https://doi.org/10.1038/nature19772, 2016.

Wilkenskjeld, S., Kloster, S., Pongratz, J., Raddatz, T., and Reick, C. H.: Comparing the influence of net and gross anthropogenic land-use and land-cover changes on the carbon cycle in the MPI-ESM, Biogeosciences, 11, 4817–4828, https://doi.org/10.5194/bg-11-4817-2014, 2014.

Wiltshire, A. J., Burke, E. J., Chadburn, S. E., Jones, C. D., Cox, P. M., Davies-Barnard, T., Friedlingstein, P., Harper, A. B., Liddicoat, S., Sitch, S., and Zaehle, S.: JULES-CN: a coupled terrestrial carbon–nitrogen scheme (JULES vn5.1), Geosci. Model Dev., 14, 2161–2186, https://doi.org/10.5194/gmd-14-2161-2021, 2021.

Woodward, F. I. and Lomas, M. R.: Vegetation dynamics – simulating responses to climatic change, Biol. Rev., 79, 643–670, https://doi.org/10.1017/S1464793103006419, 2004.

Wright, R. M., Le Quéré, C., Buitenhuis, E., Pitois, S., and Gibbons, M. J.: Role of jellyfish in the plankton ecosystem revealed using a global ocean biogeochemical model, Biogeosciences, 18, 1291–1320, https://doi.org/10.5194/bg-18-1291-2021, 2021.

Xi, F., Davis, S. J., Ciais, P., Crawford-Brown, D., Guan, D., Pade, C., Shi, T., Syddall, M., Lv, J., Ji, L., Bing, L., Wang, J., Wei, W., Yang, K.-H., Lagerblad, B., Galan, I., Andrade, C., Zhang, Y., and Liu, Z.: Substantial global carbon uptake by cement carbonation, Nat. Geosci., 9, 880–883, https://doi.org/10.1038/ngeo2840, 2016.

Xia, X., Ren, P., Wang, X., Liu, D., Chen, X., Dan, L., He, B., He, H., Ju, W., Liang, M., Lu, X., Peng, J., Qin, Z., Xia, J., Zheng, B., Wei, J., Yue, X., Yu, G., Piao, S., and Yuan, W.: The carbon budget of China: 1980–2021, Sci. Bull., 69, 114–124, https://doi.org/10.1016/j.scib.2023.11.016, 2024.

Yang, D., Liu, Y., Feng, L., Wang, J., Yao, L., Cai, Z., Zhu, S., Lu, N., and Lyu, D.: The First Global Carbon Dioxide Flux Map Derived from TanSat Measurements, Adv. Atmos. Sci., 38, 1433–1443, https://doi.org/10.1007/s00376-021-1179-7, 2021.

Yang, X., Thornton, P., Ricciuto, D., Wang, Y., and Hoffman, F.: Global evaluation of terrestrial biogeochemistry in the Energy Exascale Earth System Model (E3SM) and the role of the phosphorus cycle in the historical terrestrial carbon balance, Biogeosciences, 20, 2813–2836, https://doi.org/10.5194/bg-20-2813-2023, 2023.

You, Y., Tian, H., Pan, S., Shi, H., Bian, Z., Gurgel, A., Huang, Y., Kicklighter, D., Liang, X.-Z., Lu, C., Melillo, J., Miao, R., Pan, N., Reilly, J., Ren, W., Xu, R., Yang, J., Yu, Q., and

Zhang, J.: Incorporating dynamic crop growth processes and management practices into a terrestrial biosphere model for simulating crop production in the United States: Toward a unified modeling framework, Agr. Forest Meteorol., 325, 109144, https://doi.org/10.1016/j.agrformet.2022.109144, 2022.

Yu, Z., Ciais, P., Piao, S., Houghton, R. A., Lu, C., Tian, H., Agathokleous, E., Kattel, G. R., Sitch, S., Goll, D., Yue, X., Walker, A., Friedlingstein, P., Jain, A. K., Liu, S., and Zhou, G.: Forest expansion dominates China's land carbon sink since 1980, Nat. Commun., 13, 5374, https://doi.org/10.1038/s41467-022-32961-2, 2022.

Yue, C., Ciais, P., Zhu, D., Wang, T., Peng, S. S., and Piao, S. L.: How have past fire disturbances contributed to the current carbon balance of boreal ecosystems?, Biogeosciences, 13, 675–690, https://doi.org/10.5194/bg-13-675-2016, 2016.

Yue, X., Zhou, H., Tian, C., Ma, Y., Hu, Y., Gong, C., Zheng, H., and Liao, H.: Development and evaluation of the interactive Model for Air Pollution and Land Ecosystems (iMAPLE) version 1.0, Geosci. Model Dev., 17, 4621–4642, https://doi.org/10.5194/gmd-17-4621-2024, 2024.

Zaehle, S. and Friend, A. D.: Carbon and nitrogen cycle dynamics in the O-CN land surface model: 1. Model description, site-scale evaluation, and sensitivity to parameter estimates: Site-scale evaluation of a C-N model, Global Biogeochem. Cy., 24, GB1005, https://doi.org/10.1029/2009GB003521, 2010.

Zaehle, S., Ciais, P., Friend, A. D., and Prieur, V.: Carbon benefits of anthropogenic reactive nitrogen offset by nitrous oxide emissions, Nat. Geosci., 4, 601–605, https://doi.org/10.1038/ngeo1207, 2011.

Zaehle, S., Medlyn, B. E., De Kauwe, M. G., Walker, A. P., Dietze, M. C., Hickler, T., Luo, Y., Wang, Y.-P., El-Masri, B., Thornton, P., Jain, A., Wang, S., Warlind, D., Weng, E., Parton, W., Iversen, C. M., Gallet-Budynek, A., McCarthy, H., Finzi, A., Hanson, P. J., Prentice, I. C., Oren, R., and Norby, R. J.: Evaluation of 11 terrestrial carbon–nitrogen cycle models against observations from two temperate Free-Air CO_2 Enrichment studies, New Phytol., 202, 803–822, https://doi.org/10.1111/nph.12697, 2014.

Zeng, J., Iida, Y., Matsunaga, T., and Shirai, T.: Surface ocean CO_2 concentration and air-sea flux estimate by machine learning with modelled variable trends, Front. Mar. Sci., 9, https://doi.org/10.3389/fmars.2022.989233, 2022.

Zheng, B., Ciais, P., Chevallier, F., Chuvieco, E., Chen, Y., and Yang, H.: Increasing forest fire emissions despite the decline in global burned area, Sci. Adv., 7, eabh2646, https://doi.org/10.1126/sciadv.abh2646, 2021.

Zou, Y., Wang, Y., Ke, Z., Tian, H., Yang, J., and Liu, Y.: Development of a REgion-Specific Ecosystem Feedback Fire (RESFire) Model in the Community Earth System Model, J. Adv. Model. Earth Sy., 11, 417–445, https://doi.org/10.1029/2018MS001368, 2019.

Zscheischler, J., Mahecha, M. D., Avitabile, V., Calle, L., Carvalhais, N., Ciais, P., Gans, F., Gruber, N., Hartmann, J., Herold, M., Ichii, K., Jung, M., Landschützer, P., Laruelle, G. G., Lauerwald, R., Papale, D., Peylin, P., Poulter, B., Ray, D., Regnier, P., Rödenbeck, C., Roman-Cuesta, R. M., Schwalm, C., Tramontana, G., Tyukavina, A., Valentini, R., van der Werf, G., West, T. O., Wolf, J. E., and Reichstein, M.: Reviews and syntheses: An empirical spatiotemporal description of the global surface–atmosphere carbon fluxes: opportunities and data limitations, Biogeosciences, 14, 3685–3703, https://doi.org/10.5194/bg-14-3685-2017, 2017.